The Role of PTTG, PBF, p53 and MDM2 in Thyroid Cancer

By

Gavin Ryan

A thesis presented to the College of Medical and Dental Sciences at the University of Birmingham for the Degree of Doctor of Philosophy

School of Clinical and Experimental Medicine

College of Medical and Dental Sciences

University of Birmingham

September 2013

Abstract

Thyroid cancer is the most common endocrine malignancy and its incidence is increasing. p53, a potent tumour suppressor, is rarely mutated in thyroid cancer, and it therefore seems plausible there are other means of wild-type p53 inactivation. Overexpression of the human pituitary tumor-transforming gene, and its binding factor PBF, have been found in thyroid cancer. hPTTG1 is a multifunctional protein with roles in cell cycle control, DNA repair and apoptosis. It possesses a dual role in tumourigenesis, through initiation via increased genetic instability and aneuploidy, and progression through induction of growth factors. Research performed in this thesis has characterised a thyroidal hPTTG1-Tg overexpressing mouse model, showing reduced thyroid size due to reduced cellular proliferation. Characterisation of *Pttg1* knockout mouse thyroids showed growth factor expression dysregulation and potential senescence of thyroid cells. We identified no effect of hPTTG1 over or underexpression on goitre induction. PBF is a relatively uncharacterised protein, which is transforming *in vitro* and tumourigenic *in vivo*. PBF is capable of increasing p53 degradation via increased ubiquitination, and work in this thesis shows this is dependent on MDM2, an E3 ligase and primary regulator of p53. Furthermore interactions between PBF and MDM2 were demonstrated. We showed that PBF binds to the E3 ubiquitin ligase RAD6, which also ubiquitinaties p53, and regulates its expression. Taken together this work has identified critical and novel findings on the roles of hPTTG1 and PBF in thyroid cancer.

Dedication

I dedicate this thesis to my parents for your continual support and guidance.

Acknowledgements

I would like to acknowledge my supervisors Dr Kristien Boelaert and Professor Christopher McCabe for their excellent supervision during my PhD.

Also other members of our group, especially Gregory Lewy, Martin Read, Robert Seed and Neil Sharma for their patience and helpfulness in teaching new techniques.

Acknowledgements must also be made to all of my friends, both at Birmingham and from Wales for the great times I have had away from my PhD.

Special mention must also go to the Shadow Ninjas for the endless enjoyment I have got out of their company and the inspiration they have provided me to never give up.

Lastly I would like to acknowledge the contribution of my partner, Emily, who has provided me with continual support during my PhD.

This work was funded by the Medical Research Council.

Table of contents

List of figures

List of abbreviations

AD	Activation domain
APC	Anaphase promoting complex
AKT	Protein kinase B
AMV	Avian myeloblastosis virus
ARF	ADP Ribosylation factor
ATM	Ataxia telangiectasia mutated
ATR	Ataxia telangiectasia and Rad3 related
BAX	BCL-2 associated protein X
BRAF	Serine/threonine protein kinase
BSA	Bovine serum albumin
CBP	CREB-binding protein
CDK	Cyclin dependent kinase
CMV	Cytomegalovirus
Co-IP	Co-immunoprecipitation
COP-1	Coat protein complex
DAPI	4',6-diamidino-2-phenylindole
DBD	DNA-binding domain
DSCAM	Down syndrome cell adhesion molecule
DMSO	Dimethyl sulphoxide
EGF	Epidermal growth factor
ELISA	Enzyme-linked immunosorbent assay

FACS	Fluorescence-activated cell sorting
FGF	Fibroblast growth factor
FISH	Fluorescent in-situ hybridisation
FISSR-PCR	Fluorescence intersimple sequence repeat PCR
FNA	Fine needle aspiration
GH	Growth hormone
GST	Glutathione-S-transferase
H&E	Haematoxylin and Eosin
HGF	Hepatocyte growth factor
HSP70	Heat shock protein 70
I^{131}	Iodine 131 radiation
ID3	Inhibitor of DNA binding-3
IGF	Insulin-like growth factor
IgG	Immunoglobulin G
IRTKS	Insulin receptor tyrosine kinase substrate
LH	Luteinising hormone
LOH	Loss of heterozygosity
MAPK	Mitogen activated protein kinase
MDM2	Mouse double minute 2
MEF	Mouse embryonic fibroblast
MYC	Myelocytomatosis viral oncogene homologue
NCOA4	Nuclear receptor co-activator 4
NCS	Neonatal calf serum
NES	Nuclear export signal

NIS	Sodium iodide symporter
NLS	Nuclear localisation signal
NTRK1	Neurotrophic tyrosine receptor kinase type 1
NUE	Near upstream element
OIS	Oncogene-induced senescence
PAX8	Paired box gene 8
PBF	PTTG binding factor
PBS	Phosphate buffered saline
PCNA	Proliferating cell nuclear antigen
PI3-K	Phosphatidylinositol-3-kinase
Pirh2	p53-induced ubiquitin-protein ligase
PLA	Proximity ligation assay
PML	Promyelocytic leukaemia
PRD	Proline-rich domain
PSI	Plexin, Semaphorin, Integrin
PTTG	Pituitary tumor-transforming gene
PUMA	p53 upregulated mediator of apoptosis
RAD6/UBE2A/B	Ubiquitin conjugating enzyme E2
RAS	Rat sarcoma
Rb	Retinoblastoma
RET	Rearranged during transfection (protein kinase)
RF	Ring finger
SA-β-Gal	Senescence-associated Beta-galactosidase
SP1	Specificity protein 1

SV40	Simian virus 40
T3	Triiodothyronine
T4	Thyroxine
TAD	Transactivation domain
TAE	Tris acetate EDTA
TD	Tetramerisation domain
Tg	Thyroglobulin
TGF	Transforming growth factor
TH	Thyroid hormone
TKI	Tyrosine kinase inhibitor
TLK1	Serine/threonine protein kinase tousled 1
TNM	Tumour, node, metastasis
TSH	Thyroid stimulating hormone
TSHR	Thyroid stimulating hormone receptor
TSP-1	Thrombospondin-1
TTF	Thyroid transcription factor
USF	Upstream stimulatory factor
VEGF	Vascular endothelial growth factor
VO	Vector only
WT	Wild-type
XIAP	X-linked inhibitor of apoptosis protein
YY1	Yin Yang 1
ZF	Zinc finger

Chapter 1. General Introduction

1.1: Pathogenesis of thyroid cancer

1.1.1: Epidemiology and classification

Thyroid carcinoma is the most common endocrine cancer (Dulgeroff and Hershman, 1994) (Parameswaran et al, 2010), and its incidence has increased by 50% in the last 25 years in the USA (Hundahl et al, 1998) (Enewold et al, 2009). The observed increased incidence of 6.6% between 2000 to 2009 represents the most rapidly rising incidence among all cancers. A recent study, using the SEERS database, found there has been a 2.6-fold increase in thyroid cancer from 1973-2006 in the USA, with the majority of this increase occurring in papillary thyroid carcinomas (Cramer et al, 2010) (Figure 1.1.3). Many argue that the increased incidence is due to increased detection as a result of improved imaging techniques (Grodski et al, 2008), including high resolution thyroid ultrasonography, as well as pathological recognition of incidental neoplasms with little clinical significance. Others argue that factors such as the increased use of ionising radiation, increases in BMI, fertility drugs and changes in menstrual cycle are responsible for the increased incidence (Baker and Bhatti, 2006). Overall, thyroid cancers account for approximately 1% of all cancers and are three times more common in females when compared with males (Greco et al, 2009).

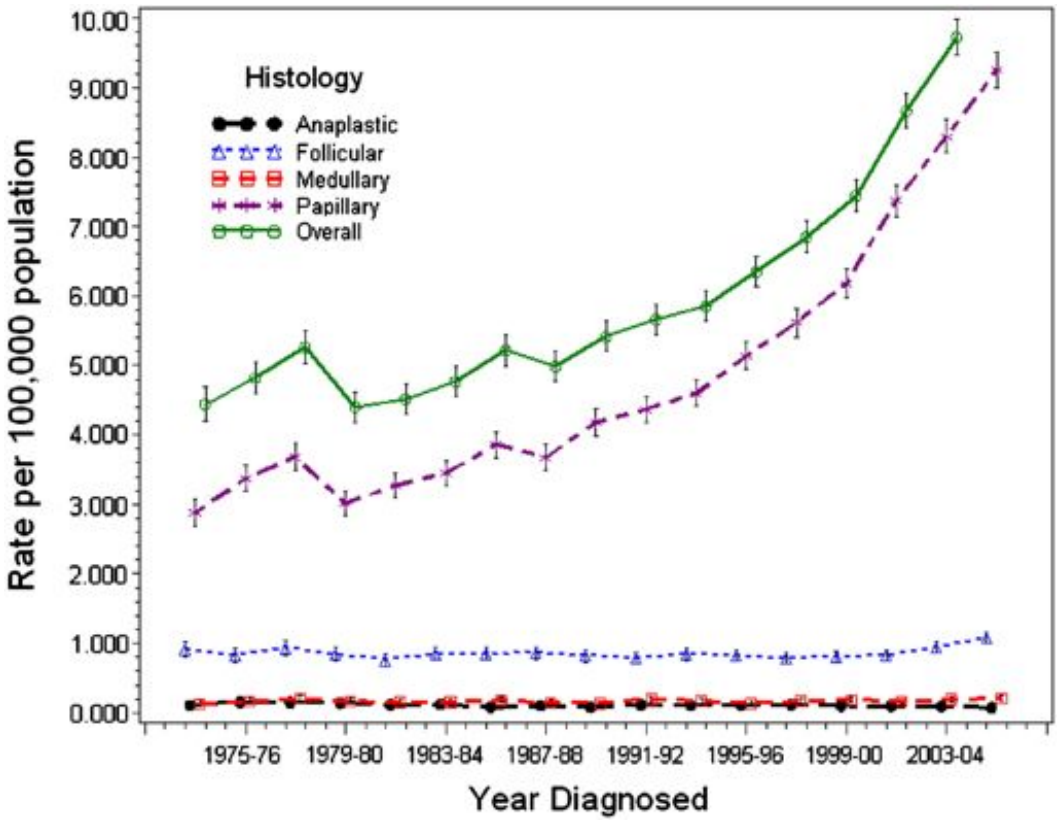

Figure 1.1.1: The incidence of thyroid cancer in the USA, from the years 1973-2006. The chart data displays the rate per 100,000 population of thyroid cancer subtypes and overall thyroid cancer incidence (Taken from Cramer et al, 2010).

Thyroid cancers arise from follicular thyrocytes, or from parafollicular C cells. Follicular cells comprise the majority of cells in the thyroid and are responsible for the production of thyroid hormones triiodothyronine (T3) and thyroxine (T4) (Figure 1.1.2). Parafollicular C cells are involved in the production and secretion of calcitonin.

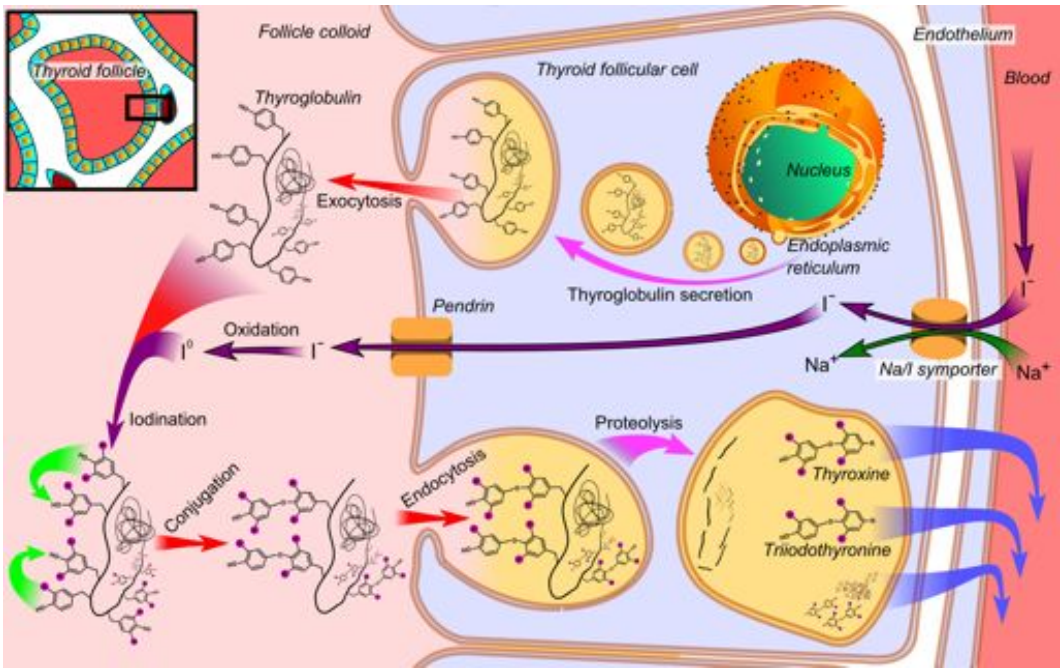

Figure 1.1.2: Thyroid hormone production, displaying a thyroid follicle, comprising follicular cells and colloid. Iodide is transported into the follicular cell via the sodium-iodide symporter, and subsequently transported into the colloid via Pendrin. Thyroglobulin is secreted to the colloid by exocytosis, where it is iodinated and endocytosed back into the follicular cell. It is then subject to proteolysis to produce thyroid hormones T3 and T4, and transported into the blood to be circulated throughout the body (Taken from Boron and Boulpaep, 2003).

Benign and malignant thyroid neoplasms consist of clonal cell populations derived from a single precursor cell, with the initial step in tumour development involving the acquisition of a somatic mutation, altering the structure of a gene and conferring cells with a growth advantage. Several genes acting at multiple steps along growth signalling pathways act as oncogenes stimulating hyperplasia and neoplasia. The majority of thyroid carcinomas are well-differentiated papillary cancers (72-85%), with the

remainder comprising follicular (10-20%), undifferentiated anaplastic (<1%) and other carcinomas (1-4%). Medullary thyroid carcinoma (1.7-3%) arise from parafollicular C cells. Differentiated thyroid carcinomas mainly originate following activation of oncogenes resulting in hyperplasia and subsequent neoplasia (Fagin, 2005), and propagation of growth is stimulated by various growth factors. Well-differentiated carcinomas are usually indolent, although can be aggressive, whereas undifferentiated anaplastic carcinomas are highly aggressive with low survival rates (Are and Shaha, 2006). Anaplastic carcinomas occasionally develop *de novo*, although many develop through de-differentiation of papillary and follicular carcinomas (Nikiforova and Nikiforov, 2009) (Nikiforova and Nikiforov, 2011).

Characteristics	Papillary carcinoma	Follicular carcinoma	Poorly-differentiated carcinoma	Anaplastic carcinoma	Medullary carcinoma
Cell type origin	Follicular	Follicular	Follicular	Follicular	C-cell
Prevalence (%)	72-85	10-15	<2	1-2	3-5
Route of spread	Local lymph-node metastasis	Haematogenous metastasis	Invasive local growth, local lymph-node and haematogenous metasases	Invasive local growth, local lymph-node and haematogenous metasases	Lymph-node and haematogenous metasases
10-year survival (%)	95-98	90-95	~50	<10	60-80
Prevalence of common mutations (%)	*BRAF* – 40-45 *RAS* – 10-20 *RET/PTC* – 10-20 *TRK* - <5	*RAS* – 40-50 *PAX8/PPARγ* – 30-35 *PIK3CA* - <10 *PTEN* - <10	*RAS* – 20-40 *TP53* – 20-30 *BRAF* – 10-20 *CTNNB1* – 10-20 *PIK3CA* – 5-10 *AKT1* – 5-10	*TP53* – 50-80 *CTNNB1* – 5-80 *RAS* – 20-40 *BRAF* – 20-40 *PIK3CA* – 10-20 *PTEN* – 5-15 *AKT1* – 5-10	Familial: *RET - >95* *Sporadic:* *RET* – 40-50 *RAS* - 25

Figure 1.1.3: Thyroid cancer classifications, origin, prevalence, route of spread, 10-year survival and prevalence of common mutations (Adapted from Nikiforov and Nikiforova, 2011).

Benign thyroid enlargement, usually in the form of a diffuse or nodular goitre, is common with prevalence rates reported between 15-50% (Hegedus et al, 2003). Their prevalence is greatly increased in areas of endemic iodine deficiency (Knudsen et al, 2002), since iodine is required for the production of thyroid hormones. Goitres are characterised by thyroid hyperplasia, which represents the response of the thyroid to TSH (Thyroid stimulating hormone), growth factors or circulating stimulatory antibodies.

1.1.2: Molecular genetics of thyroid cancer

Thyroid cancer, much like other cancers, arises through the gradual accumulation of genetic alterations. This includes activating and inactivating somatic mutations, micro RNA (miRNA) dysregulation, gene methylation changes and alteration of gene expression patterns. The majority of thyroid cancers are monoclonal, arising from a single cell somatic mutation, which can subsequently give rise to a number of different cell populations (McCarthy et al, 2006) (Fagin, 2005). The two most common molecular mechanisms of thyroid tumourigenesis are point mutations, resulting from a single nucleotide change, and chromosomal rearrangements, occurring as a result of breakage and fusion of homologous or heterologous chromosomes (Nikiforov and Nikiforova, 2011). Initiation of thyroid tumourigenesis ordinarily involves genes encoding for proteins that form part of the MAPK and PI3-K pathways. The most common of these are the cell membrane receptor tyrosine kinases NTRK1 and RET, and intracellular signal transducers RAS and BRAF.

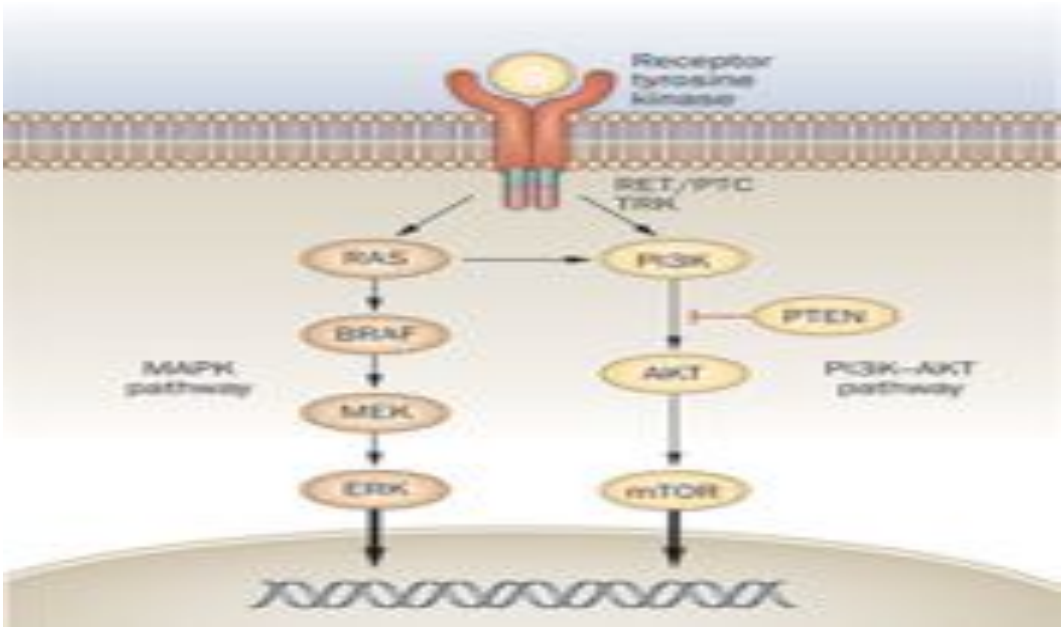

Figure 1.1.4: MAPK and PI3-K signalling cascades. These pathways regulate multiple cellular processes including cellular proliferation. Dysregulation of these pathways by mutations in thyroid follicular cells can lead to tumourigenesis (Taken from Nikiforov and Nikiforova, 2011).

1.1.3: *RAS* mutations

The *HRAS*, *KRAS* and *NRAS* genes encode for G-proteins which act to transmit signals in the MAPK, PI3-K and other signalling pathways (Nikiforov and Nikiforova, 2011). *RAS* mutations have been found in a number of thyroid carcinomas, being present in 40-50% of follicular carcinomas (Motoi et al, 2000), 20-40% of anaplastic and other poorly differentiated carcinomas (Basolo et al, 2000), and 10-20% of papillary carcinomas (Suarez et al, 1990).

The presence of mutations in the *RAS* genes in well-differentiated papillary and follicular carcinomas, as well as in highly aggressive anaplastic carcinomas, suggests that *RAS* mutations may play a role in both the initiation of thyroid tumourigenesis, as well as the promotion of its aggressiveness (Garcia-Rostan et al, 2003). *RAS* mutations have also been found in benign follicular adenomas (Esapa et al, 1999), lending further credence to the idea of *RAS* mutation as an initiator of thyroid tumourigenesis.

1.1.4: *BRAF* mutations

BRAF, another protein involved in the MAPK pathway, is a serine threonine kinase which, upon activation by RAS proteins, is translocated to the cell membrane and phosphorylates several proteins, most notably MAPK kinase. Constitutive activation of BRAF can occur through several mechanisms, the overwhelming majority consisting of a point mutation resulting in a valine to glutamate replacement at residue 600 (Kimura et al, 2003). This is the most commonly found mutation in thyroid cancer, occurring in ~45% of papillary thyroid carcinomas (Xing, 2005), and up to 40% of poorly differentiated and anaplastic carcinomas (Nikiforova et al, 2003). The presence of *BRAF* mutations in differentiated and poorly differentiated thyroid carcinomas,

often in the same tumour sample, suggests that BRAF activation, similar to RAS, is involved in the initiation and de-differentiation of thyroid cancers.

1.1.5: Chromosomal rearrangements

Chromosomal rearrangements are a common cause of thyroid tumourigenesis, in particular those of the *BRAF* and *RET/PTC* genes (Ciampi and Nikiforov, 2007). *RET/PTC* rearrangements are prevalent in papillary thyroid carcinomas (Santoro et al, 1992), occurring in 10-20%, with clonal *RET/PTC* rearrangements restricted to this tumour type (Zhu et al, 2006). *RET/PTC* rearrangement results from fusion of the tyrosine kinase domain of *RET* with the 5' portion of another gene, resulting in constitutive activation of *RET*, leading to activation of the MAPK signalling pathway and an increase in growth potential (Jhiang et al, 1996). The most common rearrangements are fusion of *RET/PTC1* with *CCD6* (Grieco et al, 1990) and *RET/PTC3* with *NCOA4* (Santoro et al, 1994), although many others have been discovered.

The gene *NTRK1*, encoding for a receptor tyrosine kinase, is also a subject of chromosomal rearrangements in papillary thyroid cancer, though not as prevalent as *RET/PTC* rearrangements. This rearrangement, which can occur through fusion of *NTRK1* with at least three different genes on homologous or non-homologous chromosomes (Radice et al, 1991) (Greco et al, 1992) (Miranda et al, 1994), is present in up to 15% of papillary thyroid carcinomas (Musholt et al, 2000).

As opposed to papillary thyroid carcinoma, fusion of the transcription factor *PAX8* and the *PPARγ* genes, causing overexpression of a chimeric PAX8/PPARγ protein, is found in ~35% of follicular carcinomas (Dwight et al, 2003). Interestingly, point mutations in *RAS* and chromosomal rearrangements of *PAX8/PPARγ* rarely occur in the same follicular thyroid sample.

1.1.6: Prognosis of thyroid cancer

Retrospective studies have confirmed specific factors which may be used in the prognostication of thyroid cancer. Several prognostic scoring systems exist, such as MACIS and AMES, although the most widely used is TNM, which focuses on tumour size, nodal metastases and distant metastases (Figure 1.1.5).

Primary tumour:
pT1: Intrathyroidal tumour, ≤1 cm in greatest dimension
pT2: Intrathyroidal tumour, >1-4 cm in greatest dimension
pT3: Intrathyroidal tumour, >4 cm in greatest dimension
pT4: Tumour of any size, extending beyond thyroid capsule
pTX: Primary tumour cannot be assessed

Regional lymph nodes (cervical or upper mediastinal):
N0: No nodes involved
N1: Regional nodes involved
If possible, subdivide
N1a: Ipsilateral cervical nodes
N1b: Bilateral, midline or contralateral cervical nodes or mediastinal nodes
NX: Nodes cannot be assessed

Distant metastases:
M0: No distant metastases
M1: Distant metastases
MX: Distant metastases cannot be assessed

Stage	Under 45 years	45 years and older	10-year cancer-specific mortality (%)
I	Any T, any M, N0	pT1, N0, M0	1.7
II	Any T, any M, N1	pT2, N0, M0 pT3, N0, M0	15.8
III		pT4, N0, M0 Any pT, N1, M0	30
IV		Any pT, any N, M1	60.9

*All undifferentiated or anaplastic carcinomas are classified as stage IV

Figure 1.1.5: The TNM scoring system, used as a measure of thyroid cancer survival rates (Taken from British Thyroid Association and Royal College of Physicians 2007).

The overall outcome for patients treated for thyroid cancer is favourable, with 10-year survival rates of 80-90% for middle-aged adults. 5-20% of patients develop recurrence of the tumour and 10-15% are subject to distant metastases. Overall 9% of patients who develop thyroid cancer will die from their disease (Mazzaferri, 1999) (Sipos and Mazzaferri, 2010). The risk of recurrence has previously been shown to be correlated with the size of the primary tumour (Simpson et al, 1987).

Fine needle aspiration (FNA) biopsy is the gold standard of thyroid cancer diagnosis, and can diagnose benign or malignant thyroid disease in the majority of patients. High resolution ultrasonography can also be performed to identify thyroid nodules and to guide FNA biopsy. Treatment of thyroid cancer generally consists of total thyroidectomy, followed by ablation therapy using ^{131}I and high doses of thyroxine to suppress serum TSH concentrations. For tumours less than 1 cm lobectomy may be considered, preserving thyroid function in 20-30% of patients (Nikiforov et al, 2013). Anaplastic tumours are usually resistant to radioiodine therapy, and so chemotherapy and external beam radiotherapy are used in their treatment, albeit with limited success (Derbel et al, 2011).

Molecular markers identifying genetic mutations are currently in use to determine thyroid cancer diagnosis, and aid in identification of its aggressiveness. A panel of mutations, which includes *BRAF* and *RAS* mutations, and *RET/PTC, PAX8/PPARγ* rearrangements, offers a significant improvement in thyroid cancer diagnosis (Nikiforov et al, 2013). Next generation sequencing is likely to result in the detection of a large number of

genes mutated in thyroid cancers, which may represent further diagnostic and therapeutic targets. A large amount of research is currently being carried out to determine treatments most suitable for specific cancer genotypes, with tyrosine kinase inhibitors (TKIs) showing promise as novel therapeutic targets (Hoffmann et al, 2006) (Okamoto et al, 2013) (Ton et al, 2013).

1.2.1: The pituitary tumor-transforming gene (PTTG)

1.2.2: Identification and characterisation of PTTG

Rat *Pttg1* was first isolated from a GH-secreting pituitary cell line (GH4) using differential mRNA display PCR (Pei and Melmed, 1997). Using rat *Pttg1* cDNA as a probe, the human homolog was identified and found to share 85% homology to rat *Pttg1* (Zhang et al, 1999). A novel gene identified by a separate group, termed *TUTR1*, was found to be identical to *hPTTG1* (Kakar and Jennes, 1999). *hPTTG1*, located to chromosome 5q33 (Prezant et al, 1999), is sized at 10 kB and contains five exons and four introns. Two other *hPTTG* genes have been identified. *hPTTG2* and *hPTTG3* are members of the hPTTG family with a strong homology to *hPTTG1* (Chen et al, 2000). *hPTTG2* was mapped to chromsome 4p15.1 with a 91% amino acid homology to *hPTTG1* (Chen et al, 2000). *hPTTG3* was mapped to chromosome 8q13.1 with

a 89% amino acid homology to *hPTTG1*. However, both hPTTG2 and hPTTG3 are expressed at low levels compared to hPTTG1.

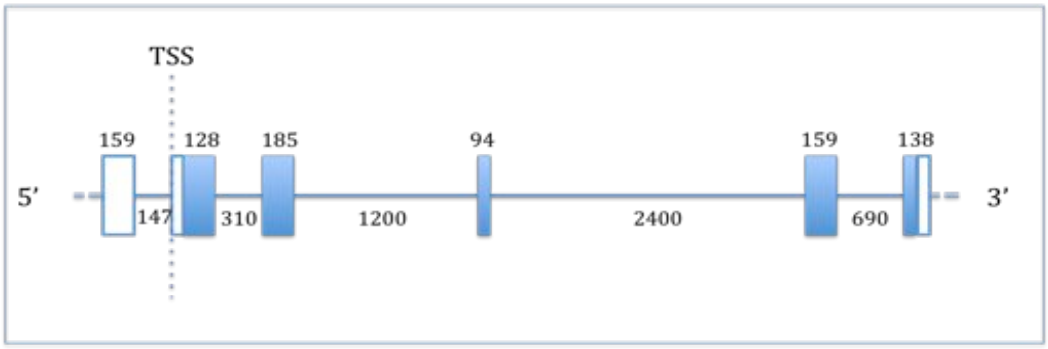

Figure 1.2.1: hPTTG1 gene structure. Exons are indicated as boxes (translated regions are blue and untranslated regions white), lines between indicate introns with sizes in bp as shown. TSS indicates the transcription start site. (Adapted from Vlotides et al, 2007).

1.2.3: PTTG protein structure

hPTTG1 codes for a 202 amino acid protein (Zhang et al, 1999) which shows a 66% structural homology to mouse *Pttg1* (Wang and Melmed, 2000). At the protein level, the expected size of hPTTG1 is 22kD. However, when run on an SDS-PAGE gel hPTTG1 migrates at approximately 28kD, suggesting post-translational modifications (Dominguez et al, 1998). Indeed, hPTTG1 can migrate as a doublet due to cell-cycle dependent phosphorylation (Ramos-Morales et al, 2000). It is localised to both the cytoplasm and

nucleus, although lacking a nuclear localisation signal it requires PTTG-binding factor (PBF) to facilitate its entry into the nucleus (Chien and Pei, 2000). Figure 1.2.2 shows a schematic of the protein structure of hPTTG1, with a functional domain at the C-terminus and a regulatory domain at the N-terminus.

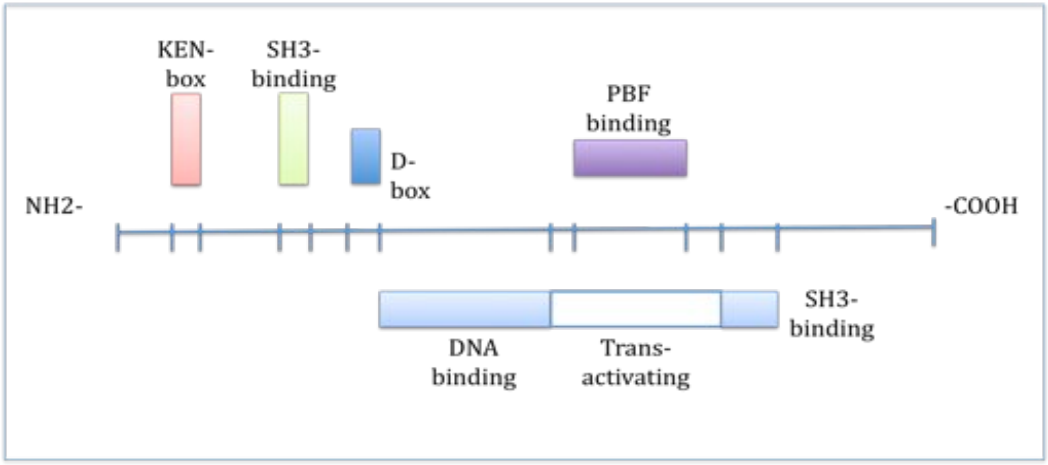

Figure 1.2.2: hPTTG1 *protein structure. Important domains in the functional C-terminus and the regulatory N-terminus are shown. D box indicates destruction box.*

The C-terminus contains a proline rich region between amino acids 163-173, which appears crucial to the transactivation and potential transforming activity of hPTTG1. A conserved Src-homology domain includes two PXXP motifs (Zhang et al, 1999). The serine at residue 165, within the SH3-binding domain, is the only known phosphorylation site of hPTTG1, and

phosphorylation is believed to play a critical role in hPTTG1 function during mitosis (Ramos-Morales et al, 2000) (Boelaert et al, 2004).

The N-terminal domain contains a KEN box (amino acids 9-11) and a Destruction box (amino acids 61-68) which are important for ubiquitination of hPTTG1 by the Anaphase Promoting Complex (APC), in order for the cell cycle to progress from metaphase to anaphase during mitosis (Zou et al, 1999) (Zur and Brandeis, 2001). A DNA-binding domain exists downstream of this (amino acids 61-118) which co-operates with the transactivating domain to facilitate hPTTG1's role as a transcription factor (Zhang et al, 1999) (Wang and Melmed, 2000). Transcriptional targets have been shown to include the oncogene C-myc (Pei, 2001), growth factors VEGF and FGF2 (Kim et al, 2006) and the sodium iodide symporter NIS (Boelaert et al, 2007).

1.2.4: PTTG functions

1.2.4.1: Securin function

During metaphase, sister chromatids are held together by the Cohesin complex, a process that is crucial in orientating chromosomes on mitotic spindles (Tanaka et al, 2000). Cleavage of the cohesin complex takes place via the protease Separase. During the majority of the cell cycle, Separase is inhibited by hPTTG1, also known as Securin, by specific binding (Uhlmann et al, 1999) (Hornig et al, 2002). hPTTG1 is subsequently degraded at the metaphase to anaphase transition after being ubiqiutinated, and therefore

targeted for degradation by the proteasome, by the ubiquitin ligase Anaphase Promoting Complex (APC) (Wirth et al, 2006). Degradation of hPTTG1 allows Separase to cleave Cohesin and equal separation of chromatids occurs.

1.2.4.2: DNA damage and repair

DNA-PK (DNA protein kinase) is an enzyme involved in DNA repair following double stranded breaks, with Ku-70 a regulatory subunit of DNA-PK. hPTTG1 has been shown to be involved in DNA repair by binding to Ku-70 (Romero et al, 2001), and upon DNA damage this binding is disrupted. This allows repair of DNA damage and implies hPTTG1 may be crucial in delaying onset of mitosis in order for DNA repair to occur. Overexpression of hPTTG1 in a colorectal cancer cell line led to an increase in genetic instability, believed to be caused at least in part by inhibition of Ku heterodimer function (Kim et al, 2007). hPTTG1 has also been shown to be required for cellular proliferation arrest following ultraviolet radiation (Romero et al, 2004). Treatment with bleomycin and doxorubicin, two potent DNA damage inducing drugs, resulted in suppression of hPTTG1 by p53, suggesting a role for p53 in regulation of hPTTG1 following DNA damage (Zhou et al, 2003). Overall, these results implicate hPTTG1 as being important in several DNA damage response pathways.

1.2.4.3: Transcription factor activity

Due to the presence of a predicted transactivation domain at the C-terminus, hPTTG1 was investigated as a potential transcription factor, and transcriptional activity was demonstrated through use of a luciferase system, using GAL4 response elements to confirm transcriptional activity (Dominguez et al, 1998). Results from DNA arrays following hPTTG1 induction showed increased expression of several genes, including the oncogene *C-myc* and *HSP70* (Pei, 2001), and hPTTG1 was further shown to bind to the *C-myc* promoter. hPTTG1 has also been shown to induce mRNA expression of Fibroblast rowth factor 2 (FGF2) in several cell lines, including NIH3T3 cells (Ishikawa et al, 2001), primary thyroid cells (Boelaert et al, 2004) and neuronal NT2 cells (McCabe et al, 2002). In order to test a large number of genes, ChIp-on-chip assays were carried out which demonstrated 746 (20,000 tested) gene promoters enriched by hPTTG1 antibody, suggesting a role for hPTTG1 as a transcription factor involved with a wide range of cellular processes (Tong et al, 2007).

1.2.5: Regulation of PTTG

The regulation of hPTTG1 expression has not been fully elucidated. mRNA expression has been shown to be regulated by both estrogen (Heaney et al, 1999) and TSH. Increased levels of calcium facilitated rapid and sustained

expression of *hPTTG1* in testicular cancer cells (Tfelt-Hansen et al, 2003), although this effect was cell-type specific. mRNA transcription is regulated by growth factors such as IGF-1 via phosphotidylinositol 3-kinase (PI3K) and MAP-kinase (MAPK) signaling (Chamaon et al, 2005). Other growth factors, for example Epidermal growth factor (EGF), Transforming growth factor-α (TGFα) and Hepatocyte growth factor (HGF) have been shown to induce *hPTTG1* mRNA expression in U87 astrocytoma cells (Tfelt-Hansen et al, 2004). Recent research by our own group has shown that hPTTG1 is regulated by growth factors EGF and TGF-α, in TPC1 and K1 thyroid papillary cancer cell lines and in human primary thyrocytes (Ryan et al, 2013). Transcription factors, including nuclear factor-γ and Sp1 (Specificity protein 1), are important for basal transcription activity of the *hPTTG1* promoter (Clem et al, 2003).

1.2.6: PTTG expression

Studies of rat *Pttg1* mRNA expression initially found expression only in adult testis and embryonic liver (Pei and Melmed, 1997). However, further studies on mouse tissue showed expression of mouse *Pttg1* in the thymus, spleen, testis and ovary (Wang and Melmed, 2000).

In normal adult human tissue, expression has been observed in the testis, thymus, colon, small intestine, placenta and spleen (Zhang et al, 1999).

After the initial finding of high hPTTG1 expression in pituitary adenomas (Pei and Melmed, 1997), various human tumours have been shown to contain high hPTTG1 expression, including thyroid (Boelaert et al, 2003) (Heaney et al, 2001) (Zatelli et al, 2010), ovary (Puri et al, 2001), breast (Puri et al, 2001), liver (Cho-Rok et al, 2006), colon (Heaney et al, 2000), lung (Rehfeld et al, 2006) and oesophagus (Shibata et al, 2002) tumours.

hPTTG1 is also expressed highly in many human cancer cell lines (Lee et al, 1999).

1.2.7: PTTG expression in thyroid cancer

Several studies have reported increased expression of hPTTG1 in thyroid cancer compared to normal thyroid tissue. Our group and others have shown increased mRNA expression in thyroid tumours compared to normal thyroid tissue (Heaney et al, 2001) (Boelaert et al, 2003) (Zatelli et al, 2010), with non-significant increases in multinodular goitres and Graves' disease samples (Boelaert et al, 2003), as shown in Figure 1.2.3. Importantly, expression of proliferating cell nuclear antigen (PCNA), a standard indicator of cellular proliferation, was unchanged, suggesting changes seen were not as a result of a change in cellular proliferation.

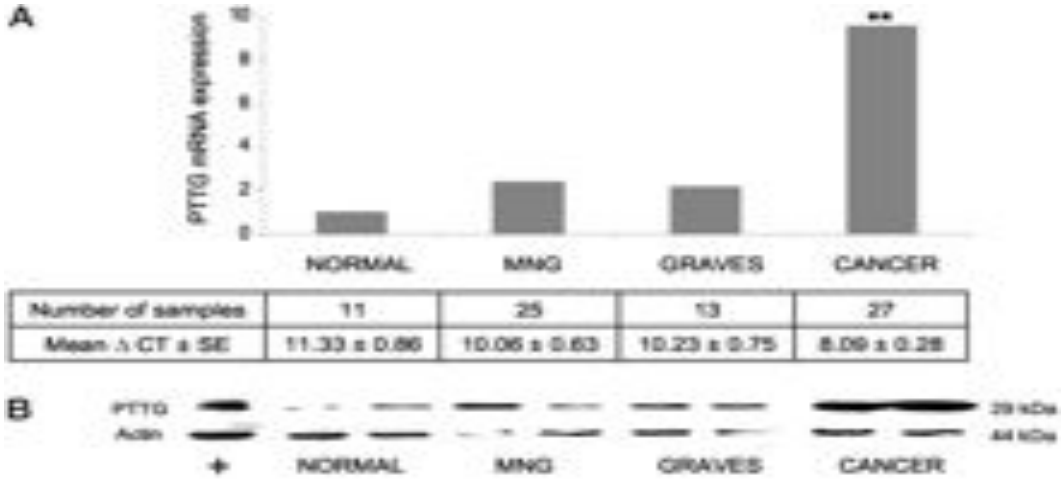

Figure 1.2.3: hPTTG1 overexpression in differentiated thyroid cancer. ***(A)*** *qPCR results of hPTTG1 mRNA expression in normal specimens compared to multi-nodular goitre, Graves' disease and thyroid cancer specimens, showing significant increases in hPTTG1 mRNA expression in cancer samples compared to normal.* ***(B)*** *Western blot analysis of two representative normal samples compared to multi-nodular goitre, graves disease and thyroid cancer samples. Results show significantly increased* hPTTG1 *protein expression in thyroid cancer samples compared to normal. Positive control used was JEG-3 choriocarcinoma cells. ** = p<0.01. (Taken from Boelaert et al, 2003).*

1.2.8: Role of PTTG in tumourigenesis

1.2.8.1: Initiation

It would seem obvious that hPTTG1s role as a securin forms the basis for its tumourigenic effect, and that high hPTTG1 expression inhibits cellular proliferation. Thus far, hPTTG1s effect on cellular proliferation has proved elusive. Stable transfection of HeLa and A549 cells with hPTTG1 resulted in reduced proliferation (Mu et al, 2003), and this was also observed in JEG-3 and H1299 cells transiently transfected with hPTTG1. However, HEK293

cells stably transfected with hPTTG1 showed increased cellular proliferation (Hamid et al, 2005). These differences may be due to differences in cell type, although results in NT2 neuronal cells suggest that relatively low overexpression of hPTTG1 (~1.7-fold) stimulated cellular proliferation, whereas high overexpression (~6-fold) resulted in reduced cellular proliferation (Boelaert et al, 2003). The phosphorylation of hPTTG1 has also been implicated in its proliferative effect. NIH3T3 cells with stably overexpressed hPTTG1 mutants which either prevented, or had constitutive phosphorylation of hPTTG1, showed increased and reduced cellular proliferation respectively (Boelaert et al, 2004). These results indicate hPTTG1s effect on cellular proliferation is complex, possibly pertaining to its cell type specificity, level of overexpression and phosphorylation status.

Chromosomal instability and aneuploidy have also been implicated in hPTTG1 mediated transformation. Indeed, aneuploidy has been shown to occur frequently in thyroid carcinomas (56%) (Joensuu et al, 1986). MG-63 osteosarcoma cells and H1299 lung cancer cells showed aneuploidy when either transiently or stably transfected with hPTTG1 (Yu et al, 2000). Live cell imaging of H1299 cells showed that hPTTG1 transfection blocked the transition from metaphase to anaphase, and cells with high levels of hPTTG1 were unable to degrade hPTTG1, resulting in chromosomal instability (Yu et al, 2003). The inactivation of hPTTG1 can also result in chromosomal instability, as demonstrated in HCT116 cells, where hPTTG1 inactivation resulted in chromosome loss (Jallepalli et al, 2001). However, hPTTG1-null HCT116 cells were chromosomally normal, and showing no signs of

aneuploidy, suggesting there may be compensatory mechanisms available to prevent instability from occurring (Pfleghaar et al, 2005).

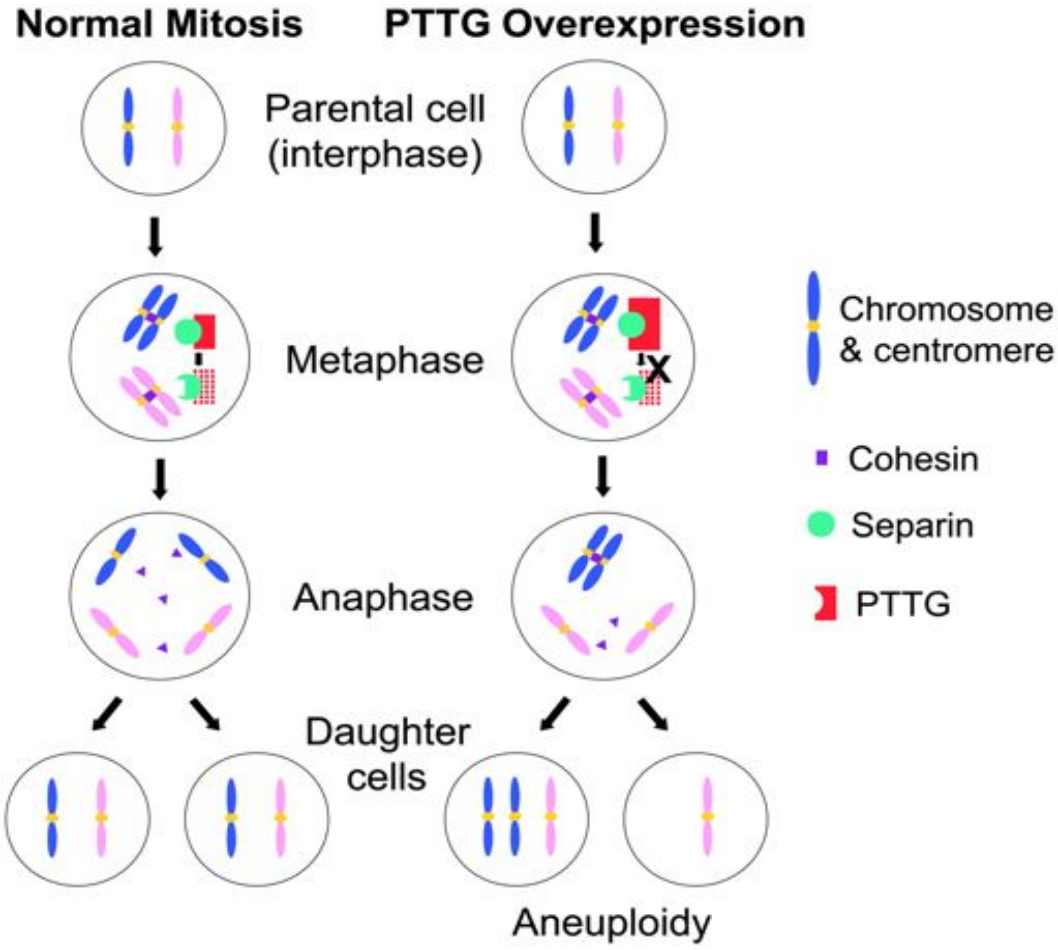

Figure 1.2.4: Normal mitosis and PTTG overexpression. Left path represents normal mitosis. hPTTG1 inhibits separin activity, while cohesin maintains sister chromatid joining. At the metaphase-anaphase transition hPTTG1 is degraded by APC, releasing separin and allowing cleavage of cohesin, releasing sister chromatids to separate equally to daughter cells. Right path represents dysregulated mitosis. Overexpression of hPTTG1 leads to dysregulation of metaphase-anaphase transition, potentially leading to aneuploidy. (Taken from Yu et al, 2003).

Similar to conflicting findings in studies investigating hPTTG1 effects on cellular proliferation, the effects of hPTTG1 on apoptosis also remain inconclusive. JEG-3 cells demonstrated increased apoptosis following overexpression of hPTTG1 (Yu et al, 2000), and studies utilising wild-type p53 MCF7 cells and p53-null MG-63 cells found hPTTG1 to be involved in both p53-dependent and p53-independent apoptosis (Yu et al, 2000). Interactions between p53 and hPTTG1 have been demonstrated *in vitro* and *in vivo*, with hPTTG1 binding p53 and blocking its transcriptional activity, resulting in reduced transcription of p53-induced genes (Bernal et al, 2002). Research into the effect of p53 on hPTTG1 found p53 is capable of transcriptionally repressing hPTTG1 following DNA damage, and also that p53 activation alone is able to suppress hPTTG1 expression by interfering with binding of the transcription factor NF-γ to the hPTTG1 promoter (Zhou et al, 2003). As with the findings of cellular proliferation effects, results from experiments investigating hPTTG1 effects on apoptosis may be dependent upon levels of hPTTG1 or may be cell-type specific. It has been suggested that the apoptosis caused by hPTTG1 is possibly a response to the induced aneuploidy.

Genetic instability facilitated by hPTTG1 is another mechanism of hPTTG1 induced cell transformation. Genetic instability is highly variable in thyroid tumours and this variability correlates with hPTTG1 expression (Kim et al, 2005). Importantly, both over- and underexpression of hPTTG1 results in genetic instability. These studies indicate that hPTTG1 is involved in a

variety of potential methods of cellular transformation, although the full role of hPTTG1 in the initiation of tumourigenesis has yet to be fully elucidated.

1.2.8.2: Progression

In respect to promoting tumour growth, hPTTG1 has been shown to induce expression of various growth factors, such as FGF-2 (Zhang et al, 1999) and VEGF (McCabe et al, 2002). High hPTTG1 expression induced expression of the pro-angiogenic factor inhibitor of DNA binding-3 (ID3) and downregulated the expression of the anti-angiogenic factor thrombospondin-1 (TSP-1) (Kim et al, 2006). These findings demonstrate a role for hPTTG1 in angiogenesis, dysregulation of which can be a major contributor to the tumourigenic process. Further research has indicated that hPTTG1 expression may be upregulated by growth factors, including IGF-1, EGF and TGF-α in human papillary cancer cell lines and human primary thyrocytes. Abrogation of hPTTG1 induction was observed when using inhibitors of MAPK and PI3-K signaling, thereby implicating these pathways in hPTTG1 regulation (Ryan et al, 2013). The association with growth factors indictates that hPTTG1 acts as an autocrine/paracrine growth factor activator, with a feedback loop occurring in which these growth factors serve to reinforce hPTTG1 expression, thereby stimulating tumour growth.

1.2.9: PTTG overexpressing mouse models

The effects of hPTTG1 overexpression have been tested using mouse models in several studies to date. Firstly, hPTTG1 overexpression was targeted to the mouse pituitary using the α subunit of the glycoprotein hormone (α-GSU) promoter. Gender specific differences were evident upon investigation. Female transgenic mice exhibited enlarged pituitary glands with elevated serum IGF-1 (Insulin-like growth factor 1) levels when compared to wild-type mice. Male transgenic mice presented with LH (Luteinizing hormone), TSH and GH (Growth hormone) cell hyperplasia and adenoma. This was associated with increased serum LH, GH, IGF-1 and testosterone levels. Pituitary glands were found to be large and irregularly shaped, and these findings provide evidence for a role for hPTTG1 in hyperplasia of the pituitary gland and a potential initiating step in pituitary tumourigenesis (Abbud et al, 2005). Another study has investigated the effect of hPTTG1 overexpression on the mouse ovary. The MISIIR gene promoter was used to ensure ovarian specific overexpression. Ovarian tumours were not evident in transgenic mice, although mice were reported to present with increased mass of the corpus luteum, generalised hypertrophy of the myometrium uteri, cystic glandular and endometrium hyperplasia (El-Naggar et al, 2007). Following this, research was conducted using the CMV (Cytomegalovirus) promoter in place of the MISIIR promoter to facilitate greater transgene expression. Results showed ovarian tumour formation at 8 months and 10 months of age in 17% of mice, and it has been proposed that this was due to

increased secretion of bFGF, which has previously been demonstrated to increase ovarian cancer invasion and promote tumour progression (Li and Jiang, 2010). These mice were subsequently crossed with *Tp53* +/- mutant mice, resulting in an increase in the percentage of tumours formed, and a reduction in the time of tumour formation, although there was no increase in ovarian cancer formation, demonstrating hPTTG1's effects to be independent of p53 (Fong et al, 2012). This study highlighted the ability of hPTTG1 to induce hyperplasia, and to potentially act as a pre-tumourigenic initiating event.

1.2.10: *Pttg1*-null mouse model

Contrary to results in both yeast (Pds1p) and *Drosophila* (Securin), where loss of the gene homologous to *hPTTG1* resulted in lethality (Stratmann et al, 1996) (Ciosk et al, 1998), loss of murine *Pttg1* resulted in viable offspring (Wang and Melmed, 2001). Tissue specific defects were present, such as testicular hypoplasia, thymic hyperplasia and thrombocytopenia. Pancreatic β-cell hyperplasia was also evident (Wang et al, 2003). While knockout mouse embryonic fibroblasts (MEFs) demonstrated similar cell cycle times (~30 hours) to wild-type mice, there were significant differences in the cell cycle. *Pttg1 -/-* MEFs presented with a shorter G1 phase and a longer G2 phase, an effect that was reversible with transfection of *Pttg1* (Wang and Melmed, 2001). MEFs from *Pttg1 -/-* mice showed chromosomal

abnormalities, such as increased aneuploidy, although these abnormalities did not appear lethal. Pituitary glands were subsequently found to be hypoplastic, presenting with reduced cellular proliferation and increased p21 expression (Chesnokova et al, 2005). It has been suggested that increased p21 expression, leading to cellular senescence, may be protective of pituitary tumour formation (Chesnokova and Melmed, 2009), however this has yet to be tested in other cell types. The tissue specific defects following *Pttg1* deletion suggest that this oncogene has cell type specific functions. The murine *Pttg1* knockout shows a viable phenotype which, given the crucial role of Pttg1 action as a securin, suggests there are compensatory mechanisms in order to prevent instances of chromosomal instability, although the precise nature of these mechanisms has yet to be fully investigated.

1.3.1: p53 the tumour suppressor

1.3.2: Mislabelling p53 as an oncogene

Oncogenes were first discovered following research into tumour viruses in the 1970s. Investigations into RNA tumour viruses found overexpression of genes adjacent to the integration sites of retroviruses, resulting in cellular transformation. This lead to the unearthing of many different oncogenes, although for a long time it was believed that tumour viruses were the cause

of tumour formation. In 1979, research using the SV40 DNA tumour virus found a cellular protein immunoprecipitated with the viral protein, which possessed a molecular mass of approximately 53 kDa. This was discovered by several groups simultaneously (Lane and Crawford, 1979) (Linzer and Levine, 1979) (Kress et al, 1979) (Melero et al, 1979), and the cellular protein was named p53. Subsequently it was found that p53 was overexpressed by other tumour viruses, such as the Abelson murine leukaemia virus (Rotter et al, 1980). Further findings demonstrated overexpression of this protein in different cancer cells, with a lack of detection in non-transformed cells, seemingly confirming suspicions of p53 as a cellular oncogene. To further characterise p53, several groups cloned its gene (*Tp53)*, although notably these clones were produced from cancer cells. Experiments subsequently suggested p53 was able to transform primary cells *in vitro*, cooperating with other recognised cellular oncogenes (Eliyahu et al, 1984) (Parada et al, 1984).

1.3.3: Identification of p53 as a tumour suppressor

Throughout the 1980s further experiments were conducted to better examine the role of p53 as an oncogene. However, it became apparent that p53 clones used in previous experiments were mutated and this was responsible for its transforming ability, with wild-type p53 unable to transform cells (Finlay et al, 1988). Following this, it was found that p53 was

inactivated or mutated in a number of different cancer clonal populations, suggesting instead that p53 acted as a tumour suppressor (Baker et al, 1989). Confirmation of this came from experiments performed using wild-type p53, which demonstrated repression of cellular transformation following overexpression of p53 (Eliyahu et al, 1989) (Finlay et al, 1989). Therefore, p53 was identified as a true tumour suppressor.

1.3.4: The structure of p53

p53 is a 393 amino-acid protein with a molecular mass of 43.7 kDa, which runs at 53 kDa on a protein gel due to its proline-rich region, to which it owes its name. Its amino-terminus contains two activation domains (AD), the first from residues 1-42 and the second from 43-92, which are involved in regulation of various genes. Both AD1 and AD2 are able to interact with histone acetyltransferases and with the basal transcription machinery (Candau et al, 1997). Experiments using p53 mutants also found AD1 and AD2 were capable of promoting transcription of different subsets of genes independently (Zhu et al, 1998).

Figure 1.3.1: Schematic diagram of p53 *protein structure. At the N-terminus an activation domain 1 (AD1) exists at residues 1-42. Activation domain 2 exists at residues 43-92 and contains a proline-rich domain (PRD). The DNA-binding domain (DBD) is present at residues 101-300, which is responsible for* p53 *binding to DNA. A nuclear-localisation signal (NLS) exists at 305-322, while a tetramerisation domain (TD) is present at residues 326-356, which is responsible for oligomerisation of* p53. *At the C-terminus is a negative regulation domain (NEG), from residues 364-393. Nuclear exclusion signal (NES) domains are present at residues 11-27 and 340-351.*

The DNA binding domain (DBD) of p53 is present from residues 101-300. It contains four highly conserved regions (Harms and Chen, 2006), which operate a critical role in binding of p53 to consensus sequences of downstream genes (Olivier et al, 2002). The ability of p53 to function as a tumour suppressor seems dependent upon the DBD, as greater than 80% of the mutations found in p53 in human tumours are present in the DBD (Olivier et al, 2002).

In order for p53 to bind to its consensus sequences with a high affinity, it requires oligomerisation to form a homo-tetramer, which is maintained through its hydrophobic core produced by its helix:helix interaction (Mateu and Fersht, 1998).

p53 exists as both a cytoplasmic and nuclear protein, shuttling to the nucleus to act as a transcription factor, and exerting other effects in the cytoplasm, such as interactions with mitochondrial proteins to facilitate

apoptosis. Due to its size, tetrameric p53 is not capable of entering the nucleus, and so requires a nuclear localisation signal (NLS) (residues 305-322) and two nuclear export signals, located at the C-terminus and N-terminus (Scoumanne et al, 2005) (Viadiu et al, 2008). Mutations of the NLS or NES are relatively rare, however p53 subcellular localisation is regularly altered in cancers due to changes in post-translational modifications of p53 (Liang and Clarke, 1999).

The regulatory domain is located at the C-terminus, present at amino acid residues 364-393. It has been labelled as a negative regulation domain, and is a site of post-translational modifications such as phosphorylation, acetylation, methylation, neddylation (conjugation of NEDD8 to target proteins) and Sumoylation (conjugation of small ubiquitin modifier proteins to target proteins) (Liu and Kulesz-Martin, 2006) (Gostissa et al, 1999) (Gu and Roeder, 1997). This is also the site of ubiquitination of p53, which is primarily regulated by MDM2, which will be covered in more depth later in this chapter.

1.3.5: Biological activities of p53

p53 has been shown to possess numerous biological activities, although its role as a tumour suppressor is most widely recognised. p53, as a transcription factor, has been demonstrated to facilitate the transcription of numerous target genes involved in the DNA damage response (Vogelstein et

al, 2000). Direct transcriptional control of the cyclin dependent kinase inhibitor p21 is activated by p53 and this process facilitates cell cycle arrest (El-Deiry, 1997), which can potentially lead to cellular senescence. Transcriptional activation of many pro-apoptotic genes has also been demonstrated. Indeed, p53 can induce apoptosis via the mitochondrial route, such as by induction of pro-apoptotic genes *BAX* (Bcl-2-associated X protein) (Miyashita and Reed, 1995) and *PUMA* (p53 upregulated modulator of apoptosis) (Nakano and Vousden, 2001), which leads to the release of cytochrome C from mitochondria and activation of APAF-1 (Apoptotic protease activating factor 1) (Green and Reed, 1998), or via the death receptor route (Vousden, 2000), such as *FAS* (Lin and Benchimol, 2000). p53 has also been shown to act as a transcriptional repressor via its interaction with histone deacetylase proteins, enzymes which remove acetyl groups from histones and allow tighter histone binding to DNA (Murphy et al, 1999).

1.3.6: Regulation of p53

As p53 has been shown to possess potent tumour suppressor activities, it is evident that p53 requires tight regulation, and in normal cells is kept at relatively low levels. It has been demonstrated that p53 is regulated transcriptionally and post-transcriptionally. It is also regulated post-translationally, via its subcellular localisation, activity and stability (Woods and Vousden, 2001). Transcriptional regulation is achieved via transcription

factors such as NF-κB (Nuclear factor kappa-light-chain-enhancer of activated B cells) (Webster and Perkins, 1999) and HOXA5 (Raman et al, 2000). However, the primary control of p53 takes place at the protein level. Subcellular localisation is an important control for p53 function, as the protein is required to be present in the nucleus to facilitate transcription of downstream genes. This is achieved through use of the NLS and NES sequences present on the p53 protein, which allow p53 to be transported to the nucleus to potentiate activation, while p53 is shuttled to the cytoplasm for interactions with the mitochondria and to enable degradation via the proteasome (Freedman and Levine, 1998). However, the main regulation of p53 is determined by MDM2 (Mouse double minute 2), a protein with an intimate relationship with p53, which will be closely described later in this chapter.

1.3.7: p53 in thyroid cancer

Mutations in the p53 gene are the most frequent in all human cancers, being present in approximately 50% of human tumours sequenced. However, as shown in Figure 1.3.3, only 11.3% of human thyroid cancers show any form of p53 mutation (Olivier et al, 2002). The vast majority of well-differentiated thyroid carcinomas show no sign of p53 mutation, while anaplastic thyroid carcinomas present with a high frequency (67-88%) of p53 mutations (Kondo et al, 2006) (Smallridge et al, 2009). This suggests p53 is not

involved in early thyroid tumourigenesis, but is important in progression to aggressive thyroid cancer. Indeed, inactivation, rather than mutation, of p53 has been implicated in well-differentiated thyroid cancer. Mechanisms for this appear to include retention of p53 in the cytoplasm (Zedenius et al, 1996) and MDM2 overexpression in papillary thyroid carcinoma (Jennings et al, 1995).

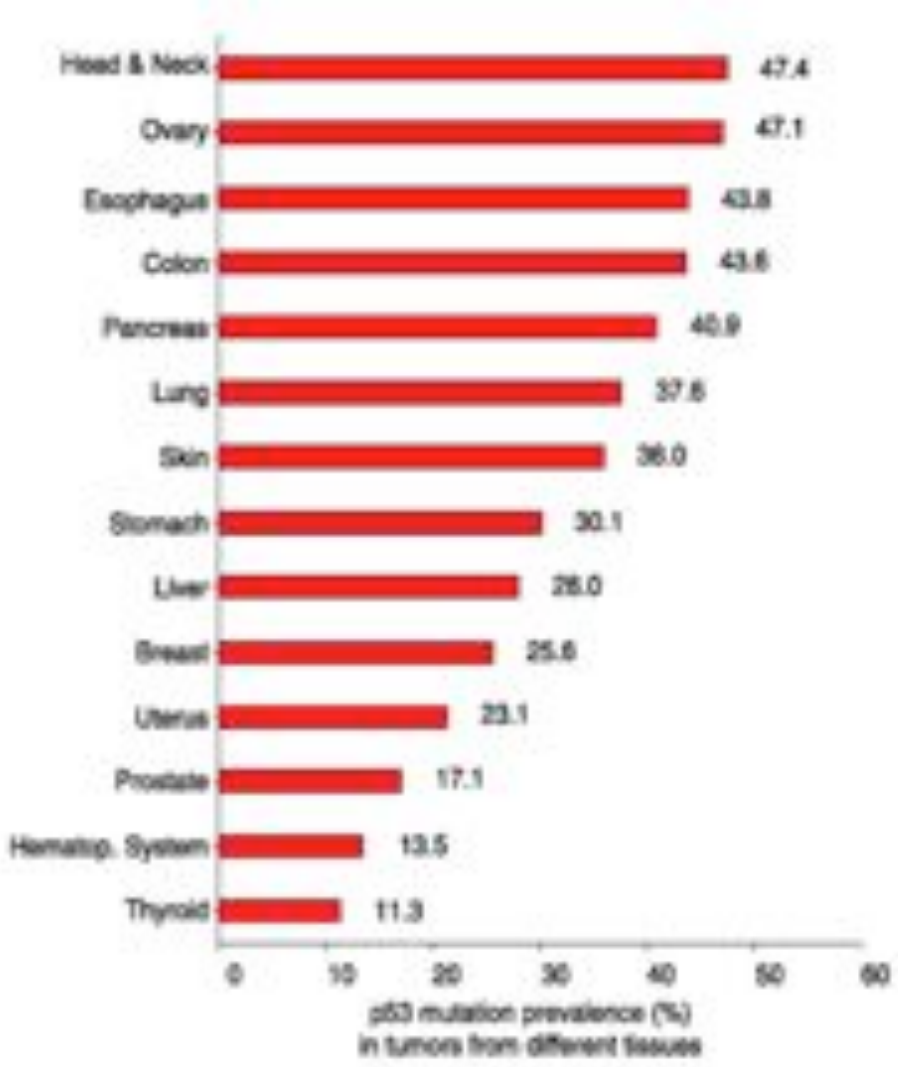

Figure 1.3.3: p53 mutation prevalence in tumours from different tissues. Thyroid cancer shows an 11.3% p53 mutation prevalence (Taken from Malaguarnera et al, 2007).

1.4.1: MDM2, the master p53 regulator

1.4.2: Identification and structure of MDM2

The *MDM2* gene was originally identified using double-minute chromsomes, which are small fragments of extrachromosomal DNA frequently found in tumours and formed from gene amplifications (Barker, 1982), in transformed mouse fibroblasts (Cahilly-Snyder et al, 1987) (Fakharzadeh et al, 1991). Investigations into the role of MDM2 revealed knockout of *MDM2* in mice resulted in embryonic lethality, later demonstrated to be caused by apoptosis (Jones et al, 1995) (Montes de Oca Luna et al, 1995). Its relationship with p53 was revealed as knockout of *p53* resulted in the rescue of the embryonic lethality caused by loss of *MDM2*, suggesting constitutive activation of p53 following deletion of *MDM2* (de Rozieres et al, 2000).

MDM2 is a 491 amino acid protein and contains several functional domains (Figure 1.4.1). The N-terminus contains the main binding site for p53, while the central acidic and zinc-finger domains are binding sites for a number of different proteins. The C-terminal ring-finger domain is the origin of the E3 ubiquitin ligase activity of MDM2, and is also the site of binding to a closely related protein named MDMX, which is structurally similar to MDM2 and can inhibit the transcriptional activity of p53 and has also been shown to inhibit the degradation of MDM2 (Tanimura et al, 1999).

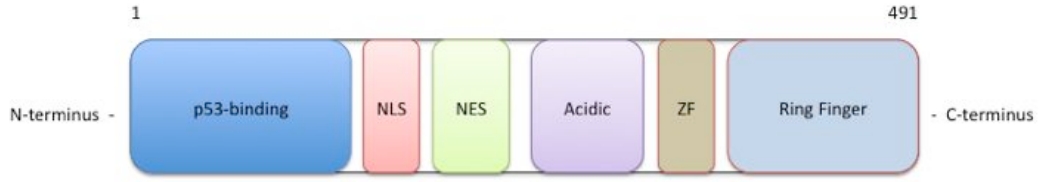

Figure 1.4.1: Structure of MDM2 *protein. The N-terminus contains a p53-binding domain, a nuclear localisation signal (NLS) and a nuclear export signal (NES). The C-terminus contains a ring-finger domain and a zinc finger domain (ZF). An acidic region is also present.*

1.4.3: The p53-MDM2 regulatory loop

MDM2 and p53 are the main constituents of an autoregulatory feedback loop designed to keep levels of p53 low in unstressed cells, but able to rapidly facilitate increased levels following DNA damage. As a transcription factor, p53 induces transcription of *MDM2* by binding to two p53 consensus sequences present on the *MDM2* gene (Barak et al, 1993) (Perry et al, 1993). MDM2 is subsequently able, via its E3 ligase activity, to ubiquitinate p53, tagging p53 for degradation by the proteasome (Haupt et al, 1997) (Honda et al, 1997). This is achieved through a cluster of lysine residues located within the C-terminus of p53 (Rodriguez et al, 2000). As p53 is degraded, protein levels decrease, which results in a reduction of *MDM2* transcription and thereby a decrease in p53 degradation. This negative feedback loop serves to keep levels of p53 low in unstressed cells. A second method of p53 inhibition

by MDM2 is via binding to the N-terminal transactivation domain of p53, thereby inhibiting induction of downstream genes by p53 (Momand et al, 1992) (Oliner et al, 1993).

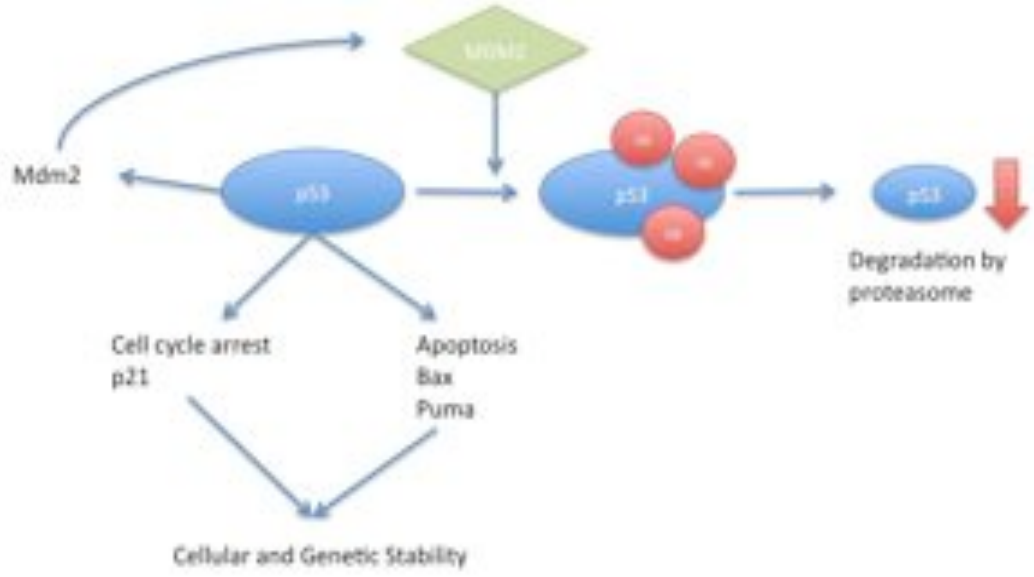

Figure 1.4.2: The p53-MDM2 *autoregulatory negative feedback loop*. p53 *induces transcription of MDM2 which ubiquitinates* p53 *leading to its degradation by the proteasome. Ub=ubiquitin protein.*

The MDM2-mediated p53 ubiquitination requires formation of protein complexes containing several MDM2 and p53 proteins, following attachment of C-terminal MDM2 to the ring-finger domain of another MDM2 protein (Poyurovsky et al, 2007) (Kostic et al, 2006). Degradation of p53 by the 26S

proteasome subsequently requires formation of a polyubiquitin chain composed of at least four ubiquitin molecules (Thrower et al, 2000). Ubiquitination results in exposure of the C-terminal NES, required for nuclear export, and dissociation of MDM2 from the p53 protein (Carter et al, 2007).

MDM2 has also been shown to mediate monoubiquitination of p53, and investigations have previously shown high levels of MDM2 to cause polyubiquitination and degradation, whereas low expression of MDM2 can result in monoubiquitination and a variety of cellular effects (Li et al, 2003). An example of this is monoubiquitination has been shown to cause nuclear export of p53, and be important in transcription-independent activities of p53 such as interacting with mitochondrial proteins in order to facilitate apoptosis (Mihara et al, 2003) (Chipuk et al, 2004). Indeed, as MDM2 is expressed at low levels in unstressed cells, where it preferentially monoubiquitinates p53, it is possible that MDM2-mediated polyubiquitination of p53 is more likely to act upon cells where p53 is stabilised due to DNA damage, returning p53 levels to previous unstressed levels.

MDM2 is considered the primary regulator of p53 degradation, however investigations have discovered other regulatory proteins. Pirh2 can promote MDM2-independent ubiquitination (Leng et al, 2003), while COP1 has also been revealed to function as an ubiquitin ligase affecting p53 (Dornan et al, 2004). The E2 ligase RAD6 has also been shown to possess an important role in the regulation of p53 (Jentsch et al, 1987). RAD6 has previously been shown to be involved in DNA damage repair by catalysing

the ubiquitination of several proteins involved in the DNA damage response (Hoege et al, 2002) (Kim et al, 2009). Overexpression of RAD6 led to a reduced half-life of the p53 protein, and it has been shown to be capable of forming a ternary complex with MDM2 and p53 in order to promote degradation of p53. Results also revealed MDM2-mediated degradation of p53 required RAD6 in HL7702 liver cells (Chen et al, 2012). The research describing Pirh2, COP1 and RAD6 demonstrates MDM2 is not alone in affecting p53 degradation, and, as p53 is an important protein, there would be expected redundancies.

Other methods of p53 regulation by MDM2 have been demonstrated, such as interacting directly with p53 mRNA and preventing its translation (Candeias et al, 2008). Also, by regulating degradation of RPL26 (a ribosomal protein), through ubiquitination, MDM2 can regulate p53 as RPL26 has been shown to participate in the regulation of p53 translation (Takagi et al, 2005) (Ofir-Rosenfeld et al, 2008).

1.4.4: Inhibition of p53-MDM2 interaction

In order for p53 to be activated in response to DNA damage, its interaction with MDM2 needs to be suppressed to allow increased expression of p53 to occur and generate the DNA damage response, leading to cell cycle arrest or apoptosis. This is primarily achieved through stabilisation of p53 by inhibition of its interaction with MDM2. Indeed, a large body of recent

research has focused on disrupting the p53-MDM2 interaction through the use of small molecule inhibitors and a number have been identified, including the inhibitor Nutlin-3 (Vassilev et al, 2004).

Numerous proteins have been demonstrated to act upon p53 and MDM2 to inhibit their interaction and facilitate activation of p53. Upon oncogene activation, ARF, an alternative reading frame of the CDKN2A locus, is increased transcriptionally and stimulates growth arrest by activating p53. This is achieved by binding of ARF to the central acidic domain of MDM2 and inhibiting its interaction with p53 (Sherr, 2001) (Kamijo et al 1998) (Pomerantz et al, 1998). Inhibition of ubiquitination by acetylation of the same lysine residues can also occur by CBP/p300, transcriptional co-activating proteins, limiting ubiquitination and stabilising p53 levels (Li et al, 2002). Additionally, MDM2 is also the subject of acetylation, with the Ring-finger domain acetylated and causing inactivation of MDM2 (Wang et al, 2004). Phosphorylation has also been shown to be a key factor in p53 regulation by MDM2. Phosphorylation of serines 15 and 20 at the N-terminal region of p53, following DNA damage, can cause inhibition of the interaction with MDM2 (Prives and Hall, 1999), while phosphorylation of MDM2 at serine 395 can also inhibit the interaction (Maya et al, 2001). Other post-translational modifications have also been implicated in regulation of the p53-MDM2 interaction, including Sumoylation, neddylation and methylation (Rodriguez et al, 1999) (Xirodimas et al, 2004) (Chuikov et al, 2004).

MDM2 stability has been shown to play a role in p53 regulation. As opposed to ubiquitinating p53, MDM2 possesses the capability to

ubiquitinate itself, and several DNA damage kinases have been demonstrated to facilitate increased self-ubiquitination, and subsequent degradation of MDM2 (Chang et al, 1998) (Stommel and Wahl, 2004).

The cellular localisation of MDM2 has also been the subject of research into its interaction with p53. As mentioned previously, ARF has a role in this process, and has been demonstrated to sequester MDM2 to the nucleoli as a means of stabilising and activating p53 (Weber et al, 1999). The protein PML (Promyelocytic leukemia protein), a phosphoprotein which localises to nuclear bodies and functions as a transcription factor and tumour suppressor, has also been found to interact with MDM2 and cause sequestration of MDM2 to the nucleolus (Wei et al, 2003) (Bernardi et al, 2004).

1.4.5: p53-independent functions of MDM2

It is widely accepted that the primary role of MDM2 is regulation of p53, however MDM2 has been to shown to possess a variety of other effects. MDM2 is capable of ubiquitinating histone proteins H2A and H2B (Minsky and Oren, 2004), implicated in transcriptional repression. MDM2 has also been demonstrated to bind to the mRNA of the anti-apoptotic protein XIAP (X-linked inhibitor of apoptosis protein), which has the effect of enhancing its translation (Gu et al, 2009). Another protein that is regulated by MDM2 is E-cadherin, crucial in the epithelial to mesenchymal transition important in

tumour formation, which is targeted for degradation, via the 26S proteasome, by MDM2 (Yang et al, 2006). Other interacting factors of MDM2 are shown in figure 1.4.3.

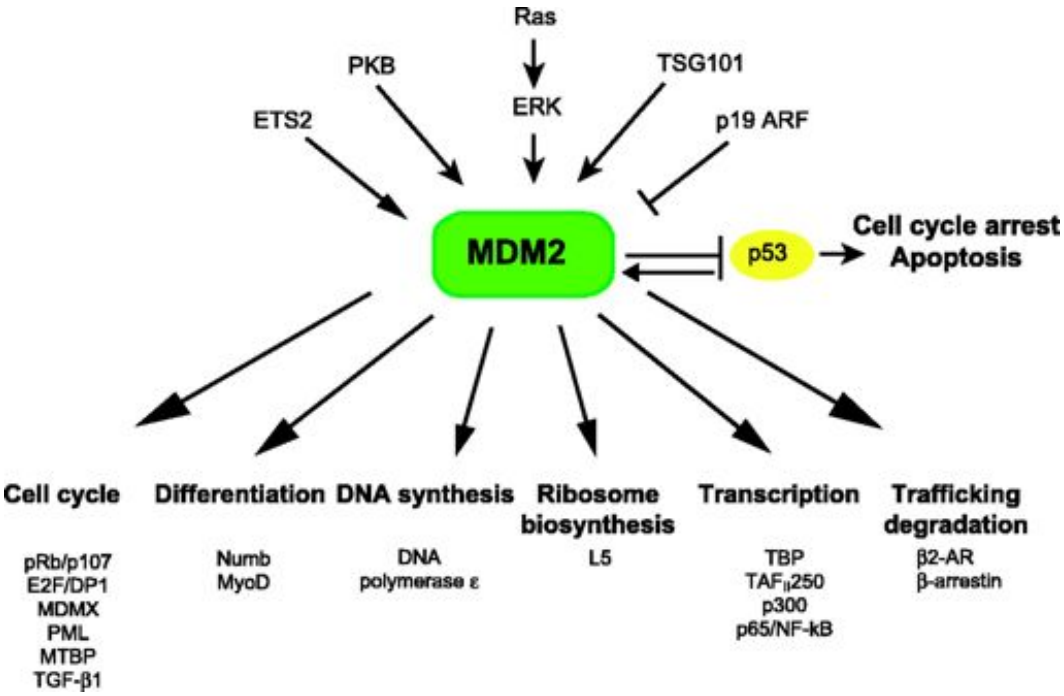

Figure 1.4.3: Schematic diagram showing identified MDM2 interacting factors. Arrows above MDM2 show factors that increase MDM2 expression. Blocked arrows above MDM2 show factors that reduce MDM2 expression (Ganguli and Wasylyk, 2003).

1.4.6: MDM2 in thyroid cancer

The role of MDM2 in thyroid cancer development is controversial. Overexpression of MDM2 has been reported in several tumour types, such as

in 6.7% of brain tumours, 5.9% of breast carcinomas and 20% of soft tissue tumours (Momand et al, 1998). Testing of MDM2 expression in thyroid carcinomas by Zou et al found a 2-3-fold increase in expression in 4 of 20 thyroid carcinomas. However, the 4 carcinomas all demonstrated a p53 mutation, which could result in increased MDM2 expression, leading investigators to conclude that MDM2 does not play a significant role in the development and progression of thyroid carcinoma (Zou et al, 1995). In contrast, another study found overexpression of MDM2 in 33% of papillary thyroid carcinomas, although there was no significant correlation between MDM2 expression and clinicopathologic features of aggressiveness (Horie et al, 2001). Furthermore, increased MDM2 nuclear staining was reported in 8/24 (33%) papillary thyroid carcinomas, implicating nuclear accumulation of MDM2 in papillary thyroid carcinoma development (Jennings et al, 1995).

1.5.1: Pituitary tumor-transforming gene binding factor

1.5.2: Identification and structure of PBF

The pituitary tumor-transforming gene binding factor, hereafter referred to as PBF (also known as PTTG1IP and c21orf3), was first identified through its interaction with the pituitary tumor-transforming gene. The PBF C-terminus was shown to bind to the C-terminus of hPTTG1, thereby causing increased

nuclear accumulation of hPTTG1, and required for transcription of FGF2 by hPTTG1 (Chien and Pei, 2000).

Human PBF consists of 6 exons spanning 24 Kb within chromosomal region 21q22.3. The gene corresponds to a 180 amino-acid protein which does not share any significant homology with any other known human protein, suggesting a unique function for PBF. It is well conserved across a wide range of species, and human PBF has 73% homology to mouse and 52% homology to zebrafish (Yaspo et al, 1998), suggesting it is evolutionarily important. The PBF protein contains a signal peptide at the N-terminus that is also the site of a nuclear export signal. A PSI (Plexin, semaphorin and integrin) domain exists which is followed by a transmembrane domain from residue 95 to 122. PBF also contains a nucleolus signal, while a nuclear localisation signal and a sorting signal are located at the C-terminus (Figure 1.5.1). Because of its structure, PBF has been labelled as a cell surface glycoprotein due to its signal peptide and transmembrane domain. However, its nuclear localisation signal also suggests PBF is possibly a nuclear protein, and research by our group has implicated roles for PBF at the cell surface and in the nucleus.

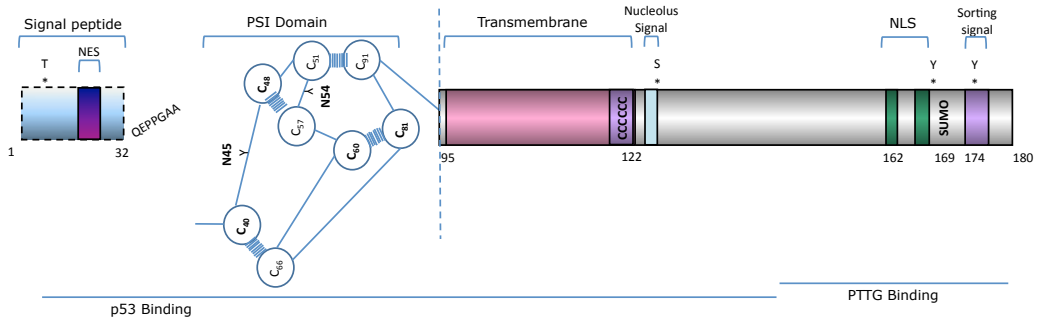

Figure 1.5.1: PBF *protein structure. The N-terminus contains a signal peptide, nuclear localisation signal (NLS) and PSI domain. The central region is the location of a transmembrane domain and nucleolus signal. The C-terminus contains a nuclear localisation signal (NLS) and a sorting signal, and is also the site of* hPTTG1 *binding. SUMO=sumoylated.*

Northern blot analysis has revealed *PBF* mRNA expression in a wide variety of normal tissue, including stomach, spleen, testis, colon and thyroid (Chien and Pei, 2000) (Yaspo et al, 1998) (Stratford et al, 2005).

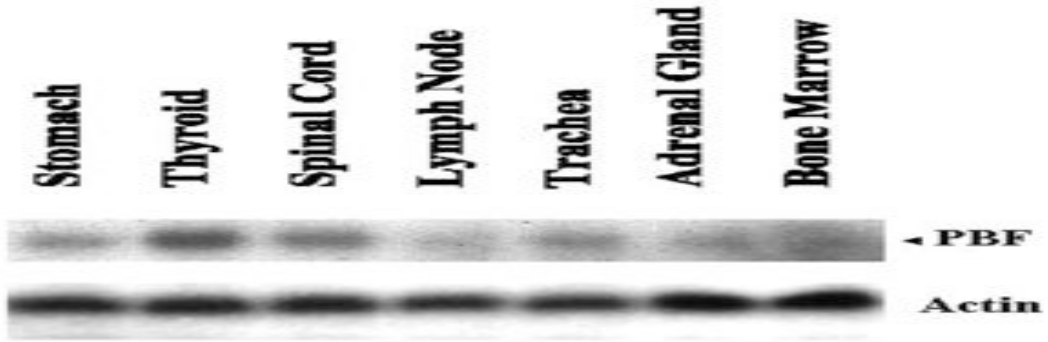

Figure 1.5.2: Northern blot showing mRNA expression of PBF in stomach, thyroid, spinal cord, lymph node, trachea, adrenal gland and bone marrow. Actin cDNA was used as a control to ensure equal loading (Taken from Chien and Pei, 2000).

1.5.3: PBF effect upon iodide uptake in thyroid cells

The sodium iodide symporter, also known as NIS, facilitates iodide uptake into thyroid cells in order to synthesise thyroid hormones. This mechanism is regularly used to deliver radioiodine to thyroid cells following surgical removal of the thyroid gland in patients with thyroid cancer. Our group has reported that PBF is able to repress NIS expression and iodide uptake via two distinct mechanisms. PBF is capable of repressing NIS mRNA expression by affecting the basal promoter activity and that of a Near Upstream Element (NUE), requiring *PAX8* and *USF1* sites present in the NUE, as PBF was unable to inhibit the NUE following mutations of *PAX8* (Paired box gene 8) and *USF1* (Upstream stimulatory factor 1) (Boelaert et al, 2007). Further investigations determined PBF is also able to bind NIS at the plasma membrane *in vitro*, and to alter its subcellular localisation by transporting it into vesicles (Smith et al, 2009). These results have shown novel effects of PBF effects upon NIS expression, localisation and subsequent iodide uptake, which have important implications for the treatment of thyroid cancer using ablative radioiodine treatment.

1.5.4: PBF in thyroid cancer

PBF overexpression has previously been found in a number of tumour types, including thyroid, colon, breast and pituitary (Stratford et al, 2005) (Watkins et al, 2010). Indeed, our group demonstrated significantly increased PBF mRNA and protein expression in papillary thyroid cancer samples compared to normal controls (Figure 1.5.3). Furthermore, PBF expression was associated with early tumour recurrence independent of known prognostic indicators (Stratford et al, 2005).

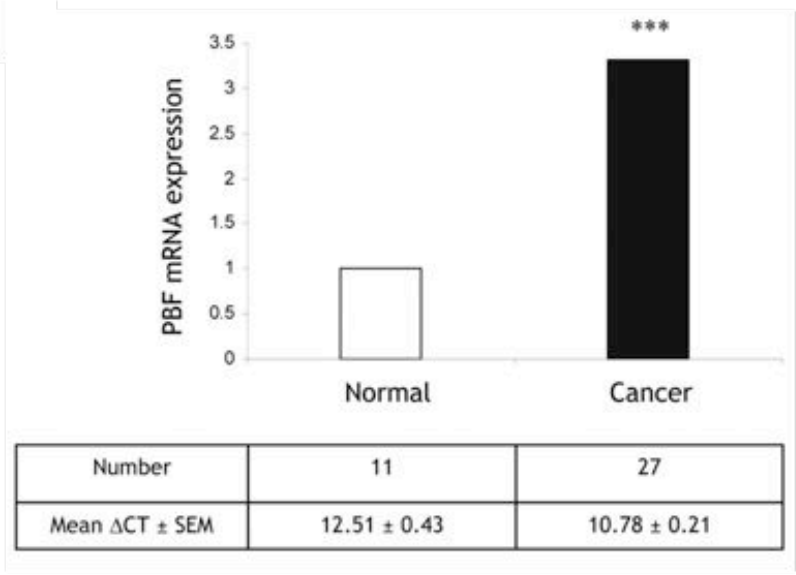

Number	11	27
Mean ΔCT ± SEM	12.51 ± 0.43	10.78 ± 0.21

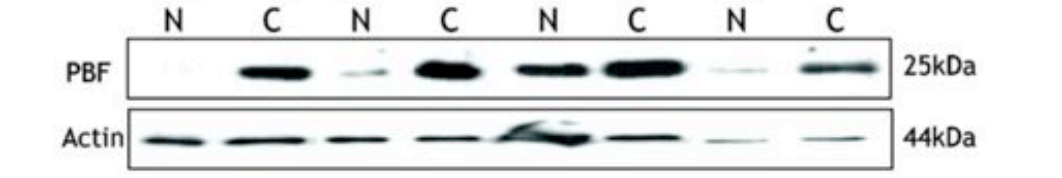

Figure 1.5.3: Significantly increased mRNA and protein expression, respectively, of PBF *in thyroid cancer samples compared to normal controls. The Western blot labels N as normal and C as thyroid cancer samples. Actin was used as a control to ensure equal protein loading (Taken from Stratford et al, 2005).*

The entire coding region of *PBF* was sequenced in 24 thyroid tumours and no mutations were found (Stratford et al, 2005), suggesting PBF overexpression is the predominating factor in thyroid cancer, rather than mutation. However, recent research has discovered 11 *PBF* mutations in a variety of human cancers, comprising 10 substitution missense mutations and 1 substitution synonomous mutation, which are documented in the *Cosmic* database (http://cancer.sanger.ac.uk/cancergenome/projects/cosmic/), although 7740 samples were tested, suggesting mutation of *PBF* is rare.

In order to determine the transforming potential of PBF *in vitro*, NIH3T3 cells were created which stably overexpressed PBF. These cells showed significant colony formation compared with vector-only cells, and subsequently nude mice were injected with NIH3T3 cells overexpressing PBF. Mice with cells overexpressing PBF showed aggressive tumour formation, indicating PBF is capable of cellular transformation *in vitro* and is tumourigenic *in vivo* (Stratford et al, 2005).

More recently, in order to determine the effect of PBF *in vivo*, a mouse model was generated possessing thyroid-specific overexpression of PBF. Although no tumour induction was found in mice aged up to 18-months, PBF transgenic mice showed 100% penetrance of significantly increased thyroid

size, comprising a significant increase in both macrofollicular and hyperplastic lesions. PBF transgenic mouse thyroids also demonstrated significantly increased TshR (TSH receptor) expression and p-Akt activation, providing a possible mechanism for the increased thyroid growth observed (Read et al, 2011).

1.5.5: Interaction of PBF with p53

Investigations into the role of PBF in tumourigenesis revealed an interaction of PBF with the tumour suppressor protein p53. GST pull-down assays showed a specific interaction of PBF with p53. Mutational studies revealed that the regions of p53 from amino acid residues 160-318 and 318-393 are required for its interaction with PBF, while mutational analysis of *PBF* demonstrated that the N-terminal region of this protein was required for p53 interaction (Figure 1.5.4).

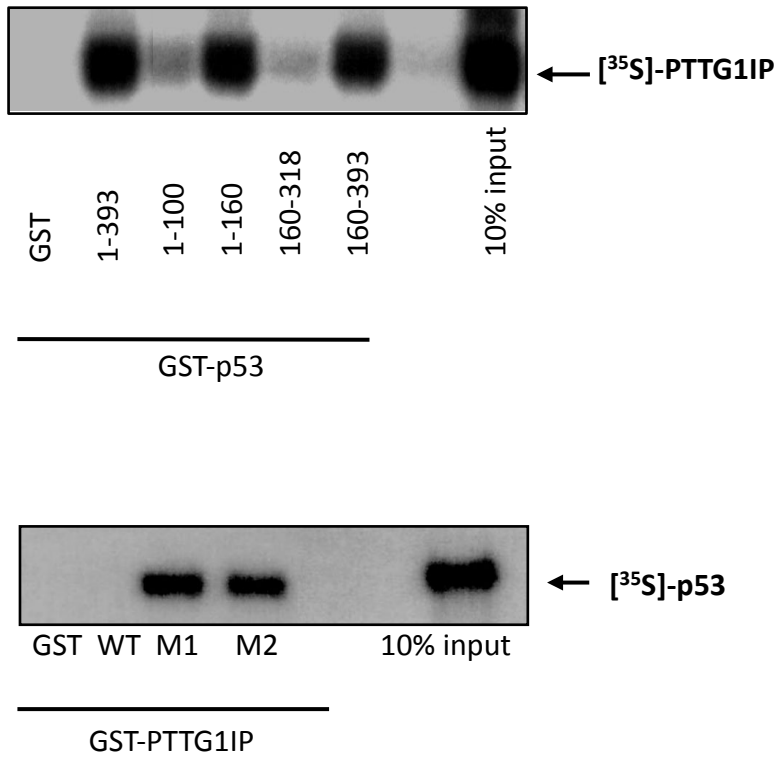

Figure 1.5.4: Specific interaction between GST tagged p53 and ^{35}S-methionine labelled PBF with inhibition of interaction using defined mutations. Interaction between GST tagged PBF and ^{35}S-methionine labelled p53 is also shown. M1=mutant 1, M2=mutant 2, 1-100=p53 with amino acids 1-100 etc (Taken from Read et al, 2013, Manuscript under revision).

Subsequently, Co-Ip (co-immunoprecipitation) assays confirmed the PBF-p53 interaction in TPC1 and K1 thyroid carcinoma cells and in HCT116 colorectal cells, suggesting the interaction is not limited to thyroid cells. Transient reporter assays revealed that p53-mediated gene regulation was affected by overexpression of PBF in H1299 cells, as, following overexpression of PBF, p53-responsive cyclin dependent kinase inhibitor

CDKN1A and *HDM2* promoter activity was repressed upon co-transfection with p53.

Further investigations into the role of PBF on p53 function revealed that PBF reduced the half-life of the p53 protein in TPC1, K1 and HCT116 cells, suggesting PBF is involved in the degradation of p53. Upon depletion of *PBF* using a specific siRNA there was an increase in the half-life of p53, providing further evidence for the role of PBF in p53 regulation. As p53 degradation is primarily achieved via ubiquitination, the proteasome inhibitor MG132, which reduces degradation of ubiquitin-tagged proteins by the proteasome, was used to analyse ubiquitination of p53. Following overexpression of PBF, p53 ubiquitination was increased (Figure 1.5.5) (Read et al, 2013, Manuscript under revision).

As increased p53 degradation may increase genetic instability, due to its role as a tumour suppressor, experiments were carried out using FISSR-PCR performed on mouse primary thyrocytes from wild-type and PBF transgenic mice to determine genetic instability. Results revealed a significant increase in genetic instability in PBF transgenic mice compared to wild-type, which correlated with the average level of genetic instability previously reported in human thyroid cancer (Kim et al, 2005). cDNA microarrays used to survey expression of DNA repair genes in mouse thyrocytes showed significant dysregulation of 17 genes, including *Xrcc2*, *Rad6* and *Tlk1* (serine/threonine-protein kinase tousled-like 1), suggesting PBF overexpression significantly affects many DNA damage repair processes.

Overall our studies have shown a potential role for PBF in the regulation of p53, however further studies are required to elucidate the complex processes underlying this.

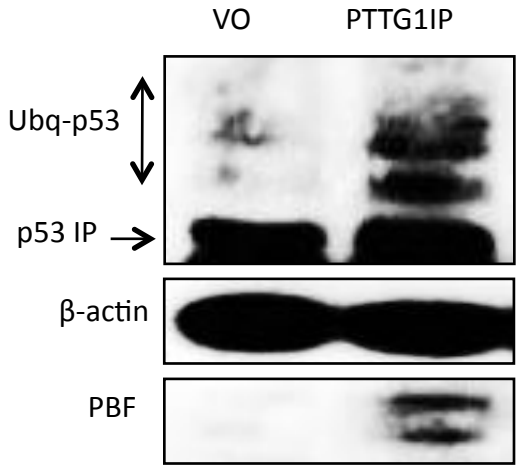

Figure 1.5.5: Ubiquitination assay of p53 following transfection with vector-only or PBF, showing increased ubiquitination of p53 with PBF overexpression. Increased ubiquitin bands for p53 are present following overexpression of PBF (Taken from Read et al, 2013, Manuscript under revision).

1.6: Hypotheses and aims

hPTTG1 is overexpressed in many cancers and plays a dual role in tumourigenesis. hPTTG1 initiates tumourigenesis through its role as the human securin, causing aneuploidy as a result of dysregulated mitosis. hPTTG1 has also been demonstrated to stimulate expression of various growth and angiogenic factors, thereby promoting transformed cell growth.

We sought to determine the effects of hPTTG1 overexpression *in vivo* through use of a transgenic mouse model of thyroid-specific overexpression of hPTTG1.

We hypothesised that hPTTG1 overexpression *in vivo* would result in hyperplasia and subsequent neoplasia of the thyroid gland. Our aim was to characterise the effect of hPTTG1 overexpression *in vivo* and to determine potential effects upon growth factor expression. We also hypothesised that stimulation of thyroid cell growth may be altered in *Pttg1* knockout mice and in hPTTG1 transgenic mice. To investigate this we employed standard methods of goitre induction using an iodine deficient diet and drugs to inhibit endogenous thyroid hormone production.

hPTTG1 interacts with p53 and approximately 50% of all cancers harbour mutations in the tumour suppressor p53. However, in thyroid cancer, p53 is rarely mutated and it is hypothesised that p53 inactivation via other mechanisms is responsible for the repression of this potent tumour suppressor. MDM2 is the primary regulator of p53 expression, causing ubiquitination of p53, and subsequent degradation, through a negative feedback loop that seeks to keep levels of p53 low until DNA damage occurs.

Increased expression of the hPTTG1 binding factor (PBF) has been observed in a number of cancers, including the thyroid, and a specific interaction with p53 has been demonstrated. PBF has been shown to significantly reduce the half-life of p53, demonstrating increased

ubiquitination of p53 following overexpression of PBF, and implicating PBF as a novel regulator of p53, which potentially has important effects in the DNA damage response. Furthermore GST pull-down assays demonstrated a potential interaction between MDM2 and PBF.

We hypothesised that the PBF-mediated increased ubiquitination and degradation of p53 occurs via MDM2, an effect that has been shown previously for proteins such as Insulin receptor tyrosine kinase substrate (Wang et al, 2011) and Yin Yang 1 (Sui et al, 2004). Our aim was to investigate this firstly by confirming the interaction between PBF and MDM2, secondly by determining if MDM2 was required for PBF-mediated increased degradation of p53, and thirdly by determining the potential mechanisms underlying these processes.

Overall our work aimed to investigate the roles of hPTTG1 and PBF in thyroid cancer and to provide mechanistic insights into the consequences of hPTTG1 and PBF overexpression previously observed in thyroid cancer.

Chapter 2. Materials and Methods

2.1: Murine studies

hPTTG1 transgenic mice were generated, bred and maintained at the Biomedical Services Unit of the University of Birmingham. All experiments were conducted in accordance with United Kingdom Home Office regulations. Cardiac punctures were performed under general anaesthesia and mice were sacrificed by overdose of anaesthetic.

2.2: Cell lines

Thyroid papillary carcinoma TPC1 cells were kindly provided by Dr Rebecca Schweppe (Division of Endocrinology, Metabolism and Diabetes, University of Colorado Denver, Aurora, Colorado). Thyroid papillary carcinoma K1 cells were obtained from the Health Protection Agency Culture Collections, United Kingdom. Thyroid papillary cancer 1 (TPC1) and thyroid papillary cancer K1 cells were routinely cultured in RPMI 1640 medium (Life Technologies Ltd, Paisley, UK) and split twice weekly. Media was supplemented with 10% foetal bovine serum (Invitrogen, Life Technologies Ltd, Paisley, UK), penicillin (10^5 U/l) and streptomycin (100 mg/l) (Invitrogen, Life Technologies Ltd, Paisley, UK). HeLa cervical cancer cells were cultured in DMEM media (Life Technologies Ltd, Paisley, UK) and split twice weekly.

Media were supplemented with 10% foetal bovine serum, penicillin (10^5 U/l) and streptomycin (100 mg/l).

2.3: Plasmid transfection

Transfection of plasmids was performed with Fugene transfection reagent (Roche, West Sussex, UK) used at a 3:1 ratio with the plasmid. Plasmids used were pcDNA3 and pci-neo vectors. Transfections were carried out 24 hours post seeding of cells. Fugene was added to OPTI-MEM media before addition of the plasmid. 2 μg plasmid was used per well of a 6-well plate. After incubation for 20 minutes for complexes to form, plasmids were added to cells. Total RNA or total protein were harvested 24, 48 or 72 hours post-transfection.

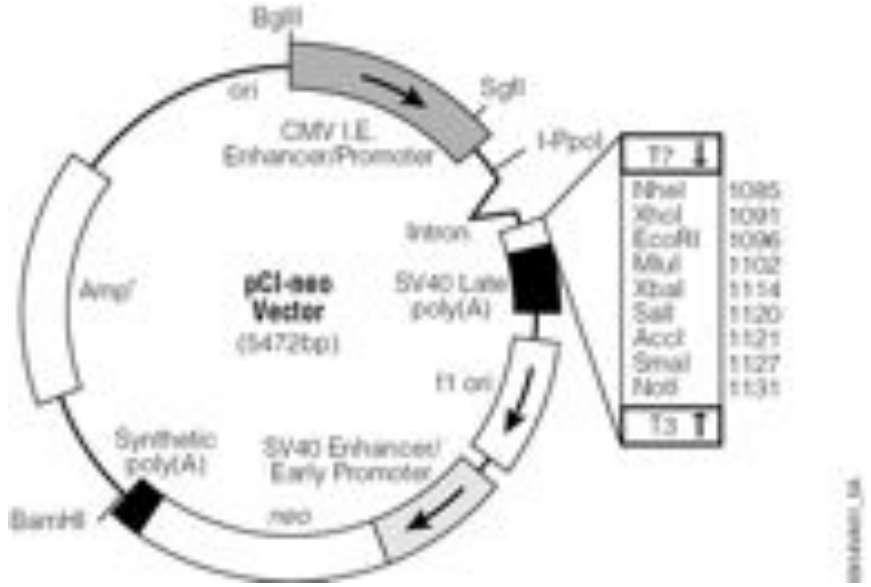

Figure 2.1: PCI-neo vector, showing origin of replication (ori) and ampicillin resistance gene (Amp^r). The restriction endonucleases are also listed.

2.4: siRNA transfection

siRNA transfection was performed using siRNA targeted to specific mRNA. Transfections were carried out using siPORT NeoFX transfection reagent (Ambion, Life Technologies Ltd, Paisley, UK) as per manufacturer's instructions. Cells were seeded and transfection was performed 24 hours later. Cells were harvested for RNA or protein 24, 48 or 72 hours post-transfection.

2.5: DNA extraction and quantification

Ear clippings from mice were provided for genotyping and stored at -20 ^{0}C until processed. DNA was extracted from mouse tissue using the DNeasy Blood & Tissue Kit (Qiagen, Manchester, UK) according to manufacturer's instructions, and RNase A (Qiagen, Manchester, UK) was added to ensure RNA free genomic DNA. DNA concentration was determined by spectroscopy of the λ260 nm wavelength using a NanoDrop Spectrometer (NanoDrop Products, Wilmington, DE, USA).

2.6: RNA extraction and quantification

RNA was extracted from mouse thyroid glands using the RNeasy Micro Kit (Qiagen, Manchester, UK) according to manufacturer's instructions, and DNase I used to ensure high RNA purity. RNA concentration was determined by spectroscopy of the λ260 nm wavelength using a NanoDrop Spectrometer(NanoDrop Products, Wilmington, DE, USA).

Total RNA was extracted from cells 24-72 hours post-transfection. Cell medium was removed and cells were washed with PBS, before adding Tri-reagent (Ambion, Life Technologies Ltd, Paisley, UK). Chloroform (Sigma

Aldrich, St louis, MO, USA) was added (200 µl/ml Tri-reagent) and samples were left to stand at room temperature for 15 minutes. Samples were subsequently centrifuged at 12,000 g for 15 minutes at 4 ^{0}C. This centrifugation separates the protein and RNA into layers with DNA forming a white precipitate. The aqueous RNA layer was extracted and isopropanol (Sigma Aldrich, St louis, MO, USA) added (500 µl/ml Tri-reagent) and mixed, prior to leaving samples to stand for 10 minutes at room temperature. After centrifuging (12,000 g) for 10 minutes at 4 ^{0}C, supernatant was removed and the pellet washed with 75% ethanol (1 ml/ml Tri-reagent). Samples were vortexed and centrifuged at 9000 g for 5 minutes at 4 ^{0}C before removal of ethanol. Samples were left to air dry at room temperature for 10 minutes. Following this 20 µl of nuclease free water was added and the pellet resuspended. Samples were stored at -80 ^{0}C and quantified using the NanoDrop Spectrometer (NanoDrop Products, Wilmington, DE, USA) as described previously.

2.7: Protein extraction and quantification

RIPA buffer containing 60 µl protease inhibitors (Sigma Aldrich, St louis, MO, USA) per ml of RIPA buffer was added to a homogeniser tube containing mouse thyroid glands. Tissue was lysed until homogenous and supernatant transferred to a fresh microcentrifuge tube following centrifugation. Protein concentration was determined using the BCA Protein Assay Kit (Thermo scientific, Nortumberland, UK). Bovine serum albumin protein at concentrations of 0–5 mg/ml was used as standards.

Total protein was extracted from cells 24-72 hours post-transfection. Cell medium was removed and cells were washed with PBS. RIPA buffer containing protease inhibitors (Sigma Aldrich, St louis, MO, USA) (60 µl/ml RIPA buffer) was added and samples were stored at -20 ^{0}C for a minimum of 20 minutes. Samples were subsequently scraped into microcentrifuge tubes, sonicated and centrifuged for 10 minutes at 12,000 g (4 ^{0}C) to pellet the debris. Supernatant was transferred to a fresh microcentrifuge tube and protein quantification was carried out using the BCA assay as described previously.

2.8: Reverse Transcription

Total-RNA (0.5 μg) was added to water to a total volume of 4.9 μl. After incubation at 70 ^{0}C for 10 minutes, a final reaction volume was prepared, consisting of 2 μl 25 mM $MgCl_2$, 1 μl RT 10X Reaction buffer, 1 μl 10 mM dNTPs, 0.25 μl RNasin (ribonuclease inhibitor), 0.5 μl random primers and 0.3125 μl Avian Myeloblastosis virus reverse transcriptase (AMV) (Promega Corporation, Madison, WI, USA). Incubation for 10 minutes at room temperature was followed by reverse transcription (42 ^{0}C for 1 hour, 95 ^{0}C for 5 minutes and 4 ^{0}C for 5 minutes). 10 μl of nuclease free water was added, followed by storage at -20 ^{0}C.

2.9: Polymerase Chain Reaction (PCR)

Sample DNA was diluted to 150 ng/ul before adding 2 μl Forward Primer (15 pmol/μl) and 2 μl Reverse Primer (15 pmol/μl) (Alta Bioscience, Birmingham, UK), 3 μl $MgCl_2$, 0.4 μl dNTPs (25 mM) and 10 μl PCR enhancer (5Prime) to give a reaction volume of 44.5 μl. After a heat start of 95 ^{0}C to denature the DNA template and limit primer dimer formation, 5 μl of PCR Buffer and 0.5 μl BioTaq DNA Polymerase (BioLine, London, UK) was added. Samples were run on a thermocycler for 35 cycles (Mastercycler Gradient) at

a reaction of 95 ^{0}C for 30 seconds (denaturation), 58/62 ^{0}C (primer annealing) for 1 minute and 72 ^{0}C for 1 minute 40 seconds (extension).

Gel electrophoresis was performed for DNA visualisation. A 1.4% agarose (Bioline, London, UK) gel was prepared in 1X TAE (Tris Acetate EDTA) Buffer (Qiagen, Manchester, UK). Gel Red (Biotium, Hayward, CA, USA) or SYBR Safe (Invitrogen, Life Technologies Ltd, Paisley, UK) was used as the fluorophore. DNA was added to 5X DNA Loading Buffer. The gel was run at 90V for approximately 1 hour before visualisation using a Gel Imager.

Primer Pair	Primer Direction	Primer Sequence
hPTTG1 Primer Set 1	Forward	CTGGTCATCATCCTGCCTTTCTC
	Reverse	GCTTGGCTGTTTTTGTTTGAGG
hPTTG1 Primer Set 2	Forward	CGTGCTGTTATTGTGCTGT
	Reverse	GAGAGGCACTCCACTCAAGG
Notch-1 Primer Set	Forward	CAGCTGCACTTCATGTACGTG
	Reverse	GGCAGACACAGCCGCATGCAGC

Figure 2.2: Table of forward and reverse primer sequences for hPTTG1 and Notch-1

2.10: Quantitative PCR (qPCR)

Relative levels of specific mRNAs or DNA were determined using quantitative Real-Time PCR. All experiments were performed using the ABI 7500 Sequence Detection System. An oligonucleotide fluorophore (probe) consists

of a 5' reporter dye (FAM 6-carboxy-fluorescein or VIC) and a 3' quencher dye (TAMRA 6-carboxy-tetramethyl-rhodamine). Quenching of the reporter, and subsequent fluorescence, is dependent on the proximity of the quencher. Breakdown of the probe by exonuclease activity, due to PCR amplification, disrupts the proximity of the quencher and reporter, allowing fluorescence emission and detection of this excitation via a laser. Therefore the greater the level of each mRNA, or DNA sequence, the greater the targeting of the reporter dye, and a proportional increase in the detected fluorescence. Primers for each sequence were designed (Alta Biosciences, Birmingham, UK) or pre-optimised specific TaqMan gene expression assays were used (Applied Biosystems, Life Technologies Ltd, Paisley, UK).

PCR was performed by adding 1.25 μl of 18s mRNA, 4.5 μl of Forward Primer (5 pmol/μl), 4.5 μl of Reverse Primer (5 pmol/μl), 0.75 μl Probe (5 pmol/μl), 12.5 μl Master Mix and 0.5 μl H_2O to 1 μl of cDNA. 18s was used as an internal housekeeping gene for mRNA (Read et al, 2009). DSCAM (Down Syndrome Cell Adhesion Molecule) was used as an alternative housekeeping gene for DNA to determine mRNA or DNA expression in relation to an internal reference. The PCR reaction was 50 ^{0}C for 2 minutes, 95 ^{0}C for 10 minutes, followed by 40 cycles of 95 ^{0}C for 15 seconds and 60 ^{0}C for 1 minute. Sample levels of fluorescence were detected after each cycle and end data was expressed as a Ct value. A ΔCt value was determined (ΔCt = Ct of target gene minus Ct of housekeeping gene 18s or DSCAM) and used to determine a ΔΔCt value (ΔCt of experimental group minus ΔCt of control

group). This value was subsequently used to determine the fold change using the equation: $2^{-\Delta\Delta Ct}$.

Sequence name	Sequence
hPTTG1 Probe	5'-CGTCTTGCCACCGGCTTCCCT-3'
hPTTG1 Forward Primer	5'-GAGAGAGCTTGAAAAGCTGTTTCAG-3'
hPTTG1 Reverse Primer	5'-TCCAGGGTCGACAGAATGCT-3'
PBF Probe	5'-CGTCTTGCCACCGGCTTCCCT-3'
PBF Forward Primer	5'-GCTTGTCTGGACTACCCAGTTACA-3'
PBF Reverse Primer	5'-AGCGTGCAGAGCTCAATTTACA-3'
DSCAM Probe	5'-TTCAAGTGCATTATCCCCTCCTCGGTG-3'
DSCAM Forward Primer	5'-CAGAAAACCATGAGAGGCAATG-3'
DSCAM Reverse Primer	5'-TTCTCCCATGAGACGACAGTGA-3'

Figure 2.3: Table of probe, forward and reverse primer sequences for hPTTG1, PBF and DSCAM used for qPCR.

2.11: Histology

Mouse thyroid glands taken for histology were fixed in formalin immediately after removal. Tissue was then paraffin embedded and either prepared for

immunohistochemistry, or stained for Haematoxylin and Eosin, by the Cellular Pathology Department of the University Hospital Birmingham.

2.12: Immunohistochemistry

Formalin fixed and paraffin embedded mouse thyroid gland tissue was used. After dewaxing in Histoclear (National Diagnostics), samples were rehydrated using an ethanol concentration gradient before washing in PBS (Oxoid Limited, Basingstoke, Hampshire, UK). Antigen retrieval was performed using 10 mM Tri-Sodium Citrate buffer (pH 6.0), subjecting samples to microwaves until the temperature of the buffer was greater than 95 ^{0}C. After further washing in PBS, samples were incubated in 0.3% Hydrogen Peroxide (Sigma Aldrich, St louis, MO, USA) in PBS to inhibit endogenous peroxidase activity. Samples were blocked in 10% Normal Goat Serum (Vector labs, Peterborough, UK) diluted in 1% IgG-free BSA and 0.1% Tween-20 in PBS for 1 hour at room temperature in a humidified chamber, to block non-specific binding. Primary antibody was subsequently added after dilution in 10% Normal Goat Serum in dilution buffer. Samples were incubated overnight (4 ^{0}C) in a humidified chamber. Following washing in PBS, a biotinylated secondary antibody (Vector ABC Kit) was added and incubated in a humidified chamber for 50 minutes at 4 ^{0}C followed by 10

minutes at room temperature. After further washing in PBS the Avidin Biotin Peroxidase Complex (Vector ABC Kit) was added. ImmPACT DABS (Vector labs, Peterborough, UK) was subsequently added for 5 minutes to develop staining. After washing in H_2O, samples were counterstained using Mayers Haemalum (VWR, Lutterworth, Leicestershire, UK) to achieve nuclear staining. Samples were dehydrated by an increasing ethanol concentration gradient before clearing with Histoclear and mounted using mounting medium (DakoCytotation, Ely, Cambridgeshire, UK). Thyroid gland section samples were viewed under a light microscope (Zeiss, Oberkochen, Germany) and imaging performed using Axiovision software.

2.13: Radioimmunoassay for circulating TH concentrations

Following cardiac puncture of mice to obtain total blood, samples were left to clot overnight at 4 ^{0}C. Samples were centrifuged at full speed for 20 minutes at 4 ^{0}C. Supernatant was subsequently extracted and serum was stored at -80 ^{0}C. Total T3 and total T4 concentrations were measured using a radioimmunoassay kit (MP Biochemicals). Mouse serum samples, and standards, were added to tubes coated with either T3 or T4 monoclonal antibodies, followed by addition of a solution containing radiolabelled T3 or T4. Competitive binding of unlabelled and labelled T3 or T4 allows the

concentration of the hormones to be determined. After 1 hour incubation, the radioactivity on the coated tubes was counted using a gamma counter.

Mouse serum TSH concentrations were determined by Professor Samuel Refetoff (University of Chicago), using a double antibody precipitation radioimmunoassay (Pohlenz et al, 1999) (Di Cosmo et al, 2010).

2.14: Western blotting

Protein (10-60 µg) was denatured at 95 ^{0}C for 5 minutes. Proteins were subsequently separated by electrophoresis in 12% Sodium Dodecyl Sulphate polyacrylamide gels. After transferring for 1 hour at 350 mA onto polyvinylidene fluoride membranes (GE Healthcare, Buckinghamshire, UK) they were incubated for 1 hour in 5% non-fat milk in Tris buffered saline with 0.1% Tween (TBS/T) (Sigma Aldrich, St louis, MO, USA) to block non-specific binding. Membranes were incubated at 4 ^{0}C overnight with the appropriate primary antibody. Following several washes in TBS/T membranes were incubated with an appropriate Horseradish peroxidase (HRP) -conjugated secondary antibody (Dakocytomation, Ely, Cambridgeshire, UK) at room temperature for 1 hour. Subsequent to several further washes in TBS/T, antigen antibody complexes were visualised using the West Pico (Thermo Scientific, Nortumberland, UK) and ECL 2 (Thermo Scientific, Nortumberland, UK) chemiluminescence detection systems onto X-ray film (Kodak). β-actin (monoclonal anti-β-Actin clone AC-15)(Sigma Aldrich, St louis, MO, USA) expression was used as a housekeeping protein to determine differential protein loading and was used at a concentration of 1:10,000. Scanning densitometry was carried out to determine quantifiable differences in protein expression (Image J software, http://rsbweb.nih.gov/ij/index.html).

2.15: Co-immunoprecipitation assay

Cells were seeded into T25 flasks and transfected 24 hours later. Protein was harvested 48 or 72 hours post-transfection. Cell media was removed and cells washed in PBS (phosphate buffered saline), prior to adding RIPA buffer containing 60 µl protease inhibitors (Sigma Aldrich, St louis, MO, USA) per ml of buffer. After scraping contents into a microcentrifuge tube, proteins were sonicated to increase protein yield and centrifuged to pellet cellular debris. After transferring the supernatant to a new microcentrifuge tube, lysates were removed and frozen, while primary antibody was added at an appropriate concentration. Samples were subsequently spun on a rotating mixer overnight at 4 ^{0}C. Sepharose beads (VWR, Lutterworth, Leicestershire, UK) were added to each sample and spun on a rotating mixer for 2 – 4 hours at 4 ^{0}C. After pulse centrifuging and discarding the supernatant, beads were washed using RIPA buffer several times, pulse centrifuging and removing supernatant after each wash. Elution buffer was added, consisting of laemmli buffer (Bio-rad, Hemel Hempstead, Hertfordshire, UK), 10% SDS (sodium dodecyl sulphate) (Sigma Aldrich, St louis, MO, USA) and β-mercaptoethanol (Sigma Aldrich, St louis, MO, USA) at a ratio of 17:2:1 respectively. Non-reducing buffer consisted of laemmli buffer alone. After incubating for 30 minutes at 37 ^{0}C, samples were pulse centrifuged and elution buffer was removed without removal of the beads. Protein binding was subsequently

visualised by performing Western blotting on samples, and lysates were used to ensure protein extraction.

2.16: Protein stability assay

The half-life of specific proteins was analysed using the protein synthesis inhibitor anisomycin (Sigma Aldrich, St louis, MO, USA). TPC1 cells were seeded and protein stability measured 24, 48 or 72 hours post-transfection. Anisomycin was added to OPTI-MEM media to a final concentration of 100 μM. Cell medium was removed and the anisomycin (diluted in OPTI-MEM) was added. Cells were subsequently harvested for protein after the timepoint had elapsed and protein concentration was measured by Western blotting.

2.17: Immunofluorescence

Immunofluorescence was performed 24, 48 or 72 hours post-transfection. Cells were seeded onto coverslips before transfection 24 hours later. Cell media was removed and, subsequent to washing with PBS (phosphate buffered saline), cells were fixed with fixing solution for 20 minutes at room temperature. Following further washing with PBS, cells were permeabilised

using chilled 100% methanol for 10 minutes. Cells were then blocked for 30 minutes with 10% NCS (neonatal calf serum) diluted in PBS. Primary antibody was added for 1 hour at room temperature, consisting of 1% BSA (bovine serum albumin) diluted in PBS, with primary antibody at appropriate concentration. Subsequent to further washing in PBS, secondary antibody was added for 1 hour at room temperature in the dark, consisting of 1% BSA and 1% NCS diluted in PBS, and secondary antibody. After further washing with PBS, coverslips were mounted onto slides using fluorescent mounting medium (Dakocytotation, Ely, Cambridgeshire, UK). Fluorescent cells were visualised using the Zeiss Axioplan fluorescent microscope (Zeiss, Oberkochen, Germany).

2.18: Table of antibodies used

Antibody	Clone	Company
Anti-hPTTG1	Rabbit anti-hPTTG	Invitrogen
Anti-Cylcin D1	Rabbit monoclonal (SP4)	Abcam
Anti-PCNA	Rabbit polyclonal (FL-261)	Santa Cruz Biotechnology
Anti-p53	Mouse monoclonal IgG_{2a} (DO-1) (sc-126)	Santa Cruz Biotechnology
Anti-p21	Rabbit polyclonal (ab7960)	Abcam
Anti-MDM2	Mouse IgG_1 (SMP14)	Santa Cruz Biotechnology
Anti-PBF	Rabbit Polyclonal	Eurogentec
Anti-Rad6	Rabbit Polyclonal (ab31917)	Abcam
Anti-β-actin	Mouse monoclonal (AC-15)	Sigma Aldrich

Figure 2.4: Table of antibodies used during thesis.

2.18: Statistics

All statistics were carried out using SPSS statistics software and Microsoft Excel spreadsheet software. Student's *t*-tests were used for the analysis of data with a normal distribution. For data that did not possess a normal distribution a Mann-Whitney U test was used for analysis. An Anderson-Darling test was used to determine a normal distribution. Samples with multiple variances were tested via analysis of variance (ANOVA). All significance values were taken as $p<0.05$. For qPCR, statistics were

performed on ΔCt values to avoid bias from transformation of data using the $2^{-\Delta\Delta Ct}$ equation.

Chapter 3. Characterisation of thyroid-specific hPTTG1 expressing transgenic mice

3.1: Introduction

hPTTG1 was first identified following discovery of rat *Pttg1* in GH4 pituitary tumour cells (Pei and Melmed, 1997). hPTTG1 was subsequently shown to be capable of cellular transformation *in vitro* and *in vivo* (Pei and Melmed, 1997) (Zhang et al, 1999). hPTTG1 was found to be important in the cell cycle through its role as the human securin (Uhlmann et al, 1999) (Hornig et al, 2002) (Wirth et al, 2006) and has also been shown to be involved in DNA damage and repair (Zhou et al, 2003) (Romero et al, 2004) (Kim et al, 2007). hPTTG1 is a potent transcription factor (Dominguez et al, 1998) and is involved in p53 dependent and independent apoptosis (Yu et al, 2000). We, and others, have shown hPTTG1 overexpression in differentiated thyroid cancer and several other cancers (Heaney et al, 2001) (Boelaert et al, 2003) (Zhang et al, 1999) (Zatelli et al, 2010) (Solbach et al, 2004). The role of hPTTG1 in tumourigenesis is complex, with hPTTG1 implicated in the initiation of tumour formation through increased genetic instability (Kim et al, 2005) (Kim et al, 2007) and aneuploidy (Yu et al, 2003). Furthermore hPTTG1 promotes cancer progression through increased cellular proliferation (Boelaert et al, 2004) and induction of growth factors such as FGF-2 (Zhang et al, 1999) and VEGF (McCabe et al, 2002), resulting in increased angiogenesis. To better elucidate the effect of hPTTG1 on organ-specific tumour formation, *in vivo* experiments using transgenic mouse models have been used. Overexpression of hPTTG1 targeted to the pituitary

resulted in hyperplasia of the pituitary gland (Abbud et al, 2005). Overexpression of hPTTG1 in mouse ovaries, using the MISIIR promoter, resulted in hyperplasia, although no tumour formation was apparent (El-Naggar et al, 2007). Subsequent research using the CMV promoter in place of the MISIIR promoter, resulted in ovarian tumour formation at 8 months of age in 17% of mice, and crossing these mice with *Tp53* +/- mice led to an increase in tumour formation. These studies demonstrate hPTTG1 overexpression may act as a pre-tumourigenic initiating event, resulting in hyperplasia but requiring a 'second hit' to cause tumour formation.

Since hPTTG1 is expressed at high levels in thyroid tumours (Stratford et al, 2005) we hypothesised that targeted hPTTG1 expression in transgenic mice would result in increased thyroid cell growth. Generation of transgenic mouse models is commonly carried out using exogenous DNA microinjected into male pronuclei of fertilised oocytes. Oocytes are then implanted into pseudopregnant foster mother mice and litters screened to determine potential founder mice (Gordon et al, 1980). There are a number of disadvantages to this method, including the need to screen large numbers of mice since successful generation of transgenic mice is rare. Furthermore the transgene is randomly integrated into the genome, which can lead to interference of endogenous gene expression. This technique has been used to generate a thyroid-specific $BRAF^{V600E}$ expressing transgenic mouse model using the bovine thyroglobulin promoter (Knauf et al, 2005). These mice developed papillary thyroid cancers after 12 and 22 weeks. Using the same promoter construct our group recently developed a transgenic mouse model

with thyroid specific overexpression of PBF, which resulted in hyperplasia of the thyroid gland and significant goitre formation (Read et al, 2011). These findings prompted successful development and characterisation of a hPTTG1 transgenic mouse model, by Dr Gregory Lewy, which is described in section 1.2.9. The transgene contained a FLAG tag, and will hereafter be referred to as hPTTG1-Tg-FLAG. hPTTG1-Tg-FLAG homozygote mice had reduced life-spans, presenting with idiopathic mortality, showing signs of sickness by 3 months of age, almost 40% dying by 6 months of age, and approximately 30% overall surviving to 18 months of age. It was felt these effects might be secondary to high levels of hPTTG1 in this model, or to random integration abrogating function of certain genes. Therefore we decided that a second mouse model with different levels of thyroid targeted hPTTG1 expression, and different integration sites, may further elucidate effects of hPTTG1 *in vivo*. Since we had technical difficulties with our original FLAG-tagged transgene construct, we generated a different transgene containing the bovine thyroglobulin promoter and hPTTG1 with a HA tag present on the C-terminus (Figure 3.1), which was performed by Dr Gregory Lewy. This was subsequently microinjected into male pronuclei of FVB/N mice and followed by implantation into pseudopregnant foster mother mice, performed by Dr Andrea Bacon.

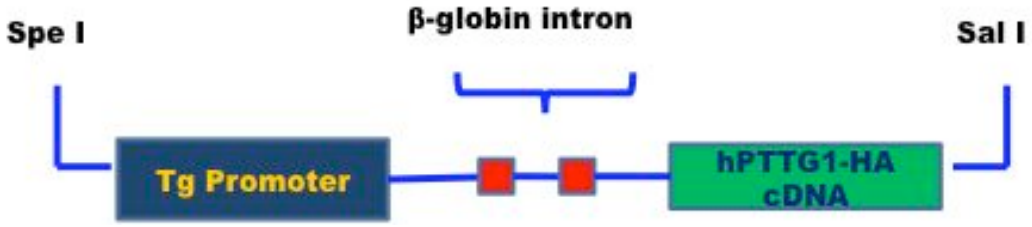

Figure 3.1: Construct used to produce transgenic mouse model of hPTTG1 thyroid specific overexpression, containing bovine thyroglobulin promoter and HA-tagged hPTTG1. β-globin intron was used to increase transcriptional efficiency (Brinster et al, 1988).

The aims of the work carried out in this chapter were to complete the generation of an alternative transgenic mouse model of thyroid-specific hPTTG1 overexpression and to fully characterise this model. We sought to confirm various *in vitro* observations, such as the effect of hPTTG1 overexpression on growth factor expression and cellular proliferation. However, we primarily sought to confirm our hypothesis that hPTTG1 overexpression would result in thyroid hyperplasia and subsequent neoplasia.

3.2: Materials and Methods

3.2.1: Murine studies

FVB/N strain mice were used for experiments. Thyroid gland dissection was carried out in sacrificed mice and thyroid glands were excised and weighed, before storage in liquid nitrogen (protein extraction), in RNA later (Sigma Aldrich, St Louis, MO, USA) on ice (RNA extraction), or in formalin (histology). A thyroid:body weight ratio was determined in order to control for mouse body weight when comparing thyroid weights.

3.2.2: DNA extraction and quantification

DNA extraction and quantification of mouse thyroid samples was performed as described in section 2.5.

3.2.3: RNA extraction and quantification

RNA was extracted from mouse thyroid glands using the RNeasy Micro Kit (Qiagen, Manchester, UK) according to manufacturer's instructions. DNase I was used to ensure high RNA purity. RNA concentration was determined by spectroscopy of the λ260 nm wavelength using a NanoDrop Spectrometer.

3.2.4: Protein extraction and quantification

Protein extraction and quantification of mouse tissue samples was performed as described in section 2.7.

3.2.5: Reverse Transcription

Total RNA was reverse transcribed to cDNA, performed as described in section 2.8.

3.2.6: Mouse genotyping

Potential founder transgenic mice were genotyped by PCR using two different primer sets to ensure reliability of results (Figure 3.2). PCR was performed as described in section 2.9 and gel electrophoresis was carried out to visualise results.

Primer Pair	Primer Direction	Primer Sequence
Primer Set 1	Forward	CTGGTCATCATCCTGCCTTTCTC
	Reverse	GCTTGGCTGTTTTTGTTTGAGG
Primer Set 2	Forward	CGTGCTGTTATTGTGCTGT
	Reverse	GAGAGGCACTCCACTCAAGG

Figure 3.2: Table of PCR primer sets 1, 2 used in conventional PCR analysis for detection of hPTTG1.

3.2.7: Quantitative PCR (qPCR)

Relative levels of specific mRNAs or DNA were determined using quantitative Real-Time PCR. All experiments were performed as described in section 2.10.

3.2.8: Histology

Mouse thyroid glands taken for histology were fixed in formalin immediately after removal. Tissue was then paraffin embedded and prepared for

immunohistochemistry, or stained for Haematoxylin and Eosin, by the Cellular Pathology Department of the University Hospital Birmingham.

3.2.9: Immunohistochemistry

Immunohistochemistry was carried out as outlined in section 2.12. Primary antibodies used were anti-hPTTG1 (1/40) (Invitrogen, Life Technologies Ltd, Paisley, UK) and anti-Cyclin D1 (Abcam, Cambridge, UK) (1/100). ImageJ software was used to count 1000 cells per sample.

3.2.10: Radioimmunoassay for circulating TH concentrations

Concentrations of mouse total T3 and total T4 were determined through radioimmunoassay as described in section 2.13. Mouse serum TSH concentrations were measured by Professor Samuel Refetoff (University of Chicago), as described in section 2.13 (Pohlenz et al, 1999) (Di Cosmo et al, 2010).

3.2.11: Western blotting

Western blotting was carried out as described in section 2.14. Antibodies used were anti-hPTTG1 (Invitrogen, Life Technologies Ltd, Paisley, UK) (1/40) and anti-PCNA (FL-261) (Santa Cruz Biotechnology, Dallas, TX, USA) (1/1000).

3.2.12: Apoptosis assay

The ApopTag peroxidase *In situ* apoptosis detection kit was used according to manufacturer's instructions (Millipore, Billerica, MA, USA). Briefly, paraffin-embedded samples were deparaffinised in histoclear and a decreasing gradient of ethanol. Samples were pre-treated using 10 mM citrate buffer (pH 3.0-6.0) and endogenous peroxidase was quenched using hydrogen peroxide. Equilibration buffer was added, followed by TdT enzyme for 1 hour in a humidified chamber at 37 ^{0}C. Subsequently stop/wash buffer was added and treated with anti-digoxigenin conjugate for 30 minutes in a humidified chamber. Peroxidase substrate was applied to samples for staining, followed by washing in dH_2O. Samples were counterstained using Mayer's Haemalum, dehydrated using an increasing ethanol gradient and mounted. Samples were subsequently viewed under a light microscope

(Zeiss, Oberkochen, Germany) using specialised software (Axiovision). ImageJ was used to count stained cells, counting 1000 nuclei per sample.

3.3: Results

3.3.1: Identification of hPTTG1 transgenic founder mice

Following microinjection of the *hPTTG1-HA* transgene construct into the pronuclei of fertilised mouse oocytes, mice were genotyped in order to identify mice with the *hPTTG1* gene integrated into their genome. Ear clippings were collected from potential founder mice and a total of 171 microinjected mice were genotyped (82 males and 89 females). Conventional PCR was performed using 2 different primer sets for *hPTTG1* (Figure 3.2), which had previously been validated by Dr Gregory Lewy, and using mouse *Notch-I* primers (Figure 3.3) to confirm the presence of genomic DNA, thereby avoiding false-negative results. DNA from wild-type mice were used as negative controls and DNA from our previous hPTTG1-FLAG transgenic mice was used as a positive control. Following conventional PCR using primer set 1, gel electrophoresis detected a band of approximately 400 bp, indicating presence of *hPTTG1* DNA (Figure 3.3).

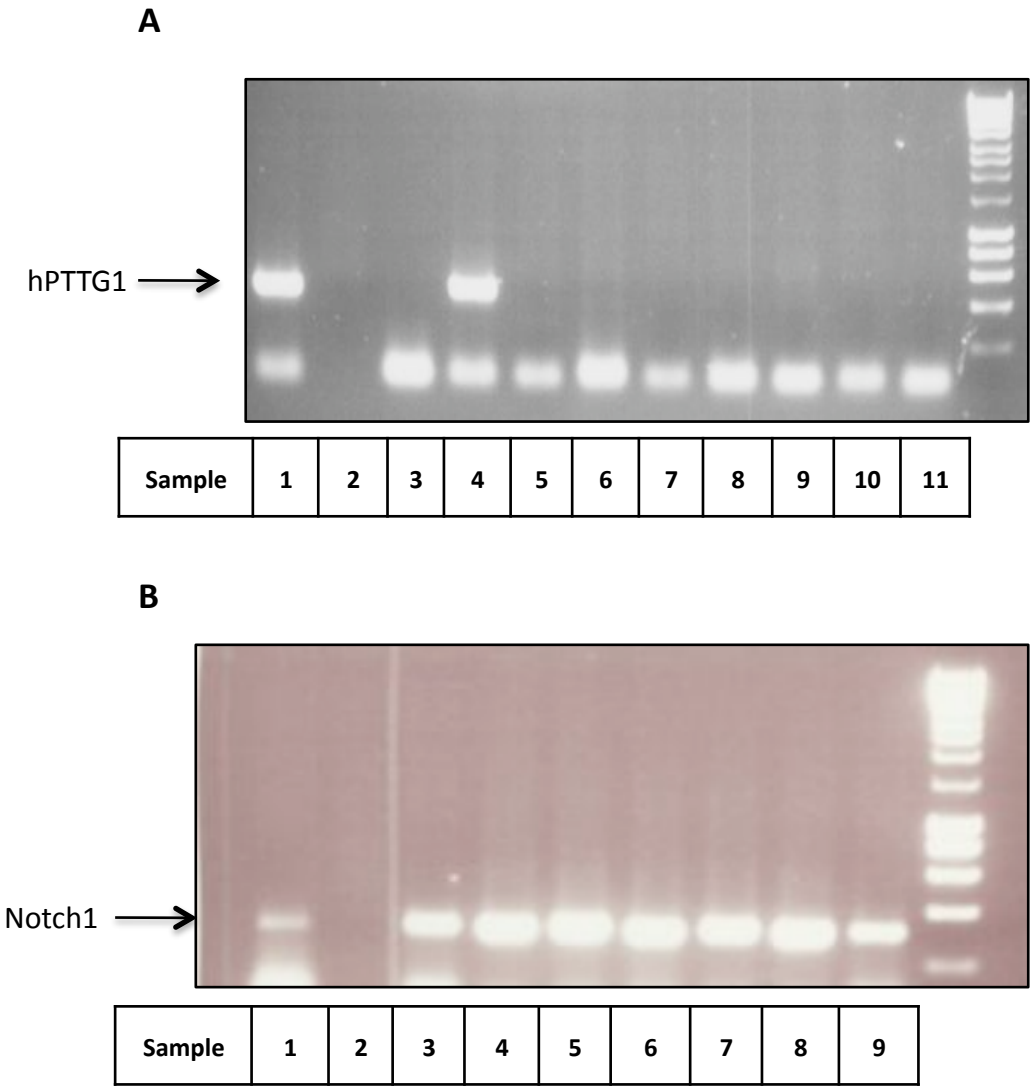

Figure 3.3: Conventional PCR genotyping for hPTTG-Tg mice. ***A.*** *Gel electrophoresis of mouse DNA samples following PCR using primers for hPTTG1. A band at 400bp indicates hPTTG1. Sample 1 – positive control, sample 2 – no primer control, sample 3 – negative control, sample 4 – positive potential founder mouse, samples 5-11 – negative potential founder mice.* ***B.*** *Gel electrophoresis of mouse DNA samples following PCR using primers for Notch1. Sample 1 – positive control, sample 2 – no primer control, sample 3 – negative control (wild-type mouse control), samples 4-9 – potential founder mice DNA samples positive for Notch1.*

Out of 171 samples, two mice tested positive for *hPTTG1* were identified and primer set 2 was used for confirmation. Subsequently TaqMan Real-time PCR was performed on DNA from mouse samples. Pre-designed and validated *hPTTG1* primers and probe were used to ensure specificity (Figure 3.4). DSCAM (Down Syndrome Cell Adhesion Molecule) primers and probe were used as an endogenous control in multiplex with *hPTTG1*, in order to normalize the data. This approach was identical to the one used to validate the hPTTG1-FLAG model by Dr Gregory Lewy. Controls used were homozygote, heterozygote and wild-type mice from the previously generated hPTTG1-FLAG mouse line. A Master Mix only control was also used to ensure there was no contamination of reagents.

Mouse DNA samples positive for *hPTTG1* in conventional PCR analysis were confirmed using qPCR. Two positive mice were identified, a female mouse with *hPTTG1* expression at a Ct value of 28 and a male mouse with *hPTTG1* expression at a Ct value of 22 (Figure 3.4). Since the Ct Value corresponds to the amount of target nucleic acid in the sample it was concluded that the male mouse (B) had a significantly greater number of *hPTTG1* transgene copies integrated into the genome than the female mouse (A). This was confirmed using the delta delta Ct method of analysis, where mouse B had a 63 fold greater amount of target nucleic acid than mouse A.

A

Sequence name	Sequence
hPTTG1 Probe	5'-CGTCTTGCCACCGGCTTCCCT-3'
hPTTG1 Forward Primer	5'-GAGAGAGCTTGAAAAGCTGTTTCAG-3'
hPTTG1 Reverse Primer	5'-TCCAGGGTCGACAGAATGCT-3'

B

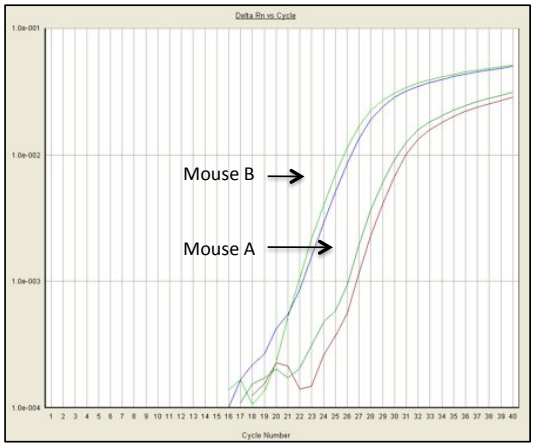

C

Sample	Ct value
Founder A	28.2
Founder B	22.4
PF 1	Undetermined
PF 2	Undetermined

Figure 3.4: Confirmation of identification of mouse DNA samples positive for hPTTG1 by TaqMan Real-time qPCR. ***A****. Table displaying sequences for hPTTG1 primers and probe, which specifically amplify hPTTG1 and do not amplify mouse Pttg1.* ***B.*** *qPCR data showing reaction curves of DNA samples of Mice A and B in duplicate.* ***C.*** *Table displaying Ct values of positive founder mice A and B and two negative potential founder mice with values, which were undetermined, showing undetectable expression of hPTTG1.*

The two mice positively identified for *hPTTG1* were mated with wild-type mice in order to propagate the transgenic lines, known as line A, propagated from mouse A, and line B, propagated from mouse B. This allowed investigation of transfer of the *hPTTG1* transgene to subsequent generations and to determine if mRNA and protein expression of hPTTG1 was present.

3.3.2: Verification of transgenic mouse *hPTTG1* mRNA expression

To verify *hPTTG1* mRNA expression present in transgenic mice, thyroids were excised from 6-week old mice and total RNA was extracted. TaqMan Real-time qPCR was performed on mice from line A (n=3) and mice from line B (n=3) and compared to wild-type mice (n=4). Hemizygous mice from line A (Mean ΔCt=4.30 ±0.27) showed a 99.7-fold (p=0.001) increase in *hPTTG1* mRNA expression compared to wild-type mice (10.89 ±0.80), while hemizygous mice from line B (5.60 ±0.17) showed a 2633.1-fold (p=0.0002) increase compared to separate wild-type mice (16.95 ±1.01) (Figure 3.5).

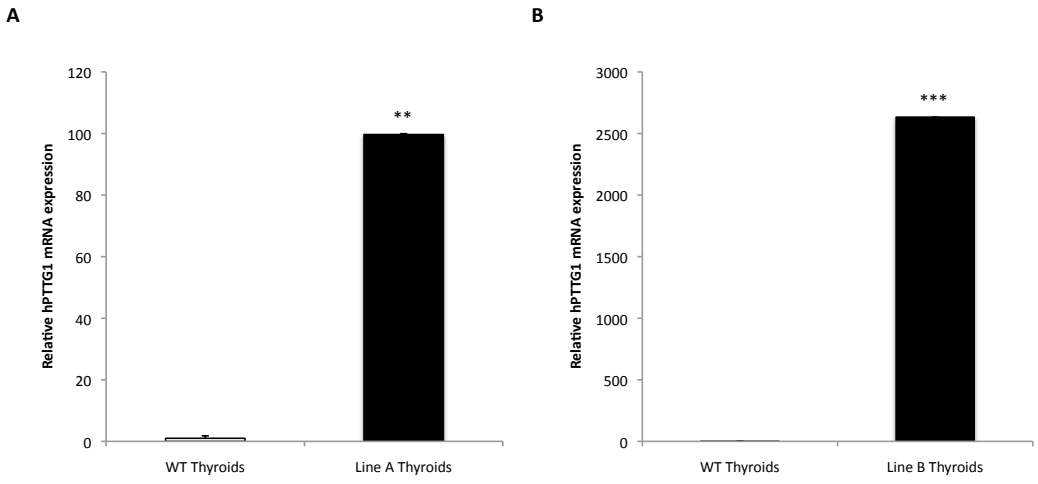

Figure 3.5: TaqMan Real-time qPCR data of hPTTG1 mRNA expression. ***A.*** *Bar chart displaying 99.7-fold increase in line A mice compared to wild-type.* ***B.*** *Bar chart displaying 2633.1-fold increase in line B mice compared to wild-type. (**=p<0.005, ***=p<0.0005).*

3.3.3: Verification of transgenic mouse hPTTG1 protein expression

To confirm hPTTG1 protein expression in transgenic mice, thyroids were excised from 6-week old mice from lines A and B. Total protein was extracted and Western blotting performed, comparing wild-type mice (n=2) to line A transgenic mice (n=3) and line B transgenic mice (n=3). HA-tagged hPTTG1 was undetectable using a commercial HA antibody (data not shown). Subsequently a hPTTG1 antibody was used, detecting bands for hPTTG1 at 28 kDa in samples from line B mice (Figure 3.6). However, there was no detectable hPTTG1 protein expression in line A mice and this line was subsequently terminated. To compare expression levels of hPTTG1 in line B mice, Western blotting tested protein samples from hemizygous line B mice. Figure 3.6 demonstrates variable expression of hPTTG1 in line B mice. Interestingly hPTTG1 frequently migrated as a doublet, indicating phosphorylation of hPTTG1 in mouse thyrocytes and suggesting that hPTTG1 was subject to normal cellular processes.

Further confirmation of hPTTG1 protein expression in thyroids of hPTTG1 transgenic mice was demonstrated by immunohistochemistry using a hPTTG1 antibody. 6-week old transgenic mice and wild-type mice were culled and thyroids excised. Thyroids were cut and paraffin-embedded slides were used for Haematoxylin and Eosin staining, as well as for immunohistochemical analysis of hPTTG1 expression and localisation. No hPTTG1 expression was found in wild-type mice while hPTTG1-Tg mice

displayed extensive nuclear and cytoplasmic staining, although this was not apparent in every thyrocyte (Figure 3.6).

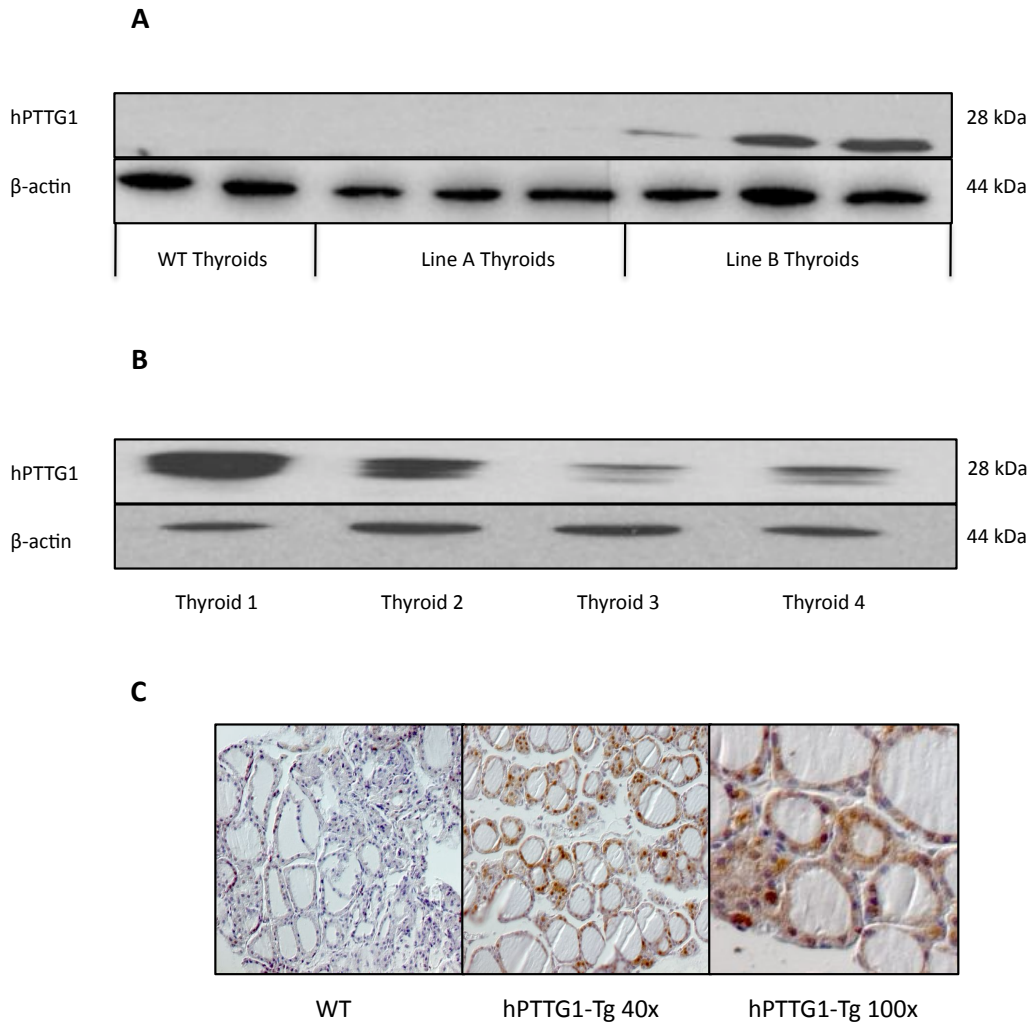

Figure 3.6: Protein expression of hPTTG1 *in transgenic mouse lines.* ***A.*** *Western blot demonstrating presence of bands for* hPTTG1 *in protein from line B mouse thyroids but not wild-type or line A thyroids.* ***B.*** *Western blot demonstrating variable expression of* hPTTG1 *in line B mice. Thyroids 1, 2 – male mice, thyroids 3,4 – female mice.* ***C.*** *Immunohistochemistry with* hPTTG1 *antibody displaying no expression of* hPTTG1 *in wild-type mice and cytoplasmic and nuclear expression of* hPTTG1 *in transgenic mice at 40x and 100x magnification.*

3.3.4: Verification of hPTTG1 transgenic mouse thyroid specificity

Having established line B as the transgenic line to pursue, we subsequently investigated thyroid specificity of the transgene. Total RNA was extracted from thyroid, heart, lungs, liver, kidneys and spleen of 6-week old wild-type (n=4) and transgenic mice (n=3). TaqMan Real-time qPCR was performed to determine expression levels of *hPTTG1* in organs listed above. There was high expression of *hPTTG1* in thyroid glands (2633.1-fold, p=0.0002) and significant expression of *hPTTG1* in lung (67.7-fold, p=0.0042), while other organs showed minimal expression levels (Figure 3.7). Since murine *Pttg1* is not amplified by *hPTTG1* primers, hPTTG1 expression was compared to wild-type murine thyroid background, which is not representative of absolute expression levels.

Total protein was also extracted from 6-week old mouse thyroids and other organs listed above. Western blotting was performed and hPTTG1 was detected in thyroids of transgenic mice but not in any other organs tested (Figure 3.7).

A

Mean ΔCt	SEM	N
15.10	±0.37	3
15.63	±0.27	3
18.25	±0.18	3
10.91	±0.25	3
14.90	±0.44	3
5.60	±0.17	3
16.94	±1.01	4

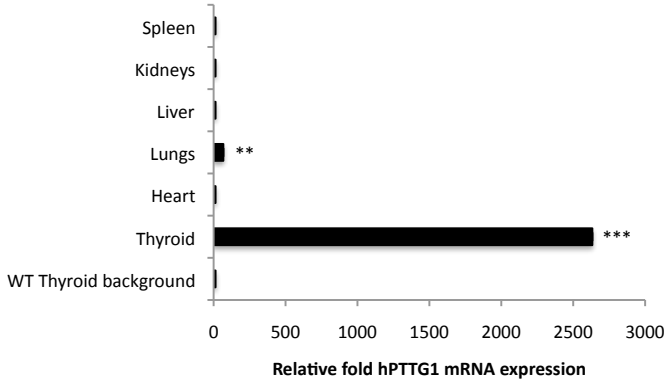

B

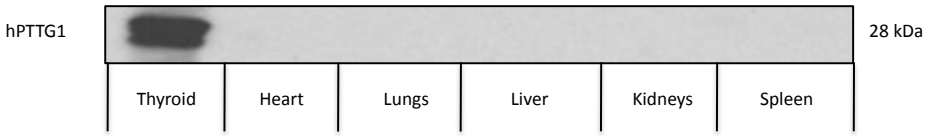

Figure 3.7: Verification of thyroid specificity of hPTTG1 transgene. ***A.*** *TaqMan Real-time qPCR data demonstrating hPTTG1 mRNA expression in thyroid, heart, lungs, liver, kidneys and spleen of transgenic mice compared to wild-type thyroid background. (**=p<0.005, ***=p<0.0005).* ***B.*** *Western blot showing* hPTTG1 *protein expression present in thyroids with no expression in heart, lungs, liver, kidneys and spleen of transgenic mice.*

3.3.5: Propagation of transgenic line

In order to propagate the transgenic line, hemizygous mice were bred together to produce wild-type, hemizygous and homozygous mice for use in subsequent investigations (Figure 3.8).

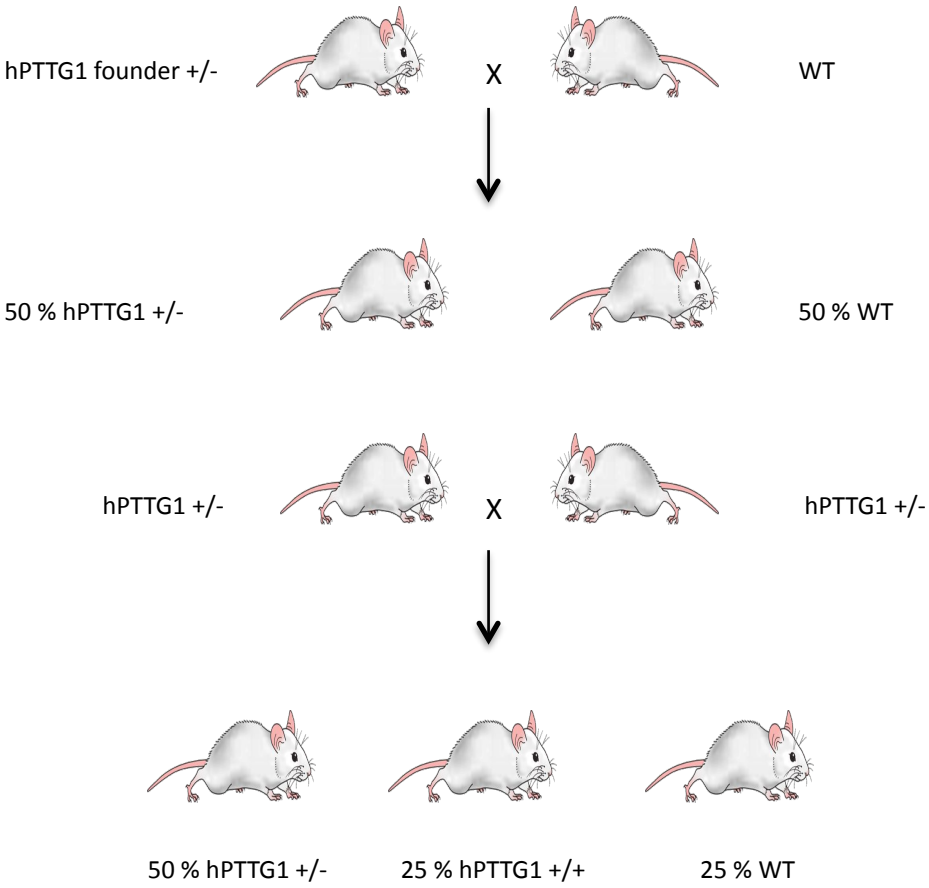

Figure 3.8: Diagram of strategy employed and mode of inheritance to propagate transgenic mouse colony.

Using human DNA controls, TaqMan Real-time qPCR was performed (Ballester et al, 2004) (Read et al, 2011) and it was estimated that the transgene copy number was approximately n=30, although this proved to be variable (Figure 3.9)

Sample	DSCAM	PTTG	ΔCt	Average controls	ΔΔCt	Fold Change	x2	Zygosity
PTTG-Tg #1	25.01	21.06	-3.95	0.09	-4.04	16.4498212	32.8996425	Hemizygote
PTTG-Tg #2	24.98	21.04	-3.94		-4.03	16.336194	32.672388	Hemizyogte
PTTG-Tg #3	25.35	21.41	-3.94		-4.03	16.336194	32.672388	Hemizygote
PTTG-Tg #4	24.98	31.52	6.54		6.45	0.01143817	0.02287634	Wild-type
PTTG-Tg #5	25.12	33.72	8.6		8.51	0.00274306	0.00548611	Wild-type
Homozygote	25.32	22.27	-3.05		-3.14	8.81524093	17.6304819	Homozygote
Hemizygote	25.16	23.27	-1.89		-1.98	3.94493082	7.88986164	Hemizygote
Wild-type	25.72	Undet.						Wild-type
MM Only	Undet.	Undet.						
Thyroid	24.68	24.8	0.12					
Placenta	25.36	25.42	0.06					

Figure 3.9: Representative example of Real-time qPCR to determine zygosity of mice using DNA from ear clippings. DSCAM is used as a housekeeping gene and multiplexed to determine differential loading. Human DNA controls used for comparison were thyroid and placenta. Homozygote, heterozygote and wild-type controls were the previous hPTTG1-FLAG transgenic mouse line.

Breeding of hemizygote mice did not appear to produce homozygote mice. Investigation of litter sizes found a 19.74% reduction ($p=1.54x10^{-5}$) in litter size in transgenic mice (Number of mice=6.26 ±0.65, n=23 litters, n=144 mice) compared to wild-type mice (9.35 ±0.34, n=52 litters, n=486 mice) (Figure 3.10). Comparison of genotype percentages from hemizygote breeding indicated 25.47% wild-type mice and 74.53% hemizygote mice (Figure 3.10).

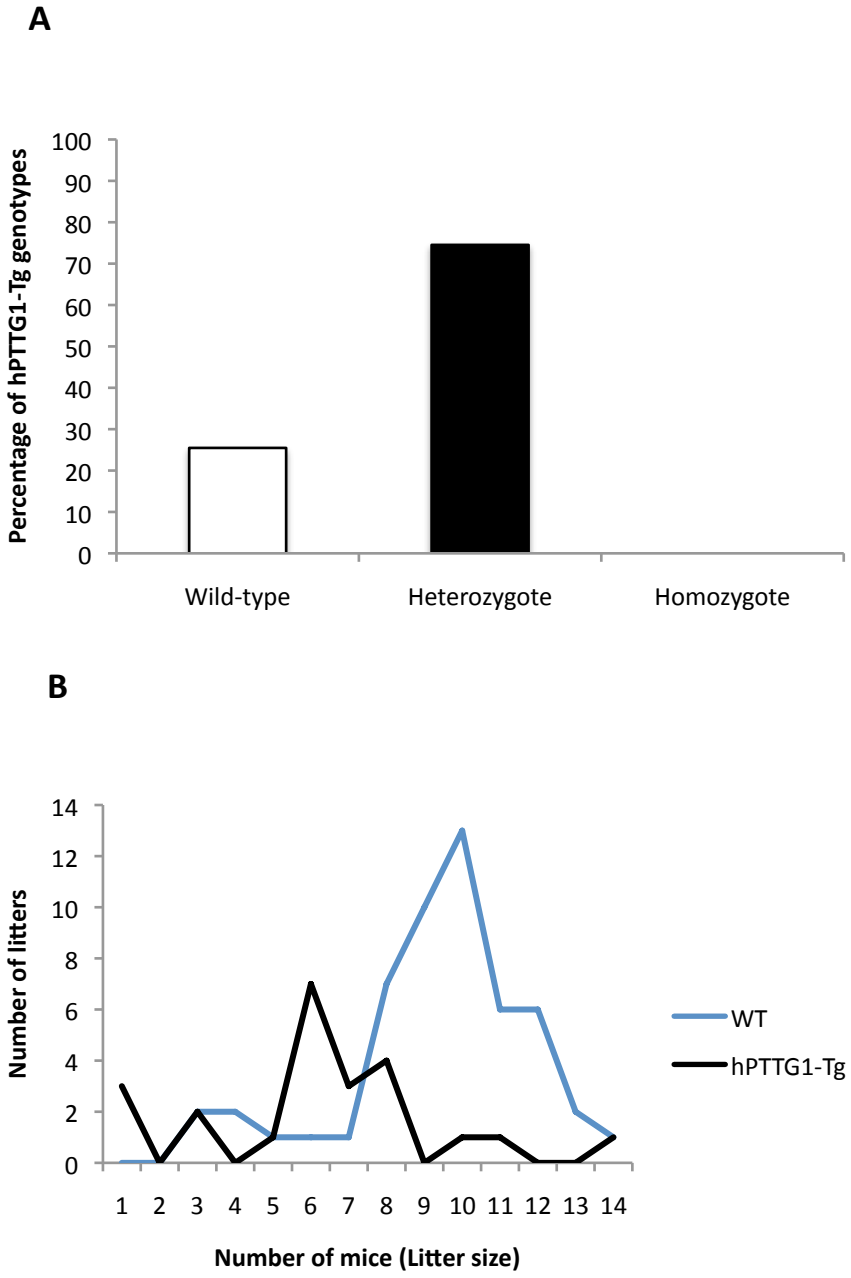

Figure 3.10: ***A.*** *Genotype percentages of offspring following breeding of hemizygote hPTTG1 transgenic mice.* ***B.*** *Number of mice per litter against number of litters comparing wild-type and hPTTG1 transgenic mice.*

3.3.6: hPTTG1 transgenic mice exhibit reduced thyroid size

Wild-type and transgenic mice were weighed to determine overally body weight and then culled at 6-weeks of age. Thyroids were excised and weighed. Body weight was not different when comparing wild-type and transgenic mice (data not shown). Mice were compared by gender to account for differences apparent in thyroid physiology between genders, such as those found in thyroid function tests in our previous PBF-Tg mouse model (lower serum TSH concentration in female mice). Thyroid:body weight ratio was significantly reduced (0.74-fold, $p=5.76x10^{-5}$) in transgenic male (0.08 mg/g ±0.005, n=24) compared to wild-type male mice (0.10 mg/g ±0.003, n=28). Transgenic females (0.10 mg/g ±0.004, n=13) also showed a significantly reduced ratio (0.88-fold, p=0.008) compared to wild-type females (0.11 mg/g ±0.003, n=22), although the reduction was not as pronounced in females compared to males (Figure 3.11).

Transgenic and wild-type mice were aged to 6-months and 12-months to determine long-term effects of hPTTG1 overexpression. At 6-months of age transgenic male mice (0.11 mg/g ±0.005, n=12) demonstrated a significantly reduced thyroid:body weight ratio (0.74-fold, p=0.0004) compared to wild-type male mice (0.14 mg/g ±0.005, n=6). At 6 months the thyroid:body weight ratio in transgenic female mice (0.10 mg/g ±0.013, n=7) was 0.61-fold (p=0.04) reduced compared with wild-type female mice (0.16 mg/g ±0.011, n=2), which represents a greater reduction compared with the difference in male mice, and which is a reversal of the trends observed at 6-

weeks (Figure 3.11). It is possible that this is in part due to a lack of available 6-month old wild-type female mice for testing. Mice at 12-months old showed similar results, with transgenic male mice (0.13 mg/g ±0.008, n=13) showing a significant reduction in thyroid:body weight ratio (0.71-fold, p=0.0027) compared to wild-type male mice (0.18 mg/g ±0.010, n=9), and transgenic female mice (0.10 mg/g ±0.006, n=9) demonstrating a greater reduction (0.57-fold, p=0.0049) compared to wild-type female mice (0.18 mg/g ±0.015, n=6) (Figure 3.11).

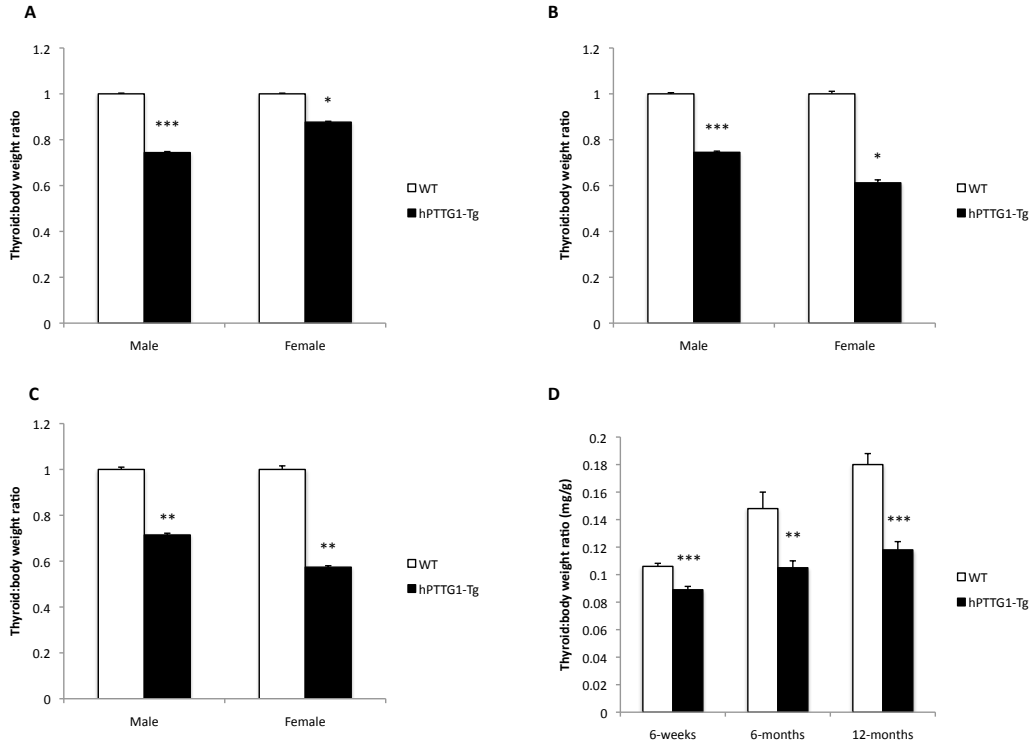

Figure 3.11: Reduced thyroid:body weight ratio in transgenic mice (gender specific) compared to wild-type. ***A.*** *Thyroid:body weight ratio of mice at 6-weeks old.* ***B.*** *Thyroid:body weight ratio of mice at 6-months old.* ***C.*** *Thyroid:body weight ratio of mice at 12-months old.* ***D.*** *Thyroid:body weight ratio of male and female mice together, comparing wild-type to transgenic mice at 6-weeks, 6-months and 12-months of age. (*=p<0.05, **=p<0.005, ***=p<0.0005).*

3.3.7: Histological evaluation of hPTTG1 transgenic thyroids

When dissecting hPTTG1 transgenic mouse thyroid glands, there were no apparent macroscopic abnormalities. Histology slides were prepared from paraffin embedded excised thyroids for use with H&E staining. Subsequent to staining, thyroids were examined at 6-months and 12-months of age, and composite images were formed of individual lobes (Figure 3.12). We confirmed normal thyroid histology in hPTTG1 transgenic mice, which was similar to wild-type mice. Dr Adrian Warfield, consultant thyroid histopathologist at UHB NHS FT, kindly confirmed that follicular structure and thyrocyte number was normal and similar between wild-type and transgenic mice at the various time points. There was no evidence of thyroid hyperplasia or neoplasia.

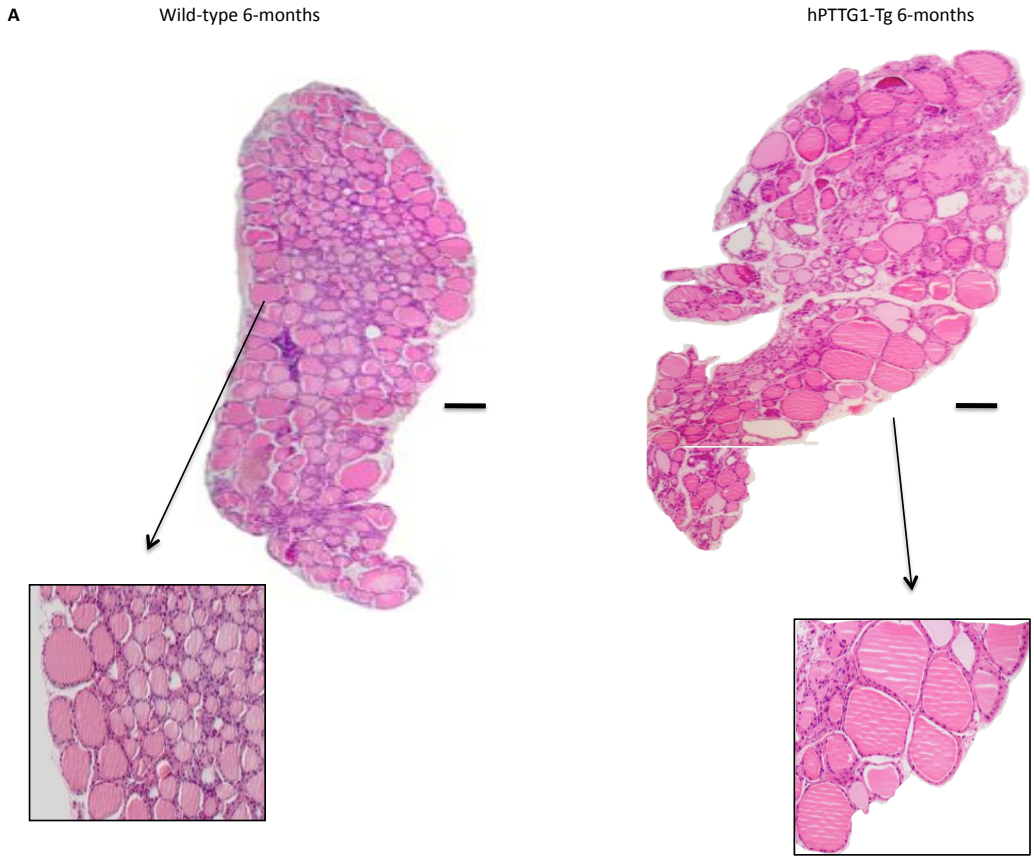
A
Wild-type 6-months
hPTTG1-Tg 6-months
B
Wild-type 12-months
hPTTG1-Tg 12-months

Figure 3.12: H&E stained thyroid lobes from wild-type and hPTTG1-Tg mice. ***A.*** *H&E stained thyroid lobes from wild-type and hPTTG1-Tg mice at 6-months of age, and a section under 20x magnification.* ***B.*** *H&E stained thyroid lobes from wild-type and hPTTG1-Tg mice at 12-months of age, and a section under 20x magnification. Scale bar=100 μm*

3.3.8: Thyroid differentiation markers in hPTTG1 transgenic mice

In order to determine thyroid cell differentiation in our hPTTG1 transgenic model we determined mRNA concentrations of *NIS*, *Tg* and *TshR* in wild-type (n=10) and transgenic mice (n=10). There were no significant differences between wild-type mice (Mean ΔCt=7.64 ±0.15) and transgenic mice (8.62 ±0.21) for *NIS* (1.25-fold, p=0.32), and *Tg* (0.93-fold, p=0.29) also showed no difference comparing wild-type mice (4.57 ±0.16) and transgenic mice (4.92 ±0.14). Likewise, *TshR* mRNA expression was not different (0.82-fold, p=0.33) comparing wild-type mice (9.40 ±0.12) and transgenic mice (9.77 ±0.15) (Figure 3.13).

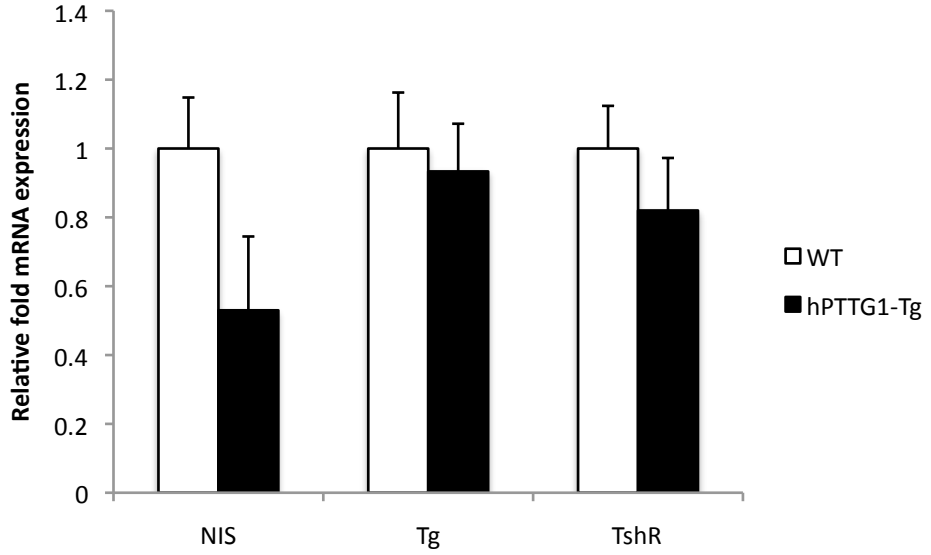

Figure 3.13: mRNA expression of thyroid differentiation markers. Relative fold mRNA expression of murine NIS, Tg and TshR, comparing hPTTG1-Tg mice and wild-type mice.

3.3.8: Thyroid hormone concentrations in hPTTG1 transgenic mice

In order to investigate the effect of hPTTG1 overexpression in the thyroid on circulating thyroid hormone concentrations, serum concentrations of total T3 and T4 were determined alongside concentrations of serum TSH. Serum was extracted from 6-week old mice and subjected to radioimmunoassay for measurement of T3 and T4. Male (n=6, 131.13 ng/dL ±10.07) and female (n=6, 115.88 ng/dL ±8.61) transgenic mice had similar T3 concentrations (male - p=0.175, female – p=0.066) compared to male (n=6, 163.50 ng/dL ±19.77) and female (n=6, 149.19 ng/dL ±13.69) wild-type mice (Figure 3.14).

Similarly there were no differences in male (n=6, 2.64 μg/dL ±0.32) and female (n=6, 4.99 μg/dL ±1.66) transgenic mice T4 concentrations (male – p=0.104, female – p=0.433) compared to male (n=6, 1.96 μg/dL ±0.21) and female (n=6, 3.54 μg/dL ±0.61) wild-type mice (Figure 3.14). To further investigate effects on thyroid function, serum TSH concentrations were determined by Professor Refetoff (University of Chicago) as described in section 2.13. Serum TSH concentrations were not different in male transgenic mice (n=6, 55 mU/L ±10.75) when compared to male wild-type mice (n=6, 48 mU/L ±13.86), however female transgenic mice (n=6, 12 mU/L ±0.52) demonstrated significantly reduced TSH concentrations (0.5-fold, $p<0.05$) compared to wild-type female mice (n=6, 24 mU/L ±3.75) (Figure 3.14). Importantly, 3 out of 5 of the female transgenic mice had a TSH concentration below the limit of detection and therefore required a nominal value to be assigned, which was the lowest value measurable (10 mU/L), and so our results may therefore not be representative of the true concentrations in these mice.

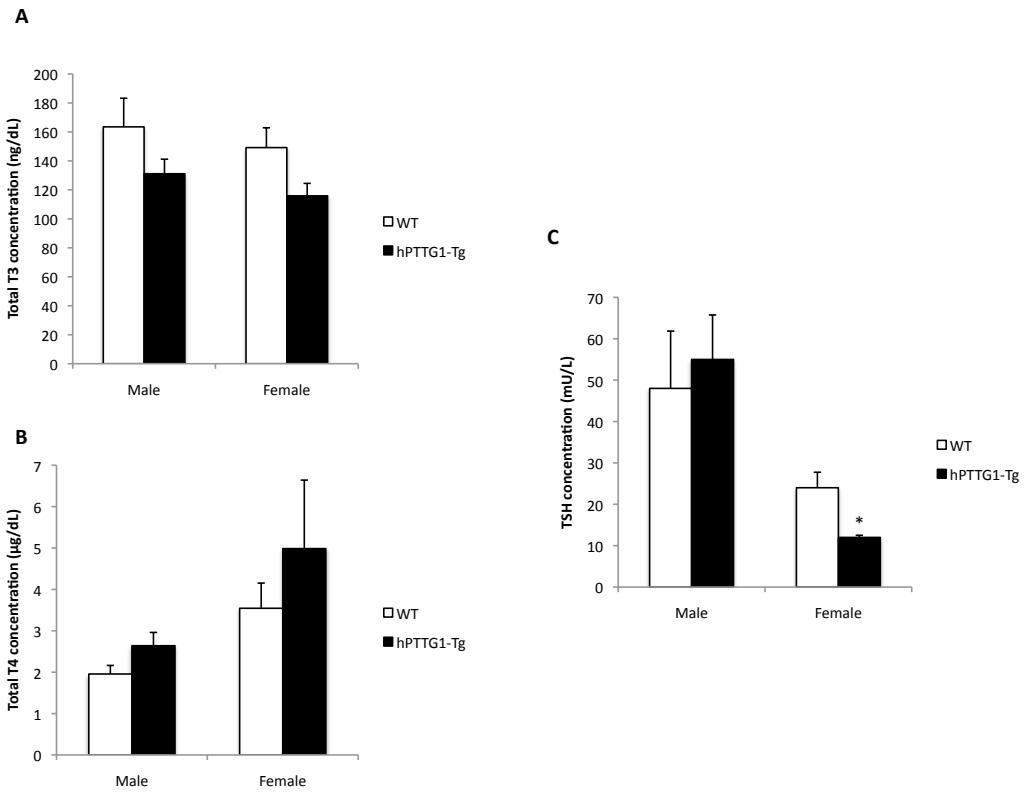

Figure 3.14: Thyroid function tests comparing wild-type mice to transgenic mice. ***A.*** *Total T3 concentration in male and female transgenic mice compared to gender specific wild-type mice.* ***B.*** *Total T4 concentration in male and female transgenic mice compared to gender specific wild-type mice.* ***C.*** *Serum TSH concentration in male and female transgenic mice compared to gender specific wild-type mice. (*=p<0.05).*

3.3.9: Growth factor expression in hPTTG1 transgenic mice

To determine expression of growth factors in hPTTG1 transgenic mice, mRNA from 6-week old wild-type (n=10) and transgenic mice (n=10), males and females grouped together, was used to perform TaqMan Real-time qPCR

using pre-validated TaqMan assays for *Egf*, *Igf1*, *Tgf-α* and *Tgf-β*. No difference was found in *Egf* expression (1.07-fold, p=0.70) when comparing wild-type mice (Mean ΔCt=18.50 ±0.17) to transgenic mice (18.40 ±0.19). Analysis for *Tgf-α* found there was no difference (1.26-fold, p=0.138) between wild-type mice (16.27 ±0.17) and transgenic mice (15.94 ±0.12). As shown in Figure 3.15, *Tgf-β* also demonstrated no difference (1.07-fold, p=0.52) comparing wild-type mice (15.03 ±0.11) to transgenic mice (14.93 ±0.11). In contrast, *Igf1* showed significantly increased mRNA expression (1.47-fold, p=0.048) when comparing wild-type mice (15.08 ±0.20) to transgenic mice (14.52 ±0.17) (Figure 3.15). Furthermore, a positive correlation (r^2=0.634, p<0.05) was found between the mRNA expression of *hPTTG1* and *Igf1* in transgenic mice (Figure 3.15).

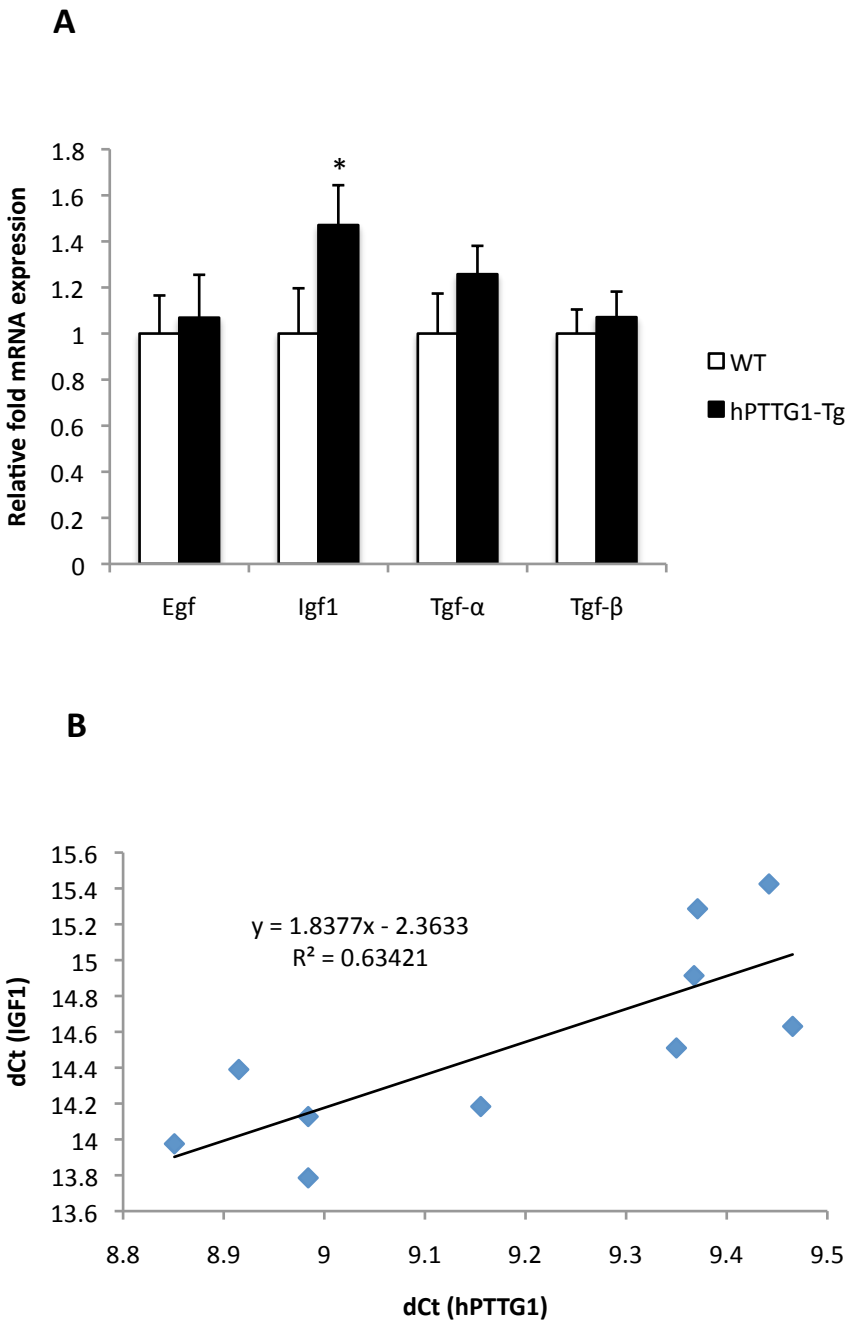

Figure 3.15: mRNA expression of growth factors in Pttg1 knockout mice compared to wild-type. ***A.*** *mRNA expression of Egf, Igf1, Tgf-α and Tgf-β, as determined from TaqMan Real-time qPCR comparing wild-type and transgenic mice.* ***B.*** *Correlation between the mRNA expression of hPTTG1 and Igf1 in transgenic mice. (*=p<0.05).*

3.3.10: Analysis of apoptosis in hPTTG1 transgenic mice

Since hPTTG1 has been shown to promote apoptosis, we set out to determine levels of apoptosis in thyroids of wild-type and transgenic mice. mRNA expression of *Bax* and *Bbc3* (PUMA), two pro-apoptotic genes, was investigated by TaqMan Real-time qPCR in 6-week old transgenic mice (n=10) compared to age-matched wild-type mice (n=10). No difference in *Bax* (0.99-fold, p=0.93) mRNA expression was found comparing wild-type mice (Mean ΔCt=14.90 ±0.25) to transgenic mice (14.92 ±0.11) (Figure 3.16). Analysis of *Bbc3* mRNA expression also showed no difference (0.94-fold, p=0.78) between wild-type mice (16.19 ±0.22) and transgenic mice (16.27 ±0.20) (Figure 3.16).

In addition, levels of apoptosis were investigated using the ApopTag Tunel assay through the use of paraffin-embedded mouse thyroid tissue from wild-type mice (n=4) and transgenic mice (n=4). We assessed 1000 nuclei and determined the percentage that were positively stained. The levels of positive nuclei were similar in wild-type mice (positive nuclei=21.75 ±4.50) and hPTTG1-Tg mice (22.75 ±2.81), confirming that levels of apoptosis were similar between genotypes.

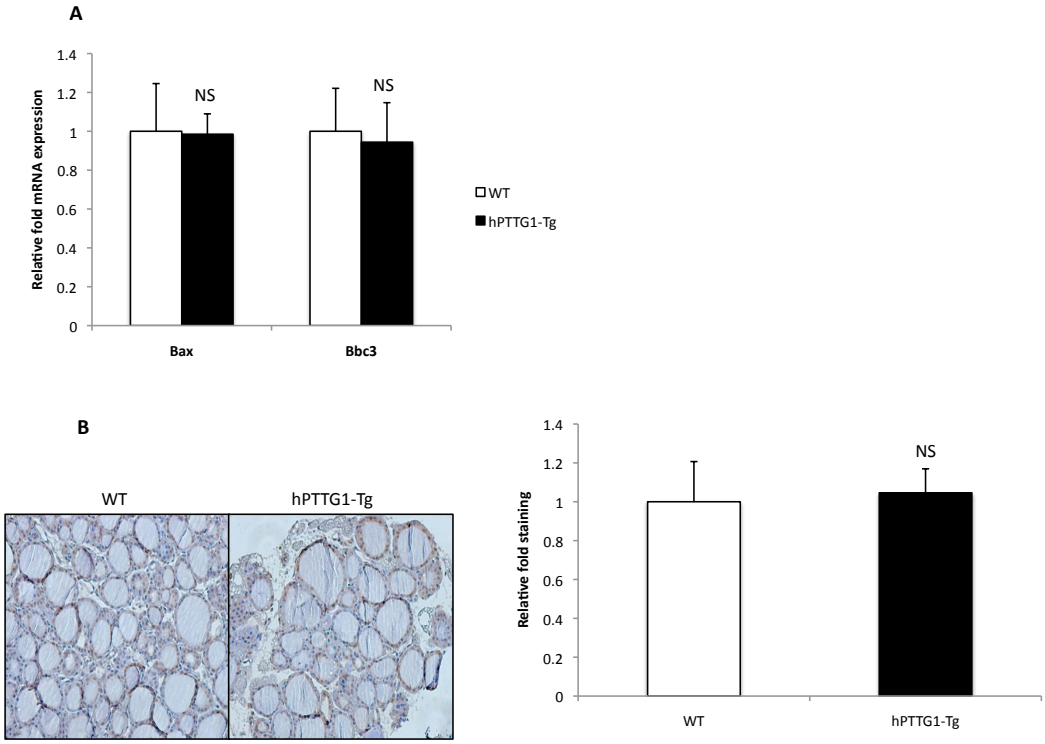

Figure 3.16: Analysis of apoptosis in transgenic mice. ***A.*** *mRNA expression, determined by TaqMan Real-time PCR, of pro-apoptotic genes Bax and Bbc3 in wild-type and transgenic mice.* ***B.*** *ApopTag assay. Pictures display representative pictures of ApopTag assay. Bar graph of ApopTag assay results, comparing wild-type and hPTTG1-Tg mice. (NS=non significant).*

3.3.11: Analysis of cellular proliferation

Investigation of cellular proliferation in mouse thyroids was carried out by measurement of the proliferation markers PCNA, Ki67 and Cyclin-D1. PCNA protein expression was determined via Western blotting, comparing 6-week

old wild-type male (n=4) and female (n=4) mice to age-matched transgenic male (n=4) and female (n=4) mice. β-actin was used as a loading control and to normalise samples for protein concentration to provide data for densitometry analysis. Thyroids from female transgenic mice had significantly reduced PCNA protein expression (0.61-fold, p=0.022) compared with female wild-type mice. Male transgenic mice showed an even greater reduction in PCNA protein expression (0.43-fold, p=0.0031) compared to male wild-type mice, suggesting the reduction in cellular proliferation in transgenic mouse thyroids is greater in males than females (Figure 3.17).

Analysis of Ki67 protein expression was also undertaken using immunohistochemistry of paraffin embedded samples, assessing 1000 nuclei per sample, comparing 6-week old wild-type mice (n=4) with age-matched transgenic mice (n=4). Transgenic mice (positive nuclei=85.0 ±7.52) showed a significantly reduced Ki67 expression (0.60-fold, p=0.0071) compared to wild-type mice (140.75 ±13.30) (Figure 3.18).

Cyclin-D1 protein expression was also measured by immunohistochemistry. Transgenic mice (n=4, positive nuclei=119.5 ±4.50) showed significantly reduced Cyclin-D1 expression (0.59-fold, p=0.015) compared to wild-type mice (203.5 ±9.50) (Figure 3.19). Subsequently, mRNA expression of Cyclin-D1 was measured to determine if the observed reduction in expression was due to a transcriptional change. 6-week old wild-type mice (n=10) were compared to age-matched transgenic mice

(n=10). Transgenic mice (Mean ΔCt=15.11 ±0.07) showed no difference (0.96-fold, p=0.64) compared to wild-type mice (15.06 ±0.09).

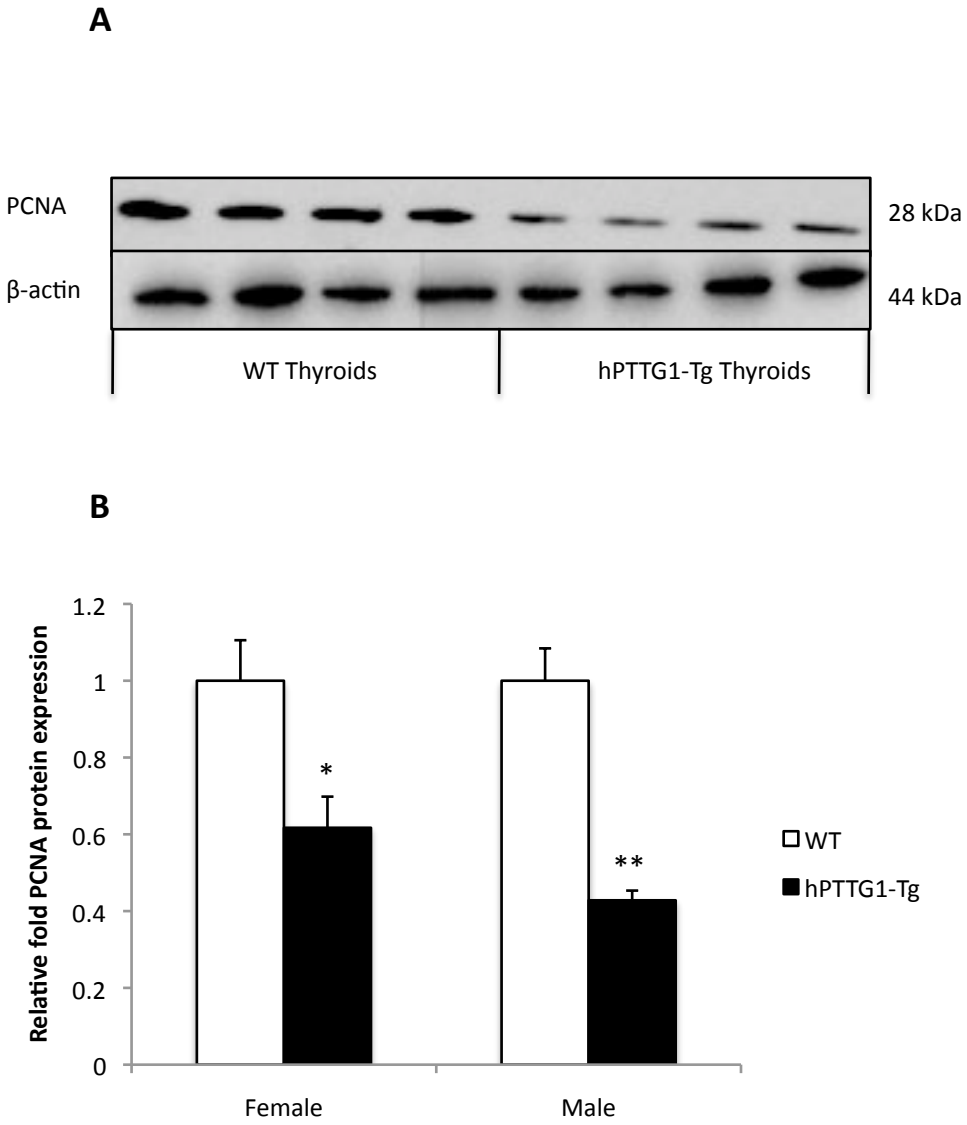

Figure 3.17: PCNA *protein expression is significantly reduced in transgenic mice compared to age-matched wild-type mice.* ***A.*** *Representative Western blot displaying reduced* hPTTG1 *expression in transgenic mouse thyroids compared to wild-type. β-actin is shown as a loading control.* ***B.*** *Densitometry of* PCNA *protein expression from Western blot studies, showing reduced* PCNA *expression in female and male transgenic mouse thyroids compared to wild-type. (*=p<0.05, **=p<0.005).*

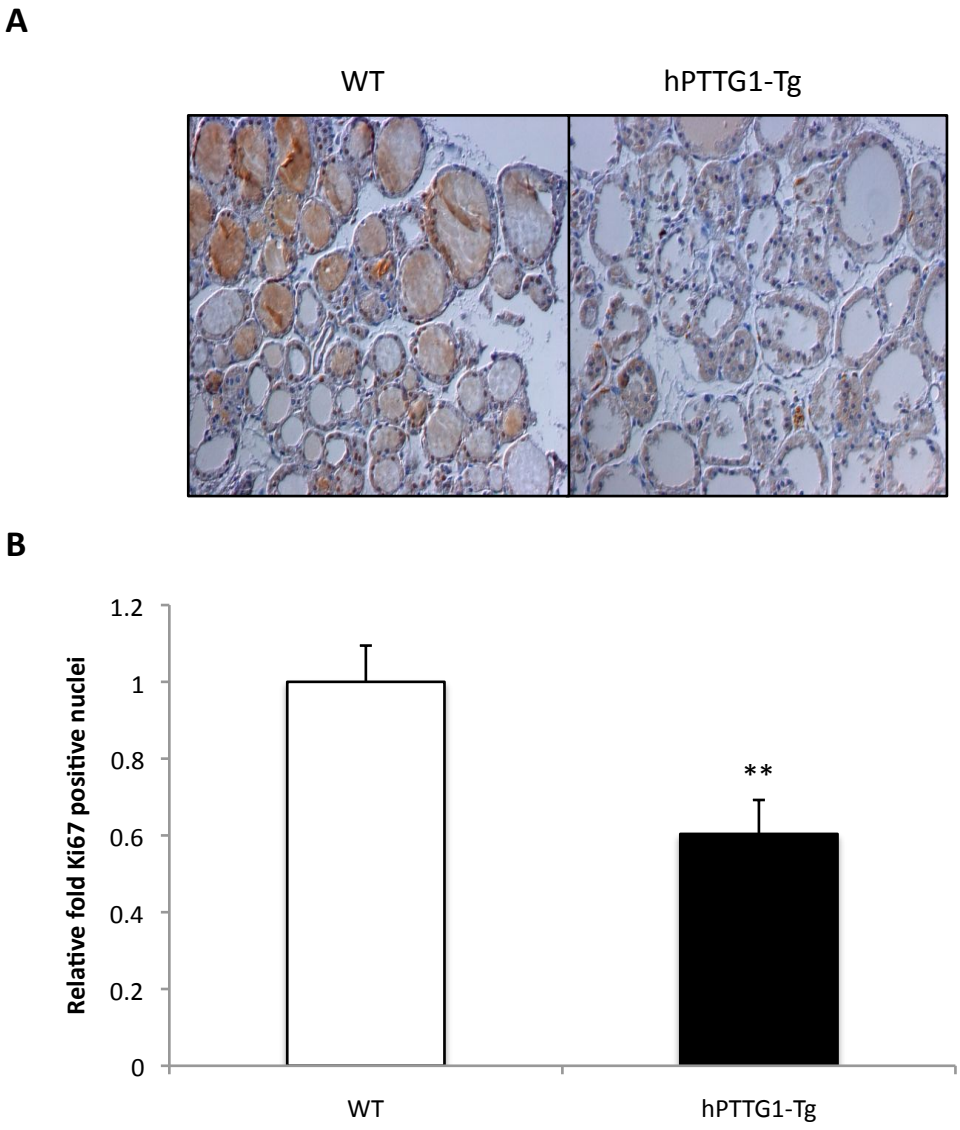

Figure 3.18: Ki67 *protein expression is significantly reduced in transgenic mice compared to age-matched wild-type mice.* ***A.*** *Representative microscope photos of wild-type and transgenic thyroids stained for* Ki67. ***B.*** *Bar graph of relative fold difference between wild-type and transgenic thyroids. (**=p<0.005).*

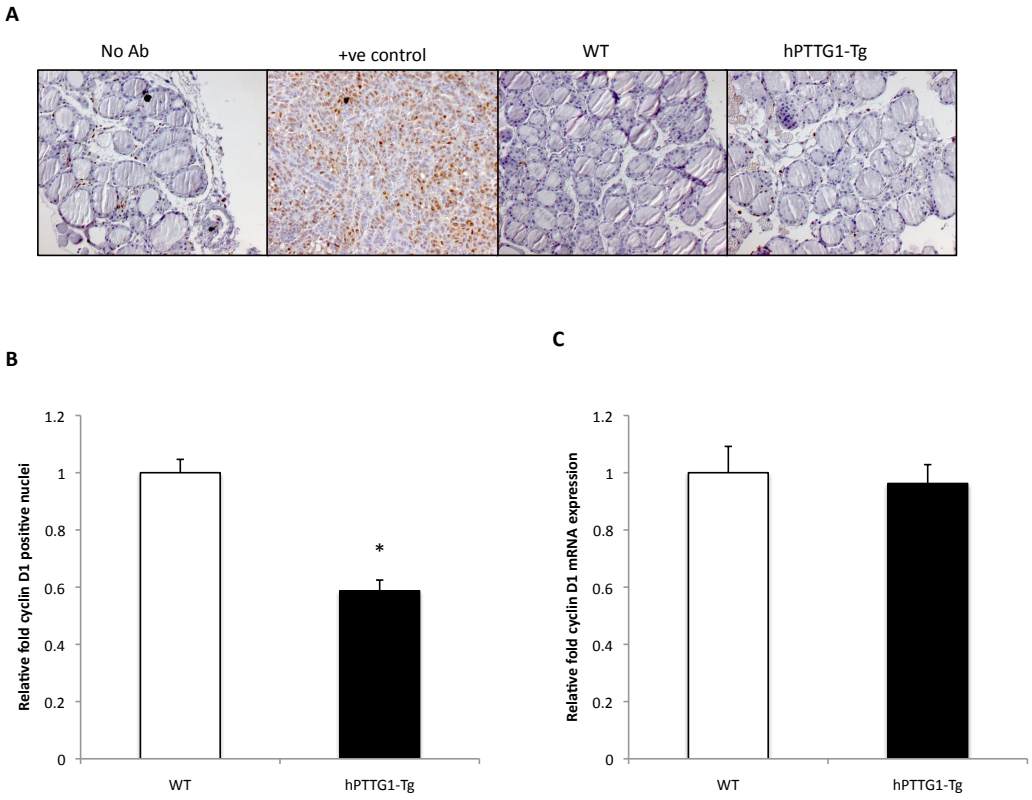

Figure 3.19: Cyclin-D1 *expression is significantly reduced in transgenic mouse thyroids compared to wild-type.* ***A.*** *Representative microscope photos of wild-type and transgenic thyroids stained for* Cyclin-D1*. A no antibody and positive lung tumour sample control are also shown.* ***B.*** *Bar graph of relative fold difference between wild-type and transgenic thyroids.* ***C.*** *Relative fold Cyclin-D1 mRNA expression in wild-type and transgenic mouse thyroids. (*=p<0.05).*

3.4: Discussion

3.4.1: Identification of hPTTG1 transgenic founder mice

Genotyping of mice to identify founder mice was performed using two methods. Conventional PCR was used with two primer sets for *hPTTG1* to increase the chance of detection (Figure 3.3), and TaqMan Real-time qPCR was also performed using specific pre-validated human primers for *hPTTG1* (Figure 3.4). A total of 171 microinjected mice were screened using these techniques and two positive mice were identified, providing a success rate of 1.17%, which seems significantly lower than the 10% success rate we had when generating our previous hPTTG1-FLAG model, although the technique is inherently quite random (Gordon et al, 1980). The two mice positively identified were labelled as 'A' and 'B', and were subsequently bred with wild-type mice to propagate the potential colonies. Following the birth of offspring from these founder mice, we found 99.7-fold *hPTTG1* mRNA expression in line A and 2633.1-fold in line B, indicating a significantly greater expression of *hPTTG1* in line B compared to line A (Figure 3.5). Subsequently we determined hPTTG1 protein expression. We had anticipated that the HA-tag present on the transgene would provide a straightforward method of testing for transgene expression, especially since the commercial antibody used by our group is extremely sensitive (Smith et al, 2009). Surprisingly, transgene expression was not detected following use of a HA antibody. This suggests that either the tag is cleaved at a point of

post-transcriptional or post-translational processing, or protein folding results in the inability of the antibody to detect the tag. Subsequent to this, probing of protein samples with a hPTTG1 antibody demonstrated expression of hPTTG1 in line B mice but no expression was detected in line A mice (Figure 3.6). It is possible that hPTTG1 protein was not present in line A mouse thyroids or that the hPTTG1 antibody lacked the sensitivity to detect low levels of expression of the hPTTG1 protein in line A mice. Following this finding, mice from line A were terminated and line B mice were used as the sole transgenic line. Use of two transgenic lines, one possessing relatively high overexpression of hPTTG1 and the other possessing a relatively low level of overexpression, more coincident with physiological expression levels found in thyroid cancer, would be the 'gold standard', although detection of hPTTG1 protein expression is clearly a requirement in a transgenic mouse model. The co-existence of a low and high expressing mouse model would have allowed us to determine dose dependent effects of hPTTG1, as these effects have been shown previously by our group to be an important factor in hPTTG1 effects on cellular proliferation (Boelaert et al, 2003). Comparing expression levels of hPTTG1 in four different transgenic mice we found differences in expression of hPTTG1, suggesting mice possessed varying levels of hPTTG1 expression (Figure 3.6). This is most likely due to differences in transgene copy number in different mice, as discussed further in this chapter in Section 3.4.3. Interestingly, hPTTG1 protein bands detected in mouse thyroids displayed a doublet at times, demonstrating phosphorylation of hPTTG1 in mice and

suggesting normal cellular processes were intact (Figure 3.6). Immunohistochemistry was subsequently performed to validate protein expression of hPTTG1 in line B mice and to determine subcellular localisation. As seen in Figure 3.6, there was nuclear and cytoplasmic localisation of hPTTG1 present in thyrocytes, suggesting normal cellular processing of hPTTG1 in mouse cells, thereby suggesting a functional role for the transgene in mouse cells (Saez et al, 1999). However, hPTTG1 expression was not evident in every thyrocyte, although a likely explanation for this is that formalin fixation, and associated cross-linking, can mask epitopes, resulting in reduced immunoreactivity (Arnold et al, 1996).

3.4.2: Verification of thyroid specificity

Having confirmed hPTTG1 expression in our transgenic line we sought to determine thyroid specificity of the transgene in our mouse model. In order to investigate effects of hPTTG1 overexpression on the thyroid gland, it is important to demonstrate that effects are not in part due to hPTTG1 overexpression in other organs. We found high levels of *hPTTG1* mRNA expression present in thyroid glands, and also 67.7-fold expression in lung tissue. Use of the bovine thyroglobulin promoter should hypothetically only be subject to activation in thyroid cells by thyroid transcription factors such as PAX8, TTF1 and TTF2 (Kang et al, 2001) (Civitareale et al, 1993) (Noseda et al, 2005). However, Tg promoter activity has not yet been fully

investigated and so-called 'leaky' activity of the promoter is possible. Further it is plausible that random integration of the transgene occurred at a site that is in close proximity to a promoter specific to lung cells, thereby causing expression in lung tissue. Our recent PBF transgenic mouse model using the same bovine thyroglobulin promoter also reported detectable *PBF* mRNA expression in lung tissue. As it is unlikely that the *hPTTG1* transgene and *PBF* transgene have integrated at an identical site, it seems likely that promoter activation in lung cells is responsible. Indeed, TTF1 expression has been reported in lung cells (Boggaram, 2009), and it is plausible that TTF1 caused promoter activity and expression of the transgene in the lung. However, there was no hPTTG1 protein expression detected in lung tissue (Figure 3.7). This could be due to degradation of *hPTTG1* mRNA by lung cells, or lack of sensitivity of the hPTTG1 antibody and failure to detect expression.

3.4.3: Propagation of transgenic line

In order to generate mice for subsequent investigations, hemizygote mice were bred. A zygosity assay using TaqMan Real-time PCR was used to determine mouse zygosity. The assay was highly reliable, with wild-type, hemizygote and homozygote controls from our previous hPTTG1-FLAG transgenic line showing consistent results, homozygote mice presenting with double the transgene copy number of hemizygote mice and no expression detected in wild-type mice. Original estimates placed transgene copy

number at n=30 (Figure 3.9), approximately double the number observed in homozygote mice of our previous hPTTG1-FLAG transgenic model. However, there was no clear doubling of transgene copy number in offspring of hemizygote mice bred, instead a range of copy numbers between 25-45 was found in the offspring. This made it extremely difficult to determine if any offspring were indeed homozygote mice. Random integration of transgenes has previously been reported as mainly occurring as head-tail concatemers at the same site (Bishop and Smith, 1989). However, if random integration of the transgene has occurred on different chromsomes, it is possible chromosomes with different transgene copy numbers are randomly distributed in meiosis, resulting in the differences observed. This has been observed previously in plant cells subject to microinjection of transgenes (Mason et al, 2003). Other techniques we could have used to distinguish between hemizygote and homozygote mice include FISH (Fluorescent in-situ hybridisation), although testing each mouse by this method was beyond the scope of this study. Whilst we were unable to test differences between hemizygote and homozygote mice, the level of hPTTG1 transgene expression was established to be several thousand fold, suggesting sufficient proto-oncogene expression was present.

Subsequent investigations of litter sizes found a significant 19.74% reduction in litter size breeding hemizygote mice compared to wild-type mice (Figure 3.10). This suggested either subfertility of mice or lethality when the transgene is expressed in homozygote mice. Embryonic lethality would explain the lack of detection of clear homozygote mice by the zygosity

assay. Indeed, homozygote mice from our previous hPTTG1-FLAG transgenic line showed significant illness resulting in death from 3-months of age, and since significantly greater expression of hPTTG1 was present in the hPTTG1-HA line, it is possible that a dose-dependent effect of hPTTG1 resulted in embryonic lethality of homozygote mice. These findings could be partially explained by our previous study, which showed that effects of hPTTG1 on cell proliferation are dependent on the level of expression (Boelaert et al, 2003). If high levels of hPTTG1 expression were present this may inhibit cell cycle division and lead to an inhibition of tissue formation.

It is also possible that random integration occured at a site which would prove lethal if present on both chromosomes, potentially resulting in silencing of important genes. Taking embryos at certain stages of development and determining zygosity could have investigated this further, however this was again not within the scope of this study. Further to these investigations it was decided to use hemizygote mice for future experiments as these provided a high level of overexpression of our transgene and we thought it unlikely that physiological differences between hemizygote and homozygote mice would be observed.

3.4.4: hPTTG1 transgenic mice exhibit reduced thyroid size

Thyroids were excised and weight was determined at 6-weeks, 6-months and 12-months. Thyroid weight was normalised for body weight of individual

mice by determining a thyroid:body weight ratio. There was a significant reduction in the thyroid:body weight ratio of male and female transgenic mice compared to wild-type mice at 6-weeks (Figure 3.11), with male mice showing a 0.26-fold reduction and female mice a 0.12-fold reduction. However, this trend was reversed by 6-months of age, with male mice showing a 0.26-fold reduction as previously, but female mice showing a 0.39-fold reduction. This was also apparent at 12-months of age, with male mice showing a 0.29-fold reduction and female mice a 0.43-fold reduction.

Histological evalutation of excised thyroids revealed normal histology (Figure 3.12), with normal follicle size and no evidence of altered thyrocyte proliferation. Normal thyroid differentiation was confirmed by mRNA expression of *NIS*, *Tg* and *TshR*, which was not different between wild-type and transgenic mice. Thyroid hormone concentrations were measured in 6-week old mice to determine if hPTTG1 overexpression resulted in changes to thyroid function. Total T3 and total T4 showed no difference between wild-type and transgenic mice, regardless of gender. Measurement of serum TSH showed no differences between male wild-type and transgenic mice, although female transgenic mice showed a significantly reduced TSH concentration (0.5-fold) compared to wild-type mice. The reliability of these results is doubtful as there were detection issues as outlined in section 3.3.8. Taken together we concluded that there was no significant change in thyroid function caused by overexpression of hPTTG1 and that the reduction in thyroid weight could not be explained by thyroid dysfunction.

3.4.5: Growth factor expression in hPTTG1 transgenic mice

Growth factors and hPTTG1 have been linked by many studies, with several implicating a role for hPTTG1 in angiogenesis through upregulation of growth factors such as VEGF and FGF-2 (Heaney et al, 1999) (Heaney et al, 2000) (Ishikawa et al, 2001). Recent research by our group (Ryan et al, 2013) has indicated that growth factors EGF, IGF-1 and TGF-α can regulate hPTTG1 expression, and their expression can in turn be regulated by hPTTG1 in thyroid cells. The association with growth factors indicates that hPTTG1 acts as an autocrine/paracrine growth factor activator, with a feedback loop occurring in which these growth factors serve to reinforce hPTTG1 expression, thereby stimulating tumour growth. Based on these data we investigated expression of growth factors in thyroids of our model to determine if the reduced thyroid weight was due to altered growth factor expression. mRNA expression of *Egf*, *Igf-1*, *Tgf-α* and *Tgf-β* was determined. There was no difference in *Egf*, *Tgf-α* and *Tgf-β* mRNA expression, while *Igf-1* mRNA expression was found to be significantly increased in transgenic mouse thyroids when compared with wild-type. Further, *Igf-1* mRNA expression was positively correlated with *hPTTG1* mRNA expression. These findings support regulation of *Igf-1* by hPTTG1 *in vivo*, lending further credence to previous findings *in vitro* (Ryan et al, 2013). In contrast, *Egf* and *Tgf-α*, which were regulated by hPTTG1 in our *in vitro* studies (Ryan et al, 2013), showed no difference in mRNA expression when comparing

transgenic mice and wild-type mice. We wanted to determine changes in protein expression of these growth factors but effective antibodies for Egf and Tgf-α proved difficult to obtain. Parallel research by our group, using ELISAs to determine protein secretion in mouse primary thyrocytes, showed no difference in Igf-1 protein levels, although Egf showed a significantly increased protein secretion in hPTTG1-FLAG transgenic mice compared to wild-type mice (Ryan et al, 2013). A possibility as to why some growth factor effects observed *in vitro* were not observed *in vivo* is that the reduced cellular proliferation is mitigating any effects of hPTTG1 on growth factors, although this would be difficult to test. Overall our transgenic mouse model has not confirmed the *in vitro* regulatory effects of hPTTG1 on growth factors, although studies have been limited by technical problems and cellular proliferation changes that were evident.

3.4.6: Analysis of apoptosis in hPTTG1 transgenic mice

Effects of hPTTG1 on apoptosis have proved controversial. Apoptosis was increased in JEG-3 cells following hPTTG1 overexpression (Yu et al, 2000), and studies involving wild-type p53 MCF7 cells and p53 null MG-63 cells showed p53-dependent and p53-independent apoptosis upon hPTTG1 overexpression (Yu et al, 2000). However, Bernal et al found that hPTTG1 was capable of binding specifically to p53 and preventing transcriptional activation of p53-induced downstream genes, thereby inhibiting apoptosis

(Bernal et al, 2002). We tested apoptosis levels in our transgenic mouse model to further characterise our model and to determine if apoptosis was a causative factor in the observed reduction in thyroid weight. mRNA expression of p53 induced pro-apoptotic genes *Bax* and *Bbc3* was not different when comparing transgenic and wild-type mice. However, since we are using a human PTTG1 transgene it is possible that the hPTTG1 protein could not interact specifically with mouse p53 as reported by Bernal et al, although phosphorylation of the transgene, found by Western blotting, and subcellular localisation of hPTTG1 in both the nucleus and cytoplasm, suggest normal cellular processing of the transgene. Use of the ApopTag Tunel assay provided another means of testing apoptosis levels. Using paraffin embedded slides of thyroid tissue from wild-type and transgenic mice we found no difference in apoptosis levels (Figure 3.15). These results indicate that there was a similar level of apoptosis in thyrocytes of our transgenic model to that in wild-type thyroid cells. As hPTTG1 induced apoptosis has been proposed to be a response to aneuploidy, it is possible that thyroid cells in our transgenic mouse model are not showing increased apoptosis levels as there is a lack of aneuploidy. Aneuploidy has been reported to be increased in MG-63 and H1299 cells overexpressing hPTTG1 (Yu et al, 2000), although compensatory mechanisms have been suggested to exist. However, these experiments were carried out in cancer cell lines, which have many DNA damage response pathways inactivated or altered, and may not be representative of conditions in thyroid cells of our transgenic mouse model.

3.4.7: Analysis of cellular proliferation

In order to investigate the cause of the reduced thyroid weight we tested expression levels of several cellular proliferation markers on 6-week old wild-type and transgenic mice. PCNA expression showed a significant 0.39-fold reduction in female transgenic mice and a significant 0.57-fold reduction in male transgenic mice, suggesting cellular proliferation is decreased in thyroid cells of our transgenic model compared to wild-type mice. The gender effect also lends credence to the implication that the effect on thyroid weight is due to cellular proliferation, as at 6-weeks male mice showed a greater reduction in thyroid weight than female mice, which is replicated by the PCNA expression data. Analysis carried out on the proliferation marker Ki67 revealed a significant 0.40-fold reduction in expression in transgenic mouse thyroids compared to wild-type mice, and testing of Cyclin D1 protein expression also revealed a significant 0.41-fold reduction in expression in transgenic mice compared to wild-type mice. These data confirm that cellular proliferation is reduced in transgenic mice compared to wild-type mice and provides a basis for the reduced thyroid weight observed. In order to test whether the reduced cell proliferation was transcriptionally regulated, we examined mRNA expression of *Cyclin-D1*. Results revealed no difference between wild-type and transgenic mice, suggesting the effect on Cyclin-D1 expression was post-transcriptional. These results confirmed previous research showing inhibition of proliferation following hPTTG1

overexpression in HeLa, A549, JEG-3 and H1299 cells (Mu et al, 2003). Hamid et al. in contrast, reported increased proliferation following hPTTG1 ovexpression in HEK-293 cells (Hamid et al, 2005), and NIH3T3 cells also showed increased proliferation (Kakar and Jennes, 1999). Results by our own group suggest hPTTG1 effects on cell proliferation are dependent on expression levels. In NT-2 cells proliferation was increased following low overexpression of hPTTG1, whereas high overexpression resulted in inhibition of cellular proliferation (Boelaert et al, 2003). These results imply cell-type specific effects and dependency on expression levels. Results from our transgenic mouse model also suggest that high expression levels inhibit cell proliferation and it would have been useful to investigate a second line with low overexpression to determine if this was the case. However, random integration of the transgene would make generating a low expression transgenic line a difficult proposition. The cause of the reduced cell proliferation is possibly due to blockage of the cell cycle, as reported in several cell lines (Yu et al, 2000) (Yu et al, 2000,b) (Bernal et al, 2002), where cells accumulated in G_2M phase. It would be useful to perform FACS analysis on primary thyrocytes from wild-type and transgenic mice to determine differences in cell cycle, but this was beyond the scope of this project. Taken together, our transgenic mouse model has provided important information regarding the *in vivo* effects of hPTTG1 overexpression on cellular proliferation.

3.4.8: Conclusions

In conclusion, we generated a transgenic mouse model with thyroid specific overexpression of hPTTG1. Levels of overexpression were high and transgenic mice showed reduced thyroid weight at 6-weeks, 6-months and 12-months of age compared to wild-type mice. Thyroid function tests demonstrated no difference between wild-type and transgenic mice, and mRNA expression tests of growth factors revealed *Igf-1* to be significantly increased and positively correlated with hPTTG1 expression. There was no difference in apoptosis levels between wild-type and transgenic mice, however expression levels of cellular proliferation markers PCNA, Cyclin D1 and Ki67 showed reduced expression in transgenic mice compared to wild-type, suggesting reduced cellular proliferation resulted in reduced thyroid size. Although there were technical difficulties and the level of overexpression was not coincident with physiological levels, the use of our transgenic mouse model and subsequent experiments provide important data on *in vivo* effects of hPTTG1 overexpression, and complements data from several *in vitro* studies suggesting reduced proliferation upon hPTTG1 overexpression.

Chapter 4. Characterisation of thyroids of *Pttg1* knockout mice

4.1: Introduction

Knockout of genes in transgenic models has led to a wealth of information on gene function and phenotypic effects of LOH and loss of protein function. Previous research has focused on generating a knockout murine model, which sought to investigate the effects of lack of *Pttg1* (Wang et al, 2001). This was achieved using a construct containing the *Pttg1* containing a 4 Kb deletion in the first exon, which included the ATG start codon, second and third exons and the middle of the third intron. The sequence was replaced by pGK-neo. The construct was subsequently injected into 800 J1 embryonic stem (ES) cells, and 5 clones were identified which had correctly inserted by homologous recombination. Following this the ES cells were injected into blastocysts from C57BL6 mice and chimeras were crossed to produce *Pttg1* knockout mice (Wang et al, 2001).

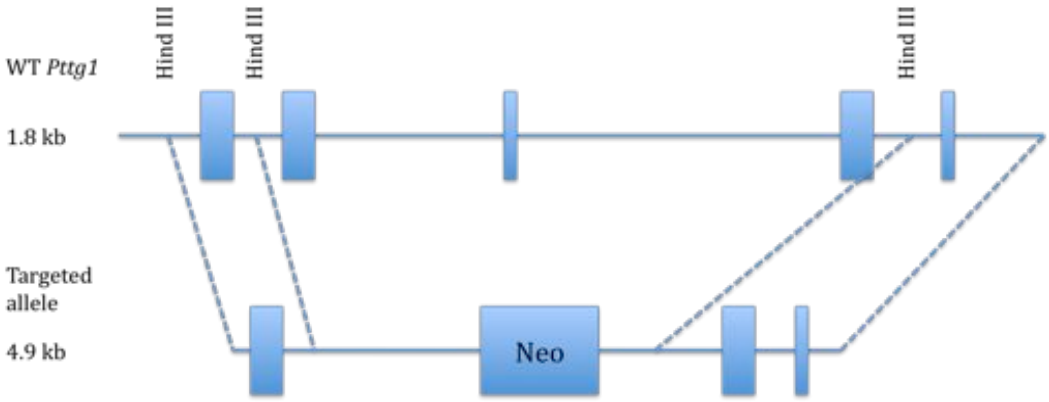

Figure 4.1: Genomic structure of wild-type Pttg1 and targeting construct. Blue bars represent exons with Neomycin labelled as Neo. HindIII-EcoRI restriction sites are labelled. Targeting construct has exons 2, 3 and part of exon 1 replaced with a Neomycin cassette.

Generation of the *Pttg1*-null mice showed deletion of the *Pttg1* gene is viable and mice are fertile (Wang et al, 2001). This confirms the function of *Pttg1* in the cell cycle (section 1.2.4.1) is not crucial for life and suggests there is more than one mechanism to ensure appropriate sister chromatid separation. It seems plausible that such a crucial process requires redundant mechanisms. Tissue specific defects were present in *Pttg1*-null mice, such as testicular and splenic hypoplasia, thymic hyperplasia and thrombocytopenia (Wang and Melmed, 2001). Testicular hypoplasia was found to be greater in sexually matured mice, although splenic hypoplasia was observed following weaning. Thymic hyperplasia was first observed four weeks following birth, and present during the full eight months of investigation. Pancreatic β-cell hyperplasia was also evident, albeit only in male mice (Wang et al, 2003). The deletion of *Pttg1* led to a disruption in glucose homeostasis and

eventually resulted in diabetes. This was found to be related to insulinopenia, a reversed α/β cell ratio and nonautoimmune islet damage. The β-cells of knockout mice also presented with pleiotropic nuclei, indicating effects of *Pttg1* deletion upon cell division.

The effect of *Pttg1* deletion on the cell cycle was less evident. Following extraction of MEFs from knockout and wild-type mice, it was observed that these cells had similar doubling times. MEFs from knockout mice displayed a shorter G1 phase and a longer G2 phase compared to wild-type mice, although this effect was partially reversible by transfecting *Pttg1* into knockout MEFs (Wang et al, 2001). On investigation, *Pttg1 -/-* MEFs displayed damaged nuclei and abnormal chromosome morphology, such as tri-radials, quadric-radials, chromosome breaks, multinucleated nuclei and signs of aneuploidy.

Research has also demonstrated an effect of Pttg1 on cellular senescence. Cellular senescence is a well-established process of permanent cell cycle arrest caused by a number of factors. It was first discovered *in vitro* in 1961 (Hayflick and Moorhead, 1961), and can be instigated by oxidative and genetic stress, such as chromosomal instability (Sharpless and Depinho, 2004). This subsequently leads to accumulation of p53, induction of p21 and Rb phosphorylation (Schmitt et al, 2002) (Campisi, 2005). Senescent cells are distinct in exhibiting a flat morphology and cells express SA- β-gal activity (Dimri et al, 1995). This was observed in experiments investigating the deletion of *Pttg1* on pituitary tumour development. Mice that contain a single Rb mutant allele develop pituitary tumours at close to 100%

penetrance (Jacks et al, 1992) (Hu et al, 1994) (Classon and Harlow, 2002). Chesnokova et al sought to examine *Pttg1* effects on pituitary tumourigenesis by generating compound *Rb* x *Pttg1* mutant mice (Chesnokova et al, 2005). *Pttg1 -/-* mice demonstrated pituitary hypoplasia, whereas compound *Rb* x *Pttg1* mice showed only 30% penetrance of pituitary tumours, suggesting the pituitary hypoplasia caused by *Pttg1* deletion can promote a reduction in pituitary tumour formation. Furthermore, *Pttg1* mouse pituitary glands had increased expression of p21, a potent cyclin-dependent kinase inhibitor, and increased p21 upregulation was linked to Cdk2 suppression, reduced phosphorylation of Rb and Cyclin A expression, which have been implicated in suppression of cell cycle progression (Chesnokova et al, 2007). Subsequently experiments showed increased p21 expression caused cellular senescence of pituitary cells, as evidenced by increased levels of senescence-associated β-galactosidase (Chesnokova et al, 2008).

In vitro experiments have confirmed that *hPTTG1* depletion in AtT20 mouse corticotrophs was associated with increased p21 expression (Chesnokova et al, 2005). However, increased p21 expression has also been observed in cells overexpressing hPTTG1, with growth arrest, by a p21-dependent mechanism, observed in human A549 lung cancer cells following hPTTG1 overexpression (Mu et al, 2003). This was also true for GH3 rat pituitary cells, which displayed increased p21 mRNA and protein levels following hPTTG1 overexpression (Chesnokova et al, 2008).

The research described has shown deletion of *Pttg1* to result in a variety of tissue specific defects. However, no research has been conducted

on the deletion of *Pttg1* in the thyroid gland. Therefore, we sought to characterise the thyroid gland of the *Pttg1* knockout mouse to discover if *Pttg1* deletion caused effects on thyroid cells. We also investigated effects of *hPTTG1* depletion in thyroid cancer cells *in vitro*.

4.2: Materials and Methods

4.2.1: Murine studies

Murine experiments were carried out as described in section 2.1. *Pttg1* knockout mice were kindly provided by Professor Melmed (Cedars Sinai Research Institute, Los Angeles, California, USA). As *Pttg1* knockout mice are sub-fertile, heterozygote mice were bred to produce wild-type and knockout mice for subsequent experiments.

4.2.2: Cell lines

TPC1 and K1 cells were cultured and maintained as outlined in section 2.2. TPC1 cells were seeded at 1.875 $x10^6$ per 25 cm^2 surface growth area. K1 cells were seeded at 2.5 $x10^6$ per 25 cm^2 surface growth area.

4.2.3: siRNA transfection

siRNA transfection was performed using siRNA targeted to *hPTTG1* (Life Technologies Ltd, Paisley, UK). Transfections were carried out in TPC-1 cells, using NeoFX siPORT (Ambion, Life Technologies Ltd, Paisley, UK) as the transfection reagent complexed with the siRNA. Cells were seeded and

transfection was performed 24 hours later according to manufacturer's instructions. Total RNA or total protein was subsequently harvested 48 hours post-transfection.

4.2.4: DNA extraction and quantification

DNA extraction and quantification of mouse thyroid samples was performed as described in section 2.5.

4.2.5: RNA extraction and quantification

RNA extraction and quantification of mouse thyroid samples were carried out as described in section 2.6.

RNA was extracted from cell lines and quantified as described in section 2.6.

4.2.6: Protein extraction and quantification

Protein extraction and quantification of mouse thyroid samples was performed as described in section 2.7.

Protein was extracted from cell lines and quantified as described in section 2.7.

4.2.7: Reverse transcription

Total RNA was reverse transcribed to cDNA, performed as described in section 2.8.

4.2.8: Mouse genotyping

Conventional PCR was used to genotype pttg knockout mice. As heterozygote mice were bred, genotyping was required to determine which mice were wild-type and knockout for subsequent experiments. Primer sequences are shown in figure 4.2. PCR was performed as described in section 2.9 and gel electrophoresis using a 1.5% agarose gel was carried out to visualise results.

4.2.9: qPCR

qPCR was used to determine expression of specific mRNAs. Experiments were performed as described in section 2.10, and pre-optimised specific gene assays (Applied Biosystems, Life Technologies Ltd, Paisley, UK) were used to determine expression levels.

4.2.10: Histology

Mouse thyroid glands taken for histology were fixed in formalin immediately after removal. Tissue was then paraffin embedded and either left for immunohistochemistry experiments, or stained for Hematoxylin and Eosin, by the Cellular Pathology Department of the University Hospital Birmingham.

4.2.11: Immunohistochemistry

Immunohistochemistry was performed as described in section 2.12. Sections of thyroid tissue were viewed under a light microscope (Zeiss Oberkochen, Germany) and imaging performed using Axiovision software.

Antibodies used were anti-Cyclin D1 (anti-rabbit) (1/500) (Abcam, Cambridge, UK).

4.2.12: Radioimmunoassay for circulating TH concentrations

Concentrations of mouse total T3 and total T4 were determined through radioimmunoassay as described in section 2.13. Mouse serum TSH concentrations were measured by Professor Samuel Refetoff (University of Chicago), as described in section 2.13 (Pohlenz et al, 1999) (Di Cosmo et al, 2010).

4.2.13: Western blotting

Western blotting was performed as described in section 2.14. Antibodies used were anti-hPTTG1 (anti-rabbit (1/40) (Invitrogen, Life Technologies Ltd, Paisley, UK)), anti-PCNA (anti-rabbit (1/1000) (FL-261) (Santa Cruz Biotechnology, Dallas, TX, USA)), anti-p53 (anti-mouse (1/500) (sc-126) (Santa Cruz Biotechnology, Dallas, TX, USA)) and anti-p21 (anti-mouse (1/500) (Abcam, Cambridge, UK)). Appropriate secondary antibodies (Dakocytomation, Ely, Cambridgeshire, UK) were used.

4.3: Results

4.3.1: Identification of *Pttg1* knockout mice

In order to identify homozygote and wild-type mice for further experiments conventional PCR was employed as described in sections 2.9 and 4.2.8, using sequences for *Pttg1* and *Neomycin*, which were provided by Professor Melmed (Wang et al, 2001) (Figure 4.2). Following PCR, gel electrophoresis was carried out. A band for mouse *Pttg1* was demonstrated at 220 bp and a band for *Neomycin* at 700 bp (Figure 4.2). A single band for *Pttg1* in a sample indicated a wild-type mouse, and a single band for *Neomycin* in a sample indicated a knockout mouse. A band for both *Pttg1* and *Neomycin* in a sample indicated a heterozygote mouse. *Notch-1* primers were used to determine DNA was of sufficient quality as described in section 3.3.1.

A

Primer Pair	Primer Direction	Primer Sequence
Pttg1	Forward	TTCTGGGGACTGAATTCAGG
	Reverse	TAGGCTTTTCGGCAACTCTGTTGAC
Neomycin	Forward	TTAGCTGTGAGCTCGTCGTG
	Reverse	GTGCTACTTCCATTTGTCACGTCC

B

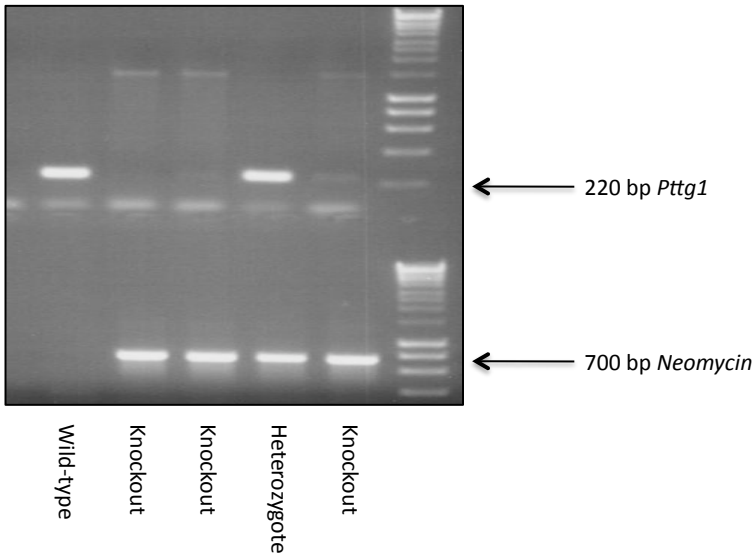

Figure 4.2: ***A.*** *PCR primer sets for Pttg1 and Neomycin displaying primer sequence and primer direction.* ***B.*** *Gel electrophoresis using hyperladder I as a DNA size marker. Pttg1 bands for mouse Pttg1 are represented at 220 bp and Neomycin at 700 bp. The gel shows examples of wild-type, heterozygote and knockout mice for mouse Pttg1.*

Mice were subsequently set up into breeding pairs to provide wild-type and knockout mouse colonies for further experiments. However, knockout mice proved to be subfertile. Therefore, hemizygote mice were bred together to provide wild-type and knockout mice.

4.3.2: Characterisation of *Pttg1* knockout mouse thyroid

Wild-type and knockout mice were culled and thyroids excised at 6-weeks of age. Thyroids were weighed and overall body weight determined. There was no difference in body weight between wild-type and knockout mice (data not shown). Body weight was used to determine a thyroid:body weight ratio. There was no difference in thyroid:body weight ratio (0.90-fold, p=0.289) between wild-type (0.074 mg/g ±0.005, n=19) and knockout mice (0.067 mg/g ±0.005, n=16) (Figure 4.3).

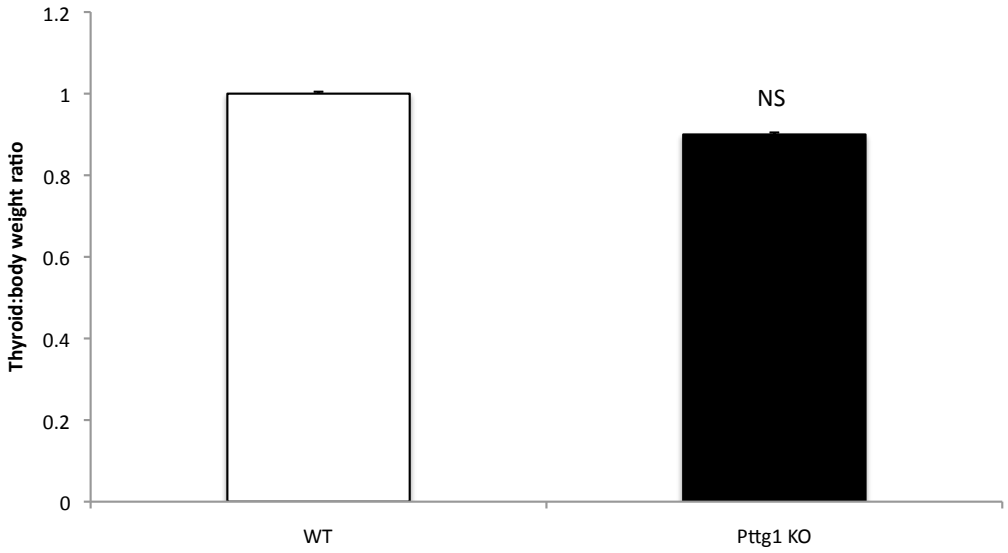

Figure 4.3: Thyroid:body weight ratio of wild-type mice compared to Pttg1 knockout mice.

Histologically knockout mouse thyroid tissues were normal, as evidenced by Figure 4.4, which shows a representative example of thyroid histology from wild-type and knockout mice. There was no change in follicular size or structure, nor any changes observed in stromal tissues (Figure 4.4).

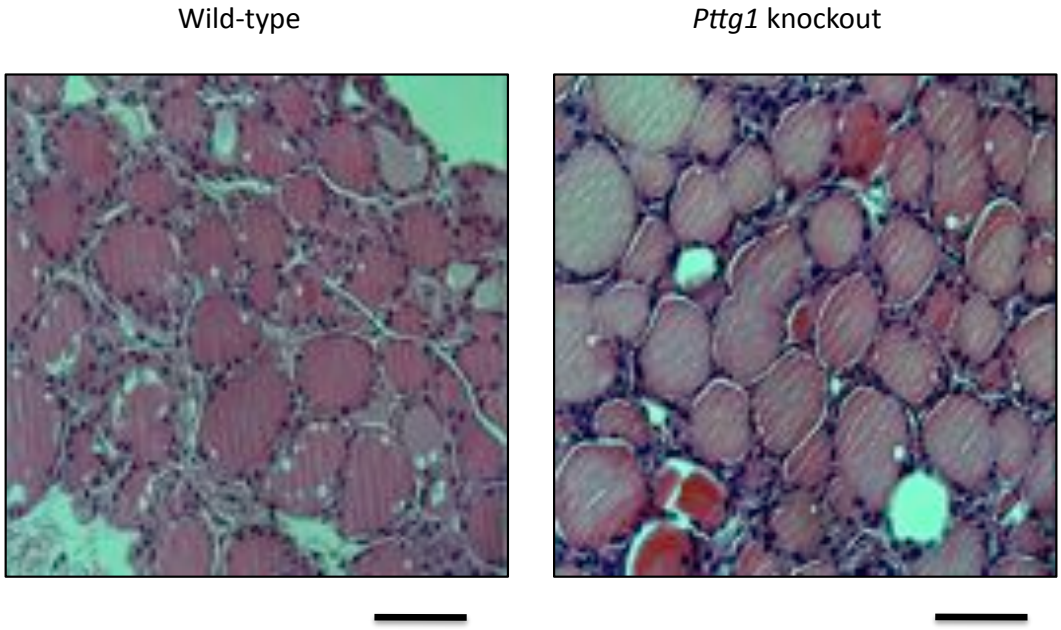

Figure 4.4: Histology pictures showing H&E staining of thyroid tissue from wild-type and Pttg1 knockout mice. Scale bars: 100μm

4.3.3: Thyroid differentiation in *Pttg1* knockout mice

Real-time qPCR was performed to determine mRNA expression levels of thyroid differentiation markers *NIS, Tg* and *TshR* using wild-type (n=5) and *Pttg1* knockout mice (n=5). Expression of *NIS* demonstrated no difference

(0.76-fold, p=0.518) comparing wild-type (Mean ΔCt = 12.95 ±0.37) and knockout mice (13.35 ±0.47). There was also no difference found in regards to *Tg* expression (1.07-fold, p=0.746) between wild-type (3.80 ±0.29) and knockout mice (3.70 ±0.09). Similarly, results showed no difference for *TshR* (1.06-fold, p=0.844) comparing wild-type (13.02 ±0.19) and knockout mice (12.94 ±0.34) (Figure 4.5).

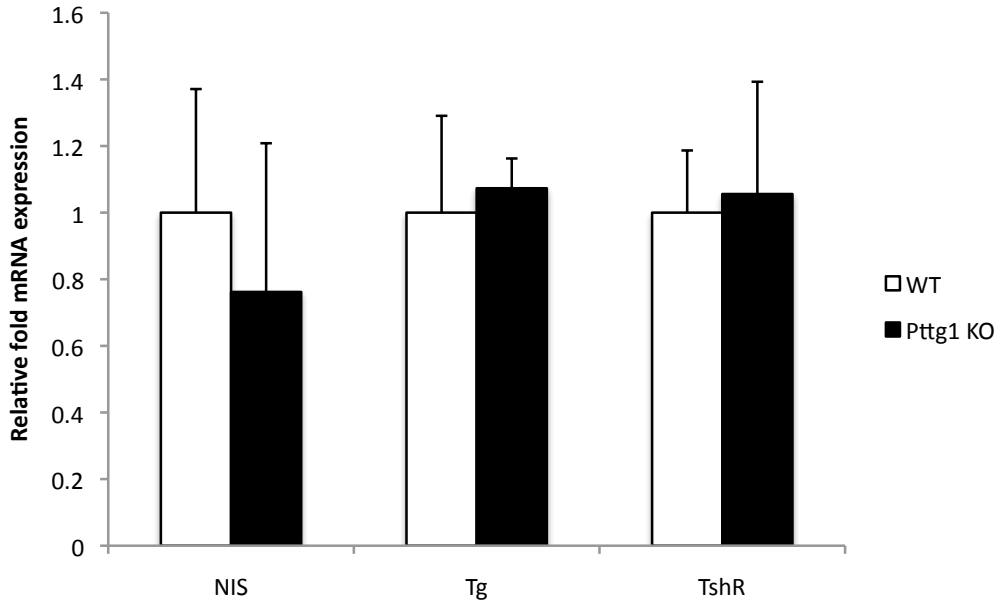

Figure 4.5: Thyroid differentiation marker mRNA expression. Relative fold mRNA expression of murine NIS, Tg and TshR in wild-type mice compared to Pttg1 knockout mice, showing no difference.

4.3.4: Thyroid function in *Pttg1* knockout mice

In order to investigate the effect of thyroidal *Pttg1* knockout on thyroid hormone concentrations, total serum T3 and T4 were determined alongside concentrations of TSH. Blood was extracted from 6-week old mice, serum was extracted, and subjected to radioimmunoassay for T3 and T4. Only male mice were used for these experiments due to a lack of female knockout mice. There was no difference in T3 concentration ($p=0.382$) when comparing wild-type (118.09 ng/dL ±11.89, n=5) and knockout mice (130.60 ng/dL ±6.45, n=5) (Figure 4.6). Similarly for T4, there was no difference ($p=0.731$) between wild-type (11.84 µg/dL ±5.91, n=5) and knockout mice (9.50 µg/dL ±2.83, n=5) (Figure 4.6). TSH concentrations were also measured to elucidate thyroid function. Results showed no difference ($p=0.553$) when comparing wild-type (50 mU/L ±7.88, n=5) and knockout mice (61 mU/L ±13.44, n=5).

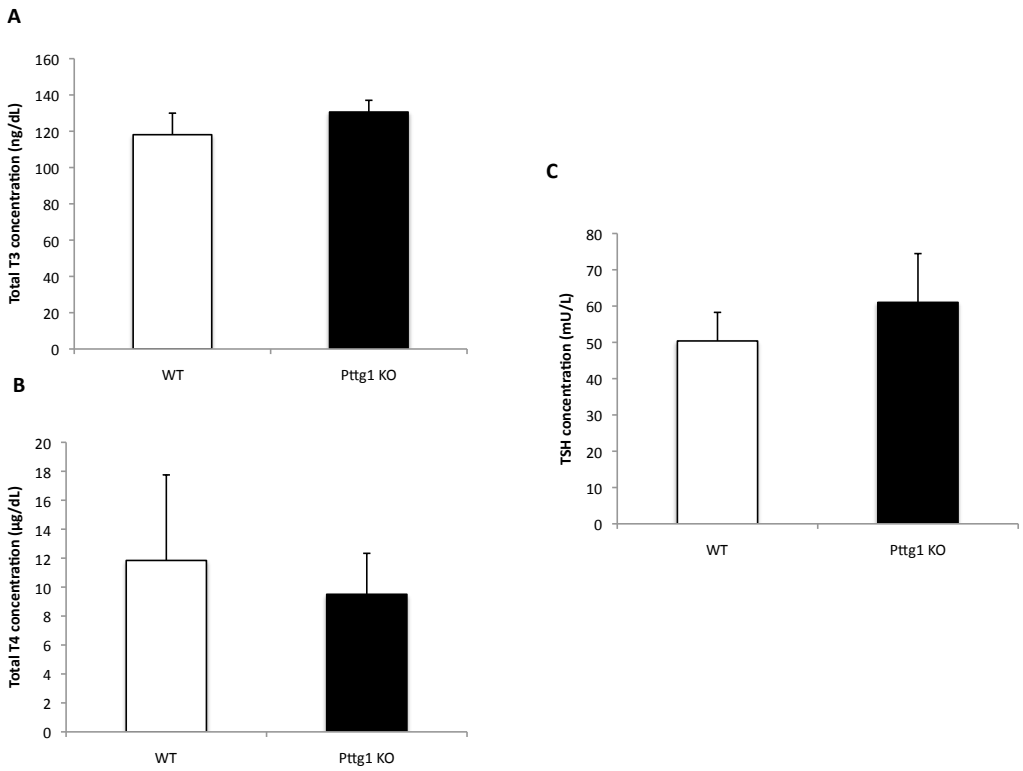

Figure 4.6: Thyroid function tests comparing wild-type mice to Pttg1 knockout mice. ***A.*** *Total serum T3 concentration of Pttg1 knockout mice compared to wild-type mice.* ***B.*** *Total serum T4 concentration of Pttg1 knockout mice compared to wild-type mice.* ***C.*** *Serum TSH concentration of Pttg1 knockout mice compared to wild-type mice.*

4.3.4: Growth factor expression in *Pttg1* knockout mice

To determine expression of growth factors in *Pttg1* knockout mouse thyroids, mRNA from 6-week old wild-type (n=5) and *Pttg1* knockout mice (n=5) was used to perform TaqMan Real-time qPCR using pre-validated TaqMan assays for *Egf*, *Igf1*, *Tgf-α*, *Tgf-β*, *Vegf* and *Fgf2*. *Egf* mRNA

expression was significantly reduced (0.61-fold, p=0.001) in *Pttg1* knockout mice (Mean ΔCt = 20.20 ±0.12) compared to wild-type mice (18.85 ±0.20). *Igf1* mRNA expression was significantly increased (1.59-fold, p=0.0036) in *Pttg1* knockout mice (13.45 ±0.10) compared to wild-type mice (14.13 ±0.13). Similarly, *Tgf-β* showed significantly increased expression (1.42-fold, p=0.04) in *Pttg1* knockout mice (13.99 ±0.16) compared to wild-type mice (14.50 ±0.14). *Tgf-α* demonstrated no difference (1.07-fold, p=0.658) between wild-type mice (14.40 ±0.15) and *Pttg1* knockout mice (14.30 ±0.17). *Vegf* expression also showed no difference (1.02-fold, p=0.923) in *Pttg1* knockout mice (11.29 ±0.13) compared to wild-type mice (11.32 ±0.18). Similarly, mRNA expression of *Fgf2*, comparing wild-type mice (16.73 ±0.17) and *Pttg1* knockout mice (16.76 ±0.19), showed no difference (0.98-fold, p=0.899) (Figure 4.7).

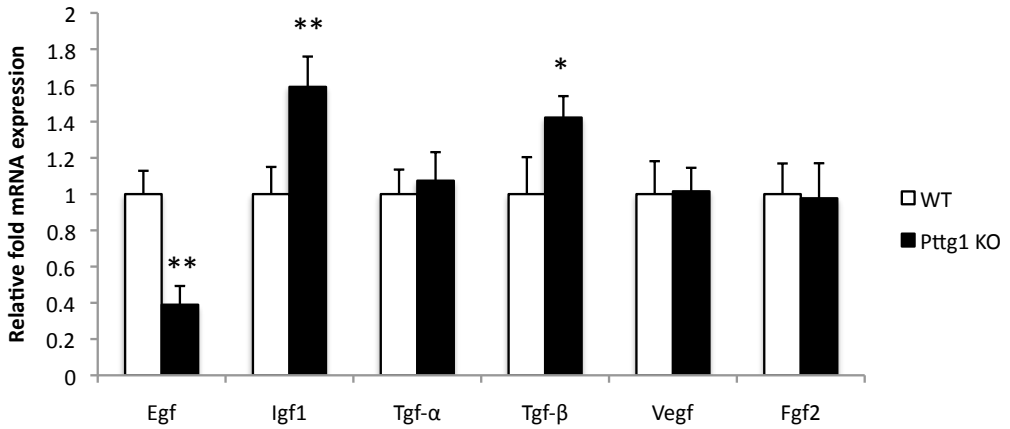

Figure 4.7: mRNA expression of growth factors Egf, Igf1, Tgf-α, Tgf-β, Vegf and Fgf2, as determined by TaqMan Real-time qPCR comparing wild-type and Pttg1 knockout mice. (=p<0.05, **=p<0.005).*

4.3.5: Associated senescence in *Pttg1* knockout mice

In order to investigate if there was evidence of senescence in *Pttg1* knockout mouse thyroids, we performed immunohistochemistry on paraffin-embedded thyroid tissue of wild-type and *Pttg1* knockout mice – and determined mRNA expression of *Cdkn1a*, which is translated to the protein p21, and protein expression of Cyclin-D1.

Immunohistochemistry of wild-type (n=4, positive nuclei=3.72 ±0.011) and knockout (n=4, 8.54 ±0.009) mice showed significantly increased protein expression of Cyclin-D1 (2.18-fold, p=0.009) (Figure 4.8). mRNA expression of *Cdkn1a* was significantly increased (2.82-fold, $p=8.31x10^{-5}$) in *Pttg1* knockout mice (Mean ΔCt = 11.95 ±0.150, n=10) compared to wild-type mice (13.45 ±0.114, n=10) (Figure 4.8). These results suggest *Pttg1* knockout mice exhibit increased Cyclin D1 expression, and upregulation of *Cdkn1a* (p21) mRNA expression.

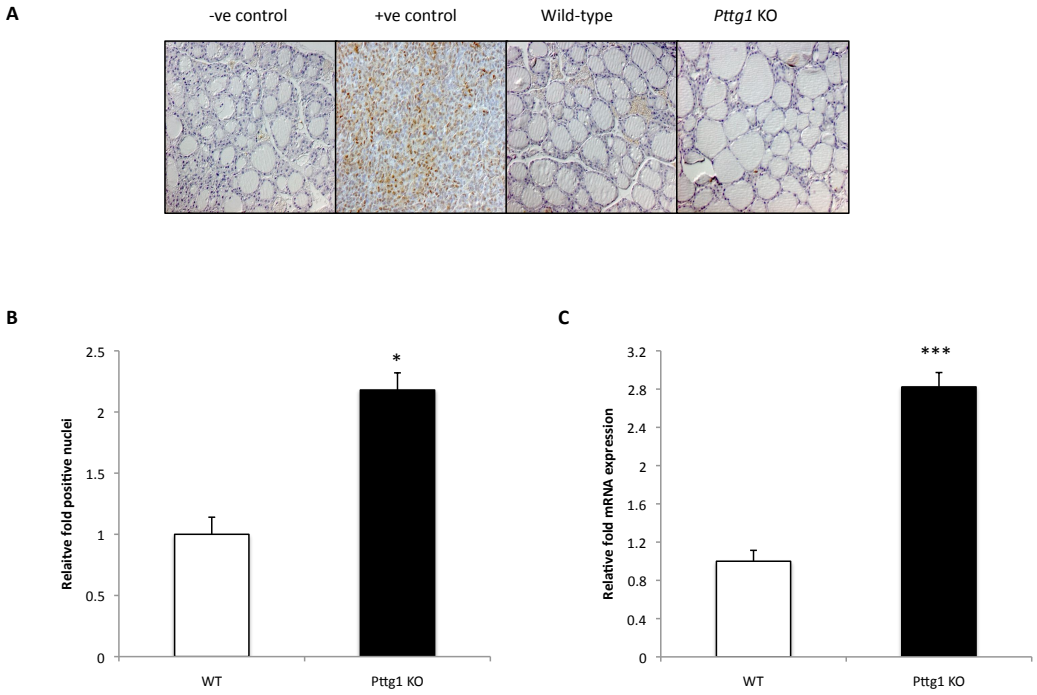

Figure 4.8: ***A.*** *Representative images of immunohistochemical analysis of paraffin embedded thyroid sections from wild-type and Pttg1 knockout mice, of Cyclin D1 negative control (a no antibody control), positive control (lung tumour tissue), wild-type mice and Pttg1 knockout mice. 40x magnification* ***B.*** *Cyclin D1 protein expression.* ***C.*** *Relative fold Cdkn1a mRNA expression, determined by Real-time qPCR. (*=p<0.05, ***=p<0.0005).*

4.3.6: Effects of *hPTTG1* depletion on thyroid cells *in vitro*

To investigate the effects of hPTTG1 depletion on thyroid cells, we used a siRNA to specifically target and reduce mRNA expression of *hPTTG1 in vitro*. Figure 4.9 shows significant knockdown of hPTTG1 expression in TPC1 cells. Repeated attempts were made to achieve similar knockdown of hPTTG1 in K1 cells, however only minimal knockdown was observed (data not shown).

Determination of mRNA expression of growth factors *EGF*, *TGF-α* and *TGF-β* (n=3) in TPC1 cells, following knockdown of *hPTTG1*, revealed a significant reduction in expression of *EGF* (0.69-fold, p=0.035) when comparing scrambled siRNA (Mean ΔCt = 19.48 ±0.02) to *hPTTG1* siRNA (20.43 ±0.01). However, mRNA expression of *TGF-α* showed no difference (1.17-fold, p=0.452) between scrambled siRNA (12.21 ±0.24) and *hPTTG1* siRNA samples (11.98 ±0.14). Similarly, *TGF-β* expression showed no difference (1.36-fold, p=0.114) comparing scrambled siRNA (12.80 ±0.22) and *hPTTG1* siRNA (12.42 ±0.15). mRNA expression of *IGF-1* was tested, however we were unable to detect *IGF-1* mRNA expression in TPC1 cells.

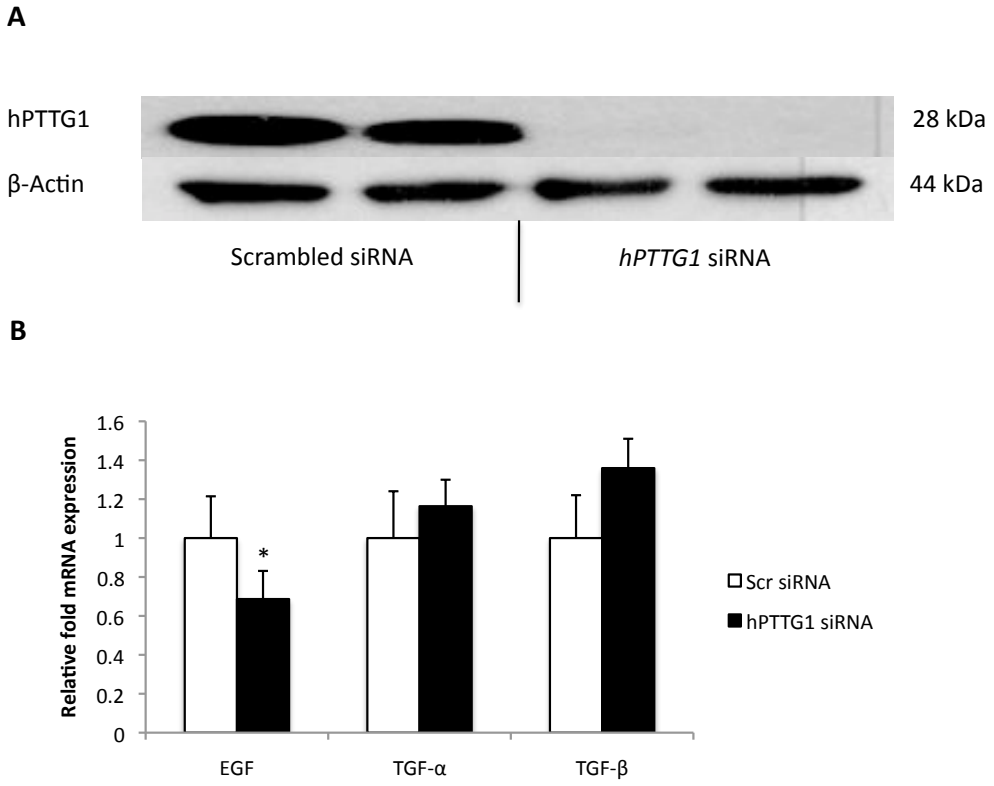

Figure 4.9: ***A.*** *Western blotting of* hPTTG1 *showing knockdown of* hPTTG1 *using a specific siRNA in TPC1 cells. β-actin was used as a loading control to normalise for protein expression.* ***B.*** *Relative mRNA expression of EGF, TGF-α and TGF-β comparing scrambled siRNA and hPTTG1 siRNA. (*=p<0.05).*

In order to investigate the effect of *hPTTG1* siRNA on p21, Real-time qPCR was performed to determine mRNA expression of *CDKN1A*. Transfection of *hPTTG1* siRNA resulted in a significant reduction (0.64-fold, p=0.0003) in *CDKN1A* mRNA expression, comparing scrambled siRNA (Mean ΔCt=11.20 ±0.16) and *hPTTG1* siRNA (11.84 ±0.09) (Figure 4.10). Similarly p21 protein expression, determined through Western blotting, was reduced following hPTTG1 knockdown. Protein expression of p53 was not different between *hPTTG1* siRNA and scrambled siRNA control (Figure 4.10).

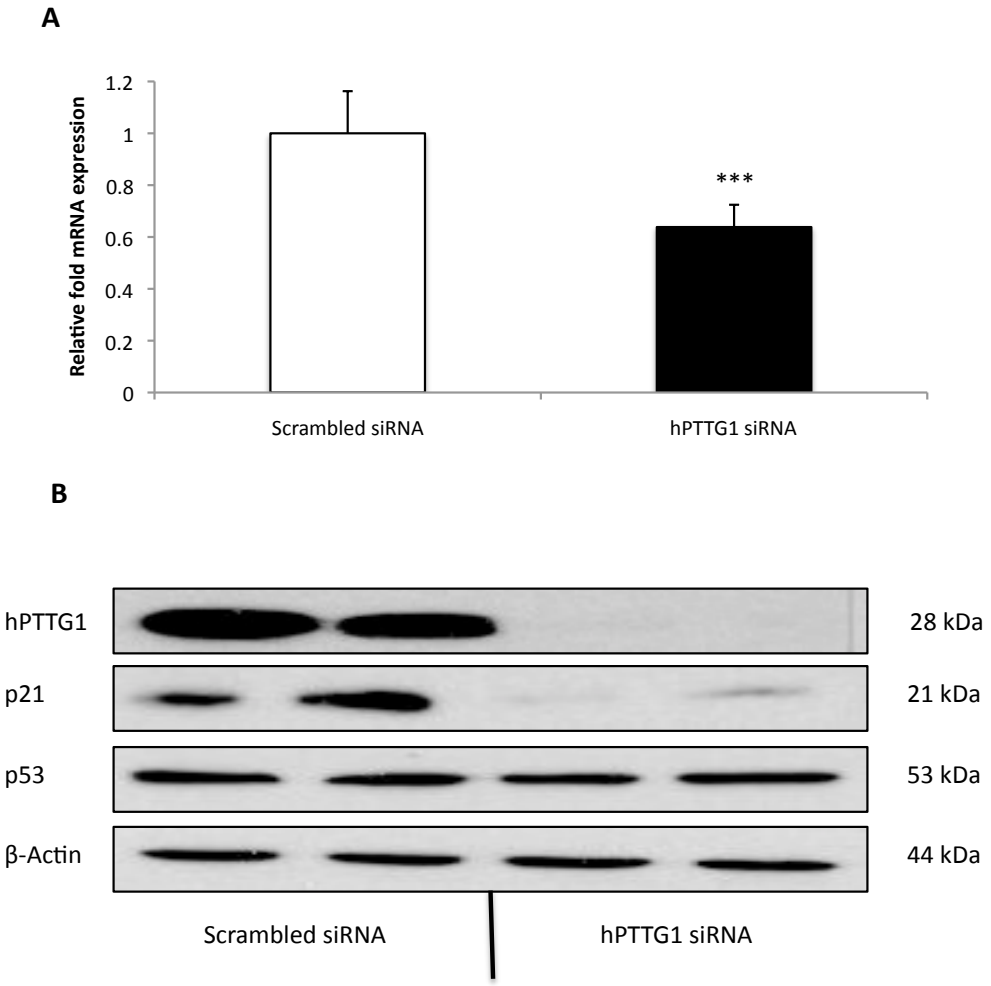

Figure 4.10: ***A.*** *Relative fold mRNA expression of CDKN1A following transfection with scrambled siRNA or hPTTG1 siRNA.* ***B.*** *Western blotting showing representative blots of protein expression of* hPTTG1, p21, p53 *and* β-actin*. (***=p<0.0005).*

4.4: Discussion

4.4.1: Effect of *Pttg1* knockout on murine thyroid phenotype

Genotyping of mice was performed using conventional PCR using pre-validated primers for *Pttg1* and *Neomycin*. Use of these primer sets, and *Notch-1* to verify DNA quality, allowed identification of wild-type, hemizygote and knockout mice (Figure 4.2). Following identification of knockout and wild-type mice, breeding pairs were set up to promote separate knockout and wild-type colonies. However, knockout mice proved to be subfertile, leading to hemizygote breeding to gain 25% knockout mice, 25% wild-type mice, which were used for further experiments, and 50% hemizygote mice, which were used for further breeding or culled. Although it would have been useful to also genotype mice using another method, such as qPCR, the lack of false positives or negatives, via observed genotype percentages versus expected, and previous use of these primers to determine genotypes (Wang et al, 2001) supported the conclusion that conventional PCR was sufficient to determine the genotyping of mice.

Previous findings have confirmed a range of tissue effects in *Pttg1* knockout mice, such as testicular and pituitary hypoplasia, and thymic hyperplasia (Wang and Melmed, 2001) (Chesnokova et al, 2003). We decided to investigate the weight and histology of thyroids of knockout mice. Macroscopic examination suggested no difference, and comparison of the thyroid:body weight ratio of *Pttg1* knockout and wild-type mice also showed

no difference (Figure 4.3). Thyroids extracted were used for histology using H&E staining. Microscopic examination of excised mouse thyroids showed no differences comparing wild-type to knockout mice, and there was no difference in mRNA expression of *NIS*, *Tg* or *TSHR* between wild-type and *Pttg1* knockout mice (Figure 4.5), indicating normal parameters of thyroid differentiation following *Pttg1* deletion and deletion of *Pttg1* did not affect thyroid phenotype. Ageing wild-type and knockout mice to 6-months and 12-months would have provided greater insight into the long-term effects of *Pttg1* deletion, as various tissue specific effects of *Pttg1* deletion were observed after a significant time period (Wang et al, 2001). However, financial constraints and difficulties breeding mice meant this was not possible.

4.4.2: Thyroid differentiation marker and thyroid function in *Pttg1* knockout mice

Thyroid hormone levels were determined to assess if deletion of *Pttg1* had any effect upon thyroid function. Concentrations of circulatory thyroid hormones (total serum T3 and T4), and serum TSH in *Pttg1* knockout mice were not different from wild-type mice (Figure 4.6), indicating *Pttg1* deletion does not result in altered thyroid function. Together with data from the previous chapter showing overexpression generated no effect upon thyroid

function or differentation, this implies PTTG1 does not directly affect thyroid function or differentiation.

4.4.3: Growth factor expression in *Pttg1* knockout mice

Growth factor expression was investigated in *Pttg1* knockout mice. mRNA expression of growth factors *Egf*, *Igf-1*, *Tgf-α*, *Tgf-β*, *Vegf* and *Fgf-2* was conducted by TaqMan Real-time qPCR. We found a significant 0.61-fold reduction in *Egf* expression in *Pttg1* knockout mice compared to wild-type mice. Previous research by other groups has shown hPTTG1 expression to be regulated by hEGF in TtT/GF pituitary cells and U87 astrocytoma cells (Tfelt-Hansen et al, 2004) (Vlotides et al, 2006). Indeed, recent research by our group has demonstrated hEGF can upregulate hPTTG1 expression, and in turn hPTTG1 overexpression promotes hEGF upregulation in TPC1 and K1 thyroid carcinoma cells (Ryan et al, 2013). The data described in this chapter show that deletion of *Pttg1* in mice results in a reduction of *Egf* expression, suggesting the regulation of EGF by PTTG1 also occurs *in vivo*. Meanwhile, *Igf-1* mRNA expression presented with significantly increased expression (1.59-fold) in *Pttg1* knockout mice compared to wild-type mice. Previous research has shown that overexpression of hIGF-1 resulted in increased *hPTTG1* mRNA expression in malignant and non-malignant astrocytes (Chamaon et al, 2005), while hPTTG1 mRNA and protein expression was upregulated in MCF7 breast cancer cells following hIGF-1 upregulation

(Thompson and Kakar, 2005). Data from our hPTTG1 overexpressing mouse model, described in Chapter 3, showed hPTTG1 thyroid-specific overexpression *in vivo* increased *Igf-1* mRNA expression. Therefore it would be expected *Pttg1* deletion may result in reduction of *Igf-1* expression. Our result did not confirm this, although our findings in *Pttg1* knockout and wild-type mice suggest dysregulation of *Igf-1* is caused both by Pttg1 over or underexpression.

Previous research has indicated that TGF-α is capable of upregulating hPTTG1 expression (Tfelt-Hansen et al, 2004), and research by our group has found TGF-α is capable of upregulating hPTTG1 expression, and that hPTTG1 can in turn increase *TGF-α* expression in thyroid cells (Ryan et al, 2013). We found no difference in *Tgf-α* mRNA expression comparing *Pttg1* knockout mice to wild-type mice. Although this contrasts with previous *in vitro* results, we also observed no difference in *Tgf-α* expression in our hPTTG1 overexpressing mouse model, compared with wild-type mice, implying that the cellular pathways are distinct in mice and Pttg1 does not directly regulate Tgf-α *in vivo*. Another explanation may be that regulation is only observed in cancer cell lines in which specific pathways are dysregulated.

In contrast, comparison of *Pttg1* knockout mice and wild-type mice showed a 1.4-fold induction of *Tgf-β* mRNA expression (Figure 4.6). This is contradictory to previous research indicating increased expression of *TGF-β* (2.6-fold) following hPTTG1 overexpression (Ryan et al, 2013), while use of a *hPTTG1* siRNA resulted in a reduction in the mRNA expression of *TGF-β* in A2780 ovarian cell line (El-naggar et al, 2007). In addition, measurement of

conditioned media revealed increased concentrations of TGF-β following hPTTG1 overexpression, and a reduction in TGF-β concentration subsequent to *hPTTG1* siRNA transfection (Shah and Kakar, 2011). Again, differences between previous research and of data demonstrated through the *Pttg1* knockout mouse model may be due to the inherent differences between transformed human cancer cell lines and *in vivo* mouse models.

mRNA expression of *Vegf* was not different between *Pttg1* knockout mice and wild-type mice. Previously, hPTTG1 overexpression has been shown to induce expression of VEGF in cell lines such as uterine leiomyoma (Tsai et al, 2005), FTC133 thyroid cells (Kim et al, 2006), NT-2, JEG-3 and MCF-7 cells (McCabe et al, 2002). However, *Pttg1* knockout mice displayed no effect upon *Vegf* expression. Similarly, hPTTG1 overexpression has demonstrated increased mRNA expression of *FGF2* in primary thyroid cells (Boelaert et al, 2004), NIH3T3 cells, (Ishikawa et al, 2001), NT-2, JEG-3 and MCF-7 cells (McCabe et al, 2002). Further, hPTTG1 has been shown to be capable of direct transactivation of *FGF2* (Chien and Pei, 2000). Results comparing *Pttg1* knockout mice to wild-type mice revealed no difference in *Fgf2* mRNA expression (Figure 4.7).

Taken together our findings demonstrate that deletion of *Pttg1* in vivo causes dysregulation of several growth factors. Previous research has shown the clear, and often direct, effects of hPTTG1 on growth factor induction, and our data corroborates that research in showing effects on growth factors. However, it is unclear whether these effects are due to direct effects mediated by Pttg1. *Pttg1*-null mice present with a distinctly altered cell

cycle, with a reduced G_1 phase and longer G_2 phase apparent. It is possible this change in the cell cycle contributes to the differences in growth factor expression observed, although experiments on cell cycle differences were performed in mouse embryonic fibroblasts and may not be representative of mouse thyroid cells *in vivo*.

4.4.4: Associated senescence in *Pttg1* knockout mice

Cellular senescence is a process of permanent cell cycle arrest caused by a number of factors (Figure 4.11), which can lead to accumulation of p53, induction of p21 and Rb phosphorylation (Schmitt et al, 2002) (Campisi, 2005). Previously, activation of oncogenes such as *BRAF* and *RAS* have been shown to promote senescence, which is termed oncogene induced senescence (OIS) (Serrano et al, 1997) (Michaloglou et al, 2005). Following this, it was discovered that OIS is associated with upregulation of a number of factors, such as IGF-1, Wnt and TGF-β, which have been implicated in forming a communication network between senescent cells (Kuilman and Peeper, 2009).

Pttg1 knockout mouse pituitary glands demonstrated high p21 expression, which is associated with increased aneuploidy observed and activation of DNA damage pathways leading to cellular senescence (Chesnokova et al, 2008).

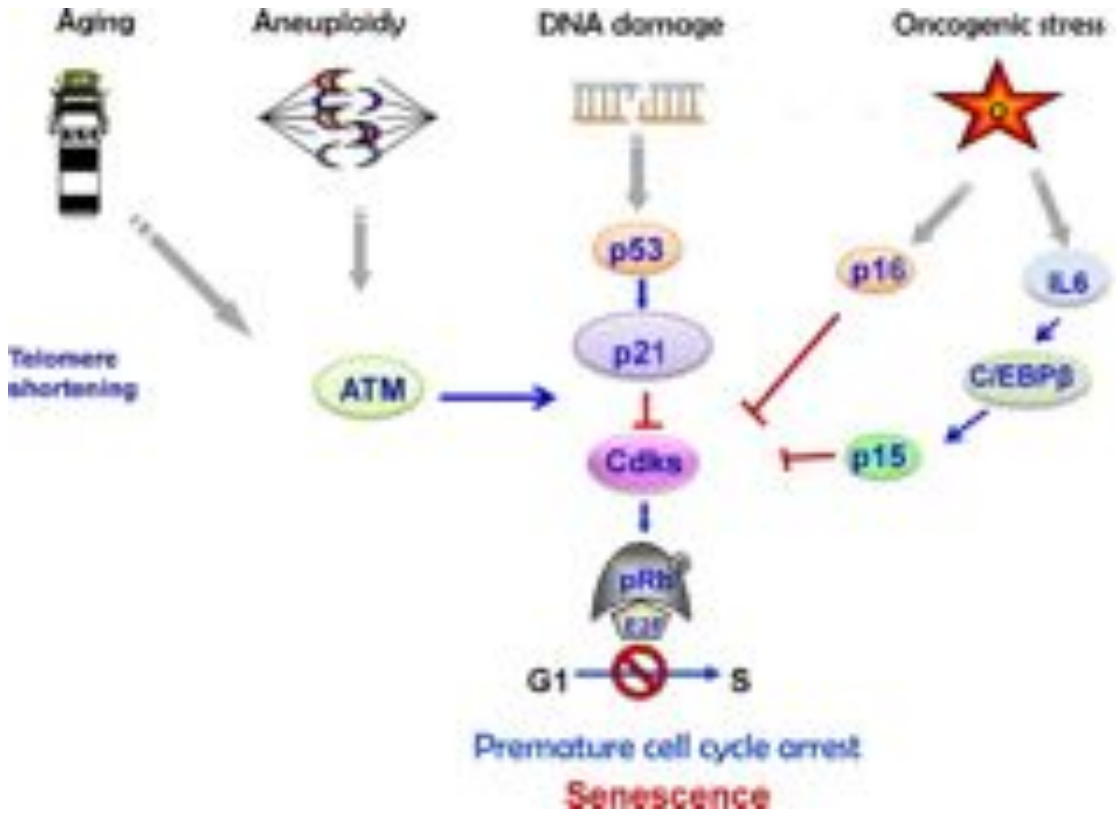

Figure 4.11: The variety of pathways responsible for promoting cellular senescence. (Taken from Chesnokova and Melmed, 2010).

Protein expression of Cyclin-D1, which forms complexes with Cdks to induce cell cycle progression (Figure 4.11), was tested via immunohistochemistry, revealing significantly increased expression in *Pttg1* knockout mice (2.18-fold) compared to wild-type mice (Figure 4.8). Following this, TaqMan Real-time qPCR was performed to investigate mRNA expression of *Cdkn1a* (p21), which showed significant 2.82-fold increased expression in *Pttg1* knockout mice compared to wild-type mice. These data are similar to findings

described previously in MEFs from *Pttg1* knockout mice where induced cellular senescence was shown (Chesnokova et al, 2007). Increased Cyclin-D1 expression has also been implicated as a consequence of increased p21, as p21 has been shown to cause degradation of Cyclin D-Cdk-4/6 complexes (Sherr and Roberts, 1999). These results therefore indicate that thyroid cells of *Pttg1* knockout mice demonstrate induced cellular senescence, potentially as a result of increased genetic stress/DNA damage. Indeed, OIS has been shown to promote upregulation of genes such as *IGF-1* and *TGF-β* (Kuilman and Peeper, 2009), and as described in section 4.3.4 there was significantly increased mRNA expression of mouse *Igf-1* and *Tgf-β* in *Pttg1* knockout mice compared to wild-type, again implying cellular senescence in *Pttg1* knockout mouse thyroids. This is a novel finding as cellular senescence caused by *Pttg1* depletion has not previously been shown *in vivo* in thyroid cells, but would seem to corroborate findings gained in pituitary cells. However, to fully characterise senescence in *Pttg1* knockout mouse thyroid cells, SA-β-gal staining would need to be conducted to determine levels of senescence in comparison to wild-type mice. Also, despite potentially increased senescence, no physiological changes were detected, unlike in the pituitary gland which displayed hypoplasia, suggesting either *Pttg1* deletion or induced sencescence is more potent in pituitary cells than thyroid cells.

4.4.5: Effects of *hPTTG1* depletion on thyroid cells

To determine if effects observed in the *Pttg1* knockout mouse could be replicated *in vitro* in human thyroid cancer cell lines, we used a *hPTTG1* siRNA to knock down hPTTG1 *in vitro*. As seen in Figure 4.9, efficient knockdown was achieved in TPC1 cells. Subsequently cells were tested for mRNA expression of growth factors *EGF*, *TGF-α* and *TGF-β*. We found a 0.31-fold reduction in expression of *EGF*, but no difference in *TGF-α* or *TGF-β*, in *hPTTG1* siRNA samples compared to scrambled siRNA controls. The reduction in *EGF* expression is complementary to results obtained from the *Pttg1* knockout mouse and previous results showing induced *EGF* expression following hPTTG1 overexpression (Ryan et al, 2013), suggesting hPTTG1 may have a role in regulating *EGF* expression in mouse and human thyroid cells. However, there was no difference in *TGF-α* or *TGF-β* expression following hPTTG1 siRNA transfection. This may be due to differences in mouse and human cells, or to increased dysregulation of growth factor pathways in transformed cancer cell lines. There is also the fact that overexpressing a protein may cause effects that are not observed as opposite effects when said protein is depleted.

CDKN1A (p21) mRNA expression was determined following transfection of TPC1 cells with either *hPTTG1* siRNA or a scrambled siRNA control. A 0.36-fold significant reduction in *CDKN1A* mRNA expression was found following *hPTTG1* siRNA transfection. This contrasts with the data obtained from the *Pttg1* knockout mouse, which demonstrated a highly

significant induction of *Cdkn1a* expression in *Pttg1* knockout mouse thyroid tissue. These differences could be related to differences in human and mouse cellular pathways. Results obtained through Western blotting confirmed a reduction in p21 expression but no change in p53 protein expression following *hPTTG1* siRNA transfection (Figure 4.10), suggesting the reduction in *CDKN1A* mRNA expression is p53-independent. Several proteins have been implicated in p53-independent *CDKN1A* regulation, such as HOXA10 (Gartel and Tyner, 1999) and members of the Klf family (Black et al, 2001). Notable among these is Sp1, which has also been shown to interact with hPTTG1 (Tong et al, 2007), and which could be responsible for *CDKN1A* induction following interaction with hPTTG1. Following depletion of hPTTG1 there may be reduced interaction with Sp1, resulting in reduced expression of *CDKN1A*. Oncogenic induction of *CDKN1A* expression has also been implicated, with RAS shown to promote increased expression (Gartel et al, 2000). It is also worth noting that hPTTG1 has been shown previously to transactivate *c-MYC* (Pei, 2001) and c-MYC has also been shown to be capable of repression of *CDKN1A* (Mukherjee and Conrad, 2005). Therefore depletion of hPTTG1 may cause increased expression of *CDKN1A* via C-myc. Dysregulated pathways or greater potency of specific pathways are possible causes of observed results, although further investigation would help in further elucidating these causes.

4.4.6: Conclusions

Results described in this chapter yield findings which will be of interest in determining further effects of *Pttg1* deletion on thyroid cells. *Pttg1* deletion has no effect on thyroid morphology, differentiation or function. However, there were significant changes to growth factor expression and associated senescence. Investigations utilising *hPTTG1* siRNA to determine *in vitro* effects of hPTTG1 depletion on thyroid cancer cell lines demonstrated effects upon *EGF* expression and p53-independent p21 expression. These experiments have provided useful data, but have also shown the difficulties involved in comparing *in vivo* findings using mouse models to *in vitro* experiments using transformed human cancer cell lines.

Chapter 5. Effect of PTTG and PBF on goitre induction

5.1: Introduction

The thyroid hormones triiodothyronine (T3) and thyroxine (T4) are produced by the follicular cells of the thyroid gland in a process regulated by thyroid stimulating hormone (TSH), released by the pituitary gland. This production is achieved by transport of sodium and iodine into the follicular cells and subsequent transport of iodine into the colloid. Following this, iodine is used in thyroid hormone synthesis when iodine atoms are attached to a tyrosine ring structure. Thyroid hormones are important in the majority of cells in the body, controlling basal metabolic rate and protein synthesis, among other functions. A negative feedback loop occurs, wherein thyroid hormones act on the pituitary to repress TSH production, leading to a repression of thyroid hormone production. Iodine deficiency may result in goitre as a compensatory mechanism and has also been shown to increase thyroid cancer risk (Knobel and Neto, 2007). Research has suggested chronic iodine deficiency is linked to an increased risk of follicular thyroid cancer, while in contrast, chronically high iodine intake has been proposed to increase the risk of papillary thyroid cancer (Feldt-Rasmussen, 2001).

hPTTG1 is the human securin, involved in the cell cycle by inhibiting the protease separase until the metaphase to anaphase transition (Wirth et al, 2006). hPTTG1 is also involved in the DNA damage and repair pathways and possesses transcription factor activity. In normal adult human tissue, expression has been observed in the testis, thymus, colon, small intestine, placenta and spleen (Zhang et al, 1999), and high hPTTG1 expression has

been found in several cancer cell lines (Lee et al, 1999). hPTTG1 has been implicated as possessing a dual role in tumourigenesis, being involved in both its initiation, and its subsequent progression. Overexpression of hPTTG1 has been reported in thyroid cancer, and a non-significant increase has also been observed in multi-nodular goitres (Boelaert et al, 2003). In this study, 25 multi-nodular goitres were tested and compared to 11 normal samples, showing a 2.4-fold non-significant increase in hPTTG1 mRNA expression (p=0.5).

PBF is a 180-amino acid protein with reported roles as a cell surface protein (Smith et al, 2012) and in the nucleus (Read et al, 2013, Manuscript under revision). PBF has also been demonstrated to be increased in thyroid cancer (Stratford et al, 2005). Transgenic mice with thyroidal overexpression of PBF have been developed by our group, and a recent publication by our group has shown PBF overexpression *in vivo* can lead to increased thyroid cell growth, due to increased cellular proliferation (Read et al, 2011).

These results led to our hypothesis that hPTTG1 overexpression may induce goitre formation and that goitregenesis may be impaired in the absence of *Pttg1*. We also decided to perform a preliminary experiment to test the effect of PBF thyroidal overexpression, using our PBF-Tg mice, on goitre induction. We decided to test this by assessing goitre induction following standard approaches in hPTTG1 overexpressing transgenic mice, and in *Pttg1* knockout mice, compared with wild-type mice. To achieve this, mice were placed on either a control diet (6 mg/kg of iodine) or an iodine

deficient diet, containing very low levels of iodine (0.05 mg/kg of iodine, or <0.05 ppm). This causes a reduction in thyroid hormone production, leading to a lack of negative feedback on the pituitary and increasing TSH production, which subsequently leads to an enlargement of the thyroid gland, or goitre formation. Mice were also given drinking water containing 0.5% sodium perchlorate and 0.02% methimazole, both of which abrogate endogenous thyroid hormone production. Sodium perchlorate acts by inhibiting the sodium-iodide symporter (NIS), therefore inhibiting iodide uptake into follicular cells (Braverman et al, 2005), and methimazole inhibits thyroperoxidase, an enzyme which is involved in the iodination and coupling of tyrosine molecules (Crescioli et al, 2007). This approach has previously been shown to promote goitre formation in mice, and the protocol used for this study was adapted from the goitregenic approach used by Professor Samuel Refetoff (Di Cosmo et al, 2010).

5.2: Materials and Methods

5.2.1: Murine studies

Murine studies were carried out as described in section 2.1. All mice were bred and maintained at the Biomedical Services Unit at the University of Birmingham by trained staff. In order to induce goitre formation mice were provided with a reduced iodine diet (Harlan Teklad), supplemented with 0.5% sodium perchlorate (Sigma Aldrich, St louis, MO, USA) and 0.02% Methimazole (Sigma Aldrich, St louis, MO, USA) in the drinking water. This diet was maintained for 4 weeks, after which mice were sacrificed and thyroids excised. Cardiac punctures were used to extract blood serum. The 2016 Harlan Teklad (6 mg/kg) diet was used as a control diet. hPTTG1 transgenic mice, and wild-type comparison mice, were the FVB/N strain, and *Pttg1* knockout mice, and wild-type comparison mice, were the c57/BL6 strain.

5.2.2: Histology

Mouse thyroid glands taken for histology were fixed in formalin immediately after removal. Tissue was then paraffin embedded and either left for immunohistochemistry experiments, or stained for Hematoxylin and Eosin, by the Cellular Pathology Department of the University Hospital Birmingham.

5.2.3: Radioimmunoassay for circulating TH concentrations

Concentrations of mouse total T3 and total T4 were determined through radioimmunoassay as described in section 2.13. Mouse serum TSH concentrations were measured by Professor Samuel Refetoff (University of Chicago), as described in section 2.13 (Pohlenz et al, 1999) (Di Cosmo et al, 2010).

5.3: Results

5.3.1: Thyroid size and histology of hPTTG1 transgenic mice

To investigate the effect of hPTTG1 overexpression on goitre induction, 6-week old wild-type and hPTTG1 overexpressing transgenic mice were subjected to either a control or iodine-deficient diet for 4 weeks. Following this, mice were culled and thyroids were weighed and harvested for histology. Representative photographs of thyroid glands from wild-type and hPTTG1-Tg mice on either the control diet or iodine-deficient diet are shown in figure 5.1. Thyroid glands from wild-type and hPTTG1-Tg mice on the iodine deficient diet were macroscopically larger than those on the control diet, and showed evidence of increased vascularisation (Figure 5.1). No difference in body weight following 4 weeks of diet change was found (data not shown). Wild-type male mice on the iodine-deficient diet (n=5, 0.164 ±0.008) showed a significantly increased thyroid:body weight ratio (1.63-fold, p=0.0003) compared to wild-type male mice on the control diet (n=5, 0.101 ±0.006). hPTTG1-Tg male mice, subjected to the iodine deficient diet (n=5, 0.142 ±0.008), also showed a significantly increased thyroid:body weight ratio (1.71-fold, p=0.0001) compared to hPTTG1-Tg male mice subjected to the control diet (n=5, 0.083 ±0.004). Comparison of wild-type and hPTTG1-Tg male mice on the iodine-deficient diet showed no difference (0.86-fold, p=0.086), suggesting hPTTG1 overexpression has no effect upon goitre formation. Similarly, wild-type female mice on the iodine deficient diet

(n=5, 0.207 ±0.011) showed a significantly increased thyroid:body weight ratio (1.66-fold, p=0.020) compared to wild-type female mice on the control diet (n=5, 0.125 ±0.023). hPTTG1 overexpressing transgenic female mice on the iodine-deficient diet (n=5, 0.197 ±0.015) had significantly increased thyroid:body weight ratio (1.88-fold, p=0.013) compared to hPTTG1-Tg female mice on the control diet (n=5, 0.104 ±0.004). Comparison of wild-type and hPTTG1-Tg female mice subjected to the iodine deficient diet showed no difference (0.95-fold, p=0.606), again demonstrating hPTTG1 overexpression has no effect upon goitre formation *in vivo* (Figure 5.1).

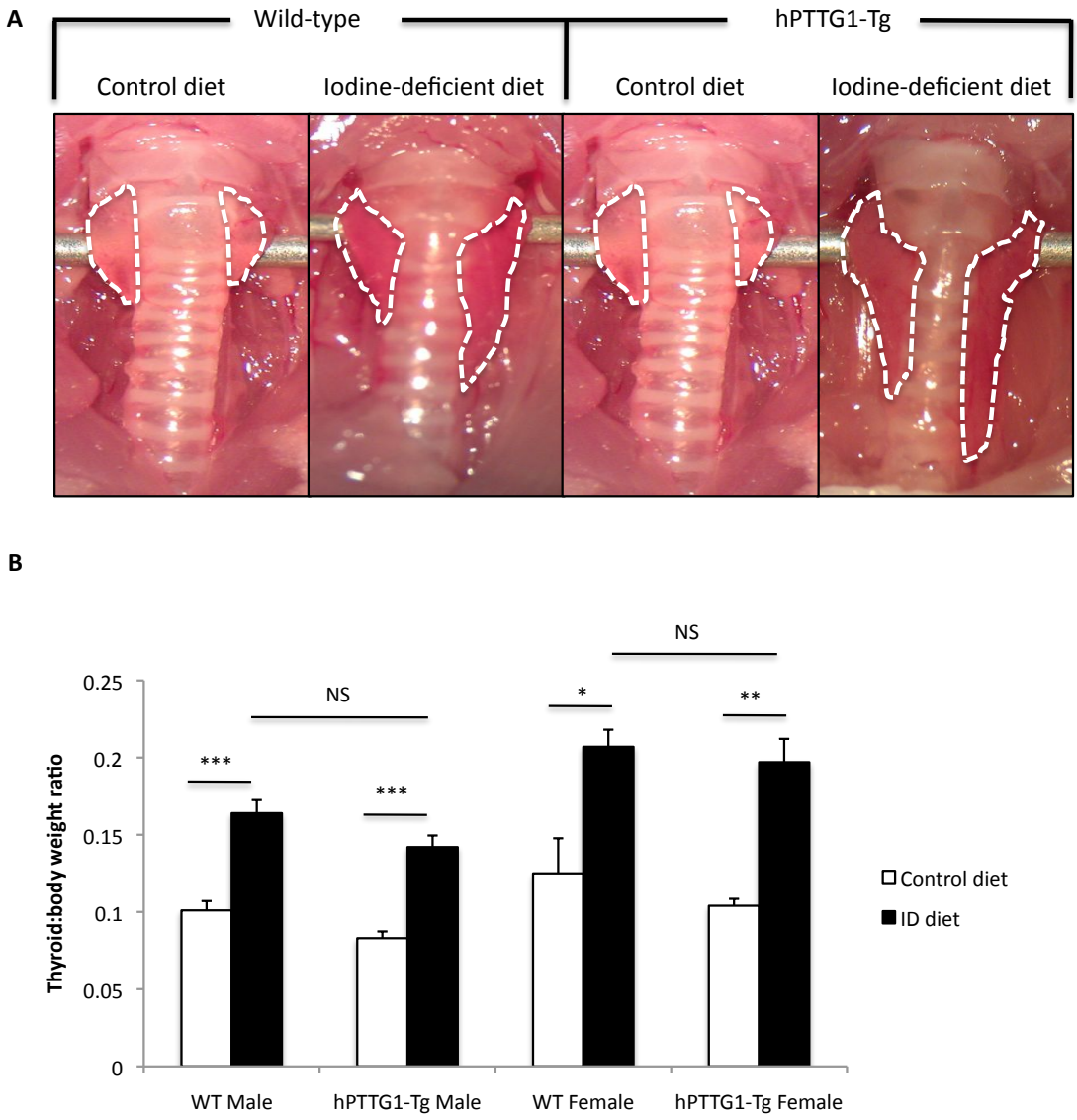

Figure 5.1: Goitre induction in hPTTG1-Tg mice. ***A.*** *Representative photographs of thyroid glands from wild-type and hPTTG1-Tg mice, subjected to control or iodine-deficient diet for 4 weeks. Thyroid glands are shown inside white dotted lines.* ***B.*** *Comparison of thyroid:body weight ratio between mice on control diet or iodine-deficient (ID) diet, for wild-type male, hPTTG1-Tg male, wild-type female and hPTTG1-Tg female. (NS=non significant, ***=p<0.0005).*

5.3.2: Serum thyroid hormone concentrations of hPTTG1 transgenic mice

Serum from wild-type and hPTTG1-Tg male and female mice, subjected to either the control or iodine-deficient diet, was extracted and total concentrations of thyroid hormones T4 and T3 were determined by radioimunnoassay. Wild-type male mice on the iodine-deficient diet (n=5, 6.83 μg/dL ±1.24) showed no difference (0.90-fold, p=0.695) in T4 concentration compared to wild-type male mice on the control diet (n=5, 7.59 μg/dL ±1.38). Similarly, hPTTG1-Tg male mice on the iodine-deficient diet (n=5, 7.13 μg/dL ±0.94) showed no difference (1.29-fold, p=0.496) in total T4 compared to hPTTG1-Tg male mice on the control diet (n=5, 5.51 μg/dL ±2.03). Comparison of male wild-type and hPTTG1-Tg mice on the iodine deficient diet revealed no difference in total T4 concentration (1.04-fold, p=0.851), suggesting hPTTG1 overexpression in thyroids of male mice has no effect upon T4 concentration following treatment with an iodine-deficient diet. Wild-type female mice on the iodine-deficient diet (n=5, 5.60 μg/dL ±0.04) showed no difference (0.77-fold, p=0.084) in T4 concentration compared to wild-type female mice on the control diet (n=5, 7.30 μg/dL ±0.52). Similarly, hPTTG1-Tg female mice on the iodine-deficient diet (n=5, 6.15 μg/dL ±0.64) showed no difference (1.42-fold, p=0.100) compared to hPTTG1-Tg female mice on the control diet (n=5, 4.32 μg/dL ±0.59). A comparison of wild-type and hPTTG1-Tg female mice on the iodine deficient diet revealed no difference in T4 concentration (1.10-fold, p=0.600), again

suggesting no effect of hPTTG1 overexpression on thyroid hormone synthesis following treatment with an iodine deficient diet.

Total T3 thyroid hormone concentrations were also determined. Wild-type male mice on the iodine-deficient diet (n=5, 64.76 ng/dL ±26.29) demonstrated significantly lower T3 concentration (0.41-fold, p=0.025) compared to wild-type male mice on the control diet (n=5, 157.61 ng/dL ±16.94). However, male hPTTG1-Tg mice on the iodine-deficient diet (n=5, 97.26 ng/dL ±26.27) showed no difference (0.66-fold, p=0.245) in total T3 compared to hPTTG1-Tg male mice subjected to the control diet (n=5, 147.62 ng/dL ±28.97). Comparison of wild-type and hPTTG1-Tg male mice on the iodine-deficient diet showed no difference (1.50-fold, p=0.415) in total T3 concentration. For female wild-type mice, those treated with the iodine-deficient diet (n=5, 85.39 ng/dL ±6.86) showed no difference (0.71-fold, p=0.322) compared to wild-type female mice on the control diet (n=5, 120.24 ±22.48). Similarly, hPTTG1-Tg female mice treated with the iodine-deficient diet (n=5, 96.51 ng/dL ±10.74) showed no difference (0.71-fold, p=0.153) compared to hPTTG1-Tg female mice treated with the control diet (n=5, 135.15 ng/dL ±16.33). Comparison of wild-type and hPTTG1-Tg female mice on the iodine-deficient diet again demonstrated no difference (1.13-fold, p=0.665).

Overall, determination of T4 concentrations revealed no differences either between mice on the control diet or iodine-deficient diet, or between wild-type and hPTTG1-Tg mice. For T3 concentrations, wild-type male mice treated with the iodine-deficient diet possessed a significantly lower

concentration compared to control diet mice, although this was not true for hPTTG1-Tg male mice or female mice. Trends towards lower total T3 and T4 concentrations in mice treated with the iodine-deficient diet indicates that larger numbers of mice may have provided statistical differences. No differences were observed when circulating thyroid hormone concentrations were compared between wild-type and hPTTG1-Tg mice.

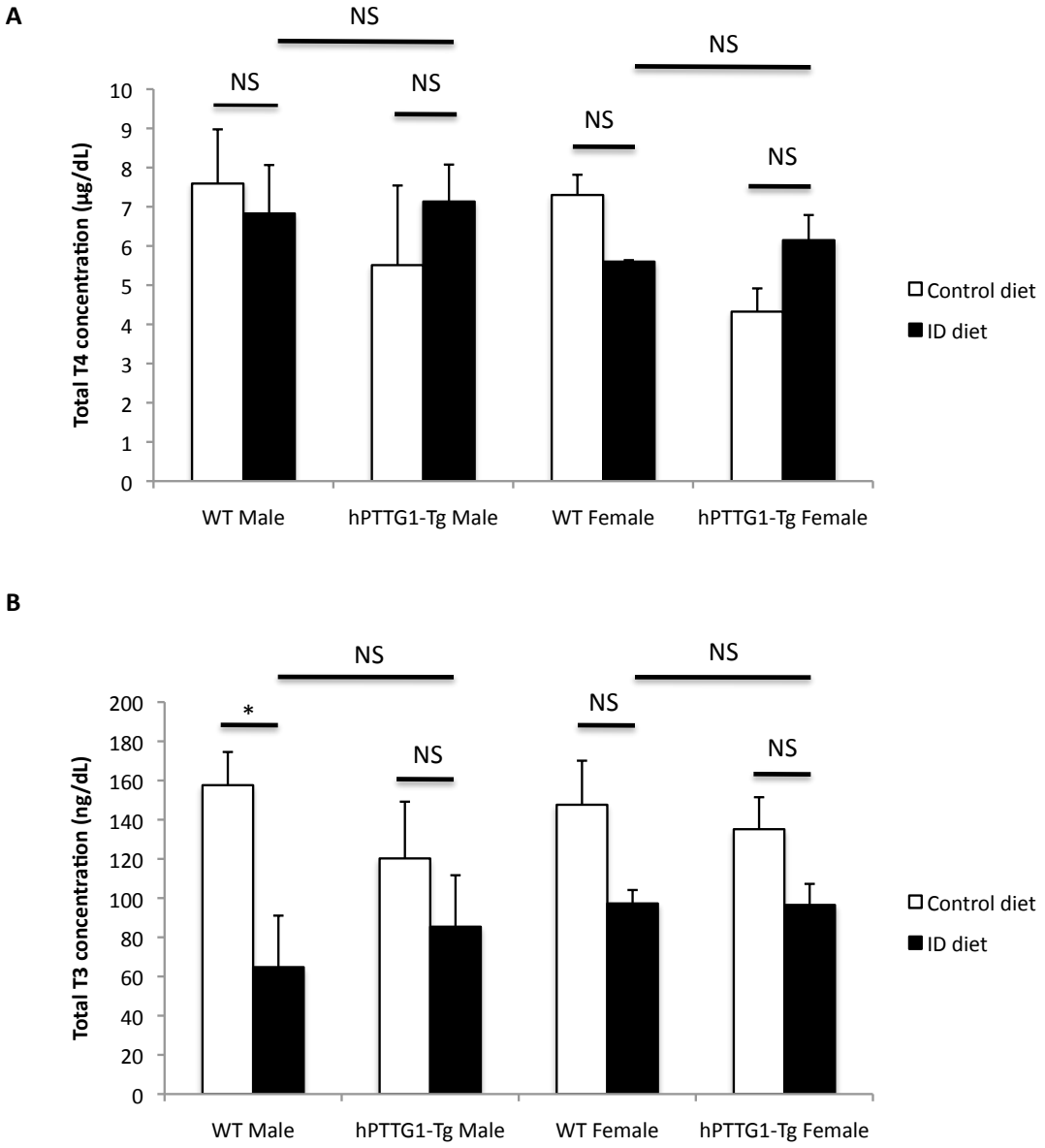

Figure 5.2: Thyroid hormone concentrations of wild-type and hPTTG1-Tg mice on either the control or iodine-deficient diet. ***A.*** *Total T4 concentration from serum of wild-type and hPTTG1-Tg male and female mice on either the control or iodine-deficient diet, showing no difference in T4 concentration across all conditions.* ***B.*** *Total T3 concentration from serum of wild-type and hPTTG1-Tg male and female mice on either the control or iodine-deficient diet, showing no difference in T3 concentration across all conditions. (NS=non-significant, *=p<0.05, **=p<0.005, ***=p<0.0005).*

5.3.3: Thyroid size and histology of *Pttg1* knockout mice

To investigate the effect of *Pttg1* knockout on goitre induction, 6-week old wild-type and *Pttg1* knockout mice were subjected to either a control or iodine-deficient diet for 4 weeks. Following this, mice were culled and thyroids were weighed and harvested for histology. Representative photographs of thyroid glands from wild-type and hPTTG1-Tg mice on either the control diet or iodine-deficient diet are shown in figure 5.3. Thyroid glands from wild-type and *Pttg1* knockout mice on the iodine deficient diet were macroscopically larger than those on the control diet, and showed evidence of increased vascularisation (Figure 5.3). No difference in body weight was found when comparing wild-type and knockout mice following 4 weeks of diet change (data not shown). Wild-type male mice on the iodine-deficient diet (n=5, 0.193 ±0.027) showed a significantly increased thyroid:body weight ratio (3.12-fold, p=0.001) compared to wild-type male mice on the control diet (n=5, 0.062 ±0.008). *Pttg1* knockout male mice, subjected to the iodine deficient diet (n=5, 0.185 ±0.012), also showed a significantly increased thyroid:body weight ratio (3.11-fold, $p=3.56x10^{-5}$) compared to *Pttg1* knockout male mice subjected to the control diet (n=5, 0.059 ±0.010). Comparison of wild-type and *Pttg1* knockout male mice on the iodine-deficient diet showed no difference (0.96-fold, p=0.780), suggesting *Pttg1* knockout has no effect upon goitre formation. Similarly, wild-type female mice on the iodine deficient diet (n=5, 0.253 ±0.027) showed a significantly increased thyroid:body weight ratio (3.65-fold,

p=0.0002) compared to wild-type female mice on the control diet (n=5, 0.069 ±0.005). *Pttg1* knockout female mice on the iodine-deficient diet (n=5, 0.196 ±0.014) had significantly increased thyroid:body weight ratio (3.34-fold, $p=9.64x10^{-6}$) compared to *Pttg1* knockout female mice on the control diet (n=5, 0.059 ±0.002). Comparison of wild-type and *Pttg1* knockout female mice subjected to the iodine deficient diet showed no difference (0.77-fold, p=0.095), again suggesting *Pttg1* knockout has no effect upon goitre formation *in vivo* (Figure 5.3).

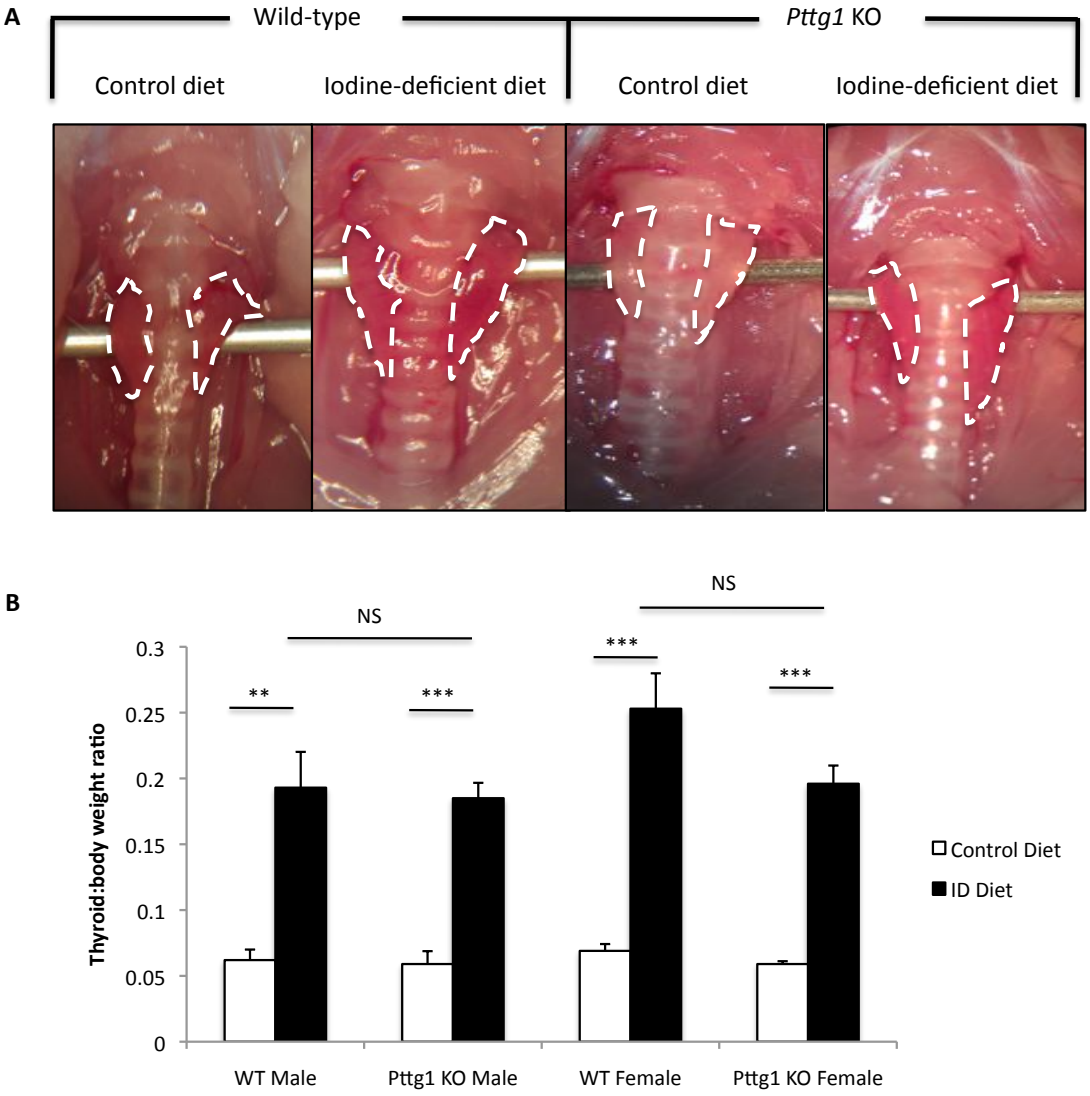

Figure 5.3: Goitre induction in Pttg1 knockout mice. ***A.*** *Representative photographs of thyroid glands from wild-type and Pttg1 knockout mice, subjected to control or iodine-deficient diet for 4 weeks. Thyroid glands are shown inside white dotted lines.* ***B.*** *Comparison of thyroid:body weight ratio between mice on control diet or iodine-deficient (ID) diet, for wild-type male, Pttg1 knockout male, wild-type female and Pttg1 knockout female. (NS=non significant, **=p<0.005, ***=p<0.0005).*

5.3.4: Serum thyroid hormone concentrations of *Pttg1* knockout mice

Serum was extracted from wild-type and *Pttg1* knockout male and female mice, subjected to either the control or iodine-deficient diet, and concentrations of total T3 and T4 were determined by radioimmunossay. Wild-type male mice on the iodine-deficient diet (n=5, 1.04 μg/dL ±0.42) showed significantly lower concentrations of T4 (0.18-fold, p=0.005) compared to wild-type male mice on the control diet (n=5, 5.83 μg/dL ±1.03), and similarly *Pttg1* knockout male mice on the iodine-deficient diet (n=5, 0.91 μg/dL ±0.14) demonstrated a significantly lower concentration of T4 (0.18-fold, p=0.003) compared to *Pttg1* knockout male mice on the control diet (n=5, 5.15 μg/dL ±0.86). Comparison between wild-type and hPTTG1-Tg male mice on the iodine deficient diet revealed no difference in T4 concentration (0.87-fold, p=0.77). Wild-type female mice on the iodine-deficient diet (n=5, 1.13 μg/dL ±0.19) showed significantly lower concentrations of T4 (0.19-fold, p=0.005) compared to wild-type female mice on the control diet (n=5, 4.91 μg/dL ±1.11), and similarly *Pttg1* knockout female mice on the iodine-deficient diet (n=5, 0.98 μg/dL ±0.30) demonstrated a significantly lower concentration of T4 (0.23-fold, p=0.0009) compared to *Pttg1* knockout female mice on the control diet (n=5, 4.74 μg/dL ±0.72). However, comparison between wild-type and hPTTG1-Tg female mice on the iodine deficient diet revealed no difference in T4 concentration (0.96-fold, p=0.76).

Wild-type male mice on the iodine-deficient diet (n=5, 51.50 ng/dL ±8.63) showed no difference in concentration of T3 (0.71-fold, p=0.124) compared to wild-type male mice on the control diet (n=5, 73.51 ng/dL ±8.77), and similarly *Pttg1* knockout male mice on the iodine-deficient diet (n=5, 61.61 ng/dL ±11.12) demonstrated no difference in the concentration of T3 (0.83-fold, p=0.173) compared to *Pttg1* knockout male mice on the control diet (n=5, 82.43 ng/dL ±7.62). Comparison between wild-type and *Pttg1* knockout male mice on the iodine deficient diet revealed no difference in T3 concentration (1.2-fold, p=0.50). Wild-type female mice on the iodine-deficient diet (n=5, 64.35 ng/dL ±9.80) showed no difference in concentrations of T3 (0.76-fold, p=0.331) compared to wild-type female mice on the control diet (n=5, 77.75 ng/dL ±8.01), and similarly *Pttg1* knockout female mice on the iodine-deficient diet (n=5, 62.01 ng/dL ±8.41) demonstrated no difference in the concentration of T3 (0.79-fold, p=0.171) compared to *Pttg1* knockout female mice on the control diet (n=5, 79.20 ng/dL ±7.00). Again, comparison between wild-type and *Pttg1* knockout female mice on the iodine deficient diet revealed no difference in T3 concentration (0.-fold, p=0.862).

These results indicate that treatment with an iodine-deficient diet and methimazole and sodium perchlorate leads to a reduction in total T4, but not T3 concentrations. Knockout of *Pttg1* had no effect upon circulating thyroid hormone concentrations compared to wild-type mice.

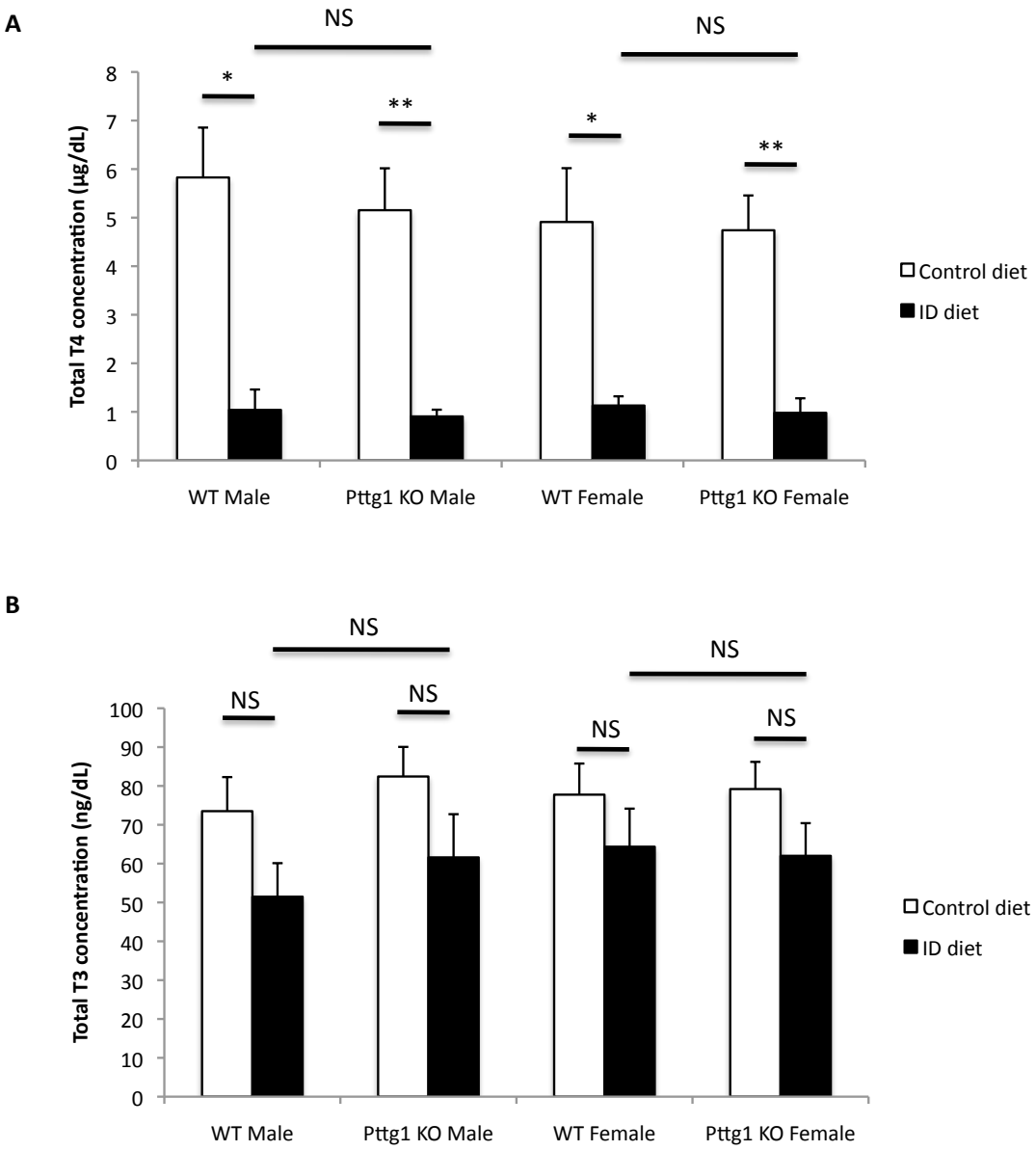

Figure 5.4: Thyroid hormone concentrations of Pttg1 knockout mice on either the control or iodine-deficient diet. ***A.*** *Total T4 concentration from serum of wild-type and Pttg1 knockout male and female mice on either the control or iodine-deficient diet.* ***B.*** *Total T3 concentration from serum of wild-type and Pttg1 knockout male and female mice on either the control or iodine-deficient diet, showing no difference in T3 concentration across all conditions. (NS=non-significant, *=p<0.05, **=p<0.005, ***=p<0.0005).*

5.3.5: Thyroid size and histology of PBF transgenic mice

A preliminary experiment to determine the effect of goitre induction on PBF overexpressing transgenic mice was also performed. Wild-type and PBF transgenic mice, at 6-weeks old, were subjected to either a control or iodine-deficient diet for 4 weeks. Following this, mice were culled and thyroids were harvested for examination. Macroscopic examination revealed thyroids were larger in PBF transgenic mice compared to wild-type, and that thyroids were larger in mice subjected to the iodine-deficient diet compared to those on the control diet. Thyroid:body weight ratio, used to normalise for body weight, showed a significant increase (1.66-fold, p=0.02) in wild-type female mice on the iodine-deficient diet (n=5, 0.207 ±0.011) compared to wild-type female mice on the control diet (n=5, 0.125 ±0.023). Similarly, PBF-Tg female mice showed a significant increase (2.17-fold, $p=3.14x10^{-5}$) in thyroid:body weight ratio on the iodine-deficient diet (n=4, 0.513 ±0.021) compared to PBF-Tg female mice on the control diet (n=4, 0.237 ±0.014). Comparison of wild-type mice and PBF-Tg mice on the control diet revealed a significantly greater (1.88-fold, p=0.006) thyroid:body weight ratio in PBF-Tg mice compared to wild-type. Also, comparison of wild-type mice and PBF-Tg mice on the iodine-deficient diet revealed a significantly greater (2.48-fold, $p=3.14x10^{-5}$) thyroid:body weight ratio in PBF-Tg mice (n=4, 0.513 ±0.021) compared to wild-type mice (n=4, 0.207 ±0.011). Using a correction factor to account for the increased thyroid:body weight ratio apparent in PBF transgenic mice on the control diet, the PBF transgenic mice on the iodine-

deficient diet still showed a significantly increased thyroid:body weight ratio (1.31-fold, p=0.006) compared to wild-type mice on the iodine-deficient diet, suggesting PBF overexpression results in increased goitre formation.

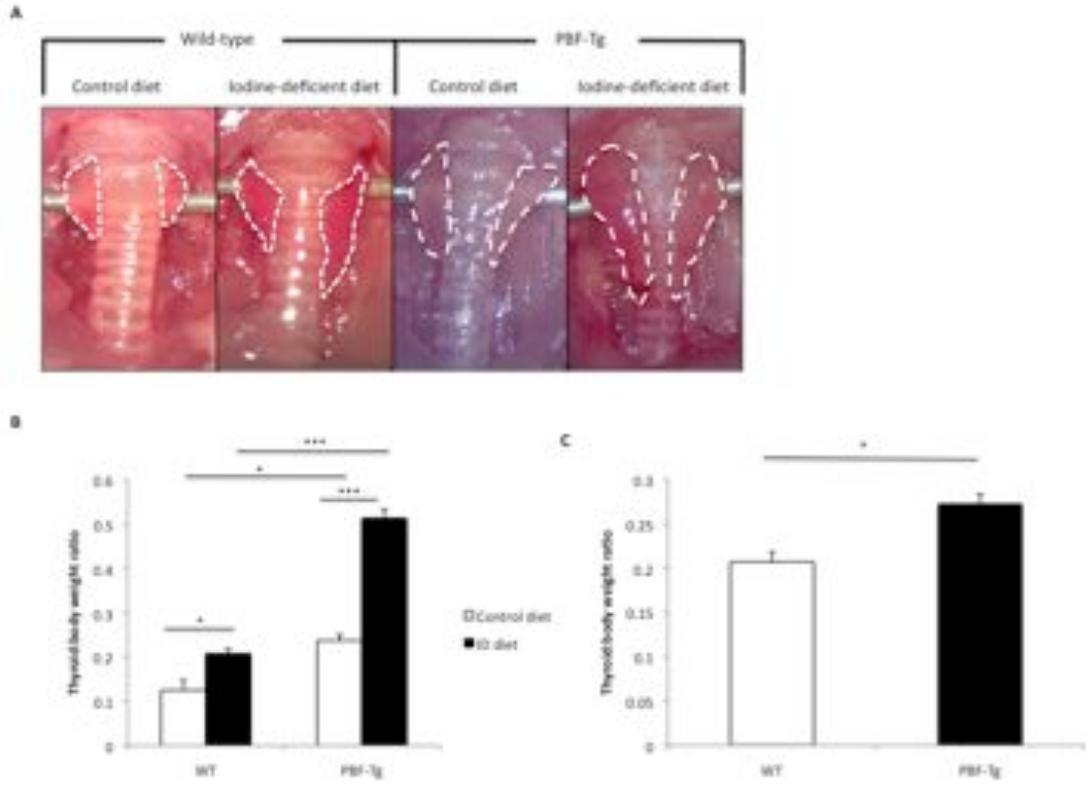

Figure 5.5: Goitre induction in PBF-Tg mice. ***A.*** *Representative photographs of thyroid glands from wild-type and PBF-Tg mice, subjected to control or iodine-deficient diet for 4 weeks. Thyroid glands are shown inside white dotted lines.* ***B.*** *Comparison of thyroid:body weight ratio between mice on control diet or iodine-deficient (ID) diet, for wild-type and PBF-Tg (female) mice.* ***C.*** *Histogram displaying comparison of thyroid:body weight ratio between wild-type and PBF-Tg (female mice) on the iodine-deficient diet, following use of a correction factor for PBF-Tg increased thyroid:body weight ratio. (*=p<0.05, ***=p<0.0005).*

5.4: Discussion

5.4.1: Goitre induction in hPTTG1 transgenic mice

To determine if hPTTG1 plays a role in goitre induction, hPTTG1 transgenic and wild-type mice were subjected to either a control or iodine-deficient diet as described in section 5.2.1. Results showed a significant approximately 1.75-fold increase in thyroid size, in wild-type and hPTTG1-Tg male and female mice, following goitre induction. However, there was no difference between wild-type and hPTTG1-Tg mice, suggesting overexpression of hPTTG1 has no effect upon goitre induction. Surprisingly, our standard methods of goitre induction did not result in reductions in total T4 concentrations in wild-type or hPTTG1-Tg mice. Total T3 concentrations were significantly reduced following administration of an iodine-deficient diet in wild-type male mice compared with those on the control diet. Other conditions did not show significant differences, although there were trends towards lower total T3 following administration of iodine-deficient diets in wild-type and hPTTG1-Tg mice. The increased thyroid:body weight ratio following our goitre induction approach is consistent with endogenous thyroid hormone suppression, and the trend towards lower total T3 concentrations in mice subjected to the iodine-deficient diet confirms this. It is plausible that a longer duration of our goitregenic approach may result in more pronounced goitre formation and more effective suppression of endogenous thyroid hormone production. Furthermore the strain of mice

used (FVB/N) is different to that used in previous experiments by Di Cosmo (Di Cosmo et al, 2010), in which c57bl6 mice were used and a greater degree of goitre induction was observed (approximately 3.0-fold).

We observed no difference in thyroid:body weight ratio when comparing wild-type and hPTTG1-Tg mice following administration of an iodine-deficient diet, indicating that hPTTG1 overexpression has no effect on goitre formaiton. Indeed, from results in chapter 3, showing reduced cellular proliferation in mice overexpressing hPTTG1, it is plausible that a reduction in goitre formation would be observed in hPTTG1-Tg mice. As stated, a longer duration of iodine-deficient diet administration may have resulted in more pronounced effects on goitre formation in wild-type and transgenic mice, and future experiments could focus on this. Future experiments should also investigate the effect on TSH concentrations, which theoretically would be induced by goitre formation, as found by Di Cosmo (Di Cosmo et al, 2010). This may prove crucial in determining the influence of hPTTG1 overexpression on goitre induction, and this experiment was only not performed due to time and financial constraints.

5.4.2: Goitre induction in *Pttg1* knockout mice

Results in *Pttg1* knockout mice revealed a significant approximately 3-fold increase in thyroid:body weight ratio in mice on the iodine-deficient diet compared to mice on the control diet. Also, there was a significant decrease

in total T4, but not total T3 concentrations in mice on the iodine-deficient diet compared to those on the control diet. These findings were evident in both wild-type and *Pttg1* knockout male and female mice, suggesting endogenous thyroid hormone suppression was achieved following administration of methimazole, sodium perchlorate and the iodine-deficient diet. A possible reason for the lack of suppression of T3 is preferential production of T3 in conditions of iodine deficiency (Obregon et al, 2005) (Pedraza et al, 2006), which was also observed by Di Cosmo et al following use of the described diet (Di Cosmo et al, 2010). Our results show differential goitre induction in c57bl6 mice (*Pttg1* knockout) and FVB/N mice (hPTTG1-Tg), with more pronounced goitre induction (3-fold v 1.75-fold) and suppression of endogenous thyroid hormone concentration observed in c57bl6 mice. The differences in T4 and T3 concentrations between c57bl6 mice on the control and iodine-deficient diet were similar to those found by Di Cosmo et al (Di Cosmo et al, 2010) in their paper on the *Mct8* knockout mice, suggesting use of the iodine-deficient diet to elicit goitre formation in c57bl6 mice was successful. However, no difference in goitre formation was found between wild-type and *Pttg1* knockout mice following administration of the goitregenic approach, indicating that *Pttg1* deletion has no effect upon goitre formation. Although these results were similar to those found by Di Cosmo, future experiments should focus on determining TSH concentrations, as it would be important to fully investigate the effect on thyroid function. As mentioned previously, these experiments would have been performed, however financial constraints prevented this.

5.4.3: Goitre induction in PBF transgenic mice

Preliminary experiments to determine the *in vivo* effect of PBF overexpression on goitre formation demonstrated interesting results. Only female PBF-Tg mice were available for this experiment. As observed in previous mouse experiments detailed in this chapter, both wild-type and PBF transgenic mice showed significantly increased thyroid:body weight ratio following our protocol of goitre induction. PBF transgenic mice had a significantly increased thyroid:body weight ratio compared with wild-type mice on the control diet, which corresponds with previous results in our group showing significantly enlarged thyroids in PBF transgenic mice (Read et al, 2011). Interestingly, results also revealed PBF transgenic mice on the iodine-deficient diet had significantly increased thyroid:body weight ratio compared to control mice on the iodine-deficient diet, suggesting that PBF overexpression may facilitate increased goitre formation. This could be through increased cellular proliferation or another mechanism, which it may prove important to determine.

To determine if endogenous thyroid hormones are suppressed, radioimunnoassays should be performed and serum TSH concentration should be measured. These experiments also need to be confirmed in larger numbers of mice and following administration of our goitregenic approach for a longer duration. Our group is currently investigating a possible *Pbf*

knockout mouse model, and should this be successfully developed, it would be interesting to test whether knockout of *Pbf* has an effect upon goitre formation.

5.4.4: Conclusions

In conclusion, neither PTTG1 overexpression nor deletion affected goitre formation in our mouse models, and it seems unlikely that PTTG1 plays an important role in early goitregenesis. However, preliminary experiments using mice overexpressing PBF targeted to the thyroid have revealed a possible role for PBF in goitre induction, although further investigations are required to confirm these findings.

Chapter 6. Relationship between PBF, p53 and MDM2

6.1: Introduction

p53 is a potent transcription factor which has been shown to be mutated in approximately 50% of all cancers (Olivier et al, 2002). However, papillary and follicular thyroid cancer, which form the vast majority of thyroid cancers, have a low incidence of p53 mutation. Indeed, only 11.3% of all thyroid cancers show evidence of p53 mutations, with the majority of these comprising aggressive anaplastic carcinomas (Kondo et al, 2006) (Smallridge et al, 2009). Therefore it seems likely another means of p53 inactivation may occur in thyroid cancer, and it will be important to understand the mechanisms surrounding this inactivation in terms of thyroid cancer tumourigenesis and progression to de-differentiation.

PBF is a 22 kDa protein, which was initially discovered as the binding factor of the pituitary tumor-transforming gene (Chien and Pei, 2000). It is involved in several cellular processes, including the DNA damage response (Read et al, 2013, Manuscript under revision), and has also been shown to be increased in thyroid cancer (Stratford et al, 2005). We have shown that PBF specifically interacts with p53 as demonstrated through GST pull-down assays using *in vitro* translated protein, and co-immunoprecipitation assays in TPC1 and K1 papillary thyroid carcinoma cells, and in HCT116 colorectal cancer cells. Investigations into this interaction, through protein stability assays, revealed overexpression of PBF significantly reduces the half-life of the p53 protein, whereas PBF knockdown through siRNA increased p53 half-life in K1, TPC1 and HCT116 cells (Read et al, 2013, Manuscript under

revision). p53 degradation is primarily achieved through ubiquitination of the protein, essentially tagging p53 for degradation by the proteasome. We performed ubiquitination assays which revealed increased ubiquitination of p53 following overexpression of PBF, thereby providing a mechanism by which the increased degradation is achieved (Read et al, 2013, Manuscript under revision).

The primary regulator of p53, via regulation of its ubiquitination, is the E3 ubiquitin ligase MDM2. MDM2 exists in a negative feedback loop with p53, whereby p53 transcribes MDM2, which subsequently degrades p53 and blocks its transactivation activity, keeping levels of p53 and MDM2 low under normal physiological conditions. Following DNA damage, the interaction between p53 and MDM2 is inhibited through a number of mechanisms such as acetylation (Li et al, 2002) and binding of proteins, such as ARF, to MDM2 (Sherr, 2001), thereby stabilising p53. Recent research has focused upon disrupting the interaction between p53 and MDM2 through the use of small molecule inhibitors; increasing p53 expression and initiating the DNA damage response to combat cancer cells. A number of inhibitors have been discovered, such as HL198, which inhibits the E3 ligase activity of MDM2 (Yang et al, 2005), and RITA, which binds to p53 to inhibit its interaction with MDM2 (Issaeva et al, 2004). The first inhibitor identified was Nutlin-3, which binds to the p53 pocket of the MDM2 protein, and inhibits the p53-MDM2 interaction efficiently at low concentrations (IC_{50}=90nM). Nutlin-3 has been shown to be capable of entering several types of cultured cells and to stabilise p53. Proliferating cancer cells were shown to be blocked in the G1

and G2 phases of the cell cycle, with nutlin-3 causing apoptosis (Vassilev et al, 2004). Nutlin-3 has been shown to have a potential role in cancer therapy (Tovar et al, 2006). Indeed, inhibitors of the p53-MDM2 interaction generally are unable to be effective when p53 is mutated. Since thyroid cancers possess low levels of p53 mutation (Olivier et al, 2002), and MDM2 overexpression has previously been shown to be a factor in p53 inactivation (Jennings et al, 1995), inhibition of the p53-MDM2 interaction could provide a therapeutic strategy in thyroid cancer.

Previous chapters in this thesis have focused on PTTG, and while these investigations have proved useful, we also sought to investigate its binding partner PBF, and the role that PBF plays in thyroid tumourigenesis. Both hPTTG1 (Heaney et al, 2001) (Boelaert et al, 2003) and PBF (Stratford et al, 2005) have increased expression in thyroid cancer, and following on from our previous research described in section 1.5.5, we determined that investigating the role of PBF in thyroid tumourigenesis may also prove important. The work carried out in this chapter comprises our investigations into the interaction between PBF and the E3 ubiquitin ligase MDM2. We sought to determine if co-localisation between PBF and MDM2 occurred in thyroid cancer cells and to investigate the role of MDM2 in the PBF-mediated p53 degradation.

6.2: Materials and Methods

6.2.1: Cell lines

Cell lines were cultured as described in section 2.2. TPC1 cells were seeded at 1.875 x10^6 per 25 cm^2 surface growth area. K1 and HeLa cells were seeded at 2.5 x10^6 per 25 cm^2 surface growth area.

6.2.2: Plasmid transfection

Transfection of plasmids was performed as described in section 2.3. Plasmids used were pcDNA3-VO, pcDNA3-PBF, pcDNA3-PBF-HA and pcDNA3-MDM2.

6.2.3: Inhibitor treatment

The Nutlin-3 inhibitor (Sigma-Aldrich, St louis, MO, USA) was used to disrupt p53-MDM2 binding by competitive inhibition. TPC1 cells were treated with the Nutlin-3 inhibitor 16 hours post-transfection. Nutlin-3 was diluted in DMSO (Dimethyl sulfoxide) (Sigma-Aldrich, St louis, MO, USA) and subsequently diluted in OPTI-MEM media to a final concentration of 10 μM

and added to cells after removal of cell media. Cells were then subsequently harvested 8 hours post-treatment.

6.2.4: Protein extraction and quantification

Total protein from cells was extracted as described in section 2.7, and protein was quantified using the BCA assay.

6.2.5: GST pull-down assay

GST pull-down assays were performed by labelling one recombinant protein with ^{35}S-methionine and tagging the other recombinant protein with a GST tag using manufacturer's instructions (TNT coupled reticulocyte lysate system) (Promega, Madison, WO, USA). GST-tagged protein was incubated with ^{35}S-methionine labelled protein for 1 hour on ice. Subsequently, low salt buffer was added together with glutathione agarose beads for 90 minutes at 4 ^{0}C with mixing. Following centrifugation and removal of supernatant, beads were washed in low salt buffer and eluted with 25 mM glutathione in 50 mM Tris at pH 8 on ice for 1 hour. Eluted protein was recovered following centrifugation and analysed by Western blotting.

6.2.6: Co-Immunoprecipitation assay

Co-immunoprecipitation assays were performed as described in section 2.15. Antibodies used were anti-MDM2 (SMP-14) (1/250) (Santa Cruz Biotechnology, Dallas, TX, USA) and anti-PBF (1/250) (Eurogentec, Southampton, Hampshire, UK). A no antibody and a random isotype antibody control were used as negative controls.

6.2.7: Protein stability assay

Protein stability assays were carried out in TPC1 cells as described in section 2.16. For p53 and MDM2 proteins, timepoints of 0, 60, 90 and 120 minutes were used.

6.2.8: Western blotting

Western blotting was performed as described in section 2.14. Antibodies used were anti-PBF (1/250) (Eurogentec, Southampton, Hampshire, UK), anti-p53 (DO-1) (1/500) (Santa Cruz Biotechnology, Dallas, TX, USA) and

anti-MDM2 (SMP-14) (1/250) (Santa Cruz Biotechnology, Dallas, TX, USA). Appropriate secondary antibodies were used.

6.2.9: Immunofluorescence

Immunofluorescence was performed as described in section 2.17. Primary antibodies used were anti-p53 (DO-1) (1/500) (Santa Cruz Biotechnology, Dallas, TX, USA), anti-MDM2 (SMP-14) (1/400) (Santa Cruz Biotechnology, Dallas, TX, USA) and anti-PBF (1/1000) (Eurogentec, Southampton, Hampshire, UK). Secondary antibodies used were Alexa Fluor 488 conjugated goat anti-mouse IgG and Alexa Fluor 594 conjugated goat anti-rabbit IgG (Invitrogen, Life Technologies Ltd, Paisley, UK) used at a concentration of 1:250. Hoescht stain was added at 1:1000 concentration to visualise DNA.

6.2.10: Proximity ligation assay

The Duolink in situ proximity ligation assay was performed according to manufacturer's instructions (Olink Bioscience, Uppsala, Sweden). Briefly, cells were seeded onto coverslips and transfected 24 hours later. Cells were harvested 48-72 hours later, before fixing and permeabilising. Samples were

blocked and primary antibody added. The PLA probes were added, consisting of a secondary antibody conjugated to an oligonucleotide, and incubated. A ligation solution was added, containing a ligase which allowed hybridisation of the probes and joining if in close proximity. Subsequently, an amplification solution (consisting of nucleotides and fluorescently labelled oligonucleotides) was added. Rolling circle amplification occurs, generating a concatermeric product, which hybridises to the fluorescently labelled oligonucleotides. Fluorescence microscopy is used to determine interaction between the two proteins.

6.3: Results

6.3.1: GST pull-down of wild-type and mutant PBF and MDM2

A GST pull-down assay was performed in order to confirm initial observations of a specific interaction between PBF and MDM2. ^{35}S-methionine labelled MDM2 was incubated *in vitro* with GST-tagged PBF, resulting in a band for GST-PBF but not for GST alone, which was used as a negative control, suggesting a specific interaction between PBF and MDM2 *in vitro* (Figure 6.1). To determine the sites of potential interaction with MDM2, mutants 1, 2 and 3 (Figure 6.2) of PBF were GST-tagged and tested for an interaction with MDM2, which was kindly performed by Dr Andrew Turnell. Results showed MDM2 appears to interact with mutants 1, 2 and 3 (Figure 6.1).

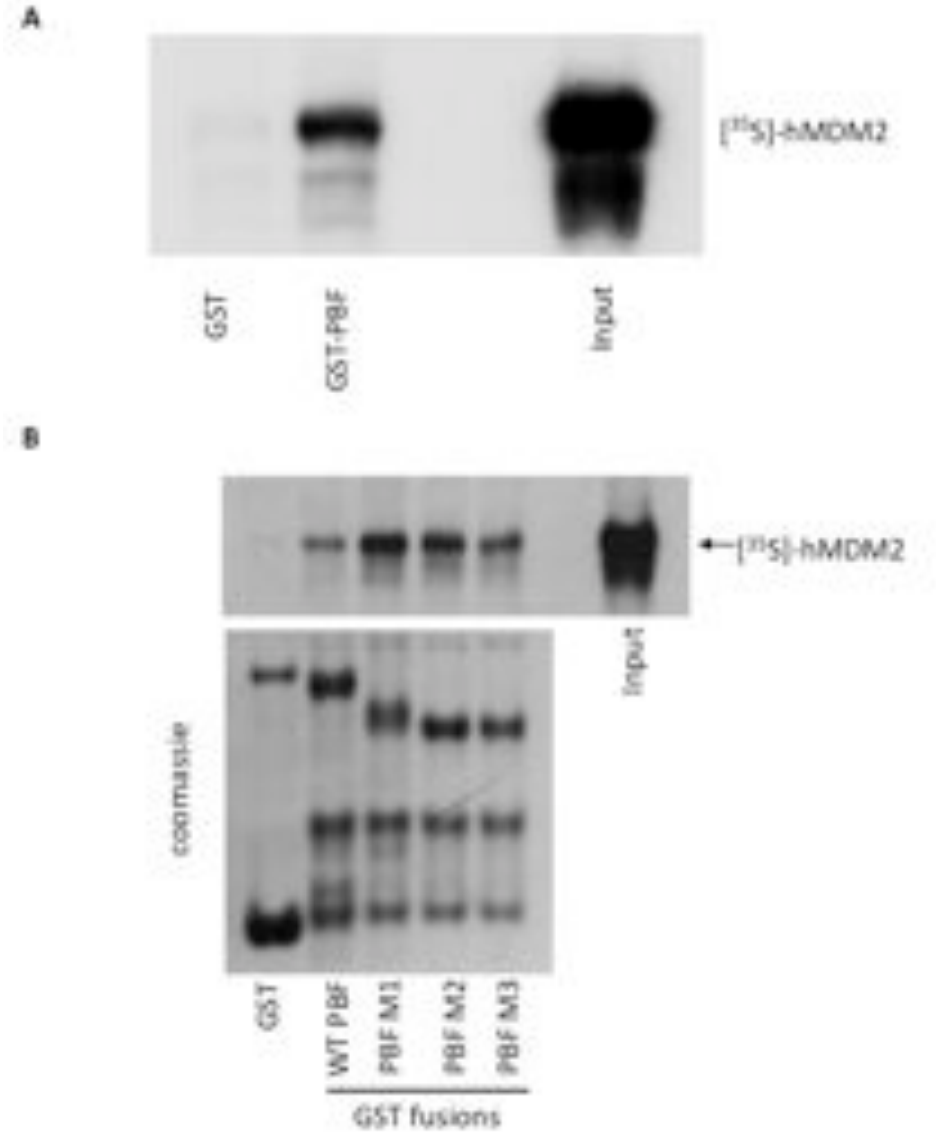

Figure 6.1: ***A.*** *GST pull-down assay displaying a specific interaction in vitro between GST-tagged* PBF *and* ^{35}*S-methionine labelled* MDM2*, with no interaction with GST alone.* ***B.*** *GST pull-down assay displaying a specific interaction in vitro between GST-tagged wild-type* PBF*, and GST-tagged* PBF *mutants 1, 2 and 3 with* ^{35}*S-methionine labelled* MDM2*. No interaction was found with GST alone.*

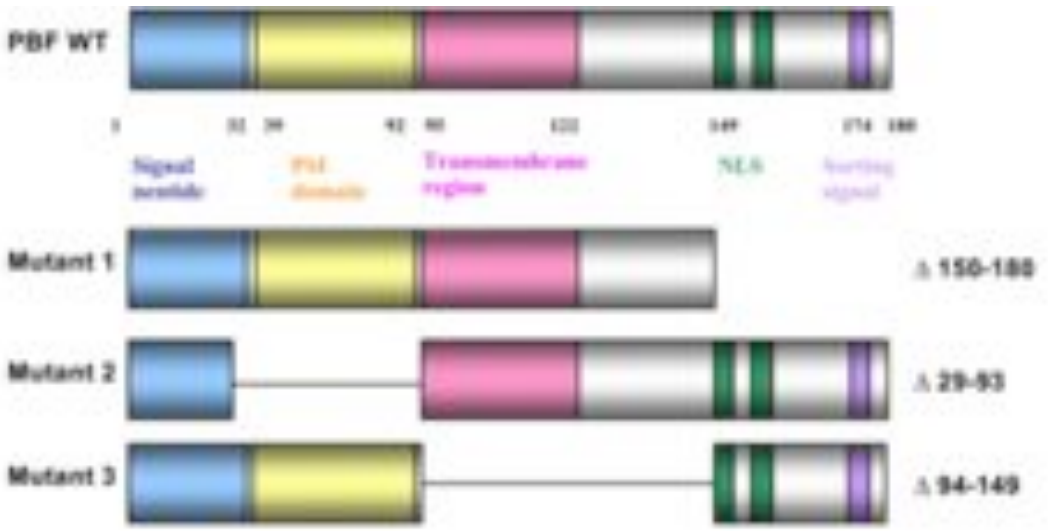

Figure 6.2: Diagram showing wild-type PBF and mutants 1, 2 and 3. Mutant 1 has the C-terminal NLS and sorting signal deleted. Mutant 2 has the PSI domain deleted. Mutant 3 has the transmembrane region deleted.

6.3.2: Co-IP of PBF and MDM2

To determine if the interaction of PBF with MDM2 occurred in cells, as opposed to *in vitro* translated protein GST-pull down assays, co-immunoprecipitation assays were performed. Co-IPs of PBF and MDM2 were attempted with wild-type and HA-tagged PBF and wild-type MDM2 using a range of different conditions. These included reducing and non-reducing elution buffer, and lysis buffers used were RIPA and NETN buffer. However, no interaction was observed in TPC1, K1 or HeLa cells (Figure 6.3).

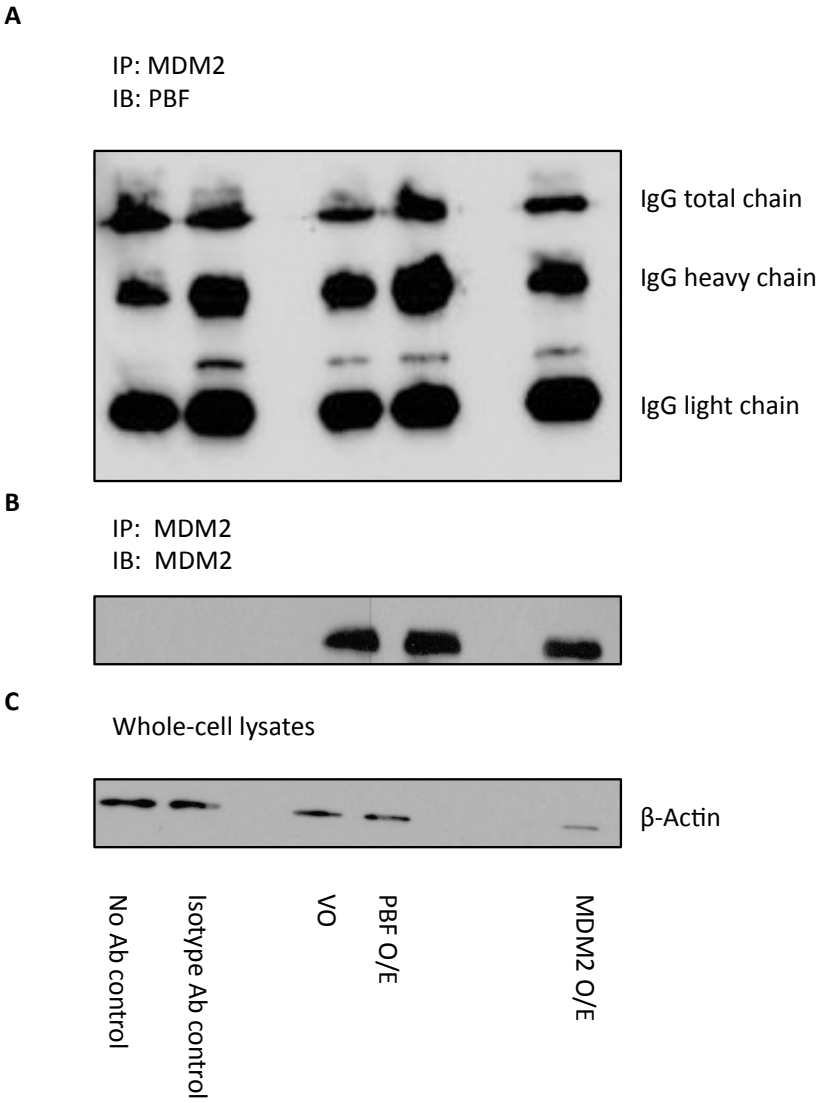

Figure 6.3: Co-immunoprecipitation of MDM2 and PBF in TPC1 cells. ***A.*** *Immunoprecipitation with* MDM2 *and immunoblotting of* PBF. IgG *light, heavy and total chain are labelled. A no antibody control and an isotype specific random antibody control were used as negative controls. VO indicates vector-only transfected cell, PBF O/E indicates pcDNA3-PBF-HA transfected cells and MDM2 O/E indicates pcDNA3-MDM2 transfected cells.* ***B.*** *Immunoprecipitation of* MDM2 *and immunoblotting of MDM2 to confirm immunoprecipitation.* ***C.*** β-actin *expression in whole-cell lysates to confirm protein extraction.*

6.3.3: Proximity ligation assay of PBF and p53, PBF and MDM2

Proximity ligation assays were performed as another method to determine if an interaction between PBF and MDM2 occurred in cells. K1 cells were used, testing the interaction between PBF and p53, and also the interaction between PBF and MDM2. A negative control with no antibody used was used to ensure specificity. A positive interaction between PBF and p53, as well as between PBF and MDM2 was demonstrated, confirming the result from the GST pull-down assays (Figure 6.4) albeit in a limited number of cells. The interaction between PBF and p53 was observed in the cytoplasm, while the interaction between PBF and MDM2 was observed to be cytoplasmic and nuclear, although without confocal microscopy it was not possible to confirm this.

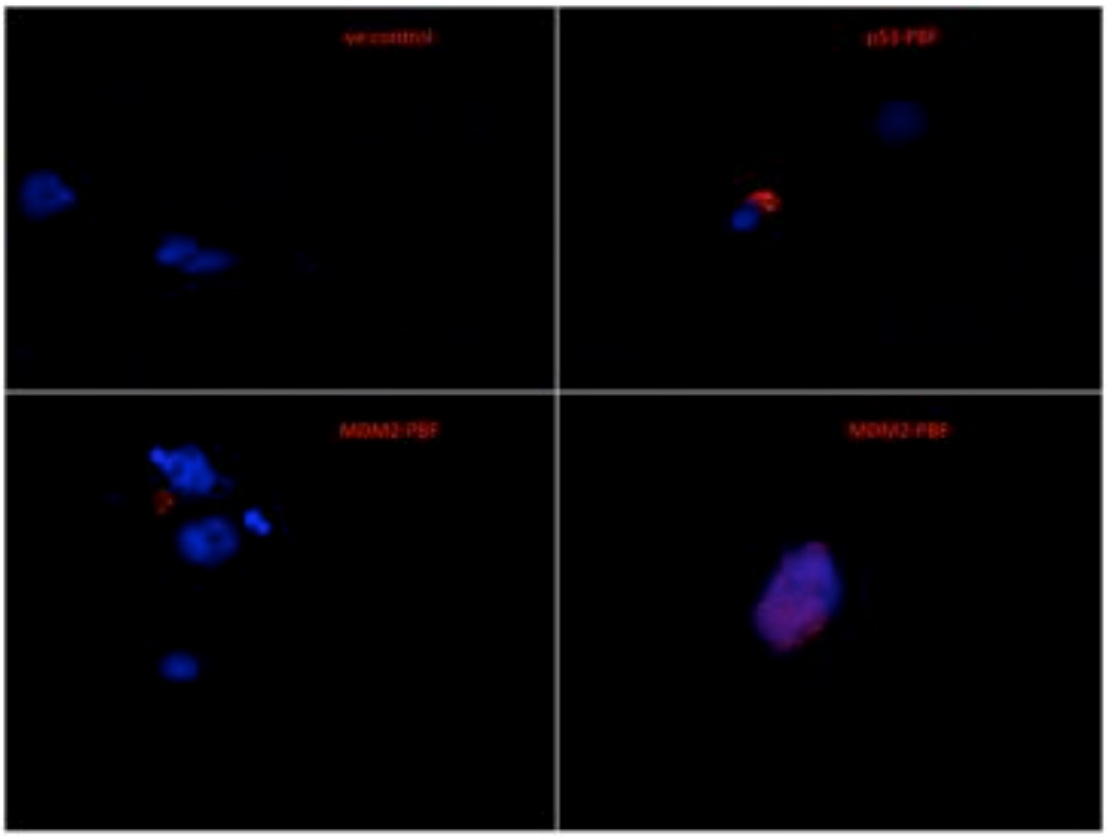

Figure 6.4: Proximity ligation assay showing negative control (no antibody), p53-PBF and MDM2-PBF interactions. Blue indicates DAPI nuclear staining, each red dot indicates a specific interaction between PBF *and* MDM2 (40x magnification).

6.3.4: Co-localisation of PBF and MDM2

Immunofluorescence was performed to investigate co-localisation of PBF and MDM2 proteins. Green indicates MDM2 staining, red indicates staining for PBF, blue indicates nuclear staining for DAPI, while yellow indicates co-localisation between PBF and MDM2. Results in K1 cells showed strong co-

localisation of PBF and MDM2 in the cytoplasm (Figure 6.5). However, no co-localisation of PBF and MDM2 was observed in HeLa cells (Figure 6.5).

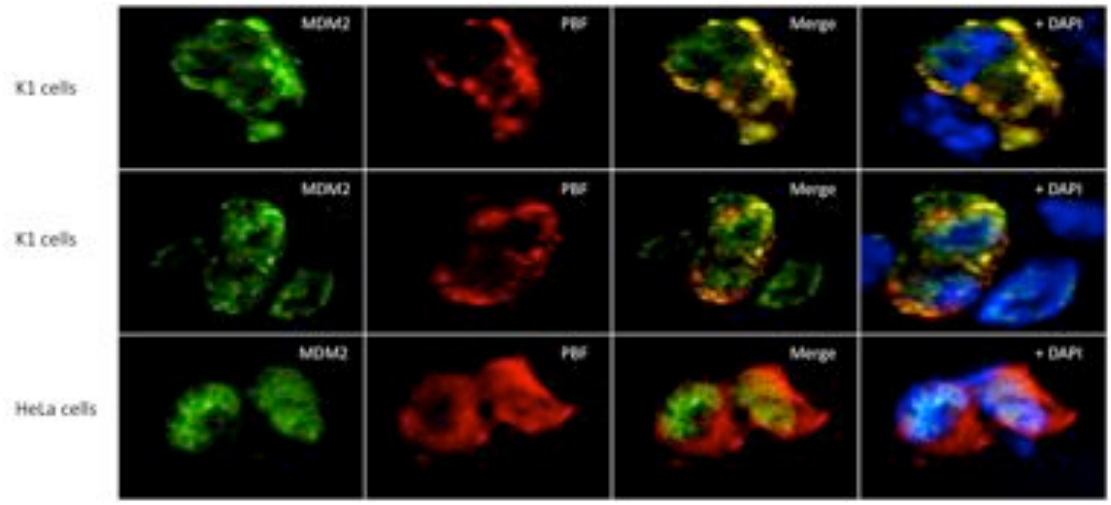

Figure 6.5: Immunofluorescence of MDM2, PBF *and merged pictures +/- DAPI. Performed in K1 and HeLa cells. Green displayed is* MDM2, *red displayed is* PBF, *blue displayed is nuclear DAPI, and yellow indicates co-localisation between* MDM2 *and* PBF.

6.3.5: MDM2 affects PBF-mediated p53 degradation

In order to investigate the effect of MDM2 upon PBF-mediated p53 degradation, the p53-MDM2 competitive inhibitor nutlin-3 was used. To validate nutlin-3 efficiency, TPC1 cells were treated with vehicle only or with nutlin-3 for 8 hours. Following this a protein stability assay was performed and cells were harvested and subjected to protein extraction and Western blotting. Results showed a marked increase in p53 protein expression

following treatment with nutlin-3 (Figure 6.6). We subsequently performed a protein stability assay following transfection with either vector only or pcDNA3-PBF-HA and treatment with either vehicle only or nutlin-3. Results in TPC1 cells (n=3) showed vehicle only cells transfected with pcDNA3-PBF-HA demonstrated a significantly reduced level of p53 at 60 (p=0.03) and 90 (p=0.03) minute time points compared to vector only. There was no difference observed at the 120 minute time point. In contrast, cells treated with nutlin-3 displayed no difference in p53 expression at 60, 90 or 120 minute time points when comparing vector only to cells transfected with pcDNA3-PBF-HA (Figure 6.6).

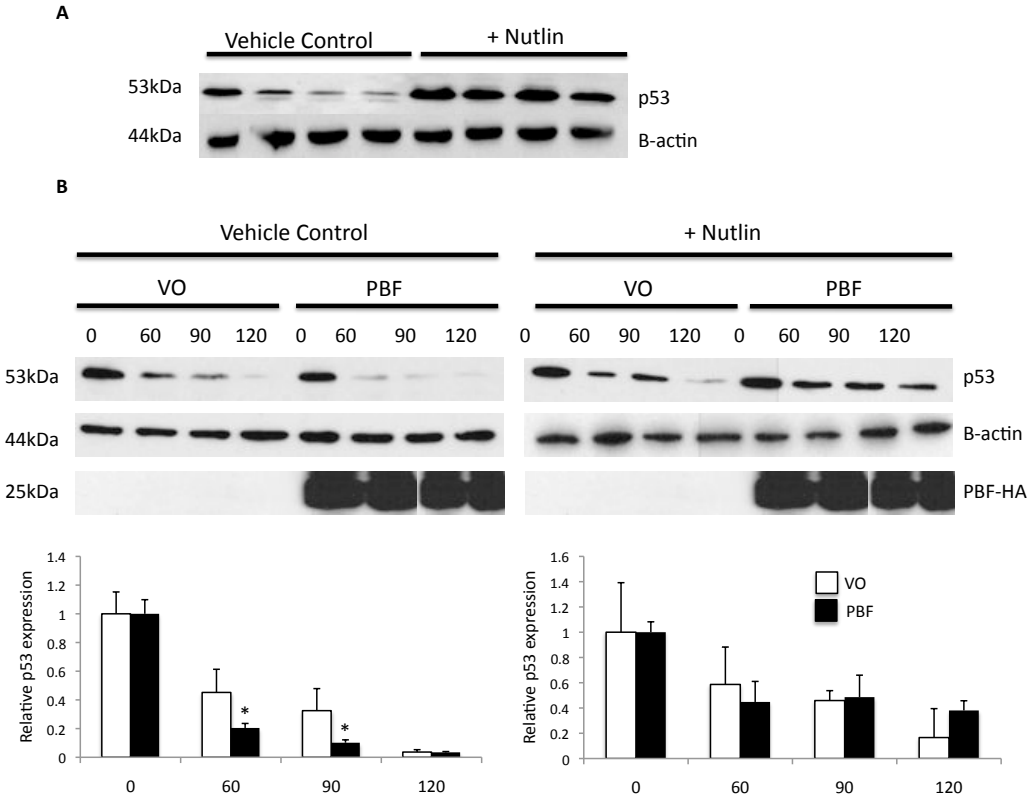

C

Vehicle only

	VO	PBF
0	1.000 ±0.152	1.000 ±0.098
60	0.452 ±0.161	0.205 ±0.031
90	0.325 ±0.154	0.102 ±0.020
120	0.037 ±0.016	0.035 ±0.006

Nutlin-3 treated

	VO	PBF
0	1.000 ±0.392	1.000 ±0.082
60	0.587 ±0.296	0.448 ±0.163
90	0.459 ±0.078	0.486 ±0.174
120	0.166 ±0.229	0.381 ±0.077

Figure 6.6: Nutlin-3 inhibitor treatment in TPC1 cells. ***A.*** *Validation of Nutlin-3 functionality. Western blotting shows increased expression of p53 following treatment with nutlin-3.* ***B.*** *p53 protein expression subsequent to protein stability assay. Cells were treated with either vehicle control or nutlin-3, following transfection of vector only or pcDNA3-PBF-HA. Densitometry is shown below.* ***C.*** *Fold change and SEM for vector-only and pcDNA3-PBF transfected TPC1 cells, with either vehicle only or nutlin-3 treatment (n=3). Timepoints are shown as 0, 60, 90 and 120 minutes. (*=p<0.05).*

6.4: Discussion

6.4.1: An interaction between PBF and MDM2

Preliminary data, obtained by Dr Andrew Turnell, revealed evidence of a potential interaction between PBF and the E3 ubiquitin ligase MDM2. In order to confirm this observation, GST pull-down assays were performed which confirmed the interaction (Figure 6.1). To investigate the site of binding of PBF and MDM2, we used mutations of PBF at different regions, and GST pull-down assays were repeated using mutants 1, 2 and 3, which possessed deletions of the NLS and sorting signal, PSI domain, and transmembrane region respectively (Figure 6.2). We demonstrated that PBF mutants 1, 2 and 3 were also capable of interacting with MDM2. This was surprising, and may indicate that MDM2 interacts with PBF at more than one region. Indeed, our previous GST pull-down assays of the interaction between PBF and p53 revealed that PBF bound to p53 at two distinct regions, indicating interactions at more than one region is plausible.

To confirm the PBF-MDM2 interaction, co-immunoprecipitation assays were attempted using TPC1, K1 HCT116 and HeLa cells (Figure 6.3). However, despite attempts using several different conditions, no interaction was observed between PBF and MDM2. Our findings obtained in a cell free environment using *in vitro* translated proteins were therefore not confirmed in different conditions using co-immunoprecipitation assay. It is possible that the interaction between PBF and MDM2 may be disrupted in

transformed human cancer cell lines. It is also possible that the interaction between PBF and MDM2 is weak, transient or only present under certain circumstances and since co-immunoprecipitation assays rely on many different factors such as antibody effectiveness, potential interactions may not have been demonstrated due to the use of poorly sensitive antibodies.

In order to investigate the lack of interaction in the co-immunoprecipitation assays, we sought to investigate the interaction between PBF and MDM2 using the proximity ligation assay, which has previously been demonstrated to have a higher sensitivity than co-immunoprecipitation assays, although it is still dependent upon antibody effectiveness (Soderberg et al, 2006). Results displayed a specific interaction between PBF and MDM2 in K1 cells, with each red dot displayed showing an interaction (Figure 6.4). However, the interaction was only observed in a subset of cells, suggesting the interaction is transient or may be dependent upon specific pathways being activated. The PLA assay also confirmed the interaction previously shown between PBF and p53, indicating that this assay is useful in demonstrating binding between two proteins. Further experiments are required to determine whether the PBF-MDM2 interaction exists in other cell subtypes and in normal cells.

An important experiment would be to determine if PBF, p53 and MDM2 bind in a specific complex. Several proteins have been demonstrated to bind in a complex with both p53 and MDM2, such as Insulin receptor tyrosine kinase substrate (Wang et al, 2011) and Ube4b (Wu et al, 2011). These further investigations were beyond the scope of this thesis.

6.4.2: Co-localisation of PBF and MDM2

Having demonstrated the interaction between PBF and MDM2, we determined the subcellular relationship of PBF and MDM2 through co-localisation studies using immunofluorescence. Results showed co-localisation between PBF and MDM2 in K1 cells, supporting findings from previously described GST pull-down assays and proximity ligation assay data, indicating a potential interaction between PBF and MDM2 (Figure 6.5). However, no co-localisation was observed in HeLa cells indicating the PBF-MDM2 interaction may not be present in other cell types. As described for the PLA assay, future experiments should focus on determining if co-localisation between PBF and MDM2 is specific to thyroid cells or extends to other cell types.

6.4.3: PBF-mediated degradation of p53 requires MDM2

MDM2 is the primary regulator of p53, being involved in both its degradation and its transactivation activity. To determine whether MDM2 played a role in the PBF-mediated degradation of p53 previously described (section 1.5.5), the p53-MDM2 inhibitor nutlin-3 was used. TPC1 thyroid carcinoma cells

were transfected with either vector only or pcDNA3-PBF-HA and subsequently treated with either vehicle only (DMSO) or nutlin-3. Following this, cells were subjected to a protein stability assay and Western blotting was performed to elucidate the effect of MDM2. Results showed a significant reduction in p53 protein following overexpression of PBF in cells treated with vehicle only, in keeping with previous findings (Manuscript under revision). However, in nutlin-3 treated cells, no reduction in p53 protein was demonstrated. This suggests the PBF-mediated degradation of p53 is dependent upon the interaction of p53 with MDM2, implicating MDM2 as an important protein in this process. Future studies should focus on determining if this mechanism is present in other cell types or is restricted to thyroid cells. Several other proteins, which cause increased degradation of p53 protein, have been shown to interact with MDM2 to accomplish this. Insulin receptor tyrosine kinase substrate is capable of binding both p53 and MDM2, enhancing levels of p53 ubiquitination when MDM2 levels were low (Wang et al, 2011). Similarly, Yin Yang 1 (YY1) physically interacts with p53 and MDM2, with YY1 able to affect MDM2-mediated p53 ubiquitination via promotion of the p53-MDM2 interaction (Sui et al, 2004). Other known proteins with a similar role include Ube4b (Wu et al, 2011) and p300 (Grossman et al, 2003). These results show that there is a complex network of proteins that control the degradation of p53, often via regulation of MDM2-mediated p53 ubiquitination. PBF effects on p53 and MDM2 seems to share similar functions to many of these proteins, indicating that PBF may

have a role in the regulation of p53 degradation, and requiring MDM2 to facilitate this regulation.

6.4.4: Conclusions

In conclusion, data from this chapter have shown PBF is capable of specifically binding to both p53 and MDM2, with its interaction with MDM2 not abrogated by mutants 1, 2 and 3. Immunofluorescence demonstrated PBF and MDM2 co-localise in K1 cells, however no co-localisation was observed in HeLa cells, suggesting binding of these proteins may be limited to certain cell subtypes. Investigations to determine the role of MDM2 in PBF-mediated p53 degradation revealed degradation of p53 caused by PBF overexpression was dependent upon MDM2, as inhibition of the interaction between p53 and MDM2 nullified the effect of PBF overexpression. This result suggests MDM2 is required for the increased ubiquitination and degradation of p53 associated with PBF overexpression. As PBF is overexpressed in thyroid cancer, it would be interesting to investigate if increased proliferation of cells caused by PBF overexpression occurs following the inhibition of the p53-MDM2 interaction. It is possible that increased degradation of p53 caused by PBF overexpression is the cause of increased proliferation in cancer cells, and inhibition of MDM2 interacting with p53 could abrogate this effect. Inhibition of the p53-MDM2 interaction,

via inhibitors such as nutlin-3, may represent a novel therapeutic strategy in thyroid cancer where PBF is overexpressed and wild-type p53 predominates.

Chapter 7. Mechanism of PBF and MDM2 mediated p53 degradation

7.1: Introduction

Originally identified through double minute chromosomes in transformed mouse fibroblasts, MDM2 is an E3 ubiquitin ligase which functions as the primary regulator of p53 and exists in an autoregulatory negative feedback loop with the tumour suppressor (Cahilly-Snyder et al, 1987). p53 transcribes *MDM2*, which subsequently ubiquitinates p53, targeting it for degradation by the proteasome (Barak et al, 1993) (Haupt et al, 1997). This leads to a reduction in the transcription of the *MDM2* gene, thereby keeping levels of both p53 and MDM2 low in normal unstressed cells.

Investigations have previously implicated MDM2 in the monoubiquitination of p53, leading to a variety of cellular effects, such as induction of apoptosis (Mihara et al, 2003) (Chipuk et al, 2004), and also in polyubiquitination, but requiring co-factors in order to induce polyubiquitination of the p53 protein (Li et al, 2003). Ubiquitination is a three-step process normally requiring three enzymes: E1, an ubiquitin activating enzyme, E2, an ubiquitin conjugating enzyme, and E3, an ubiquitin ligase. Ubiquitination occasionally requires use of a fourth enzyme (E4), which functions as an ubiquitin chain assembly factor. Indeed, many co-factors have been shown to be involved in MDM2-mediated p53 ubiquitination. Yin Yang 1 (YY1) is a transcription factor implicated in cellular differentiation and proliferation (Thomas and Seto, 1999), with a recently discovered role in p53 degradation when overexpressed. YY1 has been shown to significantly reduce endogenous p53 levels as a consequence

of induction of p53 ubiquitination. YY1 physically interacts with both p53 and MDM2 and was shown to regulate MDM2-mediated p53 ubiquitination in mouse embryonic fibroblast cells. This was further demonstrated to be due to promotion of the p53-MDM2 physical interaction; suggesting YY1 plays an important role in regulating p53 ubiquitination via MDM2 (Sui et al, 2004).

Similarly, the protein Ube4b has been identified as an E4 ubiquitin enzyme. Ube4b has been shown to function as both an E3 and E4 enzyme, with E4 functionality occurring in its role in p53 ubiquitination. In H1299 cells, Ube4b can specifically interact with both p53 and MDM2, and ubiquitination assays revealed that Ube4b is required for MDM2-mediated p53 polyubiquitination and degradation (Wu et al, 2011) (Wu and Leng, 2011). Other proteins, which have been shown to possess a role in p53 polyubiquitination, are p300, required to regulate MDM2-mediated p53 mono- or polyubiquitination (Grossman et al, 2003), and Insulin receptor tyrosine kinase substrate, which enhances low levels of MDM2-mediated p53 polyubiquitination (Wang et al, 2011). In contrast to these proteins, Pirh2 is a protein that demonstrates a MDM2-independent ubiquitin ligase activity to regulate p53 polyubiquitination (Leng et al, 2003). AKT has also been demonstrated to play a role in p53 ubiquitination, as p-AKT is able to phosphorylate MDM2 at ser^{186}, promoting MDM2-mediated p53 polyubiquitination (Ogawara et al, 2002). These data illustrate that a variety of proteins mediate p53 polyubiquitination, a process that involves a complex network of ubiquitin enzymes and co-factors.

PBF was discovered through its interaction with the human securin hPTTG1, to which it binds before translocating to the nucleus (Chien and Pei, 2000). PBF has been shown to be upregulated in several cancer types, including thyroid cancer, and our group has shown increased PBF mRNA and protein expression in thyroid cancer (Stratford et al, 2005). It has also been demonstrated that PBF is capable of cellular transformation *in vitro* and is tumourigenic *in vivo* (Stratford et al, 2005).

Recent research has shown PBF to specifically interact with p53 in TPC1 and K1 thyroid carcinoma cells, and also in HCT116 colorectal cancer cells (Read et al, 2013, Manuscript under revision). Subsequent experiments demonstrated that PBF is capable of causing increased p53 degradation following overexpression, through protein stability assays, and depletion of *PBF* using a specific siRNA was associated with an increase in p53 half-life. Further investigations demonstrated that p53 polyubiquitination is increased in TPC1 and HCT116 cells following PBF overexpression, providing a mechanism of increased p53 degradation. However, PBF does not possess enzymatic activity and it is plausible that PBF acts as a co-factor to facilitate increased p53 polyubiquitination via other enzymatic proteins or another mechanism.

Data from the previous chapter described a specific interaction between PBF and MDM2 proteins, demonstrated in GST pull-down and proximity ligation assays. Results also revealed co-localisation of PBF and MDM2 proteins, determined via immunofluorescence, in K1 thyroid carcinoma cells, but not in HeLa cervical cancer cells, suggesting cell type

specificity for PBF and MDM2 interaction and co-localisation. Investigations in TPC1 thyroid carcinoma cells showed increased degradation of p53 caused by PBF overexpression was ablated following nutlin-3 treatment, suggesting the interaction of MDM2 with p53 is required for PBF to promote degradation of the p53 protein. These results implicate MDM2 in the process of PBF-mediated p53 ubiquitination and subsequent degradation, and further elucidation of the relationship between PBF, p53 and MDM2 is required. Therefore, work in this chapter has focused on determining the mechanism of MDM2-mediated p53 ubiquitination and degradation caused by PBF overexpression.

7.2: Materials and Methods

7.2.1: Cell lines

Cell lines were cultured as described in section 2.2. TPC1 cells were seeded at 1.875 x10^6 per 25 cm^2 surface growth area. K1 and HeLa cells were seeded at 2.5 x10^6 per 25 cm^2 surface growth area.

7.2.2: Plasmid transfection

Transfection of plasmids was performed as described in section 2.3. Plasmids used were pcDNA3-VO, pcDNA3-PBF, pcDNA3-PBF-HA and pcDNA3-MDM2.

7.2.3: siRNA transfection

siRNA transfection was performed as described in section 2.4. siRNA (Ambion, Life Technologies Ltd, Paisley, UK) targeted to PBF (AM-16708) and MDM2 (s8630) were used. A scrambled siRNA was used as a negative control (AM-4635).

7.2.4: Protein extraction and quantification

Total protein from cells was extracted as described in section 2.7, and protein was quantified using the BCA assay.

7.2.5: Co-Immunoprecipitation assay

Co-immunoprecipitation assays were performed as described in section 2.15. Antibodies used were anti-MDM2 (SMP-14) (1/250) (Santa Cruz Biotechnology, Dallas, TX, USA). A no antibody and a specific isotype random antibody control were used as negative controls.

7.2.6: Protein stability assay

Protein stability assays were carried out in TPC1 cells as described in section 2.16. For p53 and MDM2 proteins, timepoints of 0, 60, 90 and 120 minutes were used.

7.2.7: Western blotting

Western blotting was performed as described in section 2.14. Antibodies used were anti-PBF (1/250) (Eurogentec, Southampton, Hampshire, UK), anti-p53 (DO-1) (1/500) (Santa Cruz Biotechnology, Dallas, Tx, USA) and anti-MDM2 (SMP-14) (1/250) (Santa Cruz Biotechnology, Dallas, TX, USA). Appropriate secondary antibodies were used.

7.2.8: Immunofluorescence

Immunofluorescence was performed as described in section 2.17. Primary antibodies used were anti-MDM2 (SMP-14) (1/400) (Santa Cruz Biotechnology, Dallas, TX, USA) and anti-PBF (1/1000) (Eurogentec, Southampton, Hampshire, UK). Secondary antibodies used were Alexa Fluor 488 conugated goat anti-mouse IgG and Alexa Fluor 594 conjugated goat anti-rabbit IgG (Invitrogen, Life Technologies Ltd, Paisley, UK) used at a concentration of 1:250. Hoescht stain was added at 1:1000 concentration to visualise DNA.

7.2.9: Nuclear and cytoplasmic fractionation

Nuclear and cytoplasmic fractionation was performed using the nuclear extract kit (Active Motif, Carlsbad, CA, USA). Cells were seeded into T25 flasks, transfected 24-hours later, and harvested for fractionation 24 or 48-hours post-transfection. Briefly, medium was aspirated and cells washed with PBS containing protease and phosphatase inhibitors, before centrifugation. Supernatant was discarded and cells resuspended in hypotonic buffer. Following incubation for 15 minutes on ice, a detergent was added, and cells were vortexed and centrifuged. The resulting supernatant consisted of the cytoplasmic fraction, which was extracted and stored at -80 ^{0}C. The leftover pellet was resuspended in lysis buffer, vortexed and incubated on ice for 30 minutes. Following vortexing and centrifugation, the supernatant, consisting of the nuclear fraction, was extracted and stored at -80 ^{0}C.

7.3: Results

7.3.1: PBF effects on MDM2 subcellular localisation

To determine if PBF is capable of affecting the subcellular localisation of MDM2, vector-only or pcDNA3-PBF constructs were transfected into K1 cells. 48 hours post-transfection, immunofluorescence was performed to investigate subcellular localisation. PBF overexpression did not result in altered MDM2 subcellular localisation (Figure 7.1), with MDM2 localised to the nucleus following vector-only and pcDNA3-PBF transfection. To investigate whether DNA damage has an effect upon MDM2 subcellular localisation, K1 cells were treated with 15 greys gamma radiation and immunofluorescence was performed 2 hours later. As shown in Figure 7.1, irradiation of K1 cells resulted in no difference in MDM2 subcellular localisation compared to non-irradiated cells, suggesting irradiation and DNA damage have no effect upon the subcellular localisation of MDM2. In contrast, PBF showed less nuclear staining following DNA damage. In addition, PBF and MDM2 co-localisation appeared to be abrogated following DNA damage. Experiments of DNA damage were also performed in HeLa cells, and there was also no difference observed in MDM2 localisation in these cells (data not shown).

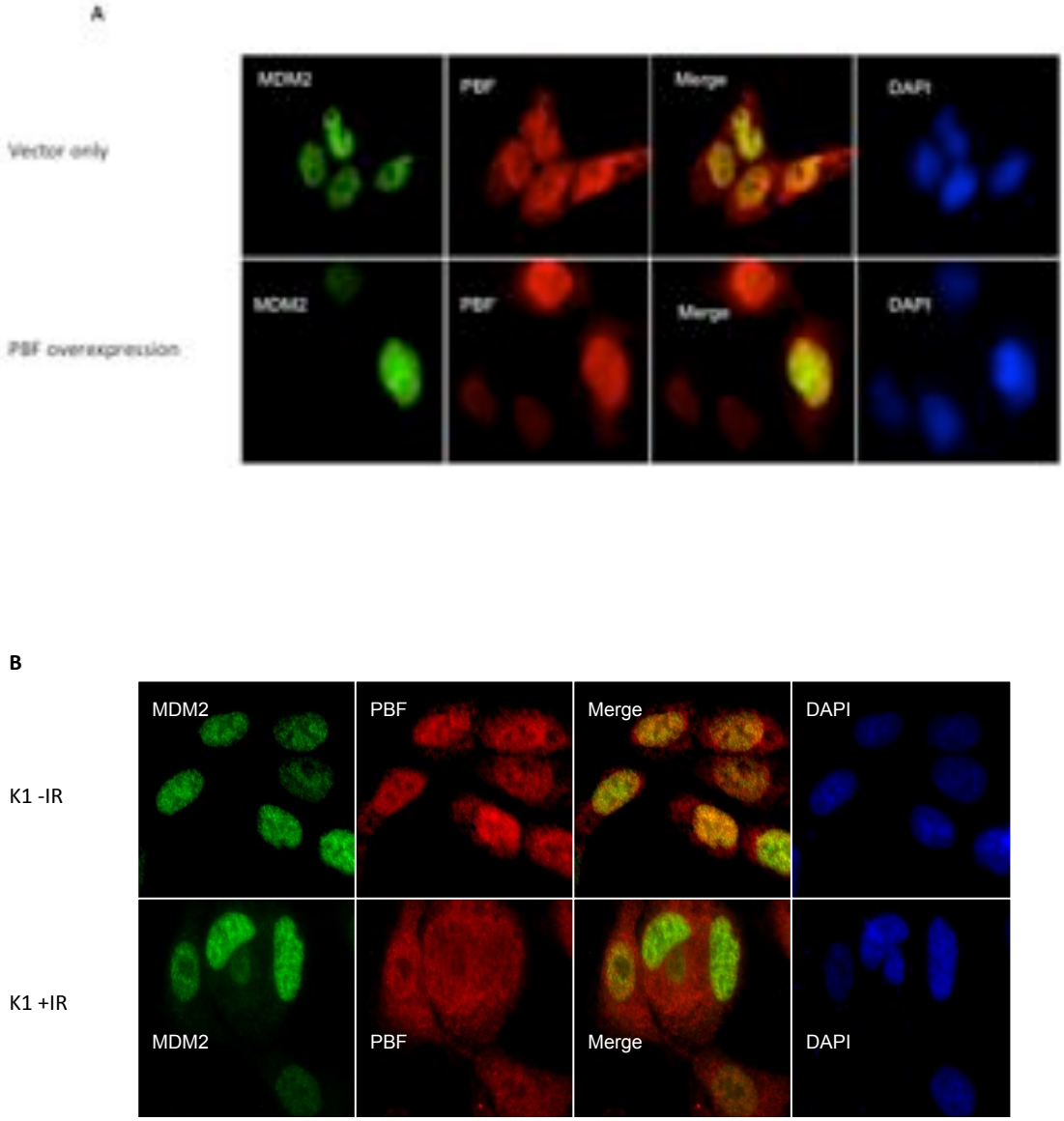

Figure 7.1: Subcellular localisation of MDM2 *and* PBF *in K1 cells.* MDM2 *is shown in green,* PBF *is shown in red, co-localisation appears yellow and DAPI is shown in blue.* ***A.*** *Localisation following transfection with either vector-only or pcDNA3-PBF.* MDM2 *was localised to the nucleus in both vector-only and pcDNA3-PBF transfected cells.* ***B.*** *Localisation following irradiation with 15 grays gamma radiation.* MDM2 *was localised to the nucleus in both non-irradiated and irradiated cells.* PBF *showed increased cytoplasmic localisation following irradiation.* PBF *and* MDM2 *co-localised in non-irradiated cells. No co-localisation between* PBF *and* MDM2 *was shown following irradiation of cells.*

7.3.2: PBF effects on MDM2 protein stability

To investigate the effect of PBF overexpression on MDM2 protein stability, we compared pcDNA3-PBF-HA to vector-only transfected TPC1 cells. Protein stability assays were performed 24-hours post-transfection and protein expression analysed by Western blotting (n=3). Results showed no difference in MDM2 protein levels at 60 (VO=0.69-fold ±0.18, PBF=0.80-fold ±0.179, p=0.47), 90 (VO=0.42-fold ±0.03, PBF=0.44-fold ±0.07, p=0.733) or 120 (VO=0.25-fold ±0.03, PBF=0.24-fold ±0.05, p=0.773) minute time points (Figure 7.2). These results indicate that PBF overexpression has no effect upon the protein stability of MDM2.

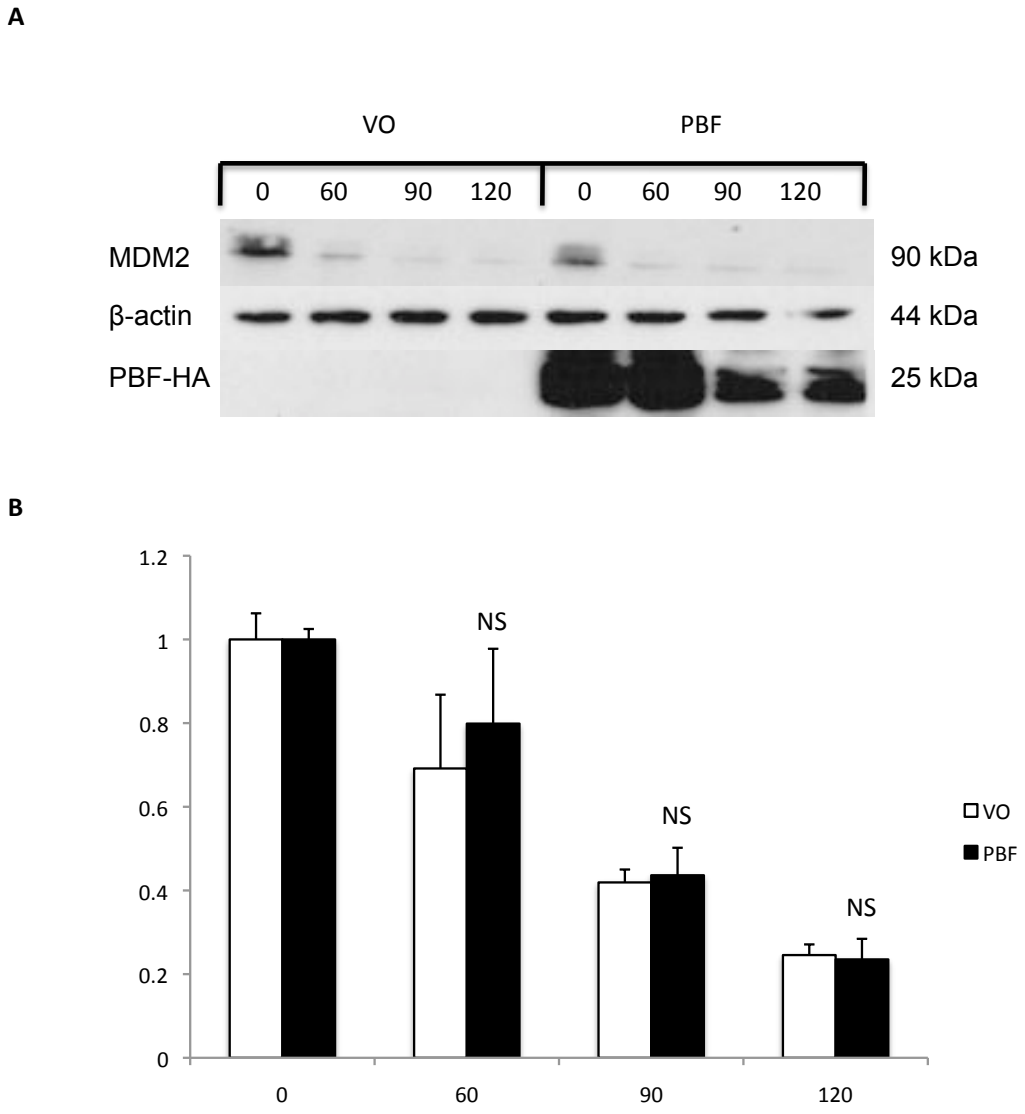

Figure 7.2: Effect of PBF *overexpression on* MDM2 *protein stability.* ***A.*** MDM2 *protein levels at time points of 0, 60, 90 and 120 minutes post-treatment with anisomycin.* β-actin *shown was used to normalise for protein loading.* PBF-HA *shown was used to validate transfection of* PBF. ***B.*** *Densitometry of Western blotting of* MDM2 *protein stability, displaying bars for VO against PBF for 0, 60, 90 and 120 minute time points.*

7.3.3: PBF effects on p-AKT levels

In order to determine if PBF overexpression affected p-AKT protein levels, TPC1 and K1 thyroid carcinoma cells were transfected with pcDNA3-PBF-HA and compared to vector-only transfected cells (n=3). Cells were harvested after 48-hours post-transfection and Western blotting was performed to investigate protein levels of p-AKT. Results revealed no difference (0.97-fold, p=0.83) between vector-only (±0.03) and pcDNA3-PBF-HA (±0.18) transfected TPC1 cells (Figure 7.3). Similarly, in K1 cells there was no difference in p-AKT expression (0.89-fold, p=0.06) between vector-only (±0.05) and pcDNA3-PBF-HA (±0.03) transfected cells (Figure 7.3).

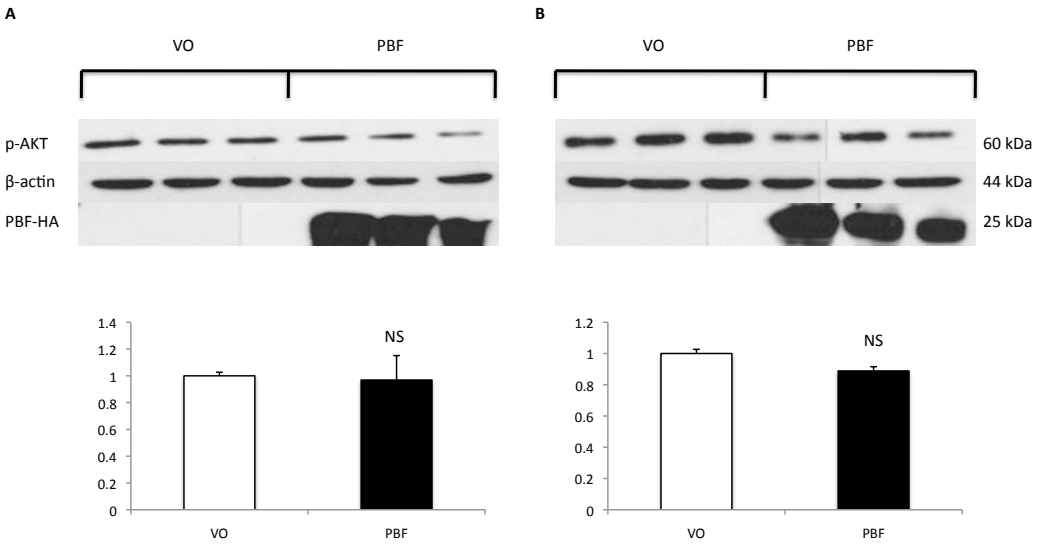

Figure 7.3: Effect of PBF *overexpression on* p-AKT *protein levels.* ***A.*** p-AKT *protein expression in TPC1 cells following vector-only or pcDNA3-PBF-HA transfection.* β-actin *is used as a loading control. Densitometry is shown in the bar graph below.* ***B.*** p-AKT *protein expression in K1 cells following vector-only or pcDNA3-PBF-HA transfection.* β-actin *is used as a loading control. Densitometry is shown in the bar graph below.*

7.3.4: PBF effects on the p53-MDM2 interaction

To investigate the effect of PBF on the interaction between p53 and MDM2, co-immunoprecipitation experiments were performed following knockdown of *PBF* using a specific siRNA. TPC1 cells were seeded and transfected 24-hours later, comparing *PBF* siRNA and scrambled siRNA for 48-hours or 72-hours. Subsequently cells were harvested and co-immunoprecipitation assays were carried out using a MDM2 antibody to immunoprecipitate MDM2 and a p53 antibody to probe for p53, thereby investigating the level of

interaction between p53 and MDM2 (n=3). There was no difference in immunoprecipitated protein following knockdown of *PBF* compared to cells treated with scrambled siRNA (Figure 7.4). This suggests that PBF did not influence the interaction between p53 and MDM2 proteins.

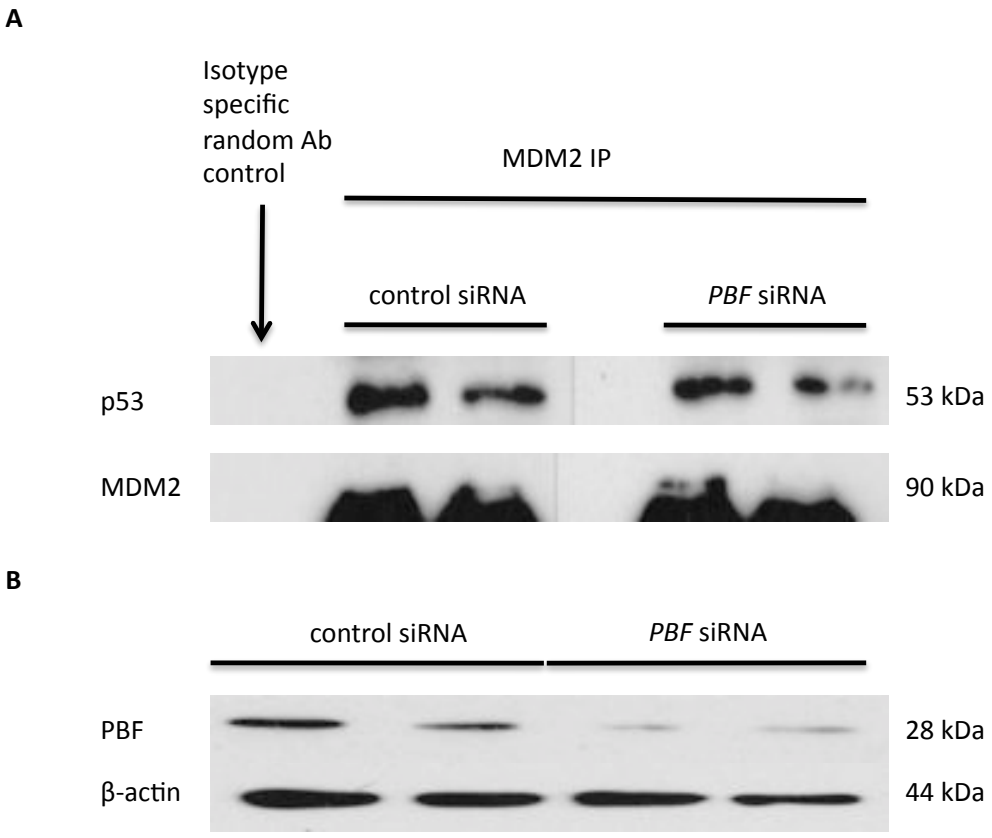

Figure 7.4: Effect of PBF knockdown on the specific interaction between p53 *and* MDM2*.* ***A.*** *Western blot of* p53 *comparing control siRNA to a PBF siRNA.* MDM2 *is shown to validate immunoprecipitation with MDM2 antibody. An isotype-specific random antibody control for* p53 *was used as a negative control.* ***B.*** *Western blot of* PBF *comparing control siRNA to a PBF siRNA to validate PBF knockdown.* β-actin is shown as a loading control.

7.4: Discussion

7.4.1: PBF effects on MDM2 subcellular localisation

To determine if PBF could influence MDM2 subcellular localisation, immunofluorescence studies were carried out. Cells were transfected with either vector-only or pcDNA3-PBF and no difference was found in the subcellular localisation of MDM2 following PBF overexpression in K1 cells (Figure 7.1). PBF has previously been shown to facilitate nuclear translocation of its binding factor hPTTG1. Transfection studies in COS-7 monkey kidney cells showed increased hPTTG1 nuclear localisation when hPTTG1 was co-transfected with PBF, with the effect abrogated following deletion of the nuclear localisation signal at the C-terminus of PBF (Chien and Pei, 2000). Therefore, it is possible that PBF interacts with MDM2 in a similar way, facilitating increased MDM2 nuclear localisation and increased ubiquitination and degradation of p53. However, there was no difference in the localisation of MDM2 following PBF overexpression, indicating that PBF does not translocate MDM2 to the nucleus. Notably, the majority of MDM2 is normally localised to the nucleus and therefore it may prove redundant to search for increased nuclear accumulation of MDM2 upon PBF overexpression. Use of a *PBF* siRNA to reduce PBF protein expression may provide a more potent experiment as it may prove easier to determine a greater cytoplasmic expression of MDM2 if MDM2 requires PBF to increase

its nuclear localisation. On the other hand, MDM2 has previously been shown to be localised to both the cytoplasm and nucleus (Mayo et al, 2002), and while hPTTG1 does not contain a nuclear localisation signal, MDM2 possesses an N-terminal nuclear localisation signal, suggesting MDM2 does not require a co-factor to facilitate nuclear entry. Recent research has reported nucleolar accumulation of MDM2 following AKT upregulation (Astle et al, 2012). Therefore, as PBF has previously been shown to increase p-AKT expression (Read et al, 2011), it was deemed possible that PBF could sequester MDM2 from the nucleolus to the nucleus to promote MDM2 ubiquitin ligase activity on p53. Only nuclear localisation of MDM2 was found in K1 cells, although no specific marker for nucleolar staining was used. Subcellular localisation studies using a nuclear and cytoplasmic fractionation kit were also attempted, but we were unable to detect MDM2 expression, via Western blotting, in K1 and TPC1 cells due to technical issues (data not shown).

To investigate the effect of DNA damage on MDM2 subcellular localisation, K1 cells were irradiated with 15 grays of gamma radiation and subsequently immunofluorescence was performed. Results showed no difference in MDM2 localisation following irradiation compared to non-irradiated cells. However, following irradiation, MDM2 and PBF appeared to no longer co-localise, and PBF showed less nuclear localisation (Figure 7.1). This suggests that DNA damage abrogates the co-localisation, and potentially disrupts the PBF-MDM2 interaction. If PBF interacts with MDM2 to facilitate

p53 polyubiquitination and degradation, this disruption could prove a method of stabilising p53.

7.4.2: PBF effects on MDM2 protein stability

Previous research has shown MDM2 ubiquitin ligase activity is not only able to ubiquitinate and degrade p53, but also to cause auto-ubiquitination and degradation (Chang et al, 1998). Increased auto-ubiquitination of MDM2 has been shown to occur following DNA damage, as a result of increased phosphorylation of MDM2 by DNA damage kinases such as ATM and ATR (Stommel and Wahl, 2004). To determine if MDM2 protein stability was altered following PBF overexpression, cells were transfected with either vector-only or pcDNA3-PBF-HA and a protein stability assay was performed using the *de novo* protein synthesis inhibitor anisomycin. Results revealed no difference in the half-life of MDM2 following PBF overexpression, suggesting PBF has no effect upon MDM2 protein stability (Figure 7.2). It may have been expected that, as p53 protein stability is decreased following PBF overexpression, that this may affect MDM2 transcription and protein expression. However, this would be likely to have no effect upon the stability of MDM2 as it would be degraded at the same rate regardless of initial MDM2 protein expression.

7.4.3: PBF effects on p-AKT levels

Research has indicated an interaction between MDM2 and AKT, suggesting MDM2 acts as a substrate for AKT, promoting phosphorylation of MDM2 (Zhou et al, 2001). Subsequent studies have found p-AKT to phosphorylate MDM2 at Ser^{186}, promoting increased MDM2-mediated p53 ubiquitination and degradation (Ogawara et al, 2002). Our own studies have investigated effects of PBF on AKT phosphorylation. Thyroids from transgenic PBF overexpressing mice displayed significantly increased p-AKT protein levels with unchanged total AKT protein, and human thyroid primary cultures also showed increased p-AKT protein expression following pcDNA3-PBF transfection (Read et al, 2011). Therefore it was hypothesised that increased PBF expression could lead to increased p-AKT protein, leading to increased phosphorylation of MDM2, and subsequent ubiquitination and degradation of p53. To investigate the effect of PBF on p-AKT levels *in vitro*, TPC1 and K1 cells were transfected with either vector-only or pcDNA3-PBF-HA, and subsequently cells were harvested and protein subjected to Western blotting. Results showed no difference in the expression of p-AKT in TPC1 and K1 cells, comparing vector-only to pcDNA3-PBF-HA transfected cells (Figure 7.3). These results imply PBF overexpression has no effect upon the level of p-AKT *in vitro*. It is plausible that these results could be caused by the use of transformed cell lines with dysregulated growth factor pathways, and more accurate results may have been obtained from primary thyroid cultures,

although use of cultures for p53-MDM2 experiments would be difficult due to the low level of expression and short half-life.

7.4.4: PBF effects on the p53-MDM2 interaction

Yin Yang 1 (YY1) is a transcription factor that has also been demonstrated to independently increase MDM2-mediated p53 polyubiquitination (Sui et al, 2004). This was due to an increase in the binding between p53 and MDM2 when YY1 was overexpressed, determined by co-immunoprecipitation, and a reduction in the binding was observed following siRNA knockdown of *YY1*. These effects were dependent upon the binding of YY1 to MDM2, with a YY1 mutant, which was defective in binding to MDM2, being unable to affect the binding of p53 and MDM2. These data demonstrate that co-factors of MDM2-mediated p53 ubiquitination are capable of affecting the interaction between p53 and MDM2, and therefore promote ubiquitination and degradation of MDM2. To assess if PBF is a co-factor in the p53-MDM2 interaction, we decided to test whether PBF knockdown affected the p53-MDM2 interaction *in vitro*. TPC1 cells were transfected with either a scrambled siRNA control or a specific *PBF* siRNA, harvested and subjected to immunoprecipitation for MDM2, and subsequently probed for p53 to determine the interaction between the two proteins. Results showed no difference in the binding between p53 and MDM2, comparing control siRNA to *PBF* siRNA, suggesting PBF has no effect upon the interaction between p53 and MDM2. However, a

future study could focus on PBF overexpression to determine if increased expression of PBF affects the interaction, as the lack of effects seen could be due to insufficient PBF knockdown. An alternative explanation is that other mechanisms are involved in the increased MDM2-mediated p53 degradation.

7.4.5: Conclusions

In conclusion, PBF overexpression or DNA damage had no effect upon the subcellular localisation of MDM2 in thyroid cells *in vitro*, and also had no effect upon the protein stability of MDM2. PBF overexpression did not affect p-AKT expression in TPC1 and K1 cells *in vitro*. Use of a *PBF* siRNA to investigate the effect of PBF on the interaction between p53 and MDM2 revealed there was no difference in binding between p53 and MDM2 following knockdown of PBF.

Work in this chapter sought to discover the mechanism behind PBF overepression resulting in increased MDM2-mediated p53 ubiquitination and degradation. Although the results have not determined the exact mechanisms involved in this process, the experiments performed provide some insight into the p53-MDM2-PBF interaction and processes. Further experiments may pertain to investigating the ubiquitination effect of MDM2 on p53 when PBF is overexpressed or reduced, to determine if PBF is required for MDM2-mediated p53 ubiquitination. MDM2 has previously been implicated as demonstrating monoubiquitination of p53, and requiring

co-factors or high expression in order to facilitate polyubiquitination (Li et al, 2003). It is possible that PBF facilitates whether MDM2 preferentially mono- or polyubiquitinates p53, thereby determining the degradation status of p53. It is also possible PBF acts upon other proteins, which regulate MDM2 to promote p53 ubiquitination, and this will be further discussed in chapter 8. If this proves true, it may be that the interaction of PBF with MDM2 may be involved in processes other than increased p53 polyubiquitination and degradation.

Chapter 8. Relationship between PBF and RAD6

8.1: Introduction

p53 is a potent tumour suppressor and is capable of transactivating numerous downstream genes, causing either cell cycle arrest (Vogelstein et al, 2000), or transactivating pro-apoptotic genes (Miyashita and Reed, 1995) (Nakano and Vousden, 2001). p53 protein expression is kept at a low level through its autoregulatory relationship with the E3 ubiquitin ligase MDM2. p53 induces transcription of *MDM2*, which subsequently ubiquitinates p53, tagging p53 for degradation by the proteasome (Barak et al, 1993) (Haupt et al, 1997). Other proteins have been shown to be involved in this process, such as Yin Yang 1 (YY1) (Sui et al, 2004) and Insulin receptor tyrosine kinase substrate (Wang et al, 2011), causing increased p53 ubiquitination and degradation through either MDM2-dependent or independent mechanisms.

RAD6 is an E2 enzyme, involved in catalysing the ubiquitination of target proteins (Jentsch et al, 1987). It plays a role in the DNA damage response by ubiquitination of PCNA, inducing either mono-ubiquitination – to facilitate the error-prone DNA repair pathway – or polyubiquitination – to facilitate the error-free DNA repair pathway (Bailly et al, 1994) (Hoege et al, 2002). RAD6 has also been shown to interact with p53, through demonstration of involvement in the degradation of DMP53 in *Drosophila* (Chen et al, 2011), as well as through identifications specific interactions with the p53 protein in mammalian cells (Lyakhovich et al, 2003). RAD6 has been shown to play a dual role in the control of the p53 protein. (i) In

unstressed cells, RAD6 is able to form a complex with MDM2 and p53 to facilitate p53 degradation via the ubiquitin pathway. (ii) In stressed cells this complex is disrupted, allowing recruitment of RAD6 to the p53 promoter region, where it was demonstrated to regulate H3K4 and H3K79 methylation at these regions, thereby promoting increased transcription of the *Tp53* gene (Chen et al, 2012).

Our group has recently demonstrated that overexpression of PBF can induce genetic instability, discovered through analysis of FISSR-PCR. Subsequently, a microarray of 84 DNA damage repair genes was performed on primary thyrocytes from wild-type and PBF transgenic mice, which showed significant dysregulation of 17 genes, including *Rad6*, which showed a greater than 2-fold induction. Protein expression of Rad6 was also induced (>2-fold) in thyroid glands of PBF transgenic mice compared to wild-type, suggesting that PBF overexpression is able to significantly induce RAD6 expression (Read et al, 2013, Manuscript under revision).

Previous chapters have shown a role for PBF in the degradation of p53, with PBF overexpression resulting in increased MDM2-dependent degradation of p53. However, the exact mechanism of this was not determined, and it is possible that PBF indirectly affects p53 degradation by affecting another protein, which subsequently increases p53 degradation. As mentioned, RAD6 has been shown to cause MDM2-mediated induction of p53 degradation, and since PBF increases *RAD6* expression in PBF transgenic mouse thyroids, we hypothesised that increased expression of RAD6 caused

by overexpression of PBF may lead to the increased MDM2-mediated p53 degradation observed.

8.2: Materials and Methods

8.2.1: Cell lines

Cell lines were cultured as described in section 2.2. TPC1 cells were seeded at 1.875 x10^6 per 25 cm^2 surface growth area. K1 cells were seeded at 2.5 x10^6 per 25 cm^2 surface growth area.

8.2.2: Plasmid transfection

Transfection of plasmids was performed as described in section 2.3. Plasmids used were pcDNA3-VO, pcDNA3-PBF and pcDNA3-Rad6.

8.2.3: siRNA transfection

siRNA transfection was performed as described in section 2.4. siRNA (Ambion, Life Technologies Ltd, Paisley, UK) targeted to PBF (AM-16708), Ube2a (s14565) and Ube2b (s14568) were used.

8.2.4: RNA extraction and quantification

RNA was extracted from cell lines and quantified as described in section 2.6.

8.2.5: Protein extraction and quantification

Total protein from cells was extracted as described in section 2.7, and protein was quantified using the BCA assay as described in section 2.7.

8.2.6: Co-Immunoprecipitation assay

Co-immunoprecipitation assays were performed as described in section 2.15. Antibodies used were anti-Ube2a (ab31917) (Abcam, Cambridge, UK) (1/2000), anti-p53 (DO-1) (Santa Cruz Biotechnology, Dallas, TX, USA) (1/500) and anti-PBF (1/250) (Eurogentec, Southampton, Hampshire, UK). A no antibody and a specific isotype random antibody were used as negative controls.

8.2.7: Reverse transcription

Total RNA was reverse transcribed to cDNA, performed as described in section 2.8.

8.2.8: qPCR

qPCR was used to determine expression of specific mRNAs. Experiments were performed as described in section 2.10, and pre-optimised specific gene assays (Applied Biosystems, Life Technologies Ltd, Paisley, UK) were used to determine expression levels.

8.2.9: Western blotting

Western blotting was performed as described in section 2.14. Antibodies used were anti-PBF (1/250) (Eurogentec, Southampton, Hampshire, UK), anti-p53 (DO-1) (Santa Cruz Biotechnology, Dallas, TX, USA) (1/500) and anti-Ube2a (ab31917) (Abcam, Cambridge, UK) (1/2000). Appropriate secondary antibodies were used.

8.3: Results

8.3.1: RAD6 regulates p53 degradation in thyroid cells

Preliminary experiments (n=1) indicated that overexpression of RAD6 in TPC1 thyroid carcinoma cells resulted in increased degradation of the p53 protein. This is shown in figure 8.1, where overexpression of RAD6 led to a reduced p53 half-life, demonstrated through half-life studies using the protein synthesis inhibitor anisomycin, and subsequent Western blotting (Figure 8.1). In cells transfected with pcDNA3-VO, there was a reduction in p53 protein, compared to the 0-minute time point, at 60 (0.91-fold), 90 (0.65-fold) and 120-minute (0.63-fold) time points. Overexpression of RAD6 following transfection with pcDNA3-RAD6 resulted in a reduction in p53 protein expression compared to VO, with a reduction, compared to a 0-minute time point, at 60 (0.65-fold), 90 (0.48-fold) and 120-minute (0.39-fold) time points (Figure 8.1). These results suggest that increased expression of RAD6 is capable of increasing the degradation of the p53 protein in thyroid cells.

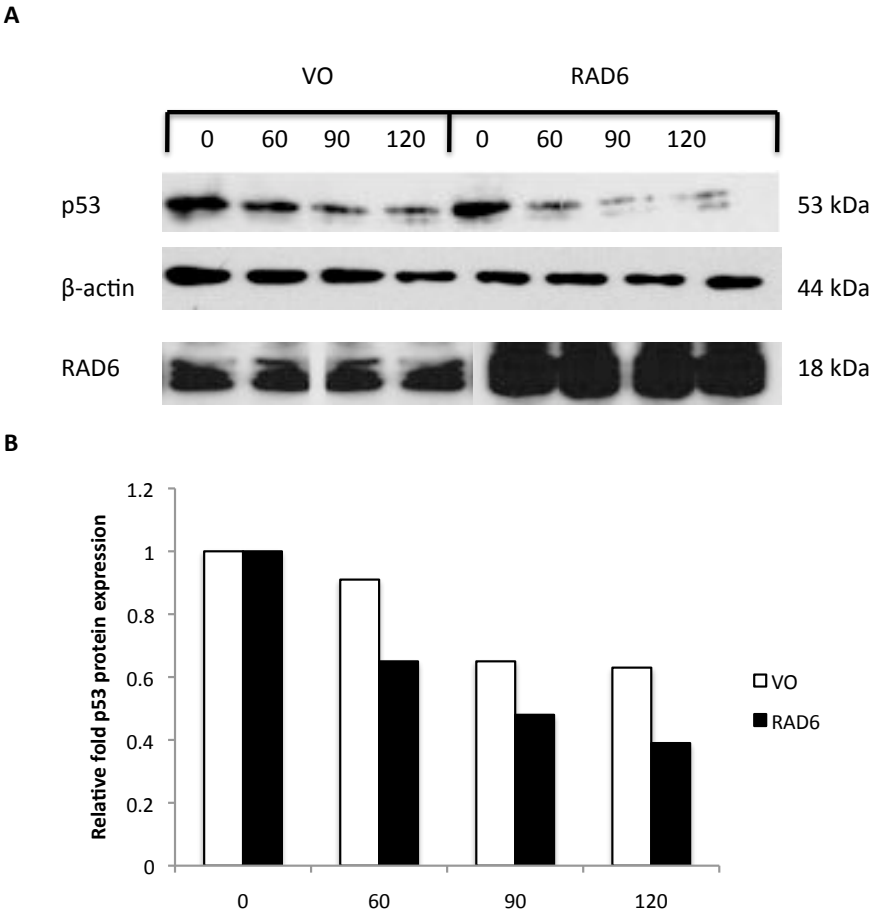

Figure 8.1: Preliminary data (n=1) on RAD6 *reduction of the half-life of the* p53 *protein in TPC1 cells.* ***A.*** p53 *protein expression at 0, 60, 90 and 120-minute time points following anisomycin treatment. Reduced* p53 *half-life was observed following transfection with pcDNA3-RAD6 compared to pcDNA3-VO.* β-actin *is shown as a protein loading control.* RAD6 *expression is shown to be increased following transfection with pcDNA3-RAD6.* ***B.*** *Densitometry of Western blotting above, showing relative fold* p53 *protein expression at 0, 60, 90 and 120 minute time points, following transfection with either pcDNA3-VO or pcDNA3-RAD6.*

8.3.2: Specific interaction between PBF and RAD6

To determine if PBF was capable of specifically binding to RAD6, co-immunoprecipitation assays were performed in TPC1 and K1 thyroid carcinoma cells. PBF was immunoprecipitated and Western blotting was performed using a RAD6 antibody to elucidate PBF-RAD6 binding. Results using endogenous protein (vector-only transfected cells) showed no binding between PBF and RAD6 (Figure 8.2). However, when RAD6 was transfected into cells, a specific interaction was observed in both TPC1 and K1 cells (Figure 8.2), suggesting PBF and RAD6 are able to bind *in vitro*, when increased levels of RAD6 protein are present.

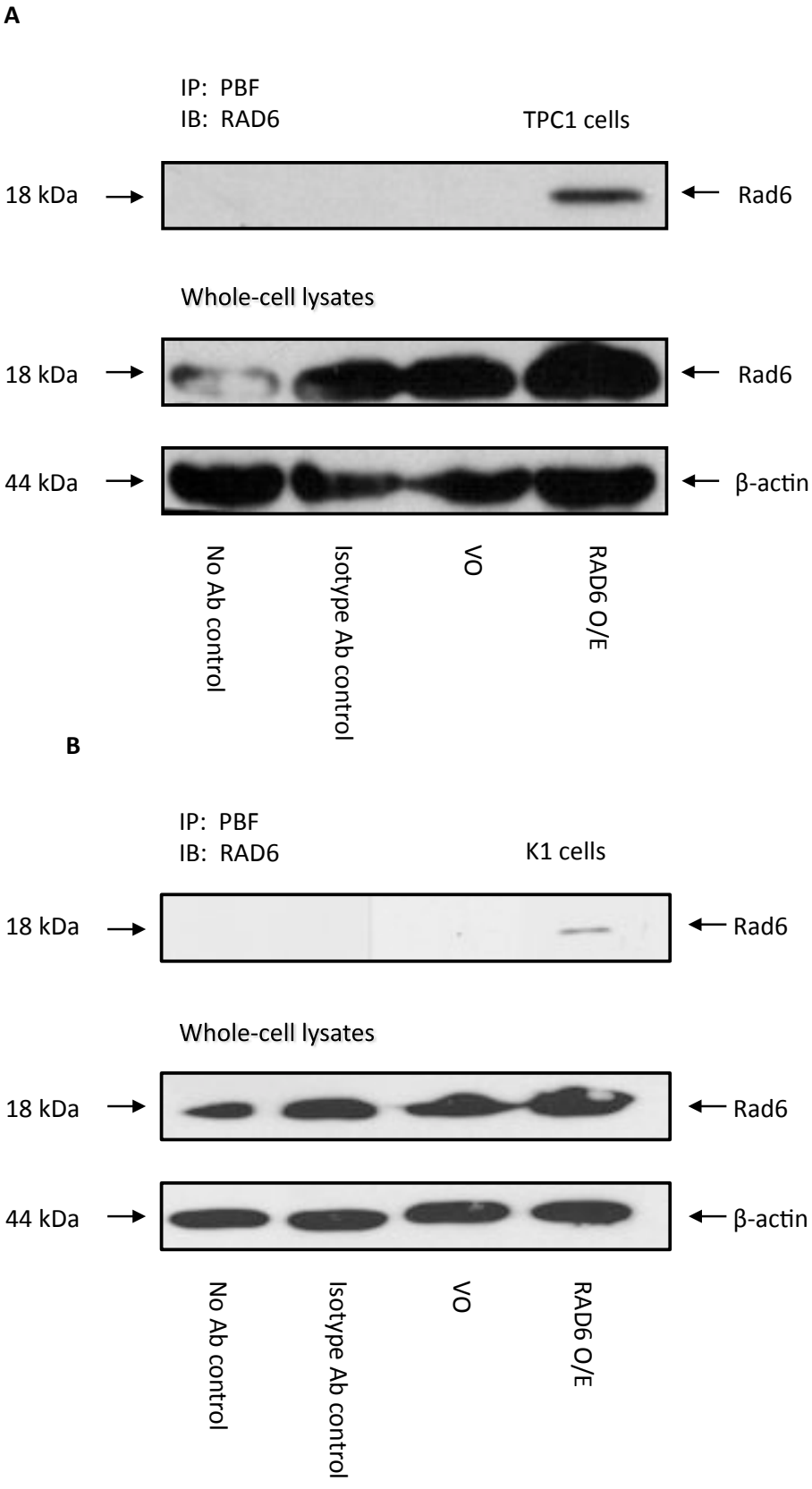
A
IP: PBF
IB: RAD6
TPC1 cells
18 kDa
Rad6
Whole-cell lysates
18 kDa
Rad6
44 kDa
β-actin
No Ab control
Isotype Ab control
VO
RAD6 O/E
B
IP: PBF
IB: RAD6
K1 cells
18 kDa
Rad6
Whole-cell lysates
18 kDa
Rad6
44 kDa
β-actin
No Ab control
Isotype Ab control
VO
RAD6 O/E

Figure 8.2: Co-immunoprecipitation assays showing specific binding between PBF *and* RAD6 *proteins.* ***A.*** *Co-immunoprecipitation assay in TPC1 cells. Negative controls were a no antibody control and an isotype specific antibody control. RAD6 O/E indicates* RAD6 *overexpression. Lysates are shown below showing* RAD6 *overexpression and* β-actin *to normalise for protein loading.* ***B.*** *Co-immunoprecipitation assay in K1 cells. Negative controls were a no antibody control and an isotype specific antibody control.*

8.3.3: Regulation of RAD6 by PBF

To further investigate the regulation of RAD6 by PBF, we determined the effects on *RAD6* mRNA expression following *PBF* knockdown through qPCR. mRNA expression of *PBF* was significantly reduced in TPC1 and K1 cells following use of the *PBF* siRNA, demonstrating successful knockdown of *PBF* at the mRNA level (Figure 8.3). mRNA expression of *RAD6* was significantly reduced (0.78-fold, p=0.001, n=3) in TPC1 cells following *PBF* knockdown, comparing scrambled siRNA (12.40 ±0.12) to *PBF* siRNA (12.75 ±0.11) (Figure 8.3). Similarly, for K1 cells, mRNA expression of *RAD6* was significantly reduced (0.53-fold, p=0.016, n=3) in cells transfected with *PBF* siRNA (12.94 ±0.16) compared to scrambled siRNA (12.01 ±0.28) (Figure 8.3).

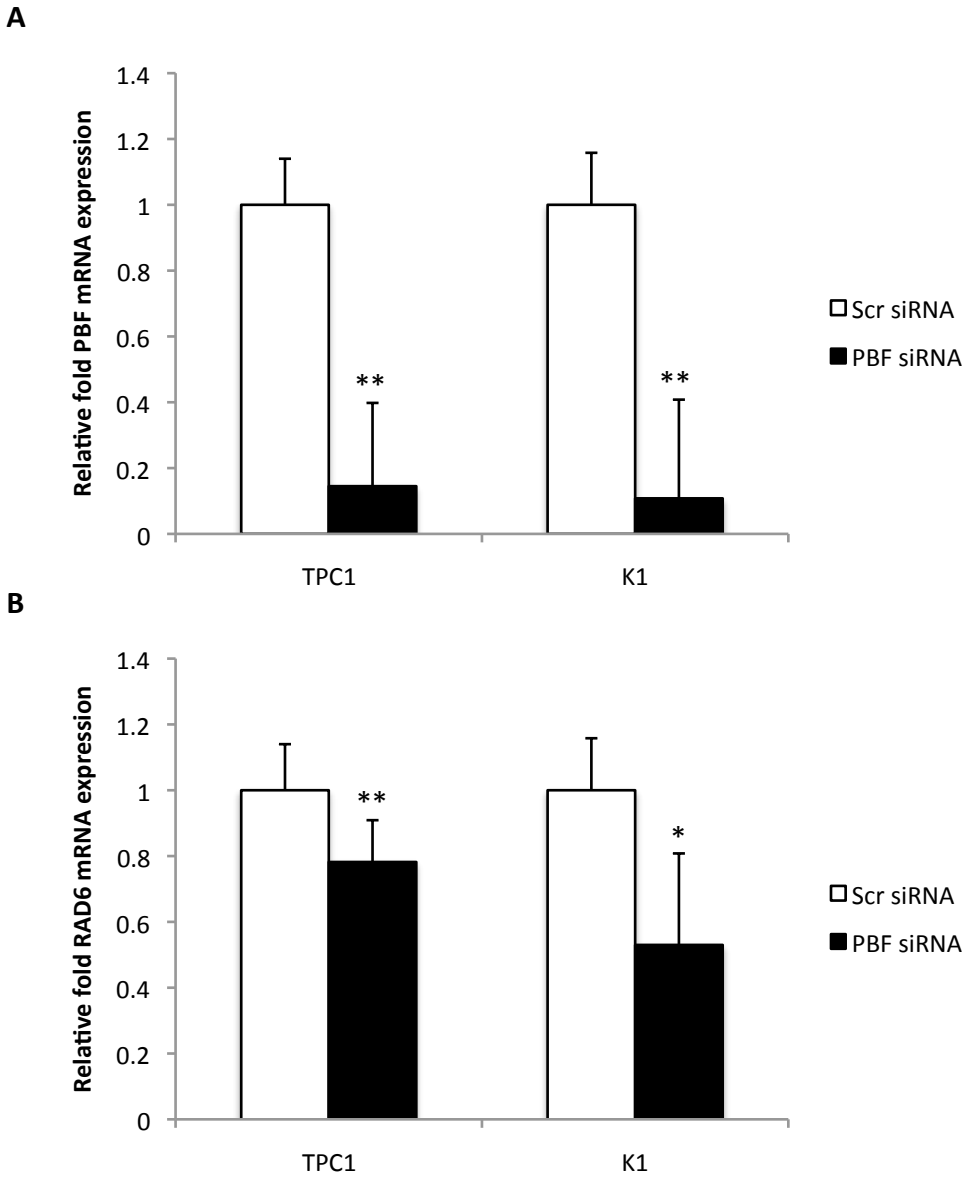

Figure 8.3: ***A.*** *Relative fold mRNA expression of PBF following transfection with scrambled siRNA or PBF siRNA, in TPC1 and K1 thyroid carcinoma cells.* ***B.*** *Relative fold mRNA expression of RAD6 following transfection with scrambled siRNA or PBF siRNA, in TPC1 and K1 thyroid carcinoma cells. (*=p<0.05, **=p<0.005).*

8.4: Discussion

8.4.1: RAD6 regulates p53 degradation in thyroid cells

RAD6 has previously been shown to be capable of binding to p53 (Lyakhovich and Shekhar, 2003) in the MCF10A normal breast cell line, and is involved in both its transcription and degradation. In HL-7702 human liver cells RAD6 forms a complex with MDM2 in order to facilitate p53 degradation under normal conditions. Following stress, the degradation complex containing RAD6, MDM2 and p53 is disrupted. RAD6 is subsequently recruited to the p53 gene, where methylation of histones H3K4 and H3K79 leads to increased transcription of the p53 gene (Chen et al, 2012).

To determine if RAD6 possessed similar capabilities in thyroid cells, RAD6 was overexpressed in TPC1 thyroid carcinoma cells and the half-life of the p53 protein was assessed following treatment with anisomycin. Preliminary experiments revealed a reduction in p53 half-life following overexpression of RAD6 (Figure 8.1), suggesting the increased degradation of p53, observed previously by Chen et al, also occurs in thyroid cells. However, these are preliminary data (n=1) and more research is needed to confirm this effect in TPC1 and other thyroid cells. If the finding of increased p53 degradation upon RAD6 overexpression is confirmed in thyroid cells this would demonstrate the effect is not specific to liver cells and this may provide further insights into the role of RAD6 and p53 in thyroid tumours.

8.4.2: Interaction and regulation of RAD6 by PBF

Previous research by our group, using cDNA microarrays of DNA damage response genes on PBF transgenic mouse primary thyrocytes, showed increased expression of *Rad6*, implicating PBF in the regulation of mouse *Rad6*. A number of other genes were found to be dysregulated (Read et al, 2013, Manuscript under revision), but due to the previously reported relationship between RAD6 and p53, we decided to investigate this protein with respect to its relationship with PBF.

Firstly, we decided to test if PBF was capable of specifically binding to RAD6 in TPC1 and K1 thyroid carcinoma cells. Co-immunoprecipitation assays using a PBF antibody to immunoprecipitate PBF and a RAD6 antibody to probe for binding between the two proteins resulted in no interaction using endogenous protein. Similarly, there was no binding observed following the overexpression of PBF. However, upon overexpression of RAD6 in TPC1 and K1 cells, binding was observed, suggesting PBF and RAD6 are capable of binding *in vitro* (Figure 8.2). Since RAD6 has previously been shown to bind p53 and MDM2 in a complex (Chen et al, 2012), and PBF has been demonstrated by our group to bind with p53, MDM2 and RAD6, it is plausible these proteins may bind in a complex in order to facilitate degradation of the p53 protein. This could be determined using two-step co-immunoprecipitation assays or gel filtration chromatography, which would

provide greater information on the method of PBF induced p53 degradation. It is also possible PBF and RAD6 binding does not have any bearing on the ability of PBF to induce increased p53 degradation, although determining if a complex is formed between these proteins would provide further information on this.

We simultaneously sought to determine if the previous effects of PBF on *RAD6* mRNA expression observed were translatable to human cell lines. Results showed (Figure 8.3) that knockdown of *PBF* resulted in a reduced mRNA expression of *RAD6*, confirming *PBF* is capable of affecting *RAD6* mRNA expression. Further experiments are required to determine if this is through transcriptional regulation or through another mechanism, such as an indirect effect, since PBF does not possess inherent transcriptional activity. Future studies should investigate whether protein expression of RAD6 is altered following either overexpression or knockdown of PBF.

8.4.3: Conclusions

In conclusion, work from this chapter has shown preliminary data suggesting RAD6 overexpression is capable of causing increased p53 degradation in thyroid cells. It has also shown evidence, via co-immunoprecipitation assays, that PBF is able to specifically bind to RAD6, and also to modulate *RAD6* mRNA expression following knockdown of *PBF*. This research suggests there may be an important relationship between PBF and RAD6, which is

potentially involved in the ubiquitin-proteasome degradation pathway of p53, although further studies are needed to elucidate this.

Chapter 9. Final discussions and future studies

The research described in this thesis follows investigations into the roles of hPTTG1 in thyroid cancer and goitre induction, as well as the relationship of hPTTG1's binding factor PBF with p53, and the role that MDM2 plays in PBF/p53 interactions was explored. hPTTG1 has been shown to be upregulated in thyroid cancer (Heaney et al, 2001) (Boelaert et al, 2003) (Zatelli et al, 2010), and we therefore hypothesised that thyroid specific overexpression of hPTTG1 in a murine model would lead to hyperplasia and subsequent neoplasia. Similarly, hPTTG1 plays important roles in cell proliferation, and protein expression was increased in multi-nodular goitres compared to normal tissue controls (Boelaert et al, 2003). This led us to hypothesise that hPTTG1 may be involved in the early steps of goitre formation, and we decided to test this in transgenic mice overexpressing hPTTG1 in the thyroid, and in *Pttg1* knockout mice. Research by our group has demonstrated that PBF is capable of inducing increased p53 degradation, which occurs through increased ubiquitination of the p53 protein. However, the mechanism behind this has not yet been elucidated. Preliminary experiments suggested a physical interaction between PBF and MDM2, the primary negative regulator of p53. Therefore we hypothesised that the PBF-mediated increased p53 degradation was dependent upon MDM2 in thyroid cells.

9.1: PTTG transgenic mice show reduced thyroid size co-incident with reduced cellular proliferation

Increased hPTTG1 expression in differentiated thyroid cancer has been shown by our group and others (Heaney et al, 2001) (Boelaert et al, 2003) (Zatelli et al, 2010). In order to test the hypothesis that overexpression of hPTTG1 results in thyroid cell hyperplasia and subsequent neoplasia, we generated a thyroid-specific transgenic mouse model overexpressing hPTTG1. Phenotypic evaluation demonstrated significant reductions in thyroid size in male and female mice at 6-weeks, 6-months and 12-months of age. Thyroid function was not altered at 6-weeks, and thyroid cell differentiation was unchanged at 6-weeks, 6-months and 12-months of age. There was no difference in the mRNA expression of growth factors *Egf* and *Tgfα*, although *Igf1* showed significantly increased expression in transgenic mice compared to wild-type, and expression of *Igf1* was positively correlated with *hPTTG1* expression, suggesting a role for hPTTG1 in *Igf1* regulation. hPTTG1 has previously been shown to be involved in apoptosis, although apoptosis levels were not different between transgenic and wild-type mice. Analysis of cellular proliferation levels, using the markers Cyclin-D1, Ki67 and PCNA revealed a significant reduction in cellular proliferation in transgenic mice compared to wild-type mice, suggesting the observed reduction in thyroid size in transgenic mice is caused by a reduction in cellular turnover, and not by increased apoptosis.

The data obtained from our mouse model provide important insights into the effects of thyroid hPTTG1 overexpression *in vivo*. Future studies may focus on the mechanism causing reduced cellular proliferation, by evaluating potential alterations in the cell cycle in mouse primary thyrocytes. It would also be interesting to determine the *in vivo* effects of hPTTG1 at levels more physiologically similar to those found in thyroid cancer, although the generation of another transgenic mouse line may prove difficult.

9.2: Characterisation of *Pttg1* knockout mouse thyroids

The knockout of genes can provide important information on gene and protein function. To determine effects of Pttg1 *in vivo*, we used an existing knockout mouse model of *Pttg1* and sought to characterise the effect of *Pttg1* deletion on the thyroid. We found no change in thyroid size, differentiation or thyroid function in *Pttg1* knockout mice compared to wild-type. Growth factor expression was dysregulated in *Pttg1* knockout mice, with a significant reduction in *Egf* mRNA expression, and significantly increased mRNA expression of *Igf1* and *Tgfβ*. Cellular senescence was also evident in *Pttg1* knockout mice compared to wild-type, with increased Cyclin-D1 protein expression and *Cdkn1a* (p21) mRNA expression observed, suggesting that, as is the case in pituitary cells of *Pttg1* knockout mice, thyrocytes are subject to cellular senescence following *Pttg1* deletion. In order to confirm this, future studies could include use of SA-β-gal on mouse primary thyrocytes from

Pttg1 knockout mice. Use of siRNA targeting *hPTTG1* in thyroid carcinoma cell lines found that, as with *Pttg1* knockout mice, *EGF* mRNA expression was significantly reduced. However, testing of *CDKN1A* mRNA expression found a significant reduction following *hPTTG1* siRNA transfection, contrasting with the significant induction of *Cdkn1a* found in *Pttg1* knockout mice. This could be due to differences in human and murine cells, or as a result of full deletion genetically in knockout mice compared to a reduction but not full abrogation of hPTTG1 levels in cell lines.

Data obtained from characterisation of *Pttg1* deletion on the thyroid correlate with previous results found in the pituitary cells of *Pttg1* knockout mice (Chesnokova et al, 2008). The dysregulation of growth factors in *Pttg1* knockout mice demonstrated the effect of Pttg1 and hPTTG1 on growth factor regulation, although it is unclear whether this is a direct effect of *Pttg1* knockout or an indirect effect caused by potential changes in the cell cycle. Furthermore our findings highlight the inherent differences between murine models and cancer cell lines.

9.3: PTTG has no effect on goitre induction

Research into the effect of PTTG upon goitre formation showed varying results. An iodine-deficient diet, together with methimazole and sodium perchlorate, were used to suppress endogenous thyroid hormone production and facilitate goitre formation. Investigations into the effect of hPTTG1

overexpression on goitre formation showed a significant 1.75-fold increase in thyroid:body weight ratio in mice on the iodine-deficient diet compared to mice on the control diet. However, there was no difference between wild-type mice and hPTTG1 transgenic mice on the iodine deficient diet, suggesting that hPTTG1 overexpression has no effect upon goitre formation. Similarly, *Pttg1* knockout mice also showed no difference compared with wild-type mice on the iodine-deficient diet to *Pttg1* knockout mice on the iodine-deficient diet, further supporting the conclusion that hPTTG1 has no effect upon goitre formation. However, hPTTG1 transgenic FVB/N mice showed a different degree of goitre induction (1.75-fold) compared to the c57/bl6 *Pttg1* knockout mice (3-fold), suggesting strain specific effects. Endogenous levels of thyroid hormones were not significantly suppressed in FVB/N mice, although there were trends towards reductions in T3 and T4, which may be the reason for the reduced goitre induction.

Preliminary experiments were also performed using PBF overexpressing transgenic mice. PBF transgenic mice showed significantly increased thyroid:body weight ratio compared to wild-type mice on both the control and iodine-deficient diet. Using a correction factor to account for the increased thyroid size of PBF transgenic mice on the control diet compared to wild-type, there was a significant increase in thyroid:body weight ratio following goitre induction. These results indicate that PBF overexpression leads to an increased goitre formation, which may have important therapeutic implications. Future investigations could focus on increasing the number of mice tested and determine if endogenous thyroid hormones have

been suppressed using radioimmunoassay for T4 and T3. In addition, our group is currently generating a *Pbf* knockout mouse, and this would provide a sound basis for determining if knockout of PBF would lead to a reduction in goitre formation.

9.4: Relationship between PBF and MDM2

hPTTG1 has also been shown to be involved in DNA damage through effects on the tumour suppressor p53 (Bernal et al, 2002) (Yu et al, 2009). Similarly, its binding factor PBF has been shown by our group to have roles in DNA damage through induction of genetic instability and also with induction of p53 ubiquitination leading to increased p53 degradation (Read et al, 2013, Manuscript under revision). MDM2 is an E3 ligase protein, and is the primary negative regulator of the p53 tumour suppressor protein through ubiquitination and subsequent degradation by the proteasome. Preliminary data, suggesting binding between PBF and MDM2 using GST pull-down assays, led us to hypothesise the PBF-mediated increased ubiquitination and subsequent degradation was MDM2 dependent. We firstly confirmed the interaction between PBF and MDM2 by GST pull-down assay and proximity ligation assay. Immunfluorescence also revealed co-localisation between PBF and MDM2 in K1 thyroid carcinoma cells. We subsequently found, using the p53-MDM2 inhibitor nutlin-3, that PBF-mediated increased degradation of p53 is MDM2 dependent. We then sought to discover the mechanism

behind this. We found no difference in localisation of MDM2 following PBF overexpression, and no difference in MDM2 stability. p-AKT expression was analysed following PBF overexpression, as p-AKT has previously been shown to induce MDM2-mediated p53 ubiquitination, but no difference was found compared to control transfected cells. We also tested if PBF could affect the interaction between p53 and MDM2, using *PBF* siRNA to deplete PBF levels, followed by a co-immunoprecipitation assay to test the interaction between p53 and MDM2. However, no difference was found comparing scrambled siRNA to *PBF* siRNA, suggesting PBF has no effect upon p53-MDM2 binding.

The research described showed an interaction between PBF and MDM2, and suggested that the increased p53 degradation upon PBF overexpression is MDM2 dependent. However, although several approaches were employed, the exact mechanism for this has yet to be elucidated. MDM2 has been suggested to either mono- or polyubiquitinate p53 depending on co-factors, and future studies could focus on discovering whether PBF is able to modulate this ubiquitination. Use of the nutlin-3 inhibitor could provide a potential therapeutic strategy in thyroid cancers overexpressing PBF, as likely wild-type p53 inactivation in thyroid cancer could be abrogated by inhibiting the interaction between p53 and MDM2.

9.6: Relationship between PBF and RAD6

RAD6 is an E2 enzyme involved in ubiquitination of many proteins such as PCNA (Hoege et al, 2002), and is also involved in p53 ubiquitination. RAD6 is able to form a complex with p53 and MDM2 to facilitate p53 degradation (Chen et al, 2012). Through use of a microarray of DNA damage response genes, our group has recently shown PBF overexpression in transgenic mice significantly induces *Rad6* mRNA expression in mouse thyroid glands. Rad6 protein expression was also significantly increased. We therefore hypothesised that increased p53 ubiquitination and degradation upon PBF overexpression, which was demonstrated to be dependent upon MDM2, was due to induced RAD6 expression, which subsequently promoted increased p53 ubiquitination. To investigate this hypothesis, we tested if PBF was able to bind to RAD6, using co-immunoprecipitation assays, and found that PBF was able to interact with RAD6 upon overexpression of RAD6. We also found reduced *RAD6* mRNA expression in TPC1 and K1 thyroid carcinoma cells following use of a *PBF* siRNA, showing PBF is capable of affecting *RAD6* expression in human thyroid cells. We simultaneously tested if RAD6 is capable of causing increased p53 degradation in thyroid cells, and preliminary data demonstrated increased degradation following RAD6 overexpression in TPC1 cells.

These data demonstrate PBF is capable of interacting with, and potentially regulating RAD6. Future studies should focus on the relationship between PBF and RAD6, and determining whether PBF is capable of causing

increased p53 degradation in the absence of RAD6, in order to investigate the role that RAD6 plays in this complex process.

9.7: Concluding statements

In conclusion, the research carried out in this thesis has provided evidence for the role of hPTTG1 in affecting cellular proliferation in thyroid cells when overexpressed, and has also shown, through use of the *Pttg1* knockout mouse and hPTTG1 transgenic mouse, that hPTTG1 can cause dysregulation of a number of growth factors involved in thyroid cell growth. Characterisation of thyroid glands from the *Pttg1* knockout mouse revealed increased Cyclin-D1 and *Cdkn1a* (p21) expression, which suggests that, as with pituitary cells from the *Pttg1* knockout mouse, knockout of *Pttg1* in thyrocytes leads to cellular senescence. Investigations into the role of hPTTG1 in goitre formation revealed that hPTTG1 does not affect goitre induction, although preliminary results indicate that its binding factor PBF may cause increased goitre induction upon overexpression. We have shown that PBF co-localises with, and is able to specifically bind to MDM2, and that the increased p53 degradation observed following PBF overexpression is dependent upon MDM2. Our findings indicate that PBF has no effect upon MDM2 subcellular localisation or stability, and that depletion of PBF did not affect the interaction between p53 and MDM2. This suggests another mechanism yet to be elucidated is responsible for the PBF associated increased degradation

of p53. The relationship of PBF with RAD6 has been expanded, with results revealing specific binding between PBF and RAD6, and showing knockdown of *PBF* results in reduced mRNA expression of *RAD6*.

Overall, this thesis has provided novel information on the roles of hPTTG1, and its binding factor PBF, in thyroid cancer and goitre formation, findings which are critical to our understanding of the role of these proto-oncogenes in thyroid cancer.

9.8: Future Studies

In terms of hPTTG1, future studies should include determining the mechanism of the reduced proliferation in the hPTTG1 transgenic mouse model. This could be due to cellular senescence, and testing of mouse primary thyrocytes with SA-β-Gal could help to elucidate this. It is also possible that the increased PTTG expression is causing a blockade in the cell cycle, and this could be tested by flow cytometry of mouse primary thyrocytes.

Future studies of the knockout mouse could also include investigations into confirming cellular senescence, which again could be tested using SA-β-Gal.

The goitre induction experiments should be performed for a longer duration in order to ascertain any effects of hPTTG1 overexpression and knockout on goitre formation, and TSH levels should be determined to

provide a full picture of the effect of these experiments on thyroid hormone synthesis. The experiment should also be repeated with PBF-transgenic mice for a longer duration and with greater numbers, also testing the levels of thyroid hormones and TSH in these mice.

In order to elucidate the mechanism by which PBF affects p53 degradation via MDM2, a ubiquitination assay should be performed to determine if PBF is capable of affecting the bias of MDM2 to preferentially mono or poly-ubiquitinate p53. It may also be useful to test if PBF is capable of cellular transformation following nutlin-3 treatment, as its transforming ability may be due to its effect on p53 degradation.

Finally, to characterise the relationship of PBF with RAD6, experiments could be performed to determine if PBF has any effect upon RAD6 protein levels. The experiments to determine if RAD6 affects p53 degradation in thyroid cells should be repeated, and it would also be useful in ascertaining whether PBF, RAD6, p53 and MDM2 bind in a complex.

Chapter 10. References

Abbud RA, Takumi I, Barker EM, Ren SG, Chen DY, Wawrowsky K, Melmed S. 2005. Early multipotential pituitary focal hyperplasia in the alpha-subunit of glycoprotein hormone-driven pituitary tumor-transforming gene transgenic mice. Mol Endocrinol 19(5):1383-1391.

Are C, Shaha AR. 2006. Anaplastic thyroid carcinoma: biology, pathogenesis, prognostic factors, and treatment approaches. Annals of surgical oncology 13(4):453-464.

Arnold MM, Srivastava S, Fredenburgh J, Stockard CR, Myers RB, Grizzle WE. 1996. Effects of fixation and tissue processing on immunohistochemical demonstration of specific antigens. Biotechnic & histochemistry : official publication of the Biological Stain Commission 71(5):224-230.

Astle MV, Hannan KM, Ng PY, Lee RS, George AJ, Hsu AK, Haupt Y, Hannan RD, Pearson RB. 2012. AKT induces senescence in human cells via mTORC1 and p53 in the absence of DNA damage: implications for targeting mTOR during malignancy. Oncogene 31(15):1949-1962.

Bailly V, Lamb J, Sung P, Prakash S, Prakash L. 1994. Specific complex formation between yeast RAD6 and RAD18 proteins: a potential mechanism for targeting RAD6 ubiquitin-conjugating activity to DNA damage sites. Genes & development 8(7):811-820.

Baker SJ, Fearon ER, Nigro JM, Hamilton SR, Preisinger AC, Jessup JM, vanTuinen P, Ledbetter DH, Barker DF, Nakamura Y and others. 1989. Chromosome 17 deletions and p53 gene mutations in colorectal carcinomas. Science 244(4901):217-221.

Baker SR, Bhatti WA. 2006. The thyroid cancer epidemic: is it the dark side of the CT revolution? European journal of radiology 60(1):67-69.

Barak Y, Juven T, Haffner R, Oren M. 1993. mdm2 expression is induced by wild type p53 activity. The EMBO journal 12(2):461-468.

Basolo F, Pisaturo F, Pollina LE, Fontanini G, Elisei R, Molinaro E, Iacconi P, Miccoli P, Pacini F. 2000. N-ras mutation in poorly differentiated thyroid carcinomas: correlation with bone metastases and inverse correlation to thyroglobulin

expression. Thyroid : official journal of the American Thyroid Association 10(1):19-23.

Bernal JA, Luna R, Espina A, Lazaro I, Ramos-Morales F, Romero F, Arias C, Silva A, Tortolero M, Pintor-Toro JA. 2002. Human securin interacts with p53 and modulates p53-mediated transcriptional activity and apoptosis. Nature genetics 32(2):306-311.

Bernardi R, Scaglioni PP, Bergmann S, Horn HF, Vousden KH, Pandolfi PP. 2004. PML regulates p53 stability by sequestering Mdm2 to the nucleolus. Nature cell biology 6(7):665-672.

Bishop JO, Smith P. 1989. Mechanism of chromosomal integration of microinjected DNA. Molecular biology & medicine 6(4):283-298.

Black AR, Black JD, Azizkhan-Clifford J. 2001. Sp1 and kruppel-like factor family of transcription factors in cell growth regulation and cancer. Journal of cellular physiology 188(2):143-160.

Boelaert K, McCabe CJ, Tannahill LA, Gittoes NJ, Holder RL, Watkinson JC, Bradwell AR, Sheppard MC, Franklyn JA. 2003. Pituitary tumor transforming gene and fibroblast growth factor-2 expression: potential prognostic indicators in differentiated thyroid cancer. The Journal of clinical endocrinology and metabolism 88(5):2341-2347.

Boelaert K, Smith VE, Stratford AL, Kogai T, Tannahill LA, Watkinson JC, Eggo MC, Franklyn JA, McCabe CJ. 2007. PTTG and PBF repress the human sodium iodide symporter. Oncogene 26(30):4344-4356.

Boelaert K, Tannahill LA, Bulmer JN, Kachilele S, Chan SY, Kim D, Gittoes NJ, Franklyn JA, Kilby MD, McCabe CJ. 2003. A potential role for PTTG/securin in the developing human fetal brain. FASEB journal : official publication of the Federation of American Societies for Experimental Biology 17(12):1631-1639.

Boelaert K, Yu R, Tannahill LA, Stratford AL, Khanim FL, Eggo MC, Moore JS, Young LS, Gittoes NJ, Franklyn JA and others. 2004. PTTG's C-terminal PXXP motifs modulate critical cellular processes in vitro. Journal of molecular endocrinology

33(3):663-677.

Boggaram V. 2009. Thyroid transcription factor-1 (TTF-1/Nkx2.1/TITF1) gene regulation in the lung. Clin Sci (Lond) 116(1):27-35.

Braverman LE, He X, Pino S, Cross M, Magnani B, Lamm SH, Kruse MB, Engel A, Crump KS, Gibbs JP. 2005. The effect of perchlorate, thiocyanate, and nitrate on thyroid function in workers exposed to perchlorate long-term. The Journal of clinical endocrinology and metabolism 90(2):700-706.

Cahilly-Snyder L, Yang-Feng T, Francke U, George DL. 1987. Molecular analysis and chromosomal mapping of amplified genes isolated from a transformed mouse 3T3 cell line. Somatic cell and molecular genetics 13(3):235-244.

Campisi J. 2005. Suppressing cancer: the importance of being senescent. Science 309(5736):886-887.

Candau R, Scolnick DM, Darpino P, Ying CY, Halazonetis TD, Berger SL. 1997. Two tandem and independent sub-activation domains in the amino terminus of p53 require the adaptor complex for activity. Oncogene 15(7):807-816.

Candeias MM, Malbert-Colas L, Powell DJ, Daskalogianni C, Maslon MM, Naski N, Bourougaa K, Calvo F, Fahraeus R. 2008. P53 mRNA controls p53 activity by managing Mdm2 functions. Nature cell biology 10(9):1098-1105.

Carter S, Bischof O, Dejean A, Vousden KH. 2007. C-terminal modifications regulate MDM2 dissociation and nuclear export of p53. Nature cell biology 9(4):428-435.

Chamaon K, Kirches E, Kanakis D, Braeuninger S, Dietzmann K, Mawrin C. 2005. Regulation of the pituitary tumor transforming gene by insulin-like-growth factor-I and insulin differs between malignant and non-neoplastic astrocytes. Biochemical and biophysical research communications 331(1):86-92.

Chang YC, Lee YS, Tejima T, Tanaka K, Omura S, Heintz NH, Mitsui Y, Magae J. 1998. mdm2 and bax, downstream mediators of the p53 response, are degraded by the ubiquitin-proteasome pathway. Cell growth & differentiation : the molecular biology journal of the American Association for Cancer Research 9(1):79-84.

Chen L, Puri R, Lefkowitz EJ, Kakar SS. 2000. Identification of the human pituitary tumor

transforming gene (hPTTG) family: molecular structure, expression, and chromosomal localization. Gene 248(1-2):41-50.

Chen S, Wang DL, Liu Y, Zhao L, Sun FL. 2012. RAD6 Regulates the Dosage of p53 by a Combination of Transcriptional and Posttranscriptional Mechanisms. Molecular and cellular biology 32(2):576-587.

Chen S, Wei HM, Lv WW, Wang DL, Sun FL. 2011. E2 ligase dRad6 regulates DMP53 turnover in Drosophila. The Journal of biological chemistry 286(11):9020-9030.

Chesnokova V, Kovacs K, Castro AV, Zonis S, Melmed S. 2005. Pituitary hypoplasia in Pttg-/- mice is protective for Rb+/- pituitary tumorigenesis. Mol Endocrinol 19(9):2371-2379.

Chesnokova V, Melmed S. 2009. Pituitary tumour-transforming gene (PTTG) and pituitary senescence. Hormone research 71 Suppl 2:82-87.

Chesnokova V, Melmed S. 2010. Pituitary senescence: the evolving role of Pttg. Molecular and cellular endocrinology 326(1-2):55-59.

Chesnokova V, Zonis S, Kovacs K, Ben-Shlomo A, Wawrowsky K, Bannykh S, Melmed S. 2008. p21(Cip1) restrains pituitary tumor growth. Proceedings of the National Academy of Sciences of the United States of America 105(45):17498-17503.

Chesnokova V, Zonis S, Rubinek T, Yu R, Ben-Shlomo A, Kovacs K, Wawrowsky K, Melmed S. 2007. Senescence mediates pituitary hypoplasia and restrains pituitary tumor growth. Cancer research 67(21):10564-10572.

Chien W, Pei L. 2000. A novel binding factor facilitates nuclear translocation and transcriptional activation function of the pituitary tumor-transforming gene product. The Journal of biological chemistry 275(25):19422-19427.

Chipuk JE, Kuwana T, Bouchier-Hayes L, Droin NM, Newmeyer DD, Schuler M, Green DR. 2004. Direct activation of Bax by p53 mediates mitochondrial membrane permeabilization and apoptosis. Science 303(5660):1010-1014.

Cho-Rok J, Yoo J, Jang YJ, Kim S, Chu IS, Yeom YI, Choi JY, Im DS. 2006. Adenovirus-mediated transfer of siRNA against PTTG1 inhibits liver cancer cell growth in vitro and in vivo. Hepatology 43(5):1042-1052.

Chuikov S, Kurash JK, Wilson JR, Xiao B, Justin N, Ivanov GS, McKinney K, Tempst P, Prives C, Gamblin SJ and others. 2004. Regulation of p53 activity through lysine methylation. Nature 432(7015):353-360.

Ciampi R, Nikiforov YE. 2007. RET/PTC rearrangements and BRAF mutations in thyroid tumorigenesis. Endocrinology 148(3):936-941.

Ciosk R, Zachariae W, Michaelis C, Shevchenko A, Mann M, Nasmyth K. 1998. An ESP1/PDS1 complex regulates loss of sister chromatid cohesion at the metaphase to anaphase transition in yeast. Cell 93(6):1067-1076.

Civitareale D, Castelli MP, Falasca P, Saiardi A. 1993. Thyroid transcription factor 1 activates the promoter of the thyrotropin receptor gene. Mol Endocrinol 7(12):1589-1595.

Classon M, Harlow E. 2002. The retinoblastoma tumour suppressor in development and cancer. Nature reviews Cancer 2(12):910-917.

Cramer JD, Fu P, Harth KC, Margevicius S, Wilhelm SM. 2010. Analysis of the rising incidence of thyroid cancer using the Surveillance, Epidemiology and End Results national cancer data registry. Surgery 148(6):1147-1152; discussion 1152-1143.

Crescioli C, Cosmi L, Borgogni E, Santarlasci V, Gelmini S, Sottili M, Sarchielli E, Mazzinghi B, Francalanci M, Pezzatini A and others. 2007. Methimazole inhibits CXC chemokine ligand 10 secretion in human thyrocytes. The Journal of endocrinology 195(1):145-155.

de Rozieres S, Maya R, Oren M, Lozano G. 2000. The loss of mdm2 induces p53-mediated apoptosis. Oncogene 19(13):1691-1697.

Derbel O, Limem S, Segura-Ferlay C, Lifante JC, Carrie C, Peix JL, Borson-Chazot F, Bournaud C, Droz JP, de la Fouchardiere C. 2011. Results of combined treatment of anaplastic thyroid carcinoma (ATC). BMC cancer 11:469.

Di Cosmo C, Liao XH, Dumitrescu AM, Philp NJ, Weiss RE, Refetoff S. 2010. Mice deficient in MCT8 reveal a mechanism regulating thyroid hormone secretion. The Journal of clinical investigation 120(9):3377-3388.

Dimri GP, Lee X, Basile G, Acosta M, Scott G, Roskelley C, Medrano EE, Linskens M, Rubelj I, Pereira-Smith O and others. 1995. A biomarker that identifies senescent human cells in culture and in aging skin in vivo. Proceedings of the National Academy of Sciences of the United States of America 92(20):9363-9367.

Dominguez A, Ramos-Morales F, Romero F, Rios RM, Dreyfus F, Tortolero M, Pintor-Toro JA. 1998. hpttg, a human homologue of rat pttg, is overexpressed in hematopoietic neoplasms. Evidence for a transcriptional activation function of hPTTG. Oncogene 17(17):2187-2193.

Dominguez A, Ramos-Morales F, Romero F, Rios RM, Dreyfus F, Tortolero M, Pintor-Toro JA. 1998. hpttg, a human homologue of rat pttg, is overexpressed in hematopoietic neoplasms. Evidence for a transcriptional activation function of hPTTG. Oncogene 17(17):2187-2193.

Dornan D, Wertz I, Shimizu H, Arnott D, Frantz GD, Dowd P, O'Rourke K, Koeppen H, Dixit VM. 2004. The ubiquitin ligase COP1 is a critical negative regulator of p53. Nature 429(6987):86-92.

Dulgeroff AJ, Hershman JM. 1994. Medical therapy for differentiated thyroid carcinoma. Endocrine reviews 15(4):500-515.

Dwight T, Thoppe SR, Foukakis T, Lui WO, Wallin G, Hoog A, Frisk T, Larsson C, Zedenius J. 2003. Involvement of the PAX8/peroxisome proliferator-activated receptor gamma rearrangement in follicular thyroid tumors. The Journal of clinical endocrinology and metabolism 88(9):4440-4445.

el-Deiry WS. 1998. Regulation of p53 downstream genes. Seminars in cancer biology 8(5):345-357.

El-Naggar SM, Malik MT, Kakar SS. 2007. Small interfering RNA against PTTG: a novel therapy for ovarian cancer. International journal of oncology 31(1):137-143.

Eliyahu D, Michalovitz D, Eliyahu S, Pinhasi-Kimhi O, Oren M. 1989. Wild-type p53 can inhibit oncogene-mediated focus formation. Proceedings of the National Academy of Sciences of the United States of America 86(22):8763-8767.

Eliyahu D, Raz A, Gruss P, Givol D, Oren M. 1984. Participation of p53 cellular tumour

antigen in transformation of normal embryonic cells. Nature 312(5995):646-649.

Enewold L, Zhu K, Ron E, Marrogi AJ, Stojadinovic A, Peoples GE, Devesa SS. 2009. Rising thyroid cancer incidence in the United States by demographic and tumor characteristics, 1980-2005. Cancer epidemiology, biomarkers & prevention : a publication of the American Association for Cancer Research, cosponsored by the American Society of Preventive Oncology 18(3):784-791.

Fagin JA. 2005. Genetics of papillary thyroid cancer initiation: implications for therapy. Transactions of the American Clinical and Climatological Association 116:259-269; discussion 269-271.

Fakharzadeh SS, Trusko SP, George DL. 1991. Tumorigenic potential associated with enhanced expression of a gene that is amplified in a mouse tumor cell line. The EMBO journal 10(6):1565-1569.

Feldt-Rasmussen U. 2001. Iodine and cancer. Thyroid : official journal of the American Thyroid Association 11(5):483-486.

Finlay CA, Hinds PW, Levine AJ. 1989. The p53 proto-oncogene can act as a suppressor of transformation. Cell 57(7):1083-1093.

Finlay CA, Hinds PW, Tan TH, Eliyahu D, Oren M, Levine AJ. 1988. Activating mutations for transformation by p53 produce a gene product that forms an hsc70-p53 complex with an altered half-life. Molecular and cellular biology 8(2):531-539.

Fong MY, Farghaly H, Kakar SS. 2012. Tumorigenic potential of pituitary tumor transforming gene (PTTG) in vivo investigated using a transgenic mouse model, and effects of cross breeding with p53 (+/-) transgenic mice. BMC cancer 12:532.

Freedman DA, Levine AJ. 1998. Nuclear export is required for degradation of endogenous p53 by MDM2 and human papillomavirus E6. Molecular and cellular biology 18(12):7288-7293.

Garcia-Rostan G, Zhao H, Camp RL, Pollan M, Herrero A, Pardo J, Wu R, Carcangiu ML, Costa J, Tallini G. 2003. ras mutations are associated with aggressive tumor

phenotypes and poor prognosis in thyroid cancer. Journal of clinical oncology : official journal of the American Society of Clinical Oncology 21(17):3226-3235.

Gartel AL, Najmabadi F, Goufman E, Tyner AL. 2000. A role for E2F1 in Ras activation of p21(WAF1/CIP1) transcription. Oncogene 19(7):961-964.

Gartel AL, Tyner AL. 1999. Transcriptional regulation of the p21((WAF1/CIP1)) gene. Experimental cell research 246(2):280-289.

Gordon JW, Scangos GA, Plotkin DJ, Barbosa JA, Ruddle FH. 1980. Genetic transformation of mouse embryos by microinjection of purified DNA. Proceedings of the National Academy of Sciences of the United States of America 77(12):7380-7384.

Gostissa M, Hengstermann A, Fogal V, Sandy P, Schwarz SE, Scheffner M, Del Sal G. 1999. Activation of p53 by conjugation to the ubiquitin-like protein SUMO-1. The EMBO journal 18(22):6462-6471.

Greco A, Borrello MG, Miranda C, Degl'Innocenti D, Pierotti MA. 2009. Molecular pathology of differentiated thyroid cancer. Q J Nucl Med Mol Imaging 53(5):440-453.

Greco A, Pierotti MA, Bongarzone I, Pagliardini S, Lanzi C, Della Porta G. 1992. TRK-T1 is a novel oncogene formed by the fusion of TPR and TRK genes in human papillary thyroid carcinomas. Oncogene 7(2):237-242.

Green DR, Reed JC. 1998. Mitochondria and apoptosis. Science 281(5381):1309-1312.

Grieco M, Santoro M, Berlingieri MT, Melillo RM, Donghi R, Bongarzone I, Pierotti MA, Della Porta G, Fusco A, Vecchio G. 1990. PTC is a novel rearranged form of the ret proto-oncogene and is frequently detected in vivo in human thyroid papillary carcinomas. Cell 60(4):557-563.

Grodski S, Brown T, Sidhu S, Gill A, Robinson B, Learoyd D, Sywak M, Reeve T, Delbridge L. 2008. Increasing incidence of thyroid cancer is due to increased pathologic detection. Surgery 144(6):1038-1043; discussion 1043.

Grossman SR, Deato ME, Brignone C, Chan HM, Kung AL, Tagami H, Nakatani Y, Livingston DM. 2003. Polyubiquitination of p53 by a ubiquitin ligase activity of

p300. Science 300(5617):342-344.

Gu L, Zhu N, Zhang H, Durden DL, Feng Y, Zhou M. 2009. Regulation of XIAP translation and induction by MDM2 following irradiation. Cancer cell 15(5):363-375.

Gu W, Roeder RG. 1997. Activation of p53 sequence-specific DNA binding by acetylation of the p53 C-terminal domain. Cell 90(4):595-606.

Hamid T, Malik MT, Kakar SS. 2005. Ectopic expression of PTTG1/securin promotes tumorigenesis in human embryonic kidney cells. Molecular cancer 4(1):3.

Harms KL, Chen X. 2006. The functional domains in p53 family proteins exhibit both common and distinct properties. Cell death and differentiation 13(6):890-897.

Haupt Y, Maya R, Kazaz A, Oren M. 1997. Mdm2 promotes the rapid degradation of p53. Nature 387(6630):296-299.

Hayflick L, Moorhead PS. 1961. The serial cultivation of human diploid cell strains. Experimental cell research 25:585-621.

Heaney AP, Nelson V, Fernando M, Horwitz G. 2001. Transforming events in thyroid tumorigenesis and their association with follicular lesions. The Journal of clinical endocrinology and metabolism 86(10):5025-5032.

Heaney AP, Singson R, McCabe CJ, Nelson V, Nakashima M, Melmed S. 2000. Expression of pituitary-tumour transforming gene in colorectal tumours. Lancet 355(9205):716-719.

Hegedus L, Bonnema SJ, Bennedbaek FN. 2003. Management of simple nodular goiter: current status and future perspectives. Endocrine reviews 24(1):102-132.

Hoege C, Pfander B, Moldovan GL, Pyrowolakis G, Jentsch S. 2002. RAD6-dependent DNA repair is linked to modification of PCNA by ubiquitin and SUMO. Nature 419(6903):135-141.

Hoffmann S, Glaser S, Wunderlich A, Lingelbach S, Dietrich C, Burchert A, Muller H, Rothmund M, Zielke A. 2006. Targeting the EGF/VEGF-R system by tyrosine-kinase inhibitors--a novel antiproliferative/antiangiogenic strategy in thyroid cancer. Langenbeck's archives of surgery / Deutsche Gesellschaft fur Chirurgie 391(6):589-596.

Honda R, Tanaka H, Yasuda H. 1997. Oncoprotein MDM2 is a ubiquitin ligase E3 for tumor suppressor p53. FEBS letters 420(1):25-27.

Horie S, Maeta H, Endo K, Ueta T, Takashima K, Terada T. 2001. Overexpression of p53 protein and MDM2 in papillary carcinomas of the thyroid: Correlations with clinicopathologic features. Pathology international 51(1):11-15.

Hornig NC, Knowles PP, McDonald NQ, Uhlmann F. 2002. The dual mechanism of separase regulation by securin. Current biology : CB 12(12):973-982.

Hu N, Gutsmann A, Herbert DC, Bradley A, Lee WH, Lee EY. 1994. Heterozygous Rb-1 delta 20/+mice are predisposed to tumors of the pituitary gland with a nearly complete penetrance. Oncogene 9(4):1021-1027.

Hundahl SA, Fleming ID, Fremgen AM, Menck HR. 1998. A National Cancer Data Base report on 53,856 cases of thyroid carcinoma treated in the U.S., 1985-1995 [see commetns]. Cancer 83(12):2638-2648.

Ishikawa H, Heaney AP, Yu R, Horwitz GA, Melmed S. 2001. Human pituitary tumor-transforming gene induces angiogenesis. The Journal of clinical endocrinology and metabolism 86(2):867-874.

Issaeva N, Bozko P, Enge M, Protopopova M, Verhoef LG, Masucci M, Pramanik A, Selivanova G. 2004. Small molecule RITA binds to p53, blocks p53-HDM-2 interaction and activates p53 function in tumors. Nature medicine 10(12):1321-1328.

Jacks T, Fazeli A, Schmitt EM, Bronson RT, Goodell MA, Weinberg RA. 1992. Effects of an Rb mutation in the mouse. Nature 359(6393):295-300.

Jallepalli PV, Waizenegger IC, Bunz F, Langer S, Speicher MR, Peters JM, Kinzler KW, Vogelstein B, Lengauer C. 2001. Securin is required for chromosomal stability in human cells. Cell 105(4):445-457.

Jennings T, Bratslavsky G, Gerasimov G, Troshina K, Bronstein M, Dedov I, Alexandrova G, Figge J. 1995. Nuclear accumulation of MDM2 protein in well-differentiated papillary thyroid carcinomas. Experimental and molecular pathology 62(3):199-206.

Jentsch S, Mcgrath JP, Varshavsky A. 1987. The Yeast DNA-Repair Gene Rad6 Encodes a Ubiquitin-Conjugating Enzyme. Nature 329(6135):131-134.

Jhiang SM, Sagartz JE, Tong Q, Parker-Thornburg J, Capen CC, Cho JY, Xing S, Ledent C. 1996. Targeted expression of the ret/PTC1 oncogene induces papillary thyroid carcinomas. Endocrinology 137(1):375-378.

Joensuu H, Klemi P, Eerola E. 1986. DNA aneuploidy in follicular adenomas of the thyroid gland. The American journal of pathology 124(3):373-376.

Jones SN, Roe AE, Donehower LA, Bradley A. 1995. Rescue of embryonic lethality in Mdm2-deficient mice by absence of p53. Nature 378(6553):206-208.

Kakar SS, Jennes L. 1999. Molecular cloning and characterization of the tumor transforming gene (TUTR1): a novel gene in human tumorigenesis. Cytogenetics and cell genetics 84(3-4):211-216.

Kamijo T, Weber JD, Zambetti G, Zindy F, Roussel MF, Sherr CJ. 1998. Functional and physical interactions of the ARF tumor suppressor with p53 and Mdm2. Proceedings of the National Academy of Sciences of the United States of America 95(14):8292-8297.

Kang HC, Ohmori M, Harii N, Endo T, Onaya T. 2001. Pax-8 is essential for regulation of the thyroglobulin gene by transforming growth factor-beta1. Endocrinology 142(1):267-275.

Kim D, Pemberton H, Stratford AL, Buelaert K, Watkinson JC, Lopes V, Franklyn JA, McCabe CJ. 2005. Pituitary tumour transforming gene (PTTG) induces genetic instability in thyroid cells. Oncogene 24(30):4861-4866.

Kim DS, Franklyn JA, Smith VE, Stratford AL, Pemberton HN, Warfield A, Watkinson JC, Ishmail T, Wakelam MJ, McCabe CJ. 2007. Securin induces genetic instability in colorectal cancer by inhibiting double-stranded DNA repair activity. Carcinogenesis 28(3):749-759.

Kim DS, Franklyn JA, Stratford AL, Boelaert K, Watkinson JC, Eggo MC, McCabe CJ. 2006. Pituitary tumor-transforming gene regulates multiple downstream angiogenic genes in thyroid cancer. The Journal of clinical endocrinology and metabolism

91(3):1119-1128.

Kim J, Guermah M, McGinty RK, Lee JS, Tang ZY, Milne TA, Shilatifard A, Muir TW, Roeder RG. 2009. RAD6-Mediated Transcription-Coupled H2B Ubiquitylation Directly Stimulates H3K4 Methylation in Human Cells. Cell 137(3):459-471.

Kimura ET, Nikiforova MN, Zhu Z, Knauf JA, Nikiforov YE, Fagin JA. 2003. High prevalence of BRAF mutations in thyroid cancer: genetic evidence for constitutive activation of the RET/PTC-RAS-BRAF signaling pathway in papillary thyroid carcinoma. Cancer research 63(7):1454-1457.

Knauf JA, Ma X, Smith EP, Zhang L, Mitsutake N, Liao XH, Refetoff S, Nikiforov YE, Fagin JA. 2005. Targeted expression of BRAFV600E in thyroid cells of transgenic mice results in papillary thyroid cancers that undergo dedifferentiation. Cancer research 65(10):4238-4245.

Knobel M, Medeiros-Neto G. 2007. Relevance of iodine intake as a reputed predisposing factor for thyroid cancer. Arquivos brasileiros de endocrinologia e metabologia 51(5):701-712.

Knudsen N, Laurberg P, Perrild H, Bulow I, Ovesen L, Jorgensen T. 2002. Risk factors for goiter and thyroid nodules. Thyroid : official journal of the American Thyroid Association 12(10):879-888.

Kondo T, Ezzat S, Asa SL. 2006. Pathogenetic mechanisms in thyroid follicular-cell neoplasia. Nature reviews Cancer 6(4):292-306.

Kostic M, Matt T, Martinez-Yamout MA, Dyson HJ, Wright PE. 2006. Solution structure of the Hdm2 C2H2C4 RING, a domain critical for ubiquitination of p53. Journal of molecular biology 363(2):433-450.

Kress M, May E, Cassingena R, May P. 1979. Simian virus 40-transformed cells express new species of proteins precipitable by anti-simian virus 40 tumor serum. Journal of virology 31(2):472-483.

Kuilman T, Peeper DS. 2009. Senescence-messaging secretome: SMS-ing cellular stress. Nature reviews Cancer 9(2):81-94.

Lane DP, Crawford LV. 1979. T antigen is bound to a host protein in SV40-transformed

cells. Nature 278(5701):261-263.

Lee IA, Seong C, Choe IS. 1999. Cloning and expression of human cDNA encoding human homologue of pituitary tumor transforming gene. Biochemistry and molecular biology international 47(5):891-897.

Leng RP, Lin Y, Ma W, Wu H, Lemmers B, Chung S, Parant JM, Lozano G, Hakem R, Benchimol S. 2003. Pirh2, a p53-induced ubiquitin-protein ligase, promotes p53 degradation. Cell 112(6):779-791.

Li M, Brooks CL, Wu-Baer F, Chen D, Baer R, Gu W. 2003. Mono- versus polyubiquitination: differential control of p53 fate by Mdm2. Science 302(5652):1972-1975.

Li M, Luo J, Brooks CL, Gu W. 2002. Acetylation of p53 inhibits its ubiquitination by Mdm2. The Journal of biological chemistry 277(52):50607-50611.

Li T, Jiang S. 2010. Effect of bFGF on invasion of ovarian cancer cells through the regulation of Ets-1 and urokinase-type plasminogen activator. Pharmaceutical biology 48(2):161-165.

Liang SH, Clarke MF. 1999. A bipartite nuclear localization signal is required for p53 nuclear import regulated by a carboxyl-terminal domain. The Journal of biological chemistry 274(46):32699-32703.

Lin Y, Ma W, Benchimol S. 2000. Pidd, a new death-domain-containing protein, is induced by p53 and promotes apoptosis. Nature genetics 26(1):122-127.

Linzer DI, Levine AJ. 1979. Characterization of a 54K dalton cellular SV40 tumor antigen present in SV40-transformed cells and uninfected embryonal carcinoma cells. Cell 17(1):43-52.

Liu Y, Kulesz-Martin MF. 2006. Sliding into home: facilitated p53 search for targets by the basic DNA binding domain. Cell death and differentiation 13(6):881-884.

Malaguarnera R, Vella V, Vigneri R, Frasca F. 2007. p53 family proteins in thyroid cancer. Endocrine-related cancer 14(1):43-60.

Mason G, Provero P, Vaira AM, Accotto GP. 2002. Estimating the number of integrations in transformed plants by quantitative real-time PCR. BMC biotechnology 2:20.

Mateu MG, Fersht AR. 1998. Nine hydrophobic side chains are key determinants of the thermodynamic stability and oligomerization status of tumour suppressor p53 tetramerization domain. The EMBO journal 17(10):2748-2758.

Maya R, Balass M, Kim ST, Shkedy D, Leal JF, Shifman O, Moas M, Buschmann T, Ronai Z, Shiloh Y and others. 2001. ATM-dependent phosphorylation of Mdm2 on serine 395: role in p53 activation by DNA damage. Genes & development 15(9):1067-1077.

Mayo LD, Dixon JE, Durden DL, Tonks NK, Donner DB. 2002. PTEN protects p53 from Mdm2 and sensitizes cancer cells to chemotherapy. The Journal of biological chemistry 277(7):5484-5489.

Mazzaferri EL. 1999. An overview of the management of papillary and follicular thyroid carcinoma. Thyroid : official journal of the American Thyroid Association 9(5):421-427.

McCabe CJ, Boelaert K, Tannahill LA, Heaney AP, Stratford AL, Khaira JS, Hussain S, Sheppard MC, Franklyn JA, Gittoes NJ. 2002. Vascular endothelial growth factor, its receptor KDR/Flk-1, and pituitary tumor transforming gene in pituitary tumors. The Journal of clinical endocrinology and metabolism 87(9):4238-4244.

Melero JA, Stitt DT, Mangel WF, Carroll RB. 1979. Identification of new polypeptide species (48-55K) immunoprecipitable by antiserum to purified large T antigen and present in SV40-infected and -transformed cells. Virology 93(2):466-480.

Michaloglou C, Vredeveld LC, Soengas MS, Denoyelle C, Kuilman T, van der Horst CM, Majoor DM, Shay JW, Mooi WJ, Peeper DS. 2005. BRAFE600-associated senescence-like cell cycle arrest of human naevi. Nature 436(7051):720-724.

Minsky N, Oren M. 2004. The RING domain of Mdm2 mediates histone ubiquitylation and transcriptional repression. Molecular cell 16(4):631-639.

Miranda C, Minoletti F, Greco A, Sozzi G, Pierotti MA. 1994. Refined localization of the human TPR gene to chromosome 1q25 by in situ hybridization. Genomics 23(3):714-715.

Miyashita T, Reed JC. 1995. Tumor suppressor p53 is a direct transcriptional activator

of the human bax gene. Cell 80(2):293-299.

Momand J, Jung D, Wilczynski S, Niland J. 1998. The MDM2 gene amplification database. Nucleic acids research 26(15):3453-3459.

Momand J, Zambetti GP, Olson DC, George D, Levine AJ. 1992. The mdm-2 oncogene product forms a complex with the p53 protein and inhibits p53-mediated transactivation. Cell 69(7):1237-1245.

Montes de Oca Luna R, Wagner DS, Lozano G. 1995. Rescue of early embryonic lethality in mdm2-deficient mice by deletion of p53. Nature 378(6553):203-206.

Motoi N, Sakamoto A, Yamochi T, Horiuchi H, Motoi T, Machinami R. 2000. Role of ras mutation in the progression of thyroid carcinoma of follicular epithelial origin. Pathology, research and practice 196(1):1-7.

Mu YM, Oba K, Yanase T, Ito T, Ashida K, Goto K, Morinaga H, Ikuyama S, Takayanagi R, Nawata H. 2003. Human pituitary tumor transforming gene (hPTTG) inhibits human lung cancer A549 cell growth through activation of p21(WAF1/CIP1). Endocrine journal 50(6):771-781.

Mu YM, Oba K, Yanase T, Ito T, Ashida K, Goto K, Morinaga H, Ikuyama S, Takayanagi R, Nawata H. 2003. Human pituitary tumor transforming gene (hPTTG) inhibits human lung cancer A549 cell growth through activation of p21(WAF1/CIP1). Endocrine journal 50(6):771-781.

Mukherjee S, Conrad SE. 2005. c-Myc suppresses p21WAF1/CIP1 expression during estrogen signaling and antiestrogen resistance in human breast cancer cells. The Journal of biological chemistry 280(18):17617-17625.

Murphy M, Ahn J, Walker KK, Hoffman WH, Evans RM, Levine AJ, George DL. 1999. Transcriptional repression by wild-type p53 utilizes histone deacetylases, mediated by interaction with mSin3a. Genes & development 13(19):2490-2501.

Musholt TJ, Musholt PB, Khaladj N, Schulz D, Scheumann GF, Klempnauer J. 2000. Prognostic significance of RET and NTRK1 rearrangements in sporadic papillary thyroid carcinoma. Surgery 128(6):984-993.

Nakano K, Vousden KH. 2001. PUMA, a novel proapoptotic gene, is induced by p53.

Molecular cell 7(3):683-694.

Nikiforov YE, Nikiforova MN. 2011. Molecular genetics and diagnosis of thyroid cancer. Nature reviews Endocrinology 7(10):569-580.

Nikiforov YE, Yip L, Nikiforova MN. 2013. New Strategies in Diagnosing Cancer in Thyroid Nodules: Impact of Molecular Markers. Clinical cancer research : an official journal of the American Association for Cancer Research.

Nikiforova MN, Kimura ET, Gandhi M, Biddinger PW, Knauf JA, Basolo F, Zhu Z, Giannini R, Salvatore G, Fusco A and others. 2003. BRAF mutations in thyroid tumors are restricted to papillary carcinomas and anaplastic or poorly differentiated carcinomas arising from papillary carcinomas. The Journal of clinical endocrinology and metabolism 88(11):5399-5404.

Nikiforova MN, Nikiforov YE. 2009. Molecular diagnostics and predictors in thyroid cancer. Thyroid : official journal of the American Thyroid Association 19(12):1351-1361.

Noseda PA, Thomasz L, Pregliasco L, Krawiec L, Pisarev MA, Juvenal GJ. 2005. Long-term effect of norepinephrine on thyroglobulin gene expression in FRTL-5 cells. Thyroid : official journal of the American Thyroid Association 15(5):417-421.

Ofir-Rosenfeld Y, Boggs K, Michael D, Kastan MB, Oren M. 2008. Mdm2 regulates p53 mRNA translation through inhibitory interactions with ribosomal protein L26. Molecular cell 32(2):180-189.

Ogawara Y, Kishishita S, Obata T, Isazawa Y, Suzuki T, Tanaka K, Masuyama N, Gotoh Y. 2002. Akt enhances Mdm2-mediated ubiquitination and degradation of p53. The Journal of biological chemistry 277(24):21843-21850.

Okamoto K, Kodama K, Takase K, Sugi NH, Yamamoto Y, Iwata M, Tsuruoka A. 2013. Antitumor activities of the targeted multi-tyrosine kinase inhibitor lenvatinib (E7080) against RET gene fusion-driven tumor models. Cancer letters 340(1):97-103.

Oliner JD, Pietenpol JA, Thiagalingam S, Gyuris J, Kinzler KW, Vogelstein B. 1993. Oncoprotein MDM2 conceals the activation domain of tumour suppressor p53.

Nature 362(6423):857-860.

Olivier M, Eeles R, Hollstein M, Khan MA, Harris CC, Hainaut P. 2002. The IARC TP53 database: new online mutation analysis and recommendations to users. Human mutation 19(6):607-614.

Parada LF, Land H, Weinberg RA, Wolf D, Rotter V. 1984. Cooperation between gene encoding p53 tumour antigen and ras in cellular transformation. Nature 312(5995):649-651.

Parameswaran R, Brooks S, Sadler GP. 2010. Molecular pathogenesis of follicular cell derived thyroid cancers. Int J Surg 8(3):186-193.

Pei L. 2001. Identification of c-myc as a down-stream target for pituitary tumor-transforming gene. The Journal of biological chemistry 276(11):8484-8491.

Pei L, Melmed S. 1997. Isolation and characterization of a pituitary tumor-transforming gene (PTTG). Mol Endocrinol 11(4):433-441.

Perry ME, Piette J, Zawadzki JA, Harvey D, Levine AJ. 1993. The mdm-2 gene is induced in response to UV light in a p53-dependent manner. Proceedings of the National Academy of Sciences of the United States of America 90(24):11623-11627.

Pfleghaar K, Heubes S, Cox J, Stemmann O, Speicher MR. 2005. Securin is not required for chromosomal stability in human cells. PLoS biology 3(12):e416.

Pohlenz J, Maqueem A, Cua K, Weiss RE, Van Sande J, Refetoff S. 1999. Improved radioimmunoassay for measurement of mouse thyrotropin in serum: strain differences in thyrotropin concentration and thyrotroph sensitivity to thyroid hormone. Thyroid : official journal of the American Thyroid Association 9(12):1265-1271.

Pomerantz J, Schreiber-Agus N, Liegeois NJ, Silverman A, Alland L, Chin L, Potes J, Chen K, Orlow I, Lee HW and others. 1998. The Ink4a tumor suppressor gene product, p19Arf, interacts with MDM2 and neutralizes MDM2's inhibition of p53. Cell 92(6):713-723.

Poyurovsky MV, Priest C, Kentsis A, Borden KL, Pan ZQ, Pavletich N, Prives C. 2007. The Mdm2 RING domain C-terminus is required for supramolecular assembly and

ubiquitin ligase activity. The EMBO journal 26(1):90-101.

Prezant TR, Kadioglu P, Melmed S. 1999. An intronless homolog of human proto-oncogene hPTTG is expressed in pituitary tumors: evidence for hPTTG family. The Journal of clinical endocrinology and metabolism 84(3):1149-1152.

Prives C, Hall PA. 1999. The p53 pathway. The Journal of pathology 187(1):112-126.

Puri R, Tousson A, Chen L, Kakar SS. 2001. Molecular cloning of pituitary tumor transforming gene 1 from ovarian tumors and its expression in tumors. Cancer letters 163(1):131-139.

Radice P, Sozzi G, Miozzo M, De Benedetti V, Cariani T, Bongarzone I, Spurr NK, Pierotti MA, Della Porta G. 1991. The human tropomyosin gene involved in the generation of the TRK oncogene maps to chromosome 1q31. Oncogene 6(11):2145-2148.

Raman V, Martensen SA, Reisman D, Evron E, Odenwald WF, Jaffee E, Marks J, Sukumar S. 2000. Compromised HOXA5 function can limit p53 expression in human breast tumours. Nature 405(6789):974-978.

Ramos-Morales F, Dominguez A, Romero F, Luna R, Multon MC, Pintor-Toro JA, Tortolero M. 2000. Cell cycle regulated expression and phosphorylation of hpttg proto-oncogene product. Oncogene 19(3):403-409.

Read ML, Lewy GD, Fong JC, Sharma N, Seed RI, Smith VE, Gentilin E, Warfield A, Eggo MC, Knauf JA and others. 2011. Proto-oncogene PBF/PTTG1IP regulates thyroid cell growth and represses radioiodide treatment. Cancer research 71(19):6153-6164.

Read ML, Mir S, Spice R, Seabright RJ, Suggate EL, Ahmed Z, Berry M, Logan A. 2009. Profiling RNA interference (RNAi)-mediated toxicity in neural cultures for effective short interfering RNA design. The journal of gene medicine 11(6):523-534.

Rehfeld N, Geddert H, Atamna A, Rohrbeck A, Garcia G, Kliszewski S, Neukirchen J, Bruns I, Steidl U, Fenk R and others. 2006. The influence of the pituitary tumor transforming gene-1 (PTTG-1) on survival of patients with small cell lung cancer

and non-small cell lung cancer. Journal of carcinogenesis 5:4.

Rodriguez MS, Desterro JM, Lain S, Lane DP, Hay RT. 2000. Multiple C-terminal lysine residues target p53 for ubiquitin-proteasome-mediated degradation. Molecular and cellular biology 20(22):8458-8467.

Rodriguez MS, Desterro JM, Lain S, Midgley CA, Lane DP, Hay RT. 1999. SUMO-1 modification activates the transcriptional response of p53. The EMBO journal 18(22):6455-6461.

Romero F, Gil-Bernabe AM, Saez C, Japon MA, Pintor-Toro JA, Tortolero M. 2004. Securin is a target of the UV response pathway in mammalian cells. Molecular and cellular biology 24(7):2720-2733.

Romero F, Multon MC, Ramos-Morales F, Dominguez A, Bernal JA, Pintor-Toro JA, Tortolero M. 2001. Human securin, hPTTG, is associated with Ku heterodimer, the regulatory subunit of the DNA-dependent protein kinase. Nucleic acids research 29(6):1300-1307.

Rotter V, Witte ON, Coffman R, Baltimore D. 1980. Abelson murine leukemia virus-induced tumors elicit antibodies against a host cell protein, P50. Journal of virology 36(2):547-555.

Saez C, Japon MA, Ramos-Morales F, Romero F, Segura DI, Tortolero M, Pintor-Toro JA. 1999. hpttg is over-expressed in pituitary adenomas and other primary epithelial neoplasias. Oncogene 18(39):5473-5476.

Santoro M, Carlomagno F, Hay ID, Herrmann MA, Grieco M, Melillo R, Pierotti MA, Bongarzone I, Della Porta G, Berger N and others. 1992. Ret oncogene activation in human thyroid neoplasms is restricted to the papillary cancer subtype. The Journal of clinical investigation 89(5):1517-1522.

Santoro M, Dathan NA, Berlingieri MT, Bongarzone I, Paulin C, Grieco M, Pierotti MA, Vecchio G, Fusco A. 1994. Molecular characterization of RET/PTC3; a novel rearranged version of the RETproto-oncogene in a human thyroid papillary carcinoma. Oncogene 9(2):509-516.

Schmitt CA, Fridman JS, Yang M, Lee S, Baranov E, Hoffman RM, Lowe SW. 2002. A

senescence program controlled by p53 and p16INK4a contributes to the outcome of cancer therapy. Cell 109(3):335-346.

Scoumanne A, Harms KL, Chen X. 2005. Structural basis for gene activation by p53 family members. Cancer biology & therapy 4(11):1178-1185.

Serrano M, Lin AW, McCurrach ME, Beach D, Lowe SW. 1997. Oncogenic ras provokes premature cell senescence associated with accumulation of p53 and p16INK4a. Cell 88(5):593-602.

Shah PP, Kakar SS. 2011. Pituitary tumor transforming gene induces epithelial to mesenchymal transition by regulation of Twist, Snail, Slug, and E-cadherin. Cancer letters 311(1):66-76.

Sharpless NE, DePinho RA. 2004. Telomeres, stem cells, senescence, and cancer. The Journal of clinical investigation 113(2):160-168.

Sherr CJ. 2001. The INK4a/ARF network in tumour suppression. Nature reviews Molecular cell biology 2(10):731-737.

Sherr CJ, Roberts JM. 1999. CDK inhibitors: positive and negative regulators of G1-phase progression. Genes & development 13(12):1501-1512.

Shibata Y, Haruki N, Kuwabara Y, Nishiwaki T, Kato J, Shinoda N, Sato A, Kimura M, Koyama H, Toyama T and others. 2002. Expression of PTTG (pituitary tumor transforming gene) in esophageal cancer. Japanese journal of clinical oncology 32(7):233-237.

Simpson WJ, McKinney SE, Carruthers JS, Gospodarowicz MK, Sutcliffe SB, Panzarella T. 1987. Papillary and follicular thyroid cancer. Prognostic factors in 1,578 patients. The American journal of medicine 83(3):479-488.

Sipos JA, Mazzaferri EL. 2010. Thyroid cancer epidemiology and prognostic variables. Clin Oncol (R Coll Radiol) 22(6):395-404.

Smallridge RC, Marlow LA, Copland JA. 2009. Anaplastic thyroid cancer: molecular pathogenesis and emerging therapies. Endocrine-related cancer 16(1):17-44.

Smith AE, Smith R, Paucha E. 1979. Characterization of different tumor antigens present in cells transformed by simian virus 40. Cell 18(2):335-346.

Smith VE, Read ML, Turnell AS, Watkins RJ, Watkinson JC, Lewy GD, Fong JC, James SR, Eggo MC, Boelaert K and others. 2009. A novel mechanism of sodium iodide symporter repression in differentiated thyroid cancer. Journal of cell science 122(Pt 18):3393-3402.

Soderberg O, Gullberg M, Jarvius M, Ridderstrale K, Leuchowius KJ, Jarvius J, Wester K, Hydbring P, Bahram F, Larsson LG and others. 2006. Direct observation of individual endogenous protein complexes in situ by proximity ligation. Nature methods 3(12):995-1000.

Solbach C, Roller M, Fellbaum C, Nicoletti M, Kaufmann M. 2004. PTTG mRNA expression in primary breast cancer: a prognostic marker for lymph node invasion and tumor recurrence. Breast 13(1):80-81.

Stommel JM, Wahl GM. 2004. Accelerated MDM2 auto-degradation induced by DNA-damage kinases is required for p53 activation. The EMBO journal 23(7):1547-1556.

Stratford AL, Boelaert K, Tannahill LA, Kim DS, Warfield A, Eggo MC, Gittoes NJ, Young LS, Franklyn JA, McCabe CJ. 2005. Pituitary tumor transforming gene binding factor: a novel transforming gene in thyroid tumorigenesis. The Journal of clinical endocrinology and metabolism 90(7):4341-4349.

Stratmann R, Lehner CF. 1996. Separation of sister chromatids in mitosis requires the Drosophila pimples product, a protein degraded after the metaphase/anaphase transition. Cell 84(1):25-35.

Suarez HG, du Villard JA, Severino M, Caillou B, Schlumberger M, Tubiana M, Parmentier C, Monier R. 1990. Presence of mutations in all three ras genes in human thyroid tumors. Oncogene 5(4):565-570.

Sui GC, El Bachir A, Shi YJ, Brignone C, Wall NR, Yin P, Donohoe M, Luke MP, Calvo D, Grossman SR and others. 2004. Yin Yang 1 is a negative regulator of p53. Cell 117(7):859-872.

Takagi M, Absalon MJ, McLure KG, Kastan MB. 2005. Regulation of p53 translation and induction after DNA damage by ribosomal protein L26 and nucleolin. Cell

123(1):49-63.

Tanaka T, Fuchs J, Loidl J, Nasmyth K. 2000. Cohesin ensures bipolar attachment of microtubules to sister centromeres and resists their precocious separation. Nature cell biology 2(8):492-499.

Tanimura S, Ohtsuka S, Mitsui K, Shirouzu K, Yoshimura A, Ohtsubo M. 1999. MDM2 interacts with MDMX through their RING finger domains. FEBS letters 447(1):5-9.

Tfelt-Hansen J, Yano S, Bandyopadhyay S, Carroll R, Brown EM, Chattopadhyay N. 2004. Expression of pituitary tumor transforming gene (PTTG) and its binding protein in human astrocytes and astrocytoma cells: function and regulation of PTTG in U87 astrocytoma cells. Endocrinology 145(9):4222-4231.

Thomas MJ, Seto E. 1999. Unlocking the mechanisms of transcription factor YY1: are chromatin modifying enzymes the key? Gene 236(2):197-208.

Thompson AD, 3rd, Kakar SS. 2005. Insulin and IGF-1 regulate the expression of the pituitary tumor transforming gene (PTTG) in breast tumor cells. FEBS letters 579(14):3195-3200.

Thrower JS, Hoffman L, Rechsteiner M, Pickart CM. 2000. Recognition of the polyubiquitin proteolytic signal. The EMBO journal 19(1):94-102.

Ton GN, Banaszynski ME, Kolesar JM. 2013. Vandetanib: a novel targeted therapy for the treatment of metastatic or locally advanced medullary thyroid cancer. American journal of health-system pharmacy : AJHP : official journal of the American Society of Health-System Pharmacists 70(10):849-855.

Tong Y, Tan Y, Zhou C, Melmed S. 2007. Pituitary tumor transforming gene interacts with Sp1 to modulate G1/S cell phase transition. Oncogene 26(38):5596-5605.

Tong Y, Tan Y, Zhou C, Melmed S. 2007. Pituitary tumor transforming gene interacts with Sp1 to modulate G1/S cell phase transition. Oncogene 26(38):5596-5605.

Tovar C, Rosinski J, Filipovic Z, Higgins B, Kolinsky K, Hilton H, Zhao X, Vu BT, Qing W, Packman K and others. 2006. Small-molecule MDM2 antagonists reveal aberrant p53 signaling in cancer: implications for therapy. Proceedings of the National

Academy of Sciences of the United States of America 103(6):1888-1893.

Tsai SJ, Lin SJ, Cheng YM, Chen HM, Wing LY. 2005. Expression and functional analysis of pituitary tumor transforming gene-1 [corrected] in uterine leiomyomas. The Journal of clinical endocrinology and metabolism 90(6):3715-3723.

Uhlmann F, Lottspeich F, Nasmyth K. 1999. Sister-chromatid separation at anaphase onset is promoted by cleavage of the cohesin subunit Scc1. Nature 400(6739):37-42.

Vassilev LT, Vu BT, Graves B, Carvajal D, Podlaski F, Filipovic Z, Kong N, Kammlott U, Lukacs C, Klein C and others. 2004. In vivo activation of the p53 pathway by small-molecule antagonists of MDM2. Science 303(5659):844-848.

Viadiu H. 2008. Molecular architecture of tumor suppressor p53. Current topics in medicinal chemistry 8(15):1327-1334.

Vlotides G, Cruz-Soto M, Rubinek T, Eigler T, Auernhammer CJ, Melmed S. 2006. Mechanisms for growth factor-induced pituitary tumor transforming gene-1 expression in pituitary folliculostellate TtT/GF cells. Mol Endocrinol 20(12):3321-3335.

Vlotides G, Eigler T, Melmed S. 2007. Pituitary tumor-transforming gene: physiology and implications for tumorigenesis. Endocrine reviews 28(2):165-186.

Vogelstein B, Lane D, Levine AJ. 2000. Surfing the p53 network. Nature 408(6810):307-310.

Vousden KH. 2000. p53: death star. Cell 103(5):691-694.

Wang KS, Chen G, Shen HL, Li TT, Chen F, Wang QW, Wang ZQ, Han ZG, Zhang X. 2011. Insulin Receptor Tyrosine Kinase Substrate Enhances Low Levels of MDM2-Mediated p53 Ubiquitination. PloS one 6(8).

Wang X, Taplick J, Geva N, Oren M. 2004. Inhibition of p53 degradation by Mdm2 acetylation. FEBS letters 561(1-3):195-201.

Wang Z, Melmed S. 2000. Characterization of the murine pituitary tumor transforming gene (PTTG) and its promoter. Endocrinology 141(2):763-771.

Wang Z, Moro E, Kovacs K, Yu R, Melmed S. 2003. Pituitary tumor transforming gene-

null male mice exhibit impaired pancreatic beta cell proliferation and diabetes. Proceedings of the National Academy of Sciences of the United States of America 100(6):3428-3432.

Wang Z, Yu R, Melmed S. 2001. Mice lacking pituitary tumor transforming gene show testicular and splenic hypoplasia, thymic hyperplasia, thrombocytopenia, aberrant cell cycle progression, and premature centromere division. Mol Endocrinol 15(11):1870-1879.

Watkins RJ, Read ML, Smith VE, Sharma N, Reynolds GM, Buckley L, Doig C, Campbell MJ, Lewy G, Eggo MC and others. 2010. Pituitary tumor transforming gene binding factor: a new gene in breast cancer. Cancer research 70(9):3739-3749.

Weber JD, Taylor LJ, Roussel MF, Sherr CJ, Bar-Sagi D. 1999. Nucleolar Arf sequesters Mdm2 and activates p53. Nature cell biology 1(1):20-26.

Webster GA, Perkins ND. 1999. Transcriptional cross talk between NF-kappaB and p53. Molecular and cellular biology 19(5):3485-3495.

Wirth KG, Wutz G, Kudo NR, Desdouets C, Zetterberg A, Taghybeeglu S, Seznec J, Ducos GM, Ricci R, Firnberg N and others. 2006. Separase: a universal trigger for sister chromatid disjunction but not chromosome cycle progression. The Journal of cell biology 172(6):847-860.

Woods DB, Vousden KH. 2001. Regulation of p53 function. Experimental cell research 264(1):56-66.

Wu H, Leng RP. 2011. UBE4B, a ubiquitin chain assembly factor, is required for MDM2-mediated p53 polyubiquitination and degradation. Cell Cycle 10(12):1912-1915.

Wu H, Pomeroy SL, Ferreira M, Teider N, Mariani J, Nakayama KI, Hatakeyama S, Tron VA, Saltibus LF, Spyracopoulos L and others. 2011. UBE4B promotes Hdm2-mediated degradation of the tumor suppressor p53. Nature medicine 17(3):347-355.

Xing M. 2005. BRAF mutation in thyroid cancer. Endocrine-related cancer 12(2):245-262.

Xing M. 2013. Molecular pathogenesis and mechanisms of thyroid cancer. Nature

reviews Cancer 13(3):184-199.

Xirodimas DP, Saville MK, Bourdon JC, Hay RT, Lane DP. 2004. Mdm2-mediated NEDD8 conjugation of p53 inhibits its transcriptional activity. Cell 118(1):83-97.

Yang JY, Zong CS, Xia W, Wei Y, Ali-Seyed M, Li Z, Broglio K, Berry DA, Hung MC. 2006. MDM2 promotes cell motility and invasiveness by regulating E-cadherin degradation. Molecular and cellular biology 26(19):7269-7282.

Yang Y, Ludwig RL, Jensen JP, Pierre SA, Medaglia MV, Davydov IV, Safiran YJ, Oberoi P, Kenten JH, Phillips AC and others. 2005. Small molecule inhibitors of HDM2 ubiquitin ligase activity stabilize and activate p53 in cells. Cancer cell 7(6):547-559.

Yaspo ML, Aaltonen J, Horelli-Kuitunen N, Peltonen L, Lehrach H. 1998. Cloning of a novel human putative type Ia integral membrane protein mapping to 21q22.3. Genomics 49(1):133-136.

Yu R, Heaney AP, Lu W, Chen J, Melmed S. 2000. Pituitary tumor transforming gene causes aneuploidy and p53-dependent and p53-independent apoptosis. The Journal of biological chemistry 275(47):36502-36505.

Yu R, Lu W, Chen J, McCabe CJ, Melmed S. 2003. Overexpressed pituitary tumor-transforming gene causes aneuploidy in live human cells. Endocrinology 144(11):4991-4998.

Yu R, Ren SG, Horwitz GA, Wang Z, Melmed S. 2000. Pituitary tumor transforming gene (PTTG) regulates placental JEG-3 cell division and survival: evidence from live cell imaging. Mol Endocrinol 14(8):1137-1146.

Zatelli MC, Tagliati F, Amodio V, Buratto M, Pelizzo M, Pansini G, Bondanelli M, Ambrosio MR, Degli Uberti EC. 2010. Role of pituitary tumour transforming gene 1 in medullary thyroid carcinoma. Anal Cell Pathol (Amst) 33(5):207-216.

Zedenius J, Larsson C, Wallin G, Backdahl M, Aspenblad U, Hoog A, Borresen AL, Auer G. 1996. Alterations of p53 and expression of WAF1/p21 in human thyroid tumors. Thyroid : official journal of the American Thyroid Association 6(1):1-9.

Zhang X, Horwitz GA, Prezant TR, Valentini A, Nakashima M, Bronstein MD, Melmed S.

1999. Structure, expression, and function of human pituitary tumor-transforming gene (PTTG). Mol Endocrinol 13(1):156-166.

Zhou BP, Liao Y, Xia W, Zou Y, Spohn B, Hung MC. 2001. HER-2/neu induces p53 ubiquitination via Akt-mediated MDM2 phosphorylation. Nature cell biology 3(11):973-982.

Zhou Y, Mehta KR, Choi AP, Scolavino S, Zhang X. 2003. DNA damage-induced inhibition of securin expression is mediated by p53. The Journal of biological chemistry 278(1):462-470.

Zhu J, Zhou W, Jiang J, Chen X. 1998. Identification of a novel p53 functional domain that is necessary for mediating apoptosis. The Journal of biological chemistry 273(21):13030-13036.

Zou H, McGarry TJ, Bernal T, Kirschner MW. 1999. Identification of a vertebrate sister-chromatid separation inhibitor involved in transformation and tumorigenesis. Science 285(5426):418-422.

Zou M, Shi Y, al-Sedairy S, Hussain SS, Farid NR. 1995. The expression of the MDM2 gene, a p53 binding protein, in thyroid carcinogenesis. Cancer 76(2):314-318.

Zur A, Brandeis M. 2001. Securin degradation is mediated by fzy and fzr, and is required for complete chromatid separation but not for cytokinesis. The EMBO journal 20(4):792-801.

Chapter 11. Bibliography

11.1: Publications relevant to thesis

Ryan GA, Lewy GD, Read ML, Fong JC, Poole V, Seed RI, Sharma N, Smith VE, Kwan PP, Stewart SL, Bacon A, Warfield A, Franklyn JA, McCabe CJ, Boelaert K. Regulation of Pituitary Tumor Transforming Gene (PTTG) expression and phosphorylation in thyroid cells. Endocrinology. 2013 Jul 18. [Epub ahead of print].

Read ML, Seed RI, Fong JCW, Modasia B, Ryan GA, Smith VE, Watkins RJ, Stratford AL, Kwan PK, Sharma N, Dixon OM, Watkinson JC, Boelaert K, Franklyn JA, Turnell AS and McCabe CJ (2013). The PTTG1-Binding Factor (PBF) regulates p53 activity in thyroid cells. *Endocrinology* (in revision).

11.2: Publications not relevant to thesis

Smith VE, Sharma N, Watkins RJ, Read ML, Ryan GA, Kwan PP, Martin A, Watkinson JC, Boelaert K, Franklyn JA, McCabe CJ. Manipulation of PBF/PTTG1IP phosphorylation status; a potential new therapeutic strategy for improving radioiodine uptake in thyroid and other tumors. J Clin Endocrinol Metab. 2013 Jul;98(7):2876-86.

Smith VE, Read ML, Turnell AS, Sharma N, Lewy GD, Fong JC, Seed RI, Kwan P, **Ryan G**, Mehanna H, Chan SY, Darras VM, Boelaert K, Franklyn JA, McCabe CJ. PTTG-binding factor (PBF) is a novel regulator of the thyroid hormone transporter MCT8. Endocrinology. 2012 Jul;153(7):3526-36.

11.3: Presentations

1. Poster Presentation at British Endocrine Society Meeting 2011
2. Poster Presenation at British Endocrine Society 2012
3. Poster Presentation at British Thyroid Association 2012
4. Oral Presenation at British Endocrine Society 2013
5. Poster Presenation at American Association For Cancer Resarch 2013